TRW

TRW Environmental
Safety Systems Inc.

Ambient Characterization of the Drift Scale Test Block

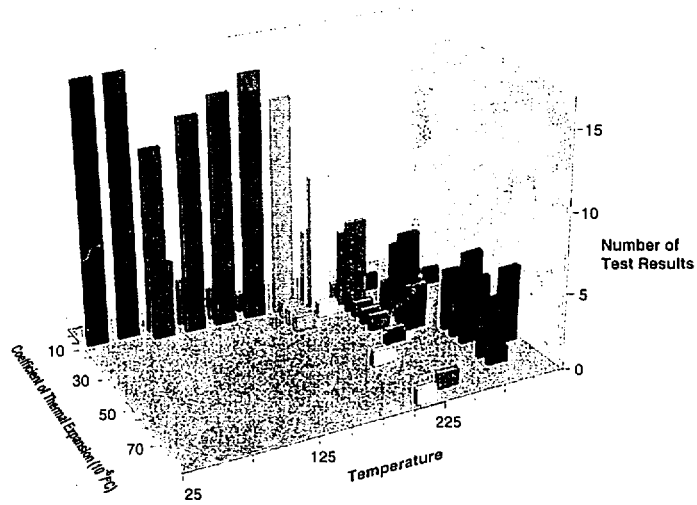

December 11, 1997

Civilian Radioactive Waste Management System

Management & Operating Contractor

B&W Federal Services
Duke Engineering & Services, Inc.
Fluor Daniel, Inc.
Framatome Cogema Fuels
Integrated Resources Group
INTERA, Inc.
JAI Corporation
JK Research Associates, Inc.
Lawrence Berkeley National Laboratory
Lawrence Livermore National Laboratory
Los Alamos National Laboratory
Morrison-Knudsen Corporation
Sandia National Laboratories
Science Applications International Corporation
TRW Environmental Safety Systems Inc.
Winston & Strawn
Woodward-Clyde Federal Services
Cooperating Federal Agency:
U.S. Geological Survey

Prepared by:
TRW Environmental Safety Systems Inc.

Prepared for:
U.S. Department of Energy
Office of Civilian Radioactive Waste Management
1000 Independence Avenue, S.W.
Washington, D.C. 20565

9903020154 990223
PDR WASTE
WM-11 PDR

WBS: 1.2.3.14
QA: L

Civilian Radioactive Waste Management System
Management & Operating Contractor

Ambient Characterization of the Drift Scale Test Block

BADD00000-01717-5705-00001 REV 01

December 11, 1997

Prepared for:

U.S. Department of Energy
Yucca Mountain Site Characterization Office
P.O. Box 30307
North Las Vegas, NV 89036-0307

Prepared by:

TRW Environmental Safety Systems Inc.
1180 Town Center Drive
Las Vegas, Nevada 89134

Under Contract Number
DE-AC01-91RW00134

DISCLAIMER

This report was prepared as an account of work sponsored by an agency of the United States Government. Neither the United States nor any agency thereof, nor any of their employees, makes any warranty, express or implied, or assumes any legal liability or responsibility for the accuracy, completeness, or usefulness of any information, apparatus, product, or process disclosed, or represents that its use would not infringe privately owned rights. Reference herein to any specific commercial product, process, or service by trade name, trademark, manufacturer, or otherwise, does not necessarily constitute or imply its endorsement, recommendation, or favoring by the United States Government or any agency thereof. The views and opinions of authors expressed herein do not necessarily state or reflect those of the United States Government or any agency thereof.

Civilian Radioactive Waste Management System
Management & Operating Contractor

Ambient Characterization of the Drift Scale Test Block

BADD00000-01717-5705-00001 REV 01

December 11, 1997

Prepared by:

Ralph A. Wagner — Date: 12.12.97

R. A. Wagner, ESF Thermal Test Team

Reviewed by:

Roger J. Henning — Date: 12/12/97

R. J. Henning, Scientific Program Operations

Approved by:

Roe. N. Datta — Date: 12/12/97

R. N. Datta, Technical Lead,
ESF Thermal Test Team

Ron Oliver for N.E. — Date: 12/18/97

N. Z. Elkins, Manager, Thermal and
Engineer Support Testing

for Larry A. Hayes — Date: 12/18/97

L. R. Hayes, Manager, Scientific Program
Operations

Civilian Radioactive Waste Management System
Management & Operating Contractor

Ambient Characterization of the Drift Scale Test Block

BADD00000-01717-5705-00001 REV 00

August 1, 1997

Prepared by:

M. R. DiBernardo, ESF Thermal Test Team — Date: 8/1/97

R. A. Wagner, ESF Thermal Test Team — Date: 8·1·97

Reviewed by:

R. J. Henning, Technical Reviewer — Date: 8/1/97

D. S. Kessel, Technical Reviewer — Date: 8/1/97

S. T. Nelson, Technical Reviewer — Date: July 31, 1997

Approved by:

R. N. Datta, Technical Lead, ESF Thermal Test Team — Date: 8/1/97

N. Z. Elkins, Manager, Thermal and Engineer Support Testing — Date: 8/1/97

L. R. Hayes, Manager, Scientific Program Operations — Date: 8/01/97

CONTENTS

Page

1. INTRODUCTION 1-1
   1.1 BACKGROUND: CHARACTERIZATION OF THE SINGLE HEATER TEST BLOCK 1-1
   1.2 OBJECTIVE 1-1
   1.3 SCOPE 1-4

2. DRIFT SCALE TEST FACILITY DESCRIPTION 2-1

3. LABORATORY TESTING: THERMAL PROPERTIES 3-1
   3.1 OBJECTIVES AND DESCRIPTION 3-1
   3.2 SAMPLES 3-1
   3.3 METHODOLOGY 3-7
      3.3.1 Thermal Conductivity 3-7
      3.3.2 Thermal Expansion 3-9
   3.4 RESULTS 3-12
      3.4.1 Thermal Conductivity 3-12
      3.4.2 Thermal Expansion 3-12

4. LABORATORY TESTING: MECHANICAL PROPERTIES 4-1
   4.1 OBJECTIVES AND DESCRIPTION 4-1
   4.2 SAMPLES 4-1
   4.3 METHODOLOGY 4-4
   4.4 RESULTS 4-6

5. LABORATORY TESTING: HYDROLOGICAL PROPERTIES 5-1
   5.1 OBJECTIVE AND DESCRIPTION 5-1
   5.2 SAMPLES 5-1
   5.3 METHODOLOGY 5-2
   5.4 RESULTS 5-3

6. LABORATORY TESTING: CHEMICAL PROPERTIES 6-1
   6.1 MINERALOGY AND PETROLOGY 6-1
      6.1.1 Objective and Description 6-1
      6.1.2 Samples 6-1
      6.1.3 Methodology 6-3
      6.1.4 Results 6-4
   6.2 PORE WATER ANALYSES 6-4
      6.2.1 Objective and Description 6-4
      6.2.2 Method 6-4
      6.2.3 Results 6-7

CONTENTS (Continued)

Page

7. FIELD MEASUREMENTS: FRACTURE MAPPING 7-1
   7.1 OBJECTIVE AND DESCRIPTION 7-1
   7.2 METHODOLOGY 7-1
   7.3 RESULTS 7-3

8. FIELD MEASUREMENTS: ROCK MASS CLASSIFICATION 8-1
   8.1 OBJECTIVE AND DESCRIPTION 8-1
   8.2 METHODOLOGY 8-1
   8.3 RESULTS 8-2

9. FIELD MEASUREMENTS: AIR PERMEABILITY TESTING 9-1
   9.1 OBJECTIVE AND DESCRIPTION 9-1
   9.2 METHODOLOGY 9-1
   9.3 RESULTS 9-7
      9.3.1 Air Permeability Estimation 9-7
      9.3.2 Interference Pressure Responses and Conceptual Model for Gas Flow in the DST Block 9-8

10. FIELD MEASUREMENTS: ADDITIONAL 10-1
   10.1 INFRARED IMAGING 10-1
      10.1.1 Objective and Description 10-1
      10.1.2 Methodology 10-1
      10.1.3 Results 10-2
   10.2 RAPID EVALUATION OF K (THERMAL CONDUCTIVITY) AND ALPHA (THERMAL DIFFUSIVITY) 10-4
      10.2.1 Objective and Description 10-4
      10.2.2 Methodology 10-4
      10.2.3 Results 10-6
   10.3 BOREHOLE VIDEO LOGS 10-8
      10.3.1 Objective and Description 10-8
      10.3.2 Methodology 10-9
      10.3.3 Results 10-9
   10.4 IN SITU STRESS MEASUREMENTS 10-9
      10.4.1 Objective and Description 10-9
      10.4.2 Methodology 10-9
      10.4.3 Results 10-15

11. SUMMARY 11-1

12. QUALITY ASSURANCE 12-1

CONTENTS (Continued)

Page

13. REFERENCES 13-1
    13.1 REFERENCED DOCUMENTS 13-1
    13.2 STANDARDS AND PROCEDURES 13-5

APPENDIX A - THERMAL EXPANSION DATA: SUMMARY SHEET FOR EACH TEST CYCLE A-1

APPENDIX B - THERMAL EXPANSION DATA: COMPARISON OF FIRST AND SECOND HEATING CYCLES B-1

APPENDIX C - MECHANICAL PROPERTIES DATA: STRESS-STRAIN DIAGRAMS . C-1

APPENDIX D - HYDROLOGICAL PROPERTIES DATA: GRAPHICAL PRESENTATION D-1

INTENTIONALLY LEFT BLANK

FIGURES

		Page
1-1	Plan View of ESF Thermal Test Facility	1-2
1-2	Schematic of the Single Heater Test: Borehole Perspective	1-3
2-1	Schematic of the Drift Scale Test: Borehole Perspective	2-3
2-2	Layout of the Drift Scale Test	2-4
2-3	Drift Scale Test Cross Section A-A	2-5
2-4	Drift Scale Test Cross Section B-B	2-6
3-1	Location of Drift Scale Test Area Within the Exploratory Studies Facility	3-2
3-2	Plan View of Drift Scale Test Area	3-3
3-3	Approximate Locations of Thermal Conductivity Test Specimens	3-4
3-4	Approximate Locations of Thermal Expansion Test Specimens	3-5
3-5	Distribution of Thermal Conductivity Values	3-14
3-6	View of DST Showing Individual Thermal Conductivities	3-15
3-7	Mean Coefficients of Thermal Expansion-Versus-Temperature During the First Heating Cycle	3-20
3-8	Distribution of Mean Coefficients of Thermal Expansion During First Heating Cycle for 17 Test Specimens	3-21
3-9	View of the DST Showing Individual Mean Coefficients of Thermal Expansion Calculated Over 25-50°C During the First Heating Cycle	3-22
3-10	View of the DST Showing Individual Mean Coefficients of Thermal Expansion Calculated Over 200-225°C During the First Heating Cycle	3-23
3-11	View of the DST Showing Individual Mean Coefficients of Thermal Expansion Calculated Over 275-300°C During the First Heating Cycle	3-24
3-12	Mean MCTEs and Standard Deviations Obtained During the First Heating Cycle for 17 DST Specimens and Nine SHT Specimens	3-25
3-13	Mean MCTEs and Standard Deviations Obtained During the First Cooling Cycle for 17 DST Specimens and Nine SHT Specimens	3-26
3-14	Mean MCTEs and Standard Deviations Obtained During the First Heating Cycle for 14 DST Specimens and Nine SHT Specimens	3-26
3-15	Mean MCTEs and Standard Deviations Obtained During the First Cooling Cycle for 17 DST Specimens and Nine SHT Specimens	3-27
4-1	Locations of Instrumentation Boreholes Used for Sample Collection	4-2
4-2	Approximate Locations of Unconfined Compressive Test Specimens	4-3
4-3	Specimen Instrumentation Assembly for Unconfined Compression Tests	4-5
4-4	Distribution of Young's Modulus	4-8
4-5	Distribution of Poisson's Ratios	4-8
4-6	Distribution of Unconfined Compressive Strengths	4-9
4-7	View of DST Block Showing Individual Young's Modulus	4-10
4-8	View of DST Block Showing Individual Poisson's Ratio	4-11
4-9	View of DST Block Showing Individual Unconfined Compressive Strength	4-12

FIGURES (Continued)

		Page
5-1	Matric Potential and Water Saturation of the SHT Samples at Room Temperature During Drying and Wetting Phases	5-11
5-2	Matric Potential and Water Saturation of the DST Samples at Room Temperature During the Wetting Phase up to 50% Relative Humidity	5-11
6-1	U Abundance in Pore-Water Leachates	6-10
7-1	Rock Mass Classification of the DST Connecting Drift from Station 0+00 to 20+00 m	7-4
7-2	Rock Mass Classification of the DST Connecting Drift from Station 20+00 to 40+00 m	7-5
7-3	Rock Mass Classification of the DST Connecting Drift from Station 40+00 to 45+00 m	7-6
7-4	Rock Mass Classification of the DST Heated Drift from Station 0+00 to 20+00 m	7-7
7-5	Rock Mass Classification of the DST Heated Drift from Station 20+00 to 40+00 m	7-8
7-6	Rock Mass Classification of the DST Heated Drift from Station 40+00 to 60+00 m	7-9
8-1	Q Values from the Thermal Test Facility Surrounding the Drift Scale Test	8-9
8-2	RMR Values from the Thermal Test Facility Surrounding the Heated Drift	8-10
8-3	Q Values for TSw2 (Tptpmn and Tptpll) for the Main Drift at Station 27+15 to 63+05 m	8-11
8-4	RMR Values for TSw2 (Tptpmn and Tptpll) for the Main Drift at Station 27+15 to 63+05 m	8-12
9-1	Plan View of DST Block	9-15
9-2	E-W Cross-Section of DST Block	9-16
9-3	Two N-S Cross-Sections of DST Block	9-17
9-4	Schematic Diagram of a Packer String with Two Packers	9-18
9-5	Packer Positions for Air Permeability Tests	9-19
9-6	Local Permeability Estimates in 41 Cross-Sections of the 14 Observation Drift Boreholes	9-20
9-7	Frequency Distribution of Permeability Values from the DST and SHT Blocks	9-21
9-8	Interference Pressure Data From Injection in 52-3	9-22
9-9	Interference Pressure Data From Injection in 51-1	9-24
9-10	Interference Pressure Data From Injection in 78-2	9-25
9-11	Interference Pressure Data From Injection in 75-1	9-26
9-12	Interference Pressure Data From Injection in 69-3	9-27
9-13	Interference Pressure Data From Injection in 51-2	9-29
9-14	Interference Pressure Data From Injection in 48-3	9-31

FIGURES (Continued)

		Page
9-15	Interference Pressure Data From Injection in 69-1	9-32
9-16	Interference Pressure Data From Injection in 53-1	9-33
9-17	Pressure Response From Nearby Boreholes From Injection in Borehole 11 in SHT Block	9-34
9-18	Pressure Response From Distant Boreholes From Injection in Borehole 11 in SHT Block	9-34
10-1	Representative Infrared Image From the DST Block	10-3
10-2	Site Locations for REKA Measurements	10-7

INTENTIONALLY LEFT BLANK

TABLES

Page

1-1 Compliance with Acceptance Criteria 1-5

3-1 Borehole Nomenclature 3-6
3-2 Nominal Dimensions of Test Specimens 3-6
3-3 Summary of Thermal Conductivity Data for Saturated Specimens from the DST Block 3-13
3-4 Summary of Thermal Expansion Data for Specimens from the DST Block for the First Heating Cycle 3-16
3-6 Summary of Thermal Expansion Data for Specimens from the DST Block for the Second Heating Cycle 3-18
3-7 Summary of Thermal Expansion Data for Specimens from the DST Area for the Second Cooling Cycle 3-19

4-1 Tabulation of Unconfined Compression Tests 4-7

5-1 Laboratory Hydrological Measurements of Dry-Drilled Cores from DST Permeability Boreholes 5-4
5-2 Laboratory Hydrological Measurements of Wet-Drilled Cores from DST Boreholes . 5-5
5-3 Laboratory Hydrological Measurements of Wet-Drilled Cores from SHT Boreholes . 5-7
5-4 Laboratory Hydrological Measurements of Grab Samples from Wet Excavation of the Observation Drift 5-8
5-5 Effective Porosities for Moisture Imbibition Potential Determination in the SHT Block 5-9
5-6 Effective Porosities for Moisture Imbibition Potential Determination in the DST Block 5-9
5-7 Relative Humidity and Water Saturation of SHT Samples in Wetting Phase at Room Temperature 5-10
5-8 Relative Humidity and Water Saturation of SHT Samples in Drying Phase at Room Temperature 5-10
5-9 Matric Potential and Water Saturation of the DST Samples at Room Temperature in the Wetting Phase 5-10

6-1 Mineral Abundances for Samples from the Drift Scale Test Block 6-2
6-2 Sample Preparation Procedures 6-5
6-3 $^{87}Sr/^{86}Sr$ Ratios 6-8
6-4 Summary of Uranium Isotopic Data on Pore-Water Leaches from Borehole Cuttings, Crushed Core, and Fracture Water 6-9
6-5 Stable δ^2H and $S^{18}O$ Values 6-11
6-6 Tritium Data 6-12
6-7 Sodium-Potassium Ratios 6-12

TABLES (Continued)

		Page
8-1	Rock Mass Rating Q for the Thermal Test Facility	8-3
8-2	Rock Mass Rating RMR for the Thermal Test Facility	8-6
8-3	RMR Indices for Topopah Spring Middle Non-Lithophysal Zone (TSw2)	8-13
9-1	As-Built Coordinates of the Collar and Diameter of Air Permeability Boreholes	9-3
9-2	Lengths of Packed-Off Zones for Air Permeability Tests	9-5
9-3	Estimated Local Permeability for the 41 Packed-Off Zones in 14 Boreholes	9-7
9-4	Estimated Permeability Values from All Injection Tests Conducted in the 14 Boreholes	9-9
10-1	REKA Results with No Background Temperature Correction	10-8
10-2	REKA Results with Background Temperature Correction	10-8
10-3	Video Logs from DST Boreholes	10-10
13-1	Tabulation of Report Location, TDIFs/DTNs, Procedures, Milestone Numbers, References, and Q-Status of Characterization Data	13-7

ACRONYMS

ASTM	American Society for Testing and Materials
C	Compressive Strength, Intact Rock Strength Rating
CRWMS	Civilian Radioactive Waste Management System
DCS	Data Collection System
DLS	Detailed Line Survey
DOE	U.S. Department of Energy
DST	Drift Scale Test
DTN	Document Transmittal Notice
ESF	Exploratory Studies Facility
FY	Fiscal Year
GENISES	Geographic Nodal Information Study and Evaluation System
GHFM	Guarded Heat Flow Meter
HFT	Heat Flux Transducer
ICTE	Instantaneous Coefficient of Thermal Expansion
ISRM	International Society for Rock Mechanics
Ja	Joint Alternation Number
Jc	Joint Condition Rating
Jn	Joint Set Number
JOA	Joint Orientation Adjustment
Jr	Joint Roughness Number
JS	Joint Set
Js	Joint Spacing Rating
Jw	Joint Water Reduction Factor (Q System), Ground Water Rating (RMR System)
LBNL	Lawrence Berkeley National Laboratory
LLNL	Lawrence Livermore National Laboratory
LVDT	Linear Variable Displacement Transducers
M&O	Management and Operating Contractor
MCTE	Mean Coefficient of Thermal Expansion
MPBX	Multiple-point Borehole Extensometer
NIST	National Institute of Standards and Technology
OCRWM	Office of Civilian Radioactive Waste Management

ACRONYMS (Continued)

psig	Pounds Per Square Inch Gauge
Q/non-Q	Quality affecting/non-Quality affecting
Q	Rock Mass Quality Indices
QA	Quality Assurance
QAIP	Quality Assurance Implementation Procedure
QAP	Quality Administrative Procedure
REKA	Rapid Evaluation of K (Thermal Conductivity) and Alpha (Thermal Diffusivity)
RMR	Rock Mass Rating
RQD	Rock Quality Designation
SHT	Single Heater Test
SLPM	Standard Liter per Minute
SNL	Sandia National Laboratories
SRF	Stress Reduction Factor
SRM	Standard Reference Materials
TDIF	Technical Data Information Form
Tptpll	**T**ertiary-Miocene (Age), **P**aintbrush (Group), **T**opopah Spring Tuff (Formation), Crystal-**P**oor (Member), **L**ower **L**ithophysal (Zone)
Tptpmn	**T**ertiary-Miocene (Age), **P**aintbrush (Group), **T**opopah Spring Tuff (Formation), Crystal-**P**oor (Member), **M**iddle **N**onlithophysal (Zone)
TSw2	Topopah Spring Welded Unit, Lithophysal-Poor Subunit
TTF	Thermal Test Facility
TU	Tritium Unit
USBR	U.S. Bureau of Reclamation
USGS	U.S. Geological Survey

1. INTRODUCTION

1.1 BACKGROUND: CHARACTERIZATION OF THE SINGLE HEATER TEST BLOCK

The Exploratory Studies Facility (ESF) Thermal Test Facility (TTF) is composed of two heater tests: the single heater test (SHT) and the drift scale test (DST) (Figure 1-1). Characterization of the SHT block was provided in a previous report, *Characterization of the ESF Thermal Test Area,* (CRWMS M&O 1996). That report compiled the results of geological and geotechnical characterization data from the SHT block to define ambient conditions prior to the onset of heating. The results of laboratory tests characterizing thermal, mechanical, hydrological, and chemical properties, and the field work characterizing local geology, in situ hydrology, and local rock mass quality were documented. This characterization data identified the initial conditions of the local rock mass to assist in the analysis and interpretation of the coupled thermal, mechanical, hydrological, and chemical processes associated with the planned SHT. The results of this characterization were generally consistent with the results of previous non-thermal test studies in the same thermal-mechanical unit and lithostratigraphic units (Brechtel et al. 1995; Kicker et al. 1996).

The SHT consists of a nominal 4 kW, 4-m long heater emplaced in one of 41 boreholes that have a cumulative length of approximately 230 m. The remaining boreholes house 530 sensors that measure the thermal (333 sensors), mechanical (45 sensors), hydrological (52 sensors), and/or chemical (100 sensors) responses from heat generated from the emplaced heater. Most of these measurements are recorded by a data collection system (DCS) on at least an hourly basis. Data from sensors located on the heater are acquired every 15 minutes. The SHT block consists of a thermomechanical alcove and a thermomechanical alcove extension, as shown in Figure 1-1. A schematic diagram of the SHT is presented in Figure 1-2.

1.2 OBJECTIVE

The objective of this report is to present the results of the characterization of the DST block of the ESF TTF. The general location and layout of the DST are shown in Figure 1-1. The data in this report were developed to define ambient conditions in the DST block prior to heater activation. Additional data, specifically hydrological data, from the SHT block were acquired since publication of the previous report (CRWMS M&O 1996), and are also provided. Where appropriate, data from the DST block and the SHT block are compared.

The ESF Thermal Test, which includes the SHT and DST, is an integral part of the program of site investigations to characterize Yucca Mountain in Nye County, Nevada, for the evaluation of its suitability as a potential site for permanent disposal of spent nuclear fuel and high level nuclear waste. The objective of the ESF Thermal Test is to better understand the coupled thermal, mechanical, hydrological, and chemical processes likely to exist from the emplacement of nuclear waste in the rock mass surrounding the potential geologic repository at Yucca Mountain.

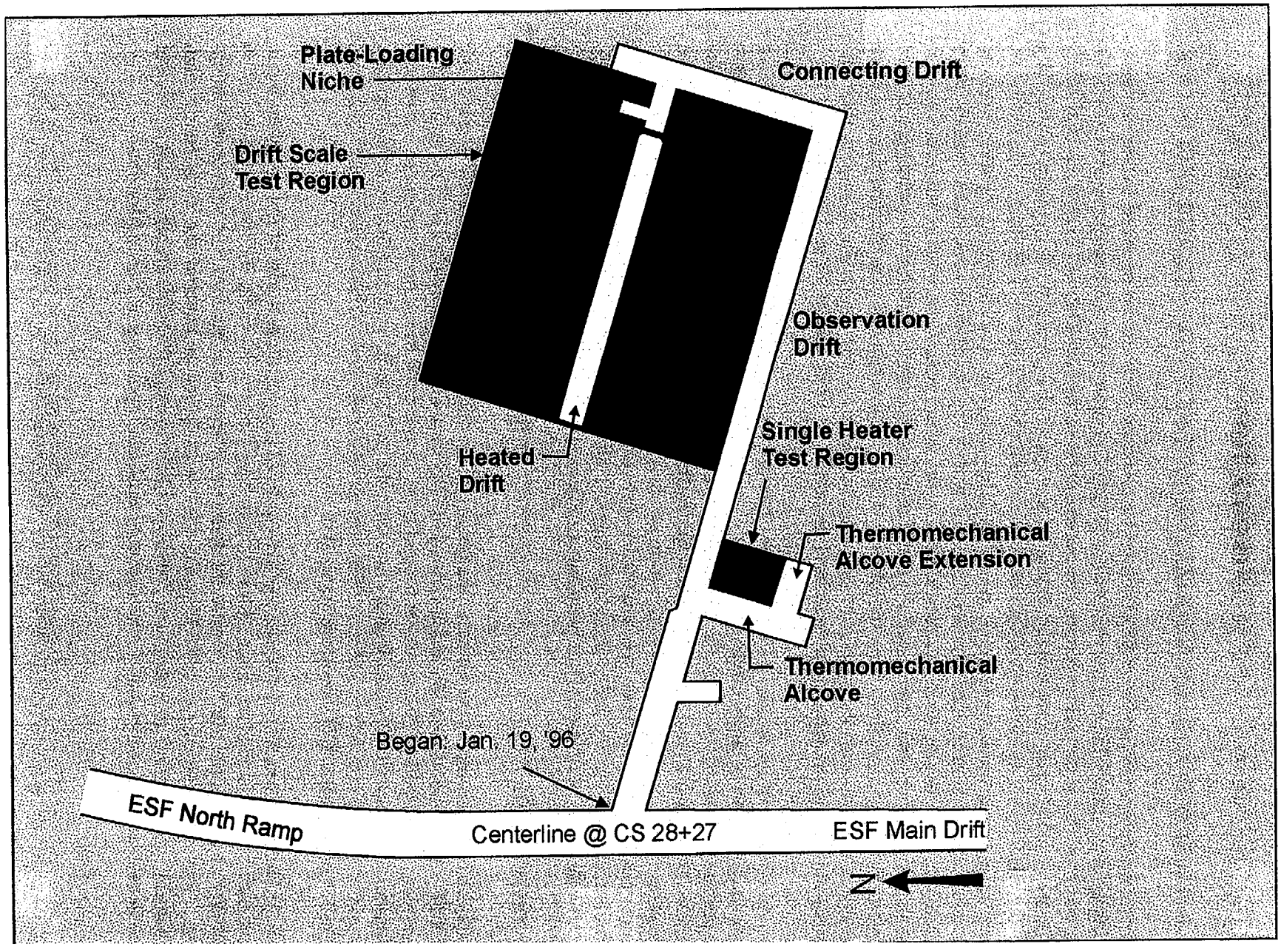

Figure 1-1. Plan View of ESF Thermal Test Facility

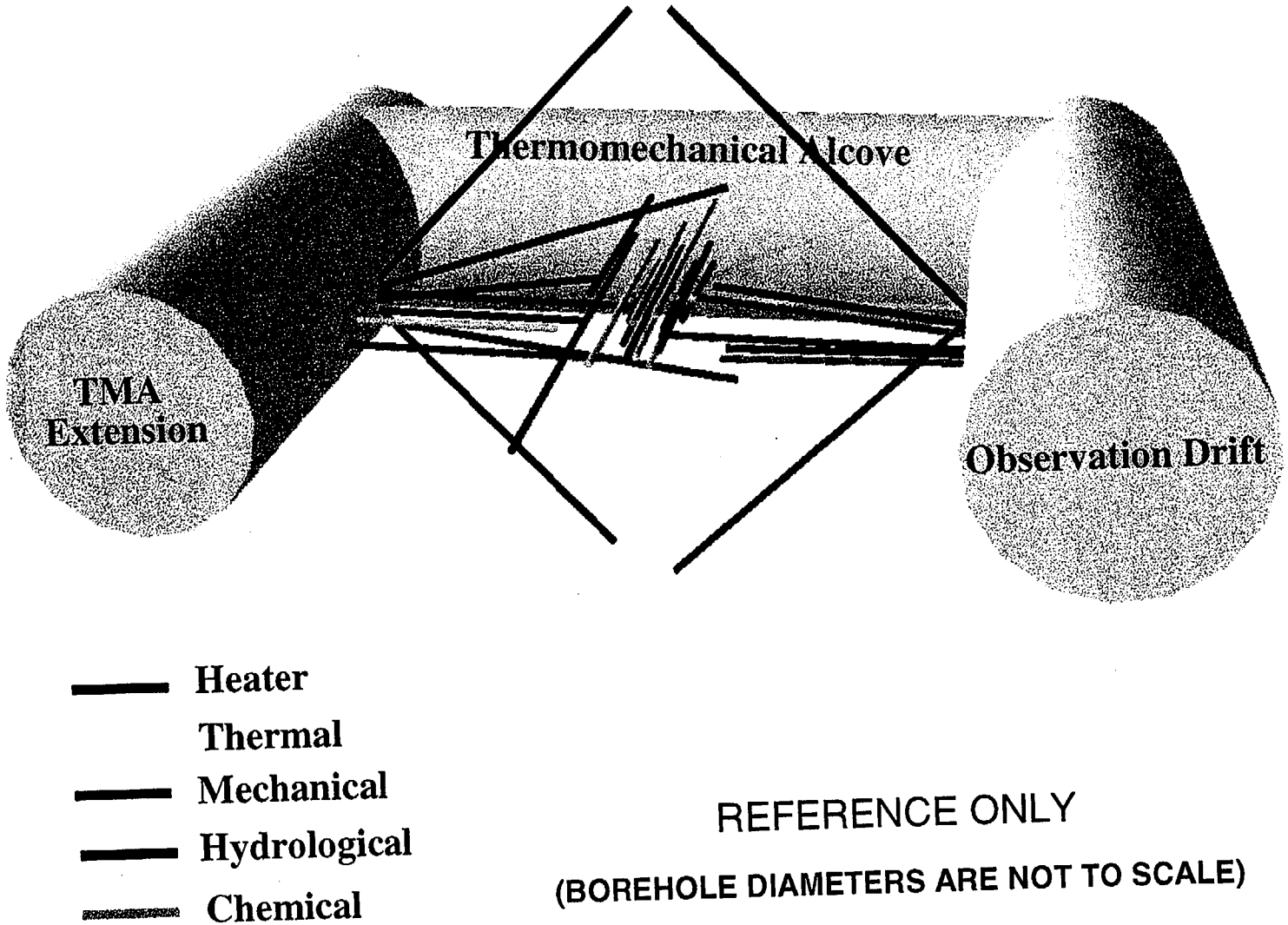

Figure 1-2. Schematic of the Single Heater Test: Borehole Perspective

1.3 SCOPE

This report documents the results of the characterization of the TTF before the start of the heating phase of the DST. This report, together with the fiscal year (FY) 96 report, largely completes the planned pre-test characterization of the ESF TTF. To this end, this report includes results of laboratory testing of hydrological properties characterizing the SHT block that could not be included in the FY 96 report (CRWMS M&O 1996). Some additional characterization data will be generated prior to activation of the DST heater and will be reported at a later date. It is beyond the scope of this report to address results obtained during the conduct of either heater test.

Results, in most cases, are presented in accordance with the reporting guidelines of the applicable and appropriate American Society for Testing and Materials, International Society of Rock Mechanics (ASTM/ISRM) standards, if any. The results of in situ bulk permeability measurements by pneumatic methods are presented. The results of other characterizations of the thermal test area are also included in this report.

This report satisfies the acceptance criteria for this deliverable. Table 1-1 outlines the criteria for this deliverable and where the criteria are met in this report. This report was prepared in accordance with the Office of Civilian Radioactive Waste Management (OCRWM)-approved quality assurance (QA) procedures, and the implementing requirements of the *Quality Assurance Requirements and Description* (QARD), DOE/RW-0333P. This report was developed on the basis of the best technical data, including both quality affecting (qualified), and non-quality affecting (non-qualified) data. The status of data used and cited in this report is appropriately noted. The stratigraphic nomenclature used is consistent with the Reference Information Base, Section 1.12(a): Stratigraphy-Geologic Lithologic Stratigraphy. Within the report's Reference Section, Section 13.2, a detailed tabulation of the report location, data tracking numbers, procedures, milestone numbers, key references, and qualified-status of the characterization data is presented in Table 13-1. Accession numbers, where available, are documented in the references in Section 13.1. Technical data contained within the deliverable which were not already incorporated in the Geographic Nodal Information Study and Evaluation System (GENISES) were submitted, if appropriate, for incorporation into the GENISES in accordance with YAP-SIII.3Q. This report is based on technical data submittal compliance which is demonstrated through the submission of individual Level-4 Milestone reports as Technical Data Information Forms. These forms can be identified in the Automated Technical Data Tracking system.

This report contains the results of geologic mapping and infra-red thermal imaging. It documents the source of the video logs of the DST boreholes. Results of geoengineering mapping provide Q system (Barton et al. 1974) and Rock Mass Rating (RMR) system (Bieniawski 1974) rock mass classifications that include rock quality designation (RQD) and spacing, length, aperture, attitude, and infilling of fractures. Results of laboratory testing include Young's modulus and Poisson's ratio; thermal conductivity and thermal expansion; porosity, density, moisture content, moisture saturation and moisture imbibition potential; and quantitative mineralogic characteristics.

Table 1-1. Compliance with Acceptance Criteria

Acceptance Criterion	Compliance Location
The FY 97 report will include those results of characterizing the SHT area that could not be included in the FY 96 report.	Section 5.4; Table 5-3; Figures D-6 through D-10.
The report will contain the results of geologic mapping.	Section 7.3; Figures 7-1 through 7-6.
The report will contain the results of infra-red thermal imaging.	Section 10.1.3; Figure 10-1.
It will document the source of the video logs of the drift scale test boreholes.	Section 10.3.
Results of geoengineering mapping will include RQD, Q and RMR as well as spacing, length, aperture, attitude and coating/infilling of fractures.	Sections 7 and 8; Tables 8-1 through 8-3; Figures 7-1 through 7-6; Figures 8-1 through 8-4.
Results of laboratory testing will include Young's modulus and Poisson's ratio.	Section 4.4; Table 4-1; Figures 4-4, 4-5, 4-7 and 4-8; Appendix C.
Results of laboratory testing will include thermal conductivity and thermal expansion.	Section 3.4.1; Tables 3-3 through 3-7; Figures 3-3 through 3-15; Section 3.4.2; Appendices A and B.
Results of laboratory testing will include porosity, density, moisture content, moisture saturation, and moisture imbibition potential.	Section 5.4; Tables 5-1 through 5-9; Appendix D.
Results of laboratory testing will include quantitative mineralogic characteristics.	Section 6.1.4; Table 6-1 through 6-7.
As far as possible, results will be presented in accordance with the reporting guidelines of applicable and appropriate ASTM/ISRM standards, if any.	Section 3.3 and 3.4; Table 13-1.
Results of in situ bulk permeability measurements by pneumatic methods will be presented in the report.	Section 9.3; Tables 9-3 and 9-4; Figures 9-7 through 9-18.
Results of any other characterization of the thermal test that have been conducted will be included in the report.	Sections 6.2, 10.2 and 10.4.
This deliverable will be prepared in accordance with OCRWM approved quality assurance procedures and the implementing requirements of the Quality Assurance Requirements Description.	Sections 3 through 10; Section 13.2; Table 13-1.
The product will be prepared on the basis of the best technical data, including both Q and non-Q data. The Q status of data used and cited in the report has been appropriately noted.	Sections 3 through 10; Section 13.2; Table 13-1.
Stratigraphic nomenclature used will be consistent with the Reference Information Base Section 1.12(a): Stratigraphy-Geologic Lithologic Stratigraphy.	Throughout report.
Within the report's Reference Section, references to data used in the report will include record Accession Numbers or Data Tracking Numbers when available.	Section 13.1 and 13.2, Table 13-1.

This report is organized as follows. A general description of the DST is given in Section 2. Characterization data, as laboratory test results and field measurements provided by various participants, are presented in Sections 3 through 10. Results are presented under the following headings:

- Laboratory testing
  - Thermal
  - Mechanical
  - Hydrological
  - Chemical

- Field testing
  - Fracture mapping
  - Rock mass classification (Q, RMR, Schmidt Hammer)
  - Air permeability testing
  - Additional field measurements: infrared imaging, borehole video, in situ stress, and REKA - Rapid Evaluation of K (Thermal Conductivity) and Alpha (Thermal Diffusivity).

Section 11 summarizes this report, and Section 12 addresses QA, including activity evaluations, input sources, procedures, and qualification status of data. References are provided in Section 13, and supplemental characterization data are documented in the appendices.

2. DRIFT SCALE TEST FACILITY DESCRIPTION

The general layout and plan view of the ESF TTF and DST area are shown in Figure 1-1, and a schematic diagram is presented in Figure 2-1.

The configuration for the DST, which is shown in Figure 1-1, includes a declining observation drift driven mostly east and downward from near the intersection of the North Ramp and main drift. Specifically, the breakout of the observation drift from the main drift of the ESF is 2,827 m from the North Ramp portal. The downward slope of the observation drift (11.5 to 14.0 percent) ensures a minimum 10 m of Tptpmn [Tertiary-Miocene (Age), Paintbrush (Group), Topopah Spring Tuff (Formation), Crystal-Poor (Member), Middle Nonlithophysal (Zone)] (Buesch et al. 1996) as the overburden for the DST. The length of the observation drift is approximately 136 m.

At the elevation of the DST crown (nominally 10 m below the upper extent of the Tptpmn), the connecting drift breaks out to the north from the observation drift, 136 m from the main drift of the ESF (see Figures 2-1, 2-2, and 2-3). The actual distance of the breakout from the main drift was determined by the requisite overburden (of at least 10 m of Tptpmn) and, to a lesser extent, by rock quality and rock-mass permeability testing determined by ambient site characterization activities. The connecting drift extends approximately 40 m to the north.

The plan view, a representative longitudinal cross-section, and the cross-section orthogonal to the heated drift axis of the DST are shown in Figure 2-2, 2-3, and 2-4 respectively. The DST consists of a nearly 50-m long, 5-m diameter heated drift. The heated drift is complemented with an 11-m long entry, a connecting drift, and an observation drift of similar diameter. Other components include plate loading and DCS niches.

Heat is generated from 50 wing heaters and 9 floor (canister) heaters. These two types of electrical heaters will have a combined power output of approximately 215 kW when operating at full capacity. The wing heaters are inserted in horizontal boreholes in the wall of the heated drift which are perpendicular to the longitudinal axis of the heated drift. Wing heaters are evenly distributed on 1.83 m spacings in boreholes located on both walls of the heated drift. Each wing heater has 10 m of heated length evenly divided between inner and outer heating elements of 1.145 kW and 1.719 kW capacity, respectively.

The thermal, mechanical, hydrological, and chemical responses are measured with approximately 3,500 sensors in 147 boreholes and on the drift surface. These sensors will be connected to a DCS with an estimated 125 miles of wire. The cumulative length of these boreholes is 3,300 m (2 miles). The sensors are divided into the following categories: 2,900 thermal; 110 mechanical; 450 hydrological, and 30 chemical. Numerous variables will be measured including temperature, heat flux, heater power, thermal conductivity, gas pressure, moisture, water flux, chemistry, displacements, and ground support behavior from sensors installed from within the DST drift and from the connecting and observation drifts. Planned durations for the heating and cooling phases are 4 years each. The heating phase should elevate temperatures of the rock above 100°C in more than 10,000 cubic meters of rock while allowing the temperature along the drift wall to reach 200°C.

The DST also includes a rock-mass deformation modulus or plate-loading test alcove near the entrance to the heated drift. This alcove, located on the unheated side of a thermal bulkhead (see Figure 2-2), will be approximately 6-m long and 2-m wide. The comparatively small width is necessary to minimize the size of the plate-loading reaction frame needed to induce a desired stress level in the rock to measure the rock-mass deformation modulus.

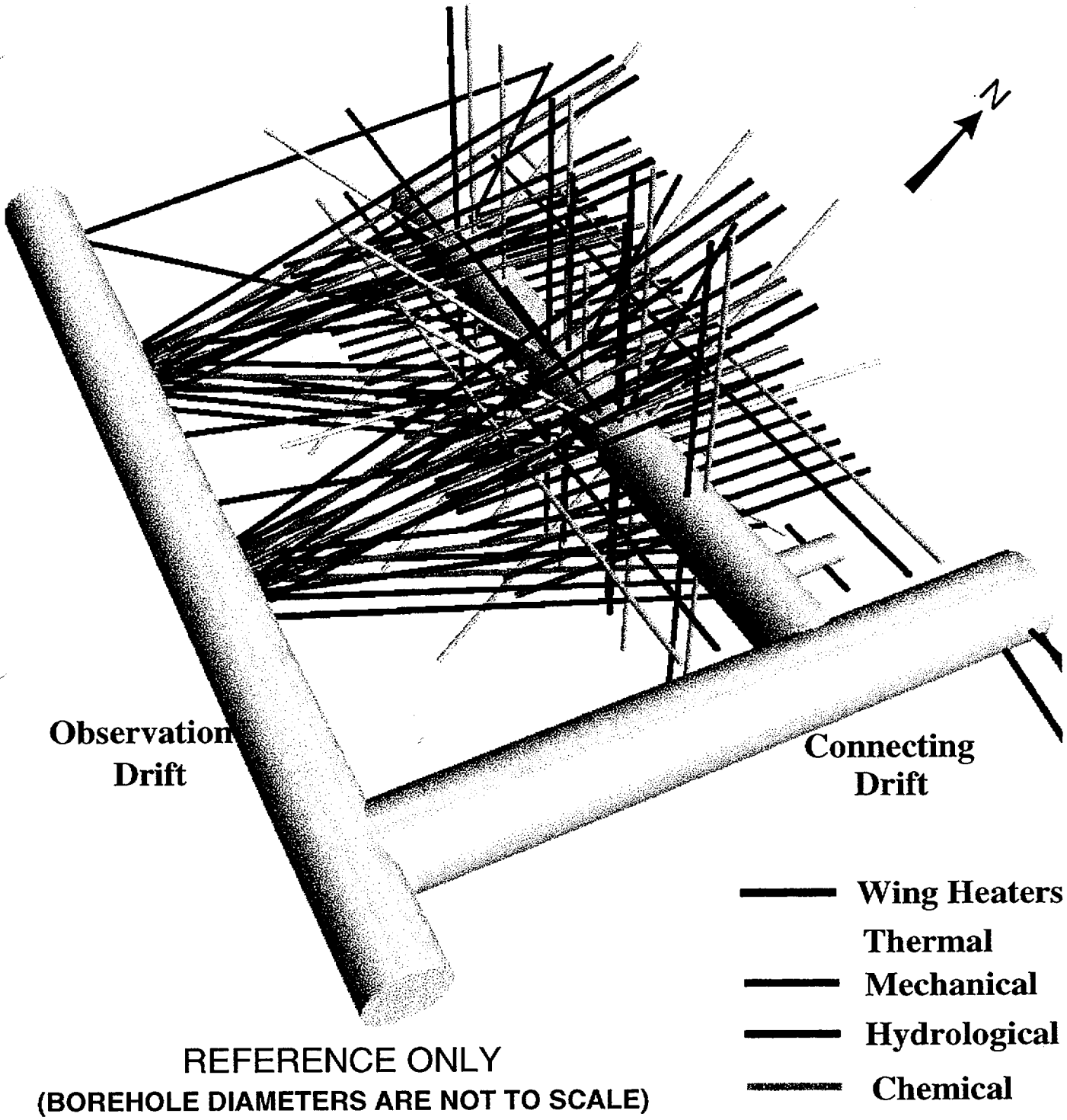

Figure 2-1. Schematic of the Drift Scale Test: Borehole Perspective

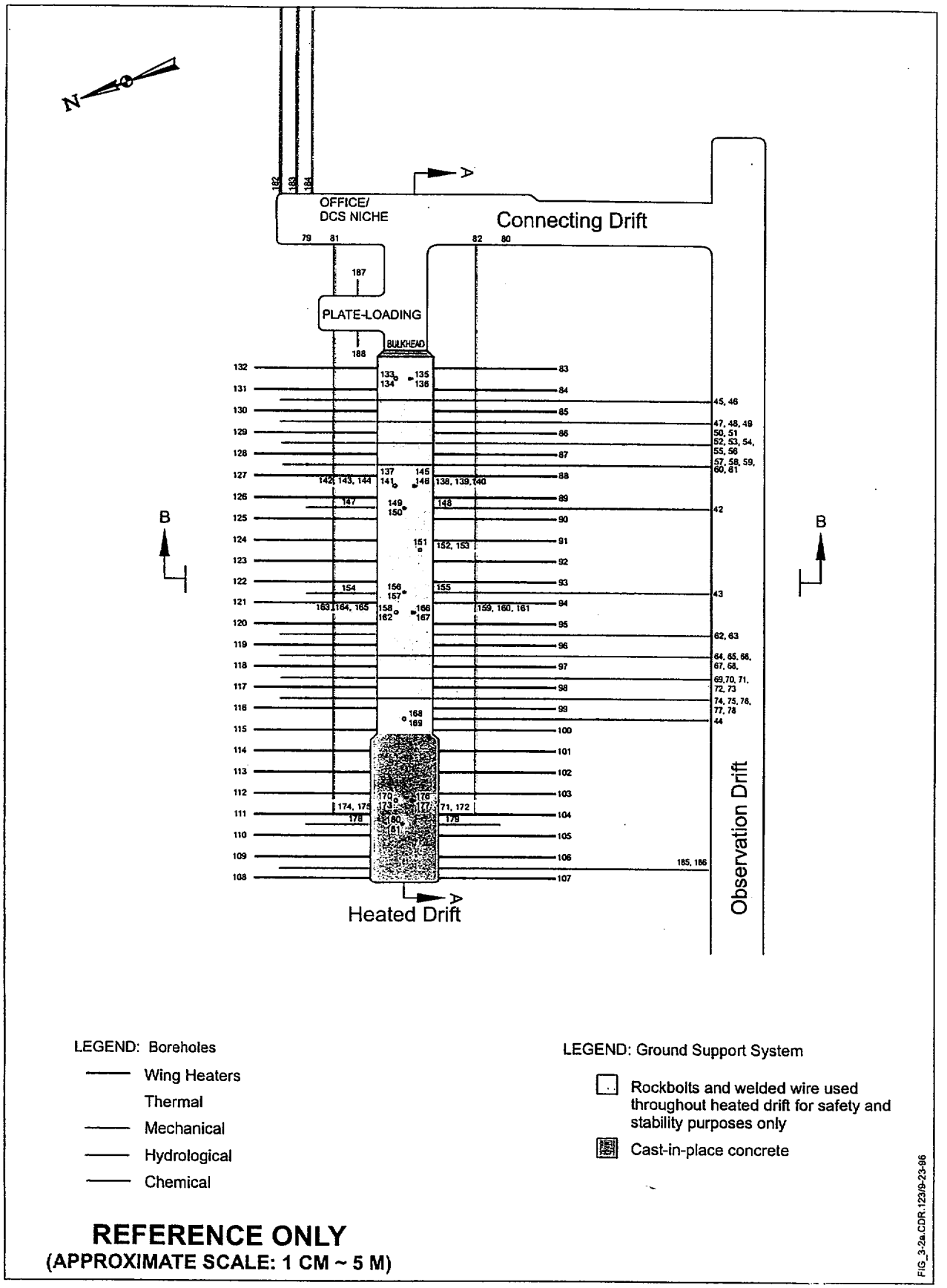

Figure 2-2. Layout of the Drift Scale Test

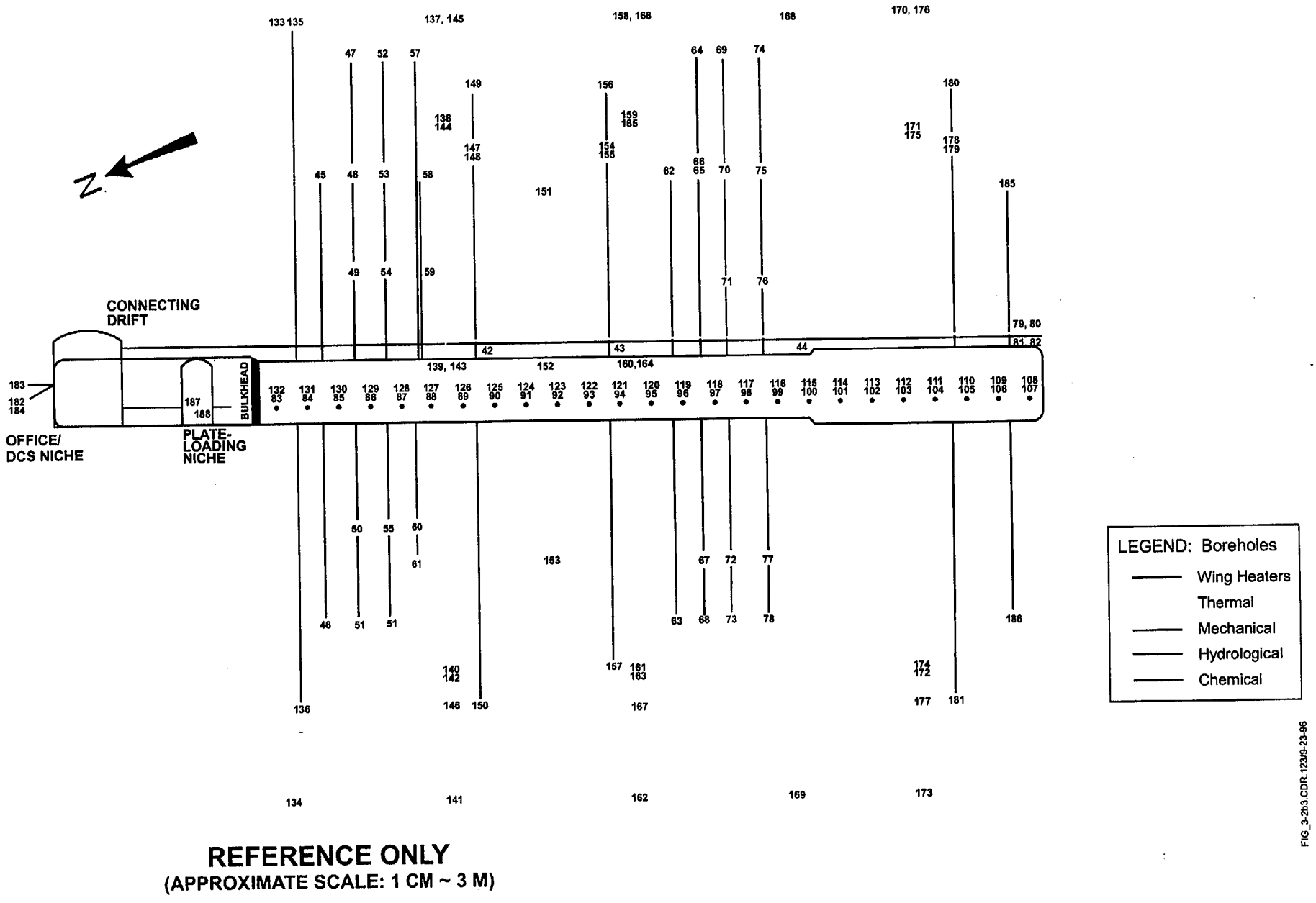

Figure 2-3. Drift Scale Test Cross Section A-A

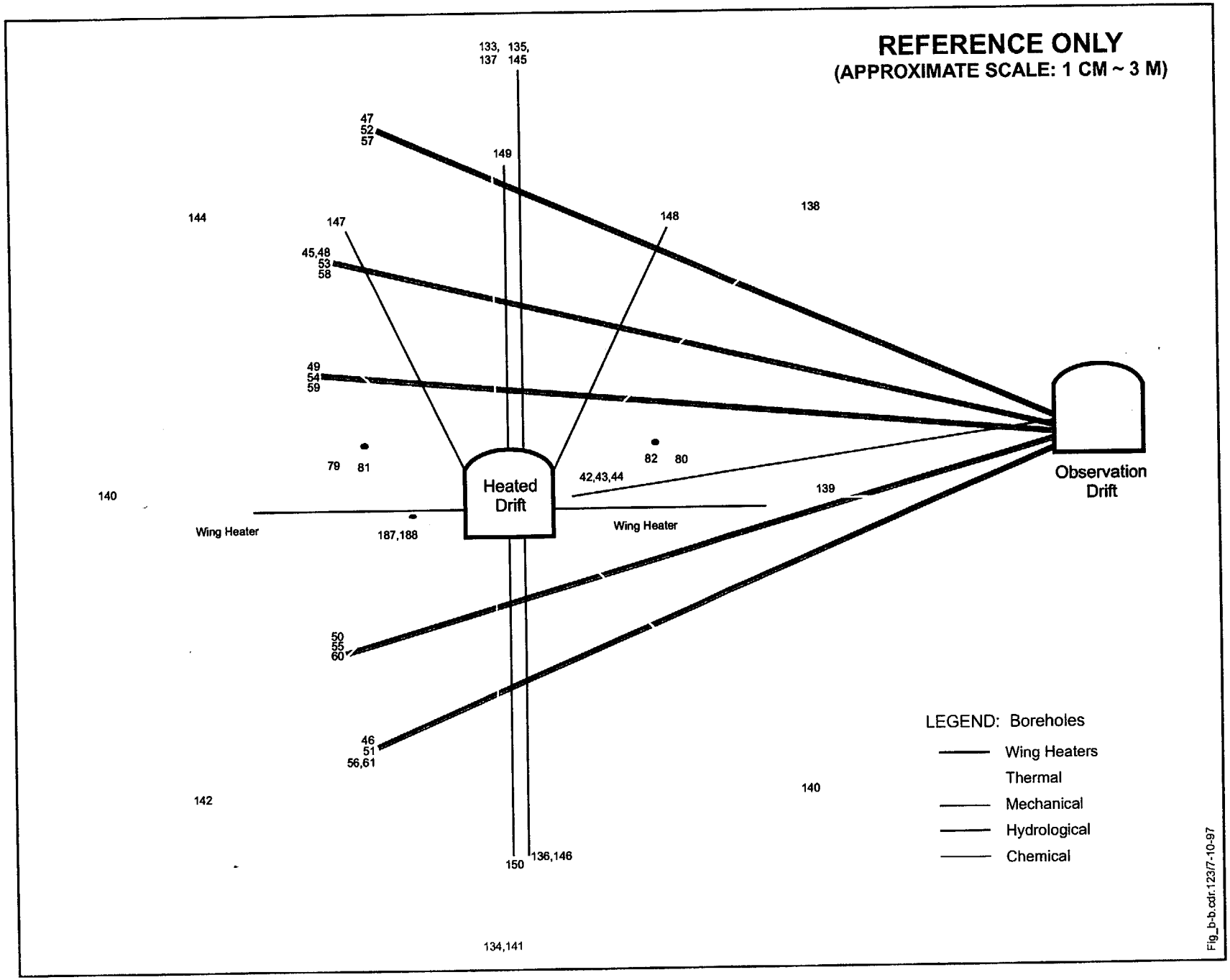

Figure 2-4. Drift Scale Test Cross Section B-B

3. LABORATORY TESTING: THERMAL PROPERTIES

3.1 OBJECTIVES AND DESCRIPTION

The objective of laboratory testing of thermal properties was two-fold:

- To characterize the thermal properties of the DST block
- To determine if significant spatial variation of these properties exists within the region.

Twenty specimens, distributed throughout part of the DST block, were measured for thermal conductivity, and 17 specimens were measured for thermal expansion. Thermal conductivity is a measure of the ability of a material to transmit heat, and so relates to the ability of the host rock to conduct heat away from the emplaced heat source. Thus, thermal conductivity is an important parameter for numerically simulating the transient temperature field from heat generated by emplaced nuclear waste. Thermal expansion is the tendency of a material to undergo a length change as a result of a change in temperature. The coefficient of thermal expansion can be defined as strain per °C.

The data in this section have been entered into automated Technical Data Tracking and were submitted to the Records Center under Document Transmittal Notice (DTN) SNL22100196001.001 and TDIF 306127. The procedures used were SNL TP-051, SNL TP-200, SNL QAIP-20-3, SNL TP-064, SNL TP-215, SNL TP-202, ASTM F433-77, and ASTM E1225-87. The work in this section was completed in satisfaction of Level 4 Milestone SP5145M4 (SNL 1997a). All data used in the preparation of this section were collected under a Sandia National Laboratories QA program and are considered qualified data.

3.2 SAMPLES

All specimens are believed to be representative of the Tptpmn lithostratigraphic unit. However, two specimens are from either the lower portion of the Tptpmn or the upper portion of the Tptpll [Tertiary-Miocene (Age), Paintbrush (Group), Topopah Spring Tuff (Formation), Crystal-Poor (Member), Lower Lithophysal (Zone)] lithostratigraphic unit: HDFR1-97.5-C (a thermal conductivity specimen) and HDFR1-97.9-B (a thermal expansion specimen). The actual lithostratigraphic location of these two specimens is not precisely known since it appears that they were taken from the gradational contact between the two units. The location of the DST block within the ESF is shown in Figure 3-1. Boreholes were drilled into the observation drift area to accommodate placement of instrumentation, and material taken from these boreholes was used to prepare specimens for both mechanical and thermal properties testing. Figure 3-2 shows the approximate locations of the boreholes used for sample acquisition. Figures 3-3 and 3-4 show enlarged views of one section of the DST block and the approximate original locations of the thermal conductivity and thermal expansion test specimens, respectively. The Multiple-Point Borehole Extensometer (MPBX) boreholes all dip approximately 10° to 11° downward so that rock from the far end of the borehole is approximately 5 m below the elevation of the borehole collar. Table 3-1 shows the full borehole designation and shows the correlation between the borehole number, given in Figures 3-2, 3-3, and 3-4 and in the text of this report.

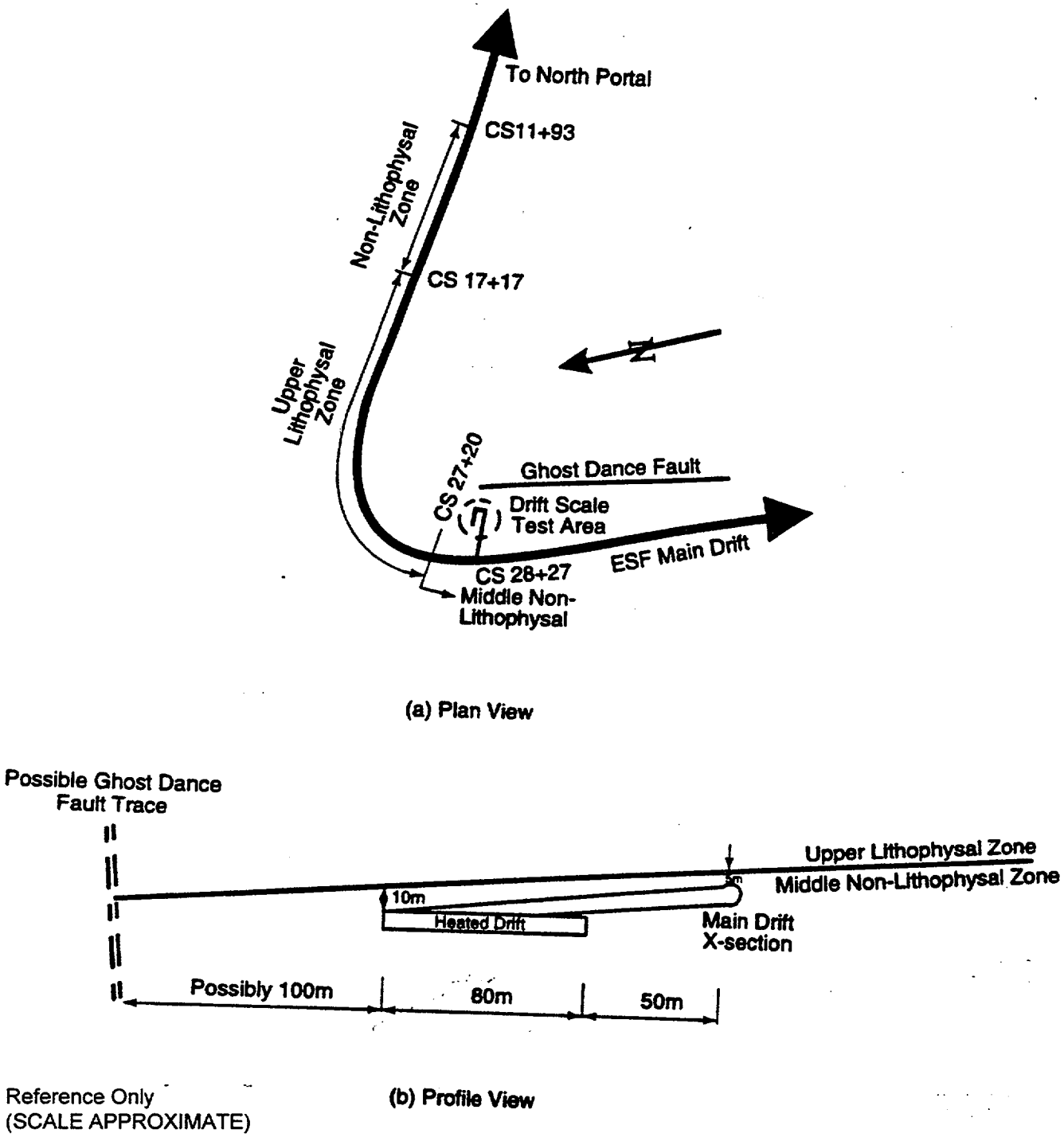

Figure 3-1. Location of Drift Scale Test Area Within the Exploratory Studies Facility

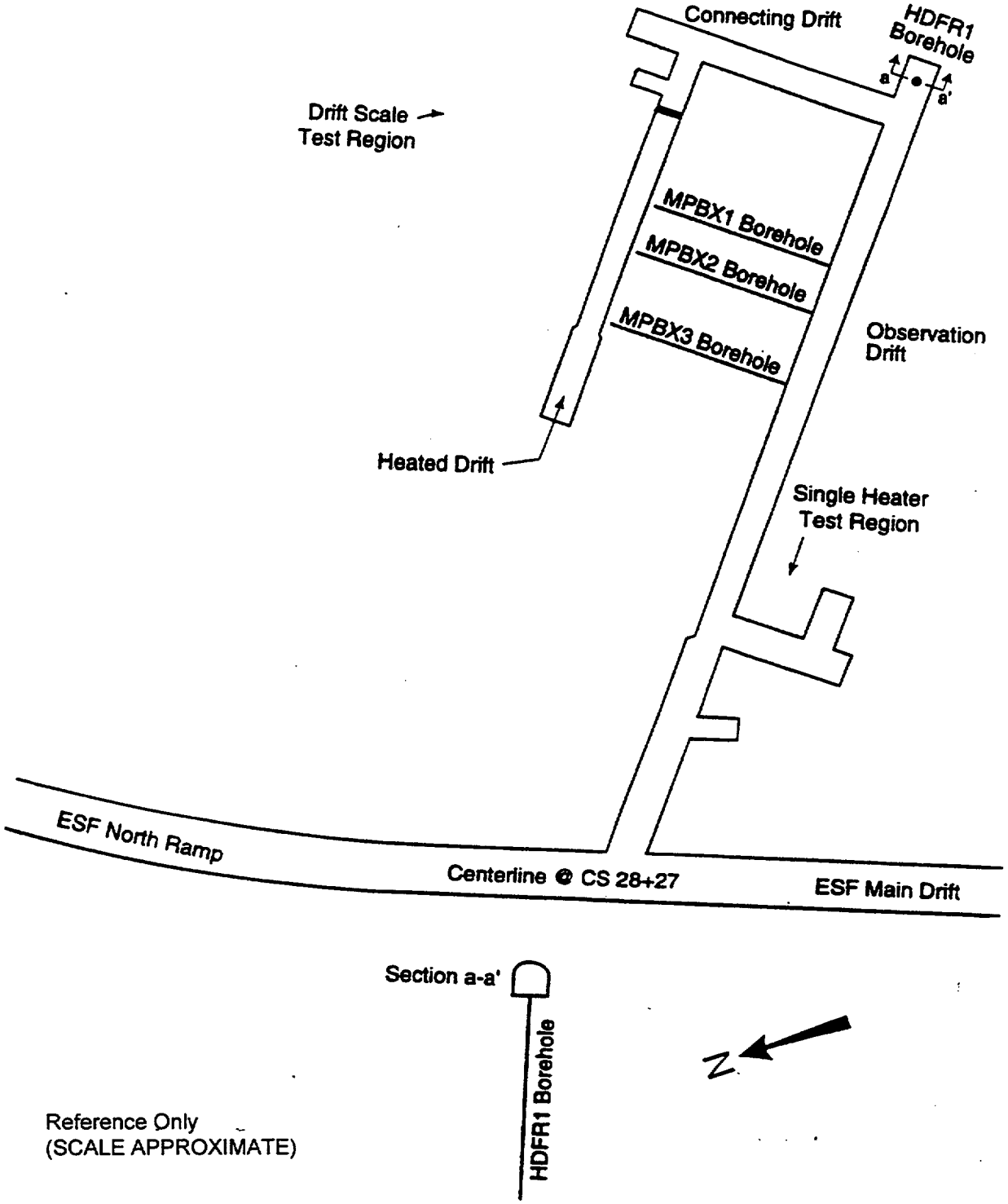

Figure 3-2. Plan View of Drift Scale Test Area

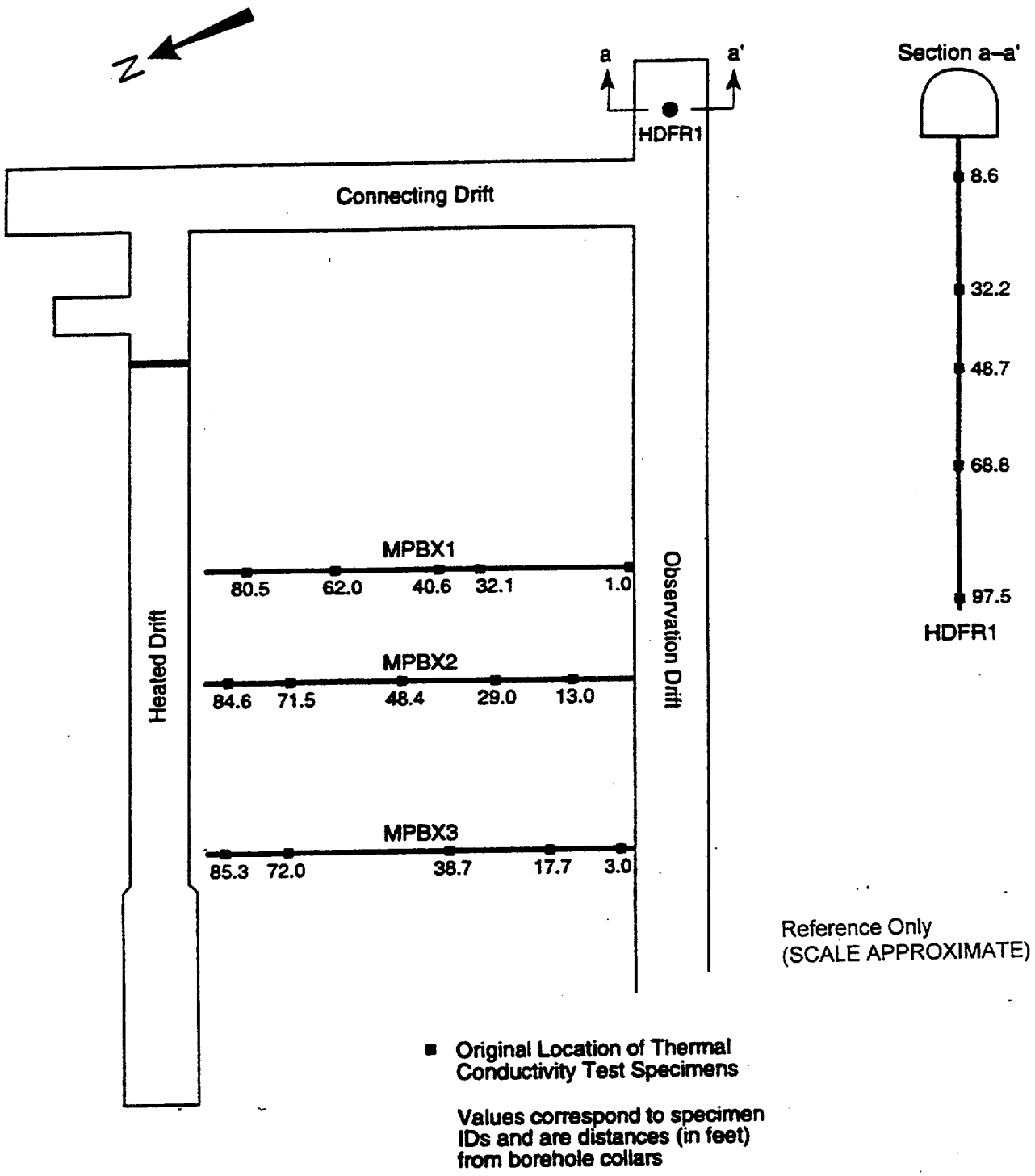

Figure 3-3. Approximate Locations of Thermal Conductivity Test Specimens

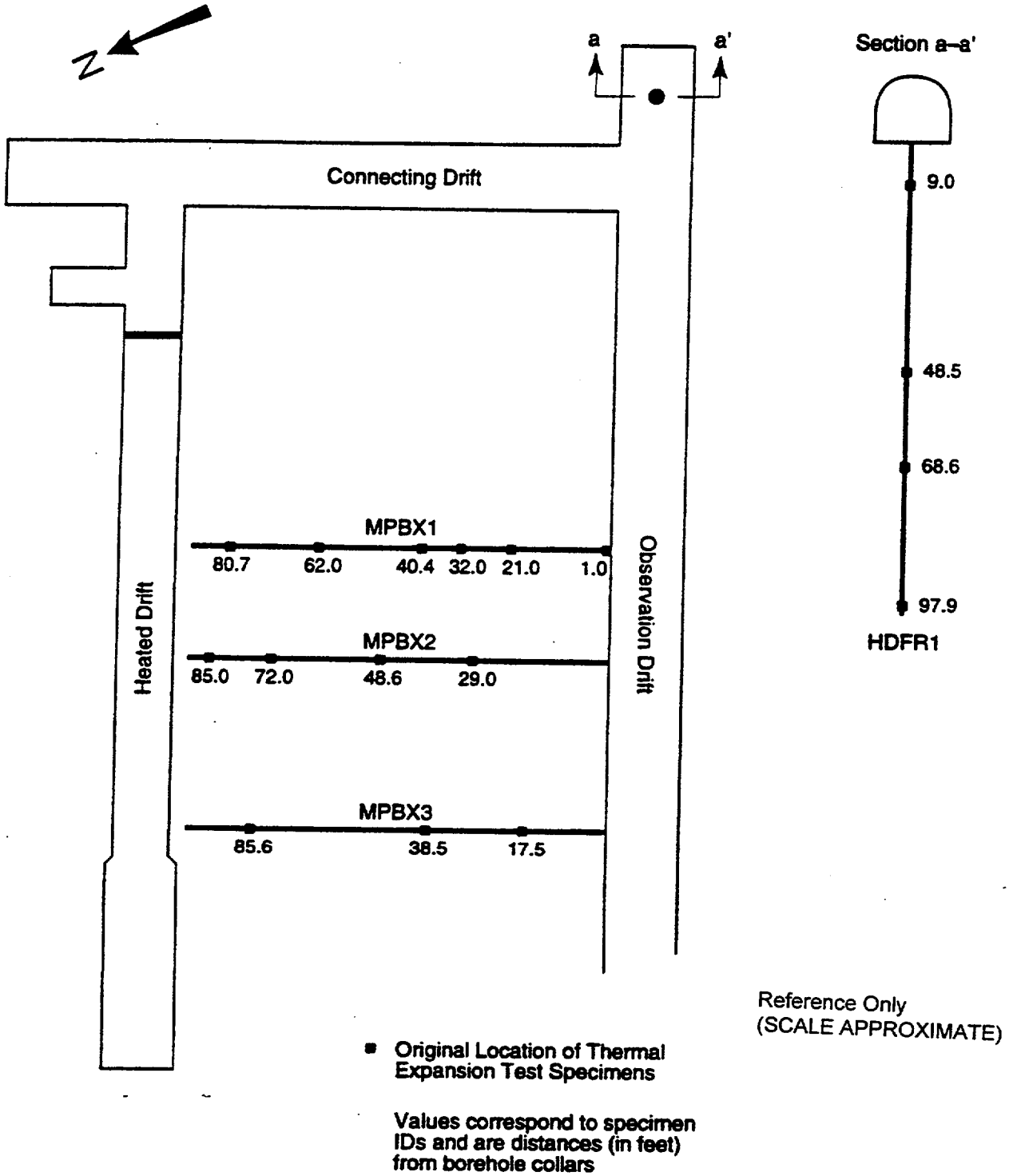

Figure 3-4. Approximate Locations of Thermal Expansion Test Specimens

Table 3-1. Borehole Nomenclature

Abbreviated Borehole Number	HDFR1	MPBX1	MPBX2	MPBX3
Borehole Designation	ESF-AOD-HDFR#1	ESF-SDM-MPBX-1	ESF-SDM-MPBX-2	ESF-SDM-MPBX-3

Thermal expansion test specimens were prepared according to Sandia National Laboratories Technical Procedure SNL TP-051, *Preparing Cylindrical Specimens Including Inspection of Dimension and Shape Tolerances.* Thermal conductivity specimens were prepared using SNL Technical Procedure TP-200, *Inspection of Samples Used in Thermal Properties Measurements.* All specimens were ground, right-circular-cylinders with nominal specimen dimensions as given in Table 3-2. The exact dimensions were checked and verified according to SNL TP-051 or SNL TP-200.

Table 3-2. Nominal Dimensions of Test Specimens

	Thermal Conductivity Test Specimens	Thermal Expansion Test Specimens
Length (mm)	12.7	50.8
Diameter (mm)	38.1	25.4

Specimens were assigned identification numbers according to Sandia National Laboratories Quality Assurance Implementation Procedure (QAIP) 20-3, *Sample Control.* The specimen identification numbers begin with the designation of the borehole, followed by the depth (distance from the collar of the borehole, in feet) of the top of the piece of core from which the specimen was prepared. If multiple test specimens were prepared from a single piece of core, then the specimens were sequentially labeled A through Z.

All thermal conductivity specimens were tested after being saturated with distilled water under a vacuum according to the procedure described in Sandia National Laboratories Technical Procedure TP-064, *Procedure for Vacuum Saturation of Geologic Core Samples.* Measurements before and after testing indicated that specimens dried out very little during testing.

All thermal expansion specimens were tested in the air-dried state, that is, in the as-received condition with no effort made to preserve or alter the moisture content. During testing the thermal expansion specimens dried out, so specimens were drier during the second cycle. Previous work has shown that for welded tuff, moisture content has no appreciable effect on thermal expansion (Brodsky, N.S.; Riggins, M.; Connolly, J.; and Ricci, P. 1997, *Thermal Expansion, Thermal Conductivity, and Heat Capacity Measurements for Boreholes UE25 NRG-4, UE25-NRG-5, USW NRG-6, and USW NRG-7/7A*, SAND95-1995, Albuquerque, New Mexico: Sandia National Laboratories. In Process.)

3.3 METHODOLOGY

3.3.1 Thermal Conductivity

The flow of heat through a material per unit time is proportional to the temperature gradient. The constant of proportionality, k, is the thermal conductivity and is a property of the material. This proportionality can be written as follows (Feynman et al. 1964):

$$\overline{h} = -k\Delta T \tag{3-1}$$

where $\overline{h}$ is a vector and represents the flow of heat across a material of cross-sectional unit area per unit time, and ΔT is the temperature gradient. For one dimensional flow this equation can be written as:

$$\frac{Q}{A} = \frac{-k\Delta T}{\Delta x} \tag{3-2}$$

where:

Q = rate of heat flow (W),
k = thermal conductivity (W/(m-K)),
ΔT = temperature difference across material (K),
Δx = thickness of material (m), and
A = cross sectional area (m^2).

Thermal conductivity measurements were made using the guarded heat flow meter (GHFM). The test specimen was placed between two heater plates controlled at different temperatures, producing heat flow through the specimen. The heat flow was measured by the heat flux transducer (HFT) between the specimen and one heater plate. Radial heat flow losses were minimized in two ways: first, a cylindrical guard heater surrounding the specimen was maintained near the mean specimen temperature, and second, specimens with lengths less than 20 mm were used.

The GHFM is calibrated by comparing theoretical values to results obtained using specimens of known thermal conductivity. A single calibration is performed to determine both the contact resistance between the specimen and heater plates and the proportionality constant relating the output of the HFT to the actual heat flux.

Calibrations were performed on reference samples of Pyrex 7740. A range of thermal resistance values was obtained using specimens of different thickness (6, 9, 12, 15, and 18 mm). Thermal resistance measurements were made at four temperatures (30, 50, 70, and 90°C) spanning the operating range. Values of ΔT and q (heat flux) were obtained from the thermocouples and the HFT, respectively. A straight line fit to Equation 3-5 was used to determine the calibration constants N and R_0. Calibrations were verified by performing measurements on reference specimens of high-purity fused quartz. Verifications were obtained using one specimen size and testing at each of the

three temperatures. Recommended thermal conductivity values for Pyrex 7740 and high-purity fused quartz are published by the National Institute of Standards and Technology (NIST). Verifications were performed periodically throughout the testing program. The thermal conductivity verification errors were 3 to 11 percent and appeared to be systematic; that is, the measured conductivities were always lower than expected for the standard material. This verification is considered acceptable because the variation is within the range specified in the procedure. The particular piece of equipment used for these measurements is identical to one used by Holometrix Inc. to obtain conductivity results for the SHT (TDIF #305593) at temperatures between 30°C and 70°C. Holometrix's test records also show conductivities that were systematically lower (5 to 8 percent) than expected for the standard, during verifications on the fused quartz standard. Although the errors reported here are sometimes larger than those obtained by Holometrix, these tests were conducted on specimens with reduced diameters inside moisture containment cells. Holometrix's SHT tests were performed on full size specimens without the moisture cells. Both the reduced size and the additional interfaces associated with the moisture containment cells add to the uncertainty of the measurement because sample size was slightly smaller than the apparatus design size and more correction is needed with the additional interfaces.

Some specimens were tested using a heat transfer compound (thermal couplant) between the specimen and endcaps to maximize reproducibility in properties across these interfaces. After the testing program was underway, it was decided to eliminate use of the thermal couplant. The errors without the couplant were 6 to 8 percent (vs. 3 to 11 percent overall), and several advantages were gained by not using the couplant. Additional discussion on this issue, including advantages and disadvantages of the couplant, are presented in the Level 4 Milestone (SNL 1997a).

Additional system components requiring calibration included thermocouples and an analog-to-digital converter. The thermocouple cold junction electronic ice reference was calibrated with a NIST-traceable, thermocouple calibrator, and the analog-to-digital converter was calibrated with a NIST-traceable precision voltage source. These calibrations were performed using SNL TP-215, *Calibration of Lawson Board Systems.*

Once the instrument was calibrated, the specimens were tested in the same manner as the reference materials. This procedure is given in SNL TP-202, *Measurement of Thermal Conductivity of Geologic Samples Using the Guarded-Heat-Flow-Meter Method,* and is summarized here. Data were obtained after the instrument had reached steady state thermal equilibrium as determined by taking readings of the thermocouples and HFT as a function of time until the readings were constant. Five readings were taken per minute and were considered to be at steady state when they were constant to within ± 0.2 percent for 10 minutes. This is within the stability criteria given in the ASTM F433, *Standard Practice for Evaluating Thermal Conductivity of Gasket Materials,* an ASTM standard based on the use of the GHFM. The measured ratio, $\Delta T/q$, was then used to determine the thermal resistance of the specimen. Thermal conductivity was calculated from R_s and specimen thickness.

The ASTM procedure that invokes the use of the GHFM is ASTM F433-77 (reapproved 1993), *Standard Practice for Evaluating Thermal Conductivity of Gasket Materials.* Although the title of this standard specifies gasket materials, the technique is applicable to solids. ASTM E1225-87, *Standard Test Method for Thermal Conductivity of Solids by Means of the Guarded Comparative-*

Longitudinal Heat Flow Technique, is based on a different experimental technique. SNL TP-202 is in full compliance with ASTM F433, and the reporting requirements of ASTM F433-77 have been addressed. In addition, those reporting requirements of ASTM E1225-87 that are not specific to test equipment or test method have also been addressed.

3.3.2 Thermal Expansion

The coefficient of linear thermal expansion, α, is the ratio of change in specimen length per degree centigrade to the length at 0°C and is given by (Weast 1974):

$$l_t = l_0(1 + \alpha T) \tag{3-3a}$$

where:

l_0 = length at 0°C, and
l_t = length at T°C.

Thermal expansion is temperature sensitive, and the more general equation is:

$$l_t = l_0(1+\alpha T+\beta T^2+\gamma T^3+...) \tag{3-3b}$$

where α, β, and γ are empirically determined constants.

All of the thermal expansion data were obtained from experiments using one of two identical push-rod dilatometer instruments manufactured by Harrop Industries. The push-rod dilatometer is one of several alternate instruments for measuring the linear coefficient of the thermal expansion of materials. The specimen is placed in a receptacle at the end of a tube made of fused silica. The tube, or specimen holder, that contains the specimen and push rod, slides into a cylindrical furnace so that the specimen is positioned near the center of the furnace. As the temperature of the specimen changes, its length changes and this motion is transmitted to the push rod. The change in length is continuously measured by a linear variable differential transformer (LVDT) which is located outside of the heated region. A type K thermocouple near the surface of the specimen monitors specimen temperature. The assembly of the specimen, specimen holder, and pushrod is inserted into the furnace.

The dilatometer system expansion was calibrated and then verified by running Standard Reference Materials (SRMs) traceable to NIST and comparing this data with the expected results. Calibration was performed using a specimen of fused silica (SRM 739), and verification was provided by measuring the expansion of SRM 731 (borosilicate glass) and SRM 738 (stainless steel). The LVDT and associated electronics were calibrated with a micrometer using an 11-point calibration. The reverification error is calculated for the dilatometer system as the difference between the expected and measured displacement versus the temperature curves. The area between the two curves is divided by the area under the expected curve and then expressed as a percentage. The system calibration was reverified twice during the testing program and also after completion of all tests. The largest reverification error was approximately 3 percent.

The thermal expansion data were corrected for system expansion using calibration data obtained as previously described. These data were then used to calculate thermal strain (ε_T) , starting at 25°C, during the heating and cooling phases as follows:

$$\varepsilon_T = \frac{L_{Tn} - L_0}{L_0} \tag{3-4}$$

where:

L_{Tn} = specimen length (m) at a particular temperature (T_n), i.e., T_n = 25°C, 50°C, 75°C,...300°C, 275°C, ...30°C, and

L_0 = specimen length (m) at the reference temperature.

The mean coefficient of thermal expansion ($\bar{\alpha}$ or MCTE) is the linear thermal expansion per unit change in temperature. It was calculated in 25°C intervals where possible, starting at 25°C during heating and cooling, that is: 25-50°C, 50-75°C, ...300-325°C, 325-300°C...50-30°C. Note that the last interval is over a smaller temperature window because the tests were terminated before complete cooling since the additional time to reach ambient conditions was not warranted. The MCTE must be accompanied by the values of the two temperatures used in the calculation. The MCTE is defined as follows:

$$\bar{\alpha} = \frac{1}{L_0}\left(\frac{L_{T2} - L_{T1}}{(T_2 - T_1)}\right) \tag{3-5a}$$

or

$$\bar{\alpha} = \frac{\Delta\varepsilon_T}{\Delta T} \tag{3-5b}$$

where:

L_{T1} = specimen length (m) at temperature T_1,

L_{T2} = specimen length (m) at temperature T_2,

L_0 = specimen length (m) at reference temperature,

$\Delta\varepsilon_T$ = change in specimen strain over temperature range T_1 -T_2, and

ΔT = T_2 - T_1 = temperature increment.

The strain-versus temperature data were fit over each temperature interval using a linear least squares regression, and the slope of the linear fit provided values of α.

The instantaneous coefficient of thermal expansion (ICTE) is calculated in a manner identical to the MCTE. The only difference is that the ICTE is calculated over a 5°C window. Values of ICTE and plots of ICTE-versus-temperature are given in Appendix A.

The ASTM procedures relevant to these tests are ASTM D 4535-85, *Standard Test Methods for Measurement of Thermal Expansion of Rock Using a Dilatometer,* and ASTM E 228-85, *Standard Test Method for Linear Thermal Expansion of Solid Materials With a Vitreous Silica Dilatometer.* ASTM D 4535 gives two test methods: one method for unconfined tests, which is very similar to that described in ASTM E 228, and one method for confined tests. The method for unconfined tests was used here. The reporting requirements for these ASTM procedures have been addressed.

The test procedure is given in the SNL TP-203, *Measurement of Thermal Expansion of Geologic Materials Using a Push Rod Dilatometer.* The test specimen was placed in the notched end of a fused silica tube and the test apparatus was set up as described. The furnace temperature was ramped up and down at a constant rate of 1 °C per minute. The rate at which the specimen temperature changed was therefore always $\leq$ 1 °C per minute. Displacement and temperature data were acquired continuously throughout the heating and cooling phases of the test and recorded by a computerized data acquisition system. Each test specimen was subjected to two complete heating cycles.

SNL TP-203 differs from ASTM E228-85, *Standard Test Method for Linear Thermal Expansion of Solid Materials with a Vitreous Silica Dilatometer,* in the following ways:

- The temperature was incremented at a constant rate (as per ASTM D4535) rather than held constant at a series of temperatures.

- If the length of a specimen changes by more than 20×10^{-6}, the ASTM standard calls for a retest or requires that the deformation be taken into account when reporting expansion values. All specimens were tested twice regardless of the permanent strain. Permanent length changes are given in Appendix A.

SNL TP-203 differs from ASTM D4535, *Standard Methods for Measurement of Thermal Expansion of Rock Using a Dilatometer,* in that the ASTM standard specifies three calibration runs, reproducible to within 5 percent, on one type of standard material. It does not call for performing verifications. Instead of the ASTM method, a single calibration on fused quartz was used to calibrate the apparatus. Verifications were then performed on two different standard materials (borosilicate glass and stainless steel). The method used here is considered an improvement over the ASTM method because the system performance is shown to be consistent over a range of thermal expansions, the system performance can be verified both before and after testing, and the verification errors were always below 5 percent.

3.4 RESULTS

3.4.1 Thermal Conductivity

Thermal conductivity values were relatively uniform throughout the sampling volume. The thermal conductivity data are summarized in Table 3-3. The mean thermal conductivities and standard deviations about the mean are given at each temperature. No temperature dependence is observed. Thermal conductivities ranged from 1.9 to 2.3 W/(m-K) with an average thermal conductivity of 2.1 ± 0.1 W/(m-K).

The distribution of thermal conductivity results obtained at 30°C is shown in Figure 3-5 to provide a visual indication of the central tendency of the data. No analysis was performed to determine the best fit distribution curve. Spatial variability of thermal conductivity is shown in Figure 3-6. This figure shows that the individual specimens with conductivities farther than one standard deviation from the mean did not cluster in particular locations. The highest thermal conductivity, 2.3 W/(m-K), was obtained for HDFR197.5-C, which is from either the lower portion of the Tptpmn or upper portion of the Tptpll unit. The mean thermal conductivity for each individual borehole was 2.1 W/(m-K). Investigations of anisotropy was considered outside the scope of this testing activity but it is scheduled to be studied. The six specimens that were tested below full saturation also had a thermal conductivity of 2.1 ± 0.1 W/(m-K).

The data obtained in this study cannot be directly compared with data obtained during characterization of the SHT area. The four SHT specimens were all tested with "as is" moisture contents rather than in the saturated state. Recent changes in testing procedure from "as is" moisture content to nearly dry or nearly saturated conditions provide for better control of test conditions and provide more representative input values for numerical simulations. Basically, saturated samples have a higher thermal conductivity than dry samples.

3.4.2 Thermal Expansion

The MCTEs are summarized in Tables 3-4 and 3-5 for heating and cooling, respectively, during the first thermal cycle. MCTEs are summarized in Tables 3-6 and 3-7 for heating and cooling, respectively, during the second thermal cycle. The mean MCTEs and standard deviations about the mean are given at each temperature for each borehole. Summary data for the entire test suite are given with standard deviations and 95 percent confidence limits at the bottom of each table. The following observations were made:

Phase Changes—The data obtained during the first heating are plotted in Figure 3-7, which shows MCTE as a function of temperature. Most thermal expansion specimens behaved similarly. However, three specimens showed behavior different from the remainder of the suite partly because of different concentrations of cristobolite and tridymite. These minerals vary substantially from their respective mean values for two of the three samples that exhibited anomalous behavior. Two of these specimens (MPBX2-85.0-B and MPBX1-40.4) appeared to initiate phase changes below 200°C, and one specimen (HDFR1-97.9-B) appeared to undergo essentially no phase change. The remaining specimens all show steep increases in MCTE beginning at approximately 200°C and

Table 3-3. Summary of Thermal Conductivity Data for Saturated Specimens from the DST Block

Distance from collar (ft)	Max. Temp. (°C)	Thermal Conductivity (W/m-K) 30°C	50°C	70°C	Mean	STD[a]	N[a]
ESF-SDM-MPBX1-C							
1.0	70	2.2	2.2	2.2	2.2	0.0	3
32.1	70	2.2	2.2	2.1	2.2	0.0	3
40.6	70	2.1	2.1	2.1	2.1	0.0	3
62.0	70	2.2	2.2	2.2	2.2	0.0	3
80.5	70	2.15	2.1	2.1	2.1	0.0	3
	N[a] =	5	5	5			
	Mean =	2.2	2.2	2.1			
	STD[a] =	0.1	0.0	0.0			
ESF-SDM-MPBX2-C							
13.0	70	2.1	2.1	2.1	2.1	0.0	3
29.0	70	2.1	2.1	2.1	2.1	0.0	3
48.4	70	2.0	2.0	2.0	2.0	0.0	3
71.5	70	2.3	2.3	2.3	2.3	0.0	3
84.6	70	2.0	2.0	2.1	2.0	0.1	3
	N[a] =	5	5	5			
	Mean =	2.1	2.1	2.1			
	STD[a] =	0.1	0.1	0.1			
ESF-SDM-MPBX3-C							
3.0	70	1.9	1.9	1.9	1.9	0.0	3
17.7	70	2.1	2.1	2.1	2.1	0.0	3
38.7	70	2.2	2.2	2.2	2.2	0.0	3
72.0	70	2.2	2.2	2.2	2.2	0.0	3
85.3	70	2.1	2.1	2.1	2.1	0.0	3
	N[a] =	5	5	5			
	Mean =	2.1	2.1	2.1			
	STD[a] =	0.1	0.1	0.1			
ESF-AOD-HDFR1-C							
8.6	70	2.0	2.0	2.0	2.0	0.0	3
32.2	70	2.1	2.1	2.1	2.1	0.0	3
48.7	70	1.9	1.9	2.0	1.9	0.0	3
68.8	70	2.1	2.1	2.0	2.1	0.0	3
97.5	70	2.3	2.3	2.3	2.3	0.0	3
	N[a] =	5	5	5			
	Mean =	2.1	2.1	2.1			
	STD[a] =	0.2	0.1	0.1			
All Drift Scale Characterization Boreholes							
	N[a] =	20	20	20			
	Mean =	2.1	2.1	2.1			
	STD[a] =	0.1	0.1	0.1			
All Specimens, All Temperatures							
	N[a] =	60					
	Mean =	2.1					
	STD[a] =	0.1					

[a]N = Number of samples; STD = Standard deviation

NOTE: Air dried. Lithostratigraphic unit: Tptpmn, except for HDFR1-97.5-C, which may be from Tptpll (see Section 3.2).

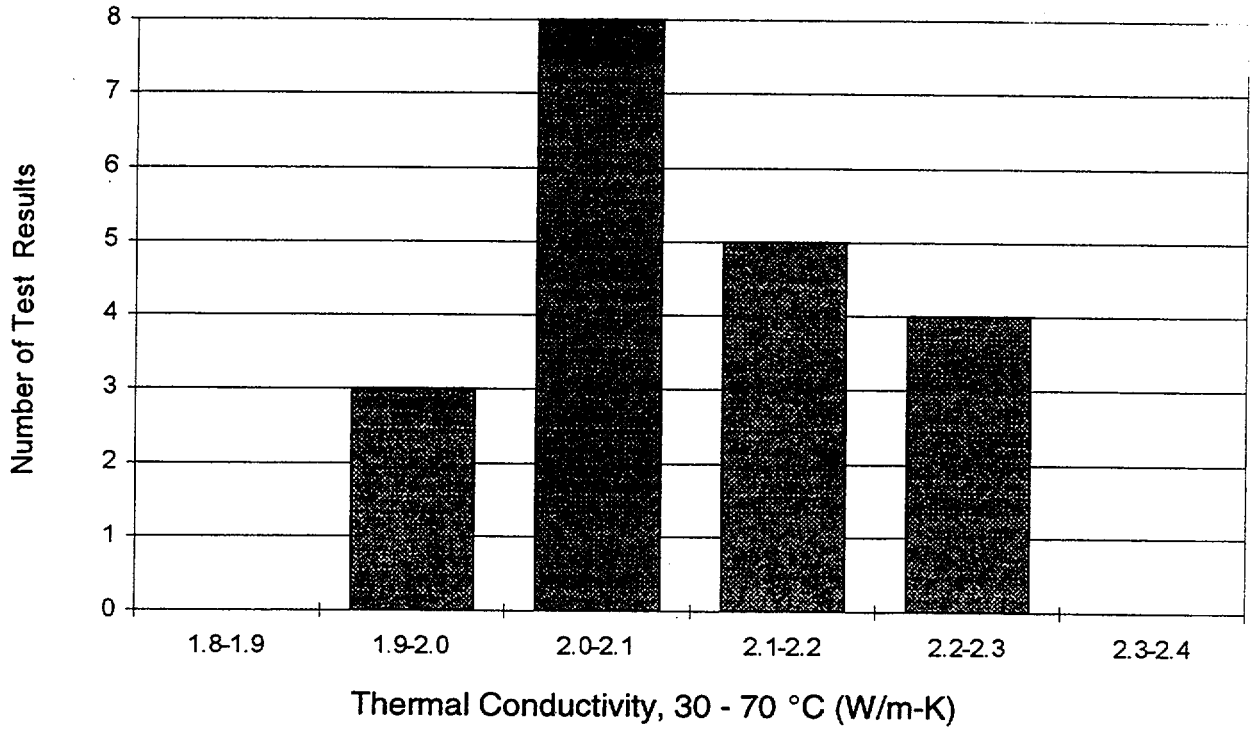

Figure 3-5. Distribution of Thermal Conductivity Values

continuing until approximately 300°C. This steep increase is attributed to phase changes in the silica mineral phases because of the presence of cristobolite and tridymite (see Table 6-1). The increase in MCTE at elevated temperatures is not attributed to thermally induced fracturing or differential expansion since these behaviors would not be significant during the second heating phase. The test data indicates sharp increases for both sets of heating/cooling cycles (see Appendix B). The decrease in MCTE at 300°C suggest that the phase changes has been completed. Also hystereses, as shown in Appendix B, are linked with phase changes. The sharp increase in MCTE at approximately 200°C is also illustrated in Figure 3-8.

Spatial Variability—Figures 3-9, 3-10, and 3-11 show the spatial distribution of MCTEs obtained at 25-50°C, 200-225°C, and 275-300°C, respectively. The spatial variations in thermal expansion properties indicate that behavior does in fact vary through the TTF. Large scale variations may indicate systematic differences between thermal expansion results obtained in this study and those obtained during SHT characterization. Small scale variations are indicated by the different behaviors of DST specimens located several meters apart. The most anomalous behavior is attributed to thermal expansion measurements of 81 and 56 (10^{-6}/°C) in the temperature range of 200-225°C (Figure 3-10). These two high values are most likely attributed to local variability rather than an overall spatial variability.

Anisotropy—All specimens from the MPBX boreholes had the same orientation. They were all subhorizontal with axes parallel to the boreholes. Specimens from HDFR1 were all vertical, but were vertically offset from the MPBX specimens, and may have slightly different lithologies. Thus, the data set is not optimal for assessing anisotropy. Within the limitations of the data set, however,

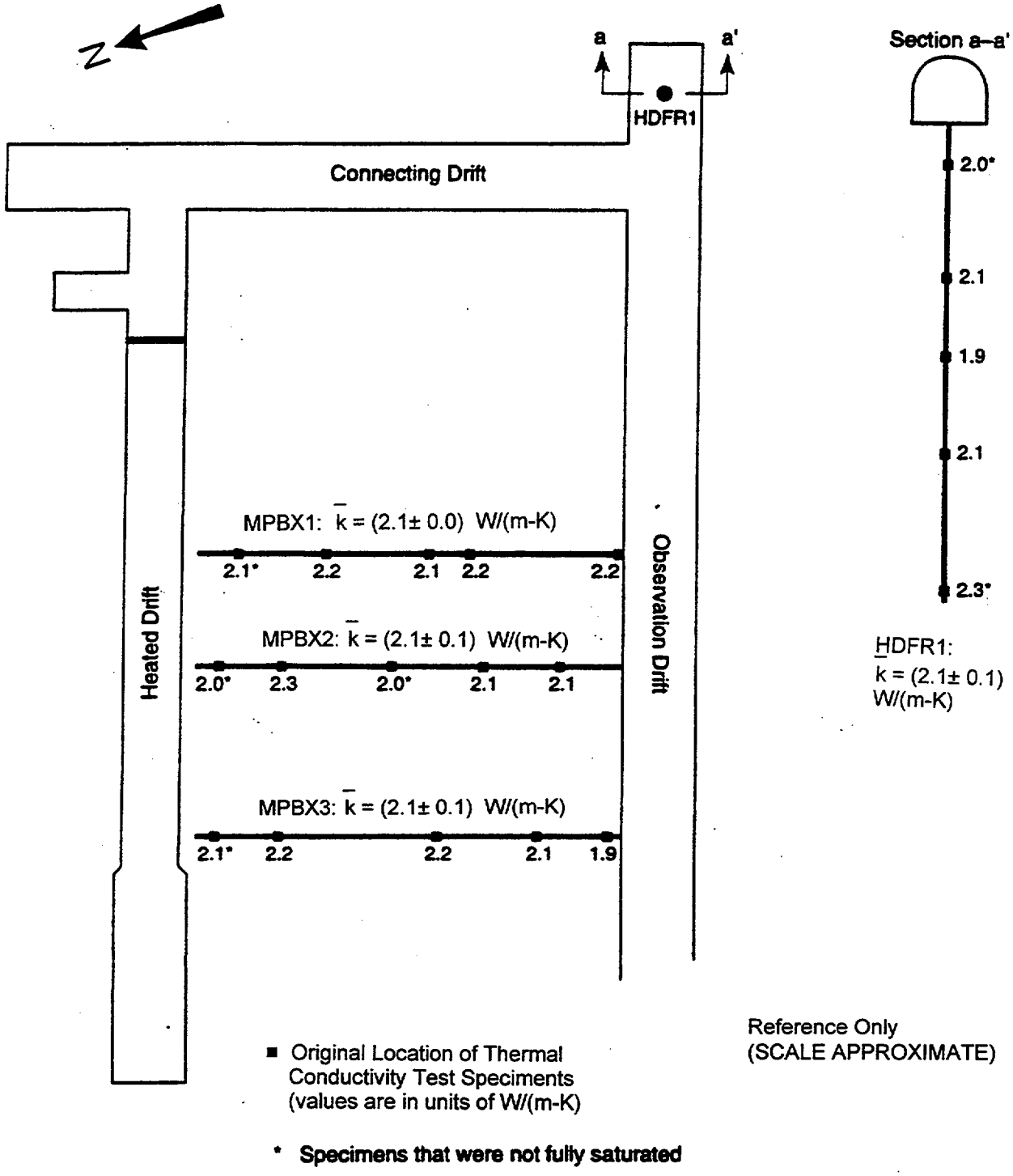

NOTE: Mean values ($\bar{k}$) and standard deviations are given for each borehole. Data are an average of all three temperature conditions.

Figure 3-6. View of DST Showing Individual Thermal Conductivities.

Table 3-4. Summary of Thermal Expansion Data for Specimens from the DST Block for the First Heating Cycle

Distance from collar (ft)	Max. Temp (°C)	MCTE on Heat-up (10^{-6}/°C)											
		25-50	50-75	75-100	100-125	125-150	150-175	175-200	200-225	225-250	250-275	275-300	300-325
ESF-SDM-MPBX-1-B													
1.0	294	5.99	8.71	9.73	10.68	11.52	12.53	13.88	17.17	19.67	32.67	59.99	-
21.0	327	7.43	9.25	9.92	10.44	11.07	11.99	12.64	14.82	19.63	30.52	57.84	64.42
32.0	326	7.88	9.49	10.42	10.93	11.54	12.47	12.91	15.25	20.44	36.22	71.46	63.09
40.4	327	7.40	9.13	10.06	10.74	11.42	14.15	29.02	80.75	78.92	42.15	46.29	47.45
62.0	326	7.68	9.15	9.73	10.06	10.62	11.60	11.94	13.52	17.70	29.01	57.27	63.98
80.7	293	6.87	9.39	10.15	10.93	11.65	12.37	13.64	16.20	21.65	38.26	66.58	-
	N[a] =	6	6	6	6	6	6	6	6	6	6	6	4
	Mean =	7.21	9.19	10.00	10.63	11.30	12.52	15.67	26.29	29.67	34.80	59.90	59.73
	STD[a] =	0.69	0.27	0.27	0.33	0.39	0.87	6.58	26.71	24.16	4.99	8.65	8.21
ESF-SDM-MPBX2-B													
29.0	325	7.84	9.06	9.69	10.11	11.05	12.50	13.30	16.04	21.77	33.93	50.98	49.55
48.6	293	6.76	8.80	9.42	10.07	10.51	11.11	12.66	17.30	28.12	42.64	57.77	-
72.0	325	7.68	9.18	9.58	10.20	9.75	11.93	12.68	14.85	19.52	32.22	46.93	39.28
85.0	325	8.11	9.57	10.57	10.12	12.30	14.17	24.58	56.34	47.64	40.73	56.99	52.31
	N[a] =	4	4	4	4	4	4	4	4	4	4	4	3
	Mean =	7.60	9.15	9.81	10.12	10.90	12.43	15.80	26.13	29.26	37.38	53.17	47.04
	STD[a] =	0.59	0.32	0.52	0.05	1.07	1.29	5.86	20.16	12.78	5.08	5.15	6.87
ESF-SDM-MPBX3-B													
17.5	293	6.70	9.11	10.16	10.60	11.27	12.10	13.78	16.20	22.95	38.27	67.89	-
38.5	327	7.60	8.94	9.77	10.20	11.00	12.16	13.66	17.33	23.14	36.40	59.65	53.30
85.6	327	7.22	8.88	9.50	9.92	10.55	11.57	12.96	18.73	33.91	35.34	54.92	62.93
	N[a] =	3	3	3	3	3	3	3	3	3	3	3	2
	Mean =	7.17	8.98	9.81	10.24	10.94	11.94	13.47	17.42	26.67	36.67	60.82	58.12
	STD[a] =	0.45	0.12	0.33	0.34	0.37	0.33	0.44	1.27	6.27	1.48	6.56	6.81
ESF-AOD-HDFR1-B													
9.0	326	7.31	9.08	9.61	10.27	10.90	11.74	12.35	13.84	17.62	26.32	49.15	64.15
48.5	326	7.99	8.93	9.67	10.10	11.05	13.28	16.92	22.22	35.73	37.16	47.52	45.58
68.6	327	7.57	8.81	9.43	9.98	10.54	11.95	13.52	17.46	24.28	30.43	52.55	56.59
97.9	326	6.69	7.43	8.07	8.34	8.79	9.79	10.09	11.19	12.11	13.68	16.36	17.05
	N[a] =	4	4	4	4	4	4	4	4	4	4	4	4
	Mean =	7.39	8.56	9.20	9.68	10.32	11.69	13.22	16.18	22.44	26.90	41.40	45.84
	STD[a] =	0.54	0.76	0.75	0.90	1.04	1.44	2.85	4.78	10.17	9.88	16.82	20.65
All Drift Scale Characterization Boreholes													
	N[a] =	17	17	17	17	17	17	17	17	17	17	17	13
	Mean =	7.34	8.99	9.73	10.22	10.91	12.20	14.74	22.31	27.34	33.88	54.13	52.28
	STD[a] =	0.57	0.47	0.54	0.58	0.79	1.04	4.79	18.09	15.70	6.94	12.18	13.42
	95% [a]	0.27	0.22	0.26	0.28	0.38	0.49	2.28	8.60	7.46	3.30	5.79	7.29

[a]N = Number of samples; STD = Standard deviation; 95% = 95 percent confidence limit.

NOTE: Air dried. Lithostratigraphic unit: Tptpmn, except for HDFR1-97.9, which may be from Tptpll (see Section 3.2).

Table 3-5. Summary of the Mean Thermal Expansion Coefficients for Specimens from DST Block for the First Cooling Cycle

Distance from collar (ft)	Max. Temp. (°C)	Mean CTE on Cool-Down (10^{-6}/°C)											
		325-300	300-275	275-250	250-225	225-200	200-175	175-150	150-125	125-100	100-75	75-50	50-30
ESF-SDM-MPBX1-													
1.0	294	-	19.12	32.86	29.46	22.32	17.74	16.15	14.11	12.64	11.77	-	-
21.0	327	17.80	30.35	43.99	40.13	27.24	20.99	15.43	13.50	12.03	11.46	10.36	10.20
32.0	326	15.95	29.45	49.79	52.55	29.79	20.24	15.89	14.03	12.67	11.68	10.77	10.31
40.4	327	13.17	20.20	25.53	27.93	29.79	47.17	34.79	21.80	14.40	11.95	14.21	10.10
62.0	326	17.73	30.23	43.48	41.91	26.49	18.74	14.75	13.21	11.91	11.11	10.50	10.03
80.7	293	-	20.56	30.61	31.10	21.94	17.13	14.27	12.63	11.48	10.57	9.84	-
	N(a) =	4	6	6	6	6	6	6	6	6	6	5	4
	Mean=	16.16	24.98	37.71	37.18	26.26	23.67	18.55	14.88	12.52	11.42	11.14	10.16
	STD(a)=	2.17	5.53	9.39	9.48	3.47	11.61	7.99	3.43	1.03	0.51	1.75	0.12
ESF-SDM-MPBX2-													
29.0	325	16.55	28.27	40.63	41.13	27.11	19.26	15.31	13.33	11.88	10.79	10.04	9.47
48.6	293	-	11.81	31.81	34.40	26.83	22.06	15.36	12.20	11.01	10.14	9.47	9.32
72.0	325	17.03	27.17	36.81	36.39	24.12	17.58	14.39	12.68	11.24	10.40	9.75	9.25
85.0	325	14.12	26.39	34.80	35.52	30.76	42.84	38.38	17.78	17.59	11.93	9.17	10.34
	N(a)=	3	4	4	4	4	4	4	4	4	4	4	4
	Mean=	15.90	23.41	36.01	36.86	27.20	25.43	20.86	14.00	12.93	10.82	9.61	9.59
	STD(a)=	1.56	7.77	3.70	2.96	2.72	11.75	11.69	2.56	3.13	0.79	0.38	0.51
ESF-SDM-MPBX3-													
17.5	293	-	21.82	34.34	34.20	25.87	19.99	15.13	13.38	12.11	11.07	10.27	9.41
38.5	327	16.08	27.42	42.00	44.91	28.98	22.20	16.25	13.57	12.07	11.13	10.23	9.58
85.6	327	16.05	26.73	38.50	39.07	29.40	32.74	17.81	14.05	12.32	11.35	10.29	10.09
	N(a)=	2	3	3	3	3	3	3	3	3	3	3	3
	Mean=	16.07	25.32	38.28	39.40	28.08	24.98	16.40	13.66	12.17	11.18	10.26	9.69
	STD(a)=	0.03	3.05	3.84	5.36	1.93	6.82	1.34	0.35	0.14	0.15	0.03	0.35
ESF-AOD-HDFR1-													
9.0	326	17.76	29.17	40.52	36.38	24.81	18.51	14.87	13.06	11.77	10.94	10.14	9.85
48.5	326	14.74	21.22	28.04	34.32	33.24	37.55	24.13	16.75	13.61	11.71	10.45	9.72
68.6	327	16.06	26.06	38.22	39.46	29.38	24.23	17.23	14.50	12.51	11.28	10.31	9.80
97.9	326	11.58	13.21	13.72	13.33	12.49	12.34	11.04	9.86	8.95	8.52	8.10	7.67
	N(a)=	4	4	4	4	4	4	4	4	4	4	4	4
	Mean=	15.03	22.42	30.13	30.87	24.98	23.16	16.82	13.54	11.71	10.61	9.75	9.26
	STD(a)=	2.61	6.95	12.21	11.88	9.01	10.75	5.50	2.89	1.99	1.43	1.11	1.06
All Drift Scale Characterization Boreholes													
	N(a) =	13	17	17	17	17	17	17	17	17	17	16	15
	Mean =	15.74	24.07	35.63	36.01	26.50	24.19	18.30	14.14	12.36	11.05	10.24	9.67
	STD(a) =	1.88	5.70	8.39	8.32	4.69	9.82	7.37	2.61	1.76	0.84	1.24	0.66
	95% (a)	1.02	2.71	3.99	3.96	2.23	4.67	3.50	1.24	0.84	0.40	0.61	0.33

(a) N = Number of samples; STD = Standard deviation

NOTE: Air dried. Lithostratigraphic Unit: Tptpmn; Thermal/mechanical Unit TSw2 (See Section 3.2).

Table 3-6. Summary of Thermal Expansion Data for Specimens from the DST Block for the Second Heating Cycle

Distance from collar (ft)	Max. Temp (°C)	MCTE on Heat-up (10^{-6}/°C)											
		25-50	50-75	75-100	100-125	125-150	150-175	175-200	200-225	225-250	250-275	275-300	300-325
ESF-SDM-MPBX-1-B													
1.0	331	5.32	8.97	10.04	10.54	11.44	12.02	13.19	15.81	19.18	25.85	39.39	47.97
21.0	327	7.67	9.01	9.88	10.46	11.19	12.28	14.32	19.02	23.99	40.69	58.17	36.66
32.0	326	7.30	9.36	10.10	10.60	11.29	12.73	13.60	16.84	24.43	50.93	64.29	32.73
40.4	328	7.00	9.04	9.77	10.83	13.59	23.69	68.42	50.62	30.28	31.03	34.14	26.00
62.0	326	7.42	8.89	9.66	10.42	10.90	12.22	13.30	16.13	22.02	38.55	56.74	35.84
80.7	326	7.44	8.90	9.73	10.43	11.86	12.18	13.41	15.86	20.29	29.84	40.94	48.06
	N[a] =	6	6	6	6	6	6	6	6	6	6	6	6
	Mean =	7.03	9.03	9.86	10.55	11.71	14.19	22.71	22.38	23.37	36.15	48.95	37.88
	STD[a] =	0.87	0.17	0.18	0.16	0.97	4.66	22.40	13.89	3.95	9.13	12.30	8.70
ESF-SDM-MPBX2-B													
29.0	326	7.70	9.35	9.87	10.69	11.69	13.38	14.87	18.80	26.97	45.52	49.43	29.37
48.6	326	7.12	8.78	9.37	9.91	10.55	11.54	12.23	19.05	23.84	36.88	47.25	47.85
72.0	326	7.00	8.76	9.48	10.11	11.09	12.30	13.69	16.74	23.22	38.64	42.24	28.17
85.0	324	9.12	10.53	10.78	11.36	12.89	16.00	45.87	41.14	35.77	46.78	42.41	27.52
	N[a] =	4	4	4	4	4	4	4	4	4	4	4	4
	Mean =	7.76	9.36	9.88	10.52	11.56	13.31	21.66	23.93	27.45	41.96	45.33	33.23
	STD[a] =	1.02	0.83	0.64	0.65	1.00	1.95	16.18	11.52	5.78	4.92	3.59	9.78
ESF-SDM-MPBX3-B													
17.5	326	6.93	8.63	9.89	10.26	10.73	11.90	13.06	16.54	21.42	31.27	50.12	53.72
38.5	326	7.47	8.67	9.58	10.19	11.19	12.59	15.21	21.02	28.15	53.43	54.98	30.09
85.6	326	7.37	8.37	9.36	10.11	10.88	12.47	16.30	29.43	27.75	42.54	54.57	33.00
	N[a] =	3	3	3	3	3	3	3	3	3	3	3	3
	Mean =	7.26	8.56	9.61	10.19	10.93	12.32	14.86	22.33	25.78	42.41	53.23	38.94
	STD[a] =	0.29	0.16	0.27	0.08	0.24	0.37	1.65	6.54	3.77	11.08	2.70	12.88
ESF-AOD-HDFR1-B													
9.0	327	6.90	8.70	9.49	9.96	10.95	12.30	13.87	18.75	23.30	38.25	55.08	35.99
48.5	326	7.25	8.63	9.38	9.98	11.70	14.61	22.65	37.53	33.41	39.67	37.89	23.61
68.6	327	7.31	8.60	9.23	9.78	10.73	12.51	14.67	20.19	25.35	39.21	52.66	34.73
97.9	326	6.35	7.57	8.10	8.42	9.04	9.96	10.65	11.71	12.49	14.14	14.99	14.41
	N[a] =	4	4	4	4	4	4	4	4	4	4	4	4
	Mean =	6.95	8.37	9.05	9.54	10.61	12.34	15.46	22.04	23.64	32.82	40.16	27.19
	STD[a] =	0.44	0.54	0.64	0.75	1.12	1.90	5.10	10.97	8.61	12.47	18.42	10.17
All Drift Scale Characterization Boreholes													
	N[a] =	17	17	17	17	17	17	17	17	17	17	17	17
	Mean =	7.22	8.87	9.63	10.24	11.28	13.22	19.37	22.66	24.82	37.84	46.78	34.46
	STD[a] =	0.76	0.59	0.54	0.61	0.98	2.98	14.97	10.66	5.47	9.52	11.63	10.17
	95% [a]	0.36	0.28	0.26	0.29	0.46	1.42	7.12	5.07	2.60	4.52	5.53	4.84

[a]N = Number of samples; STD = Standard deviation; 95% = 95 percent confidence limit.

NOTE: Air dried. Lithostratigraphic unit: Tptpmn, except for HDFR1-97.9, which may be from Tptpll (see Section 3.2).

Table 3-7. Summary of Thermal Expansion Data for Specimens from the DST Area for the Second Cooling Cycle

Distance from collar (ft)	Max. Temp (°C)	MCTE on Cool-down (10^{-6}/°C)											
		325-300	300-275	275-250	250-225	225-200	200-175	175-150	150-125	125-100	100-75	75-50	50-30
ESF-SDM-MPBX-1-B													
1.0	331	16.31	28.67	36.82	33.75	24.43	19.07	15.58	13.74	12.30	11.21	10.63	10.31
21.0	327	18.86	30.47	44.14	39.09	27.06	21.42	15.36	13.36	11.88	11.10	10.53	9.78
32.0	326	17.65	29.92	48.39	48.98	27.09	18.16	14.64	13.28	12.06	11.14	10.39	9.71
40.4	328	14.13	20.40	24.67	26.99	28.71	45.77	29.89	18.99	13.87	12.18	10.41	10.94
62.0	326	18.83	30.08	42.50	38.88	25.10	18.28	14.49	13.00	11.65	11.00	10.20	9.88
80.7	326	18.32	30.36	38.95	33.64	23.50	18.05	14.67	12.87	11.78	11.09	10.38	9.66
	N[a] =	6	6	6	6	6	6	6	6	6	6	6	6
	Mean =	17.35	28.32	39.24	36.89	25.98	23.46	17.44	14.21	12.26	11.29	10.42	10.05
	STD[a] =	1.84	3.93	8.20	7.39	1.96	11.00	6.12	2.36	0.82	0.44	0.15	0.49
ESF-SDM-MPBX2-B													
29.0	326	17.50	29.50	40.91	40.88	28.23	20.16	15.70	13.49	12.03	10.89	10.24	9.82
48.6	326	17.88	28.81	40.39	37.67	26.16	19.22	15.03	12.96	11.69	10.92	10.16	9.74
72.0	326	16.82	26.36	36.00	36.06	24.13	17.74	14.35	12.15	10.81	10.44	9.72	8.86
85.0	324	13.21	21.45	30.44	35.20	30.86	42.65	35.27	17.52	14.27	12.53	11.13	10.83
	N[a] =	4	4	4	4	4	4	4	4	4	4	4	4
	Mean =	16.35	26.53	36.94	37.45	27.35	24.94	20.29	14.03	12.20	11.19	10.31	9.81
	STD[a] =	2.14	3.64	4.86	2.51	2.88	11.85	10.14	2.39	1.47	0.92	0.59	0.81
ESF-SDM-MPBX3-B													
17.5	326	17.93	30.83	42.98	37.87	25.63	18.03	14.51	12.43	11.26	10.65	10.20	10.20
38.5	326	16.49	26.55	42.70	49.10	30.83	22.20	15.93	13.13	12.07	17.67	10.36	9.93
85.6	326	16.96	27.38	39.36	39.21	27.30	24.61	16.34	13.48	11.98	10.71	10.04	9.69
	N[a] =	3	3	3	3	3	3	3	3	3	3	3	3
	Mean =	17.13	28.25	41.68	42.06	27.92	21.62	15.60	13.01	11.77	13.01	10.20	9.94
	STD[a] =	0.73	2.27	2.01	6.13	2.65	3.33	0.96	0.54	0.45	4.04	0.16	0.25
ESF-AOD-HDFR1-B													
9.0	327	17.46	28.08	39.60	37.86	25.67	22.04	15.81	13.54	11.79	10.93	10.19	10.11
48.5	326	13.80	20.23	29.64	33.17	34.30	38.82	22.03	16.01	13.51	11.33	10.22	9.81
68.6	327	17.60	28.09	39.17	36.88	27.95	23.51	16.51	13.96	12.17	10.89	10.03	9.65
97.9	326	10.78	13.02	13.39	13.46	12.59	12.14	10.77	9.86	9.00	8.41	7.92	7.83
	N[a] =	4	4	4	4	4	4	4	4	4	4	4	4
	Mean =	14.91	22.36	30.45	30.34	25.13	24.13	16.28	13.34	11.62	10.39	9.59	9.35
	STD[a] =	3.27	7.24	12.27	11.44	9.12	11.02	4.61	2.56	1.89	1.33	1.12	1.03
All Drift Scale Characterization Boreholes													
	N[a] =	17	17	17	17	17	17	17	17	17	17	17	17
	Mean =	16.50	26.48	37.06	36.39	26.44	23.64	17.46	13.75	12.01	11.36	10.16	9.81
	STD[a] =	2.23	4.89	8.42	7.94	4.51	9.46	6.15	2.08	1.18	1.83	0.65	0.70
	95% [a]	1.06	2.32	4.00	3.77	2.14	4.50	2.92	0.99	0.56	0.87	0.31	0.33

[a]N = Number of samples; STD = Standard deviation; 95% = 95 percent confidence limit.

NOTE: Air dried. Lithostratigraphic unit: Tptpmn, except for HDFR1-97.9, which may be from Tptpll (see Section 3.2).

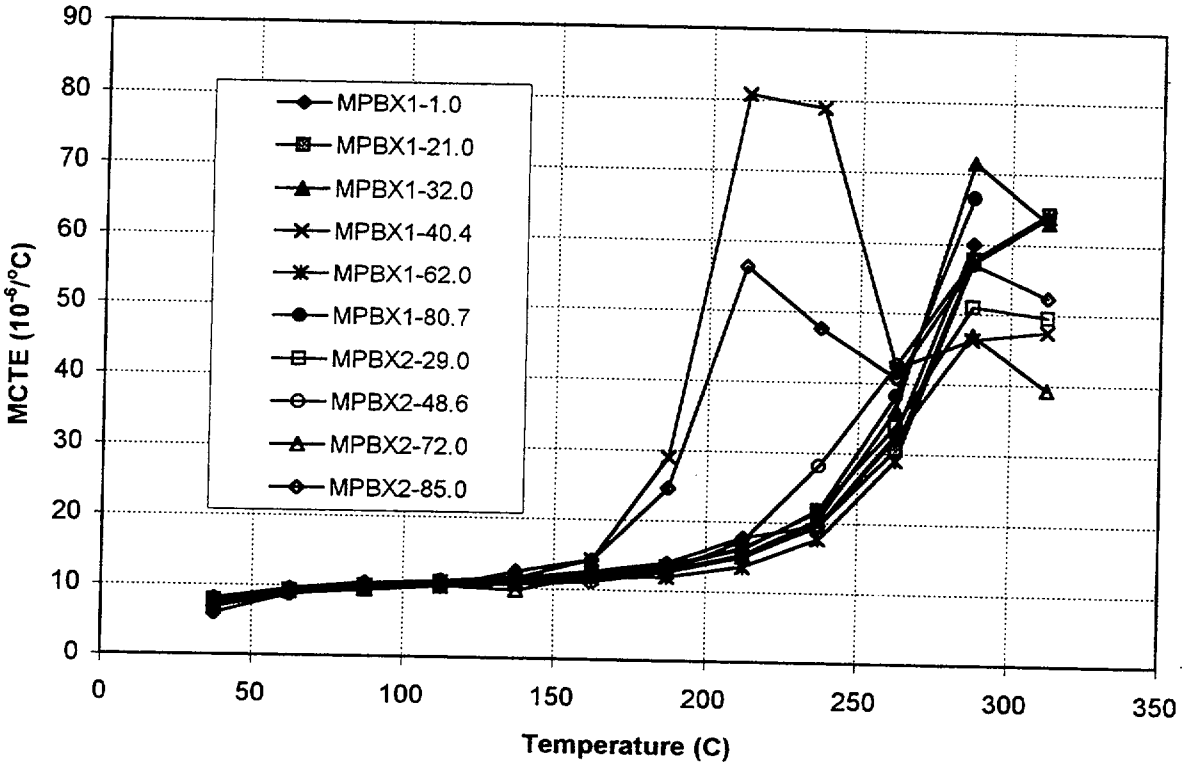

(a)

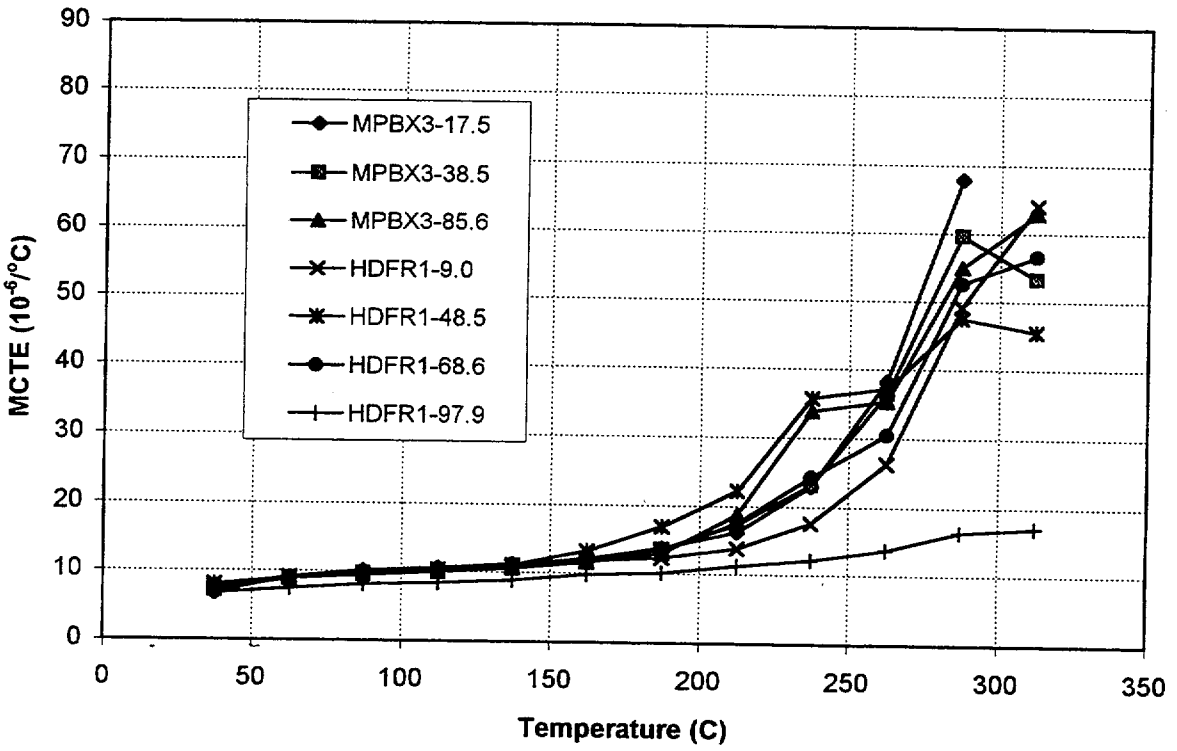

(b)

Figure 3-7. Mean Coefficients of Thermal Expansion-Versus-Temperature During the First Heating Cycle

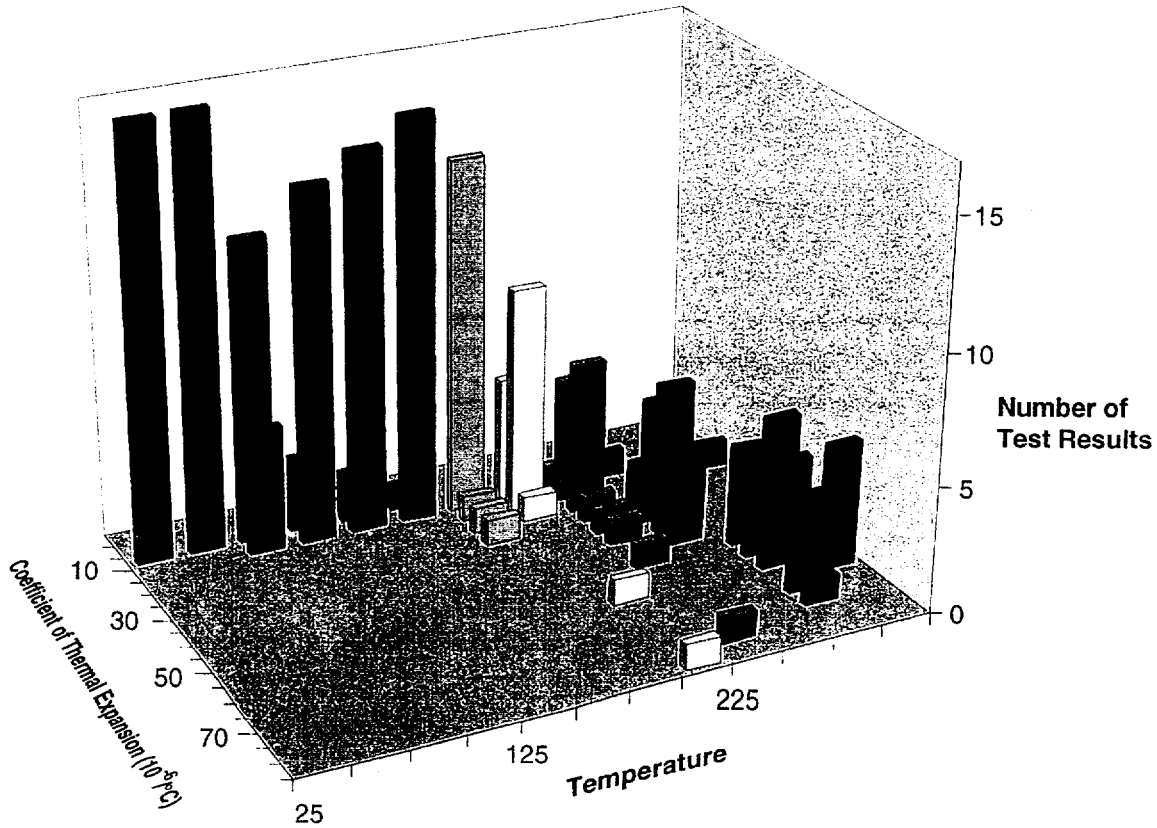

Figure 3-8. Distribution of Mean Coefficients of Thermal Expansion During First Heating Cycle for 17 Test Specimens

there is a suggestion that lower coefficients of thermal expansion may be obtained on vertically, rather than horizontally oriented specimens.

Comparison of First and Second Thermal Cycles—Appendix B provides a comparison of data obtained during the two heating cycles for each test. Each specimen is represented by two plots. The first plot shows strain-versus-temperature where the strain measured during the second cycle is offset by the permanent strain that accumulated during the first cycle. The second plot shows MCTE-versus temperature for the two cycles. For specimens cycled consistently to the same maximum temperature, the following observation can be made. With the exception of the development of permanent strains during the first cycle, the data are generally reproducible from cycle to cycle. The MCTE-versus-temperature curves and strain-versus-temperature curves obtained during cooling almost overlay one another for many specimens.

Central Tendency—The central tendency of the data set is indicated in Figures 3-7 and 3-8. Although at some temperatures, notably 200-225°C and 275-300°C, the data are not symmetric around the mean values but are skewed, for other temperatures a normal distribution may be appropriate.

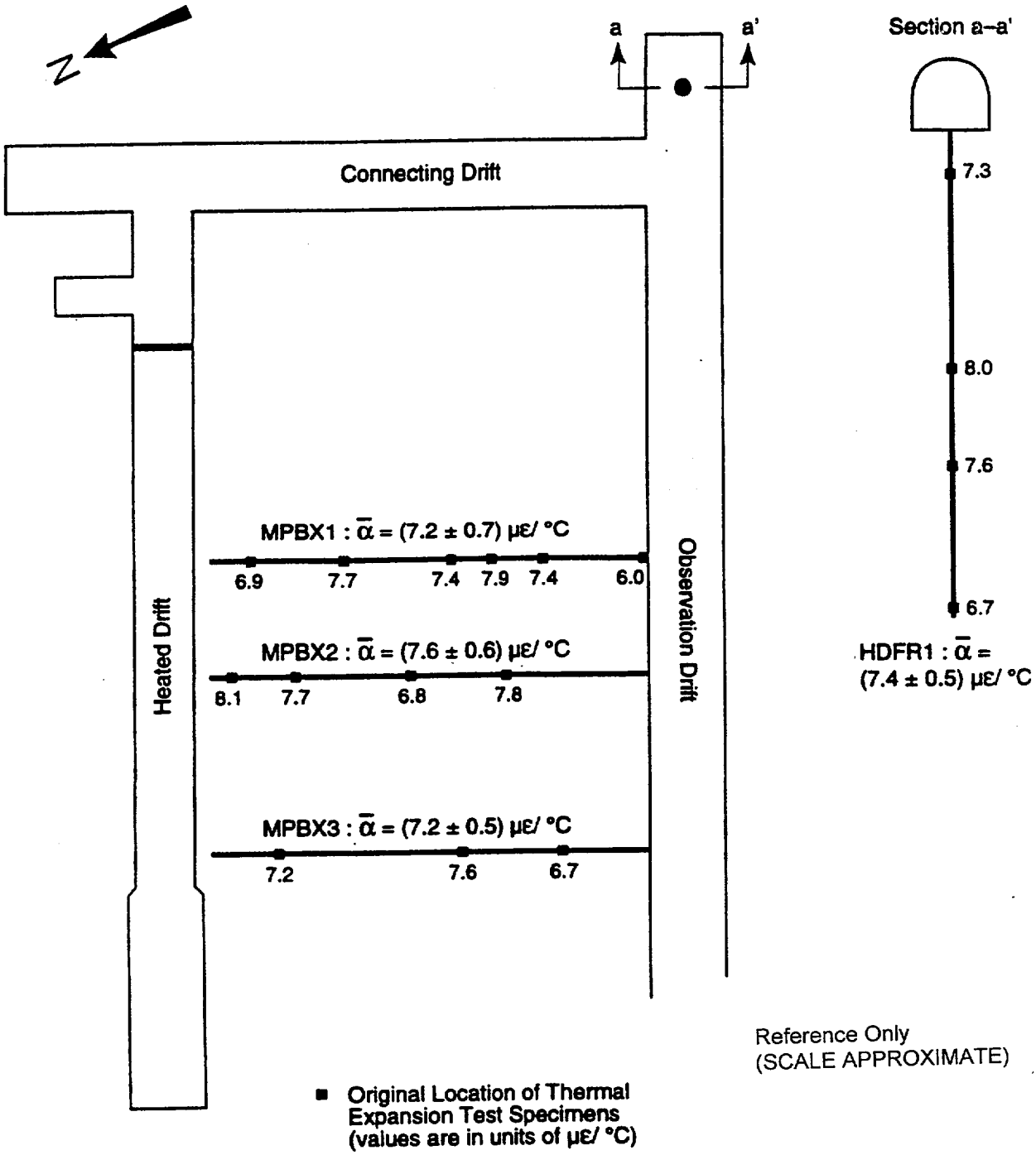

NOTE: Mean values ($\bar{\alpha}$) and standard deviations are given for each borehole.

Figure 3-9. View of the DST Showing Individual Mean Coefficients of Thermal Expansion Calculated Over 25-50°C During the First Heating Cycle

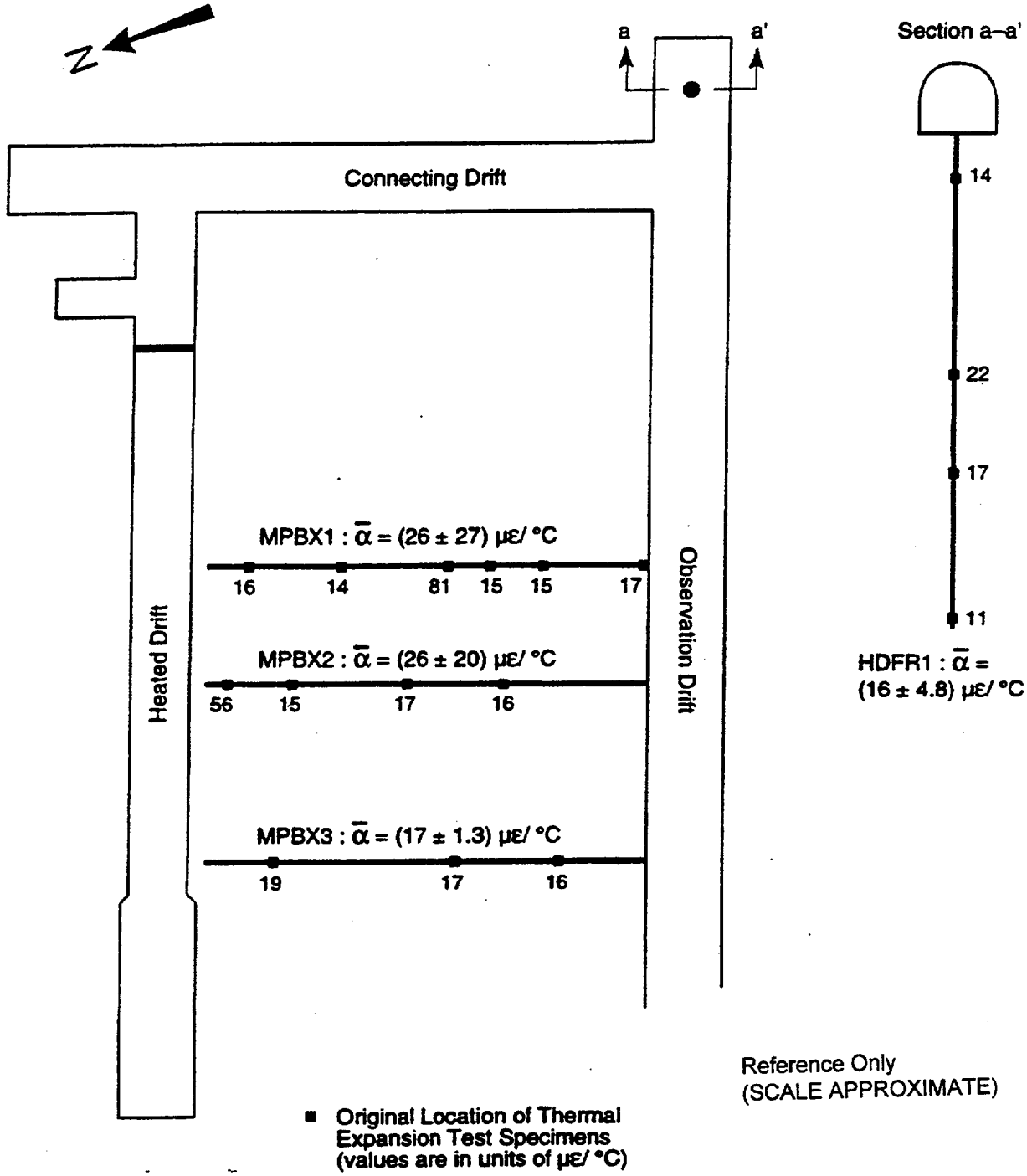

NOTE: Mean values ($\bar{\alpha}$) and standard deviations are given for each borehole.

Figure 3-10. View of the DST Showing Individual Mean Coefficients of Thermal Expansion Calculated Over 200-225°C During the First Heating Cycle

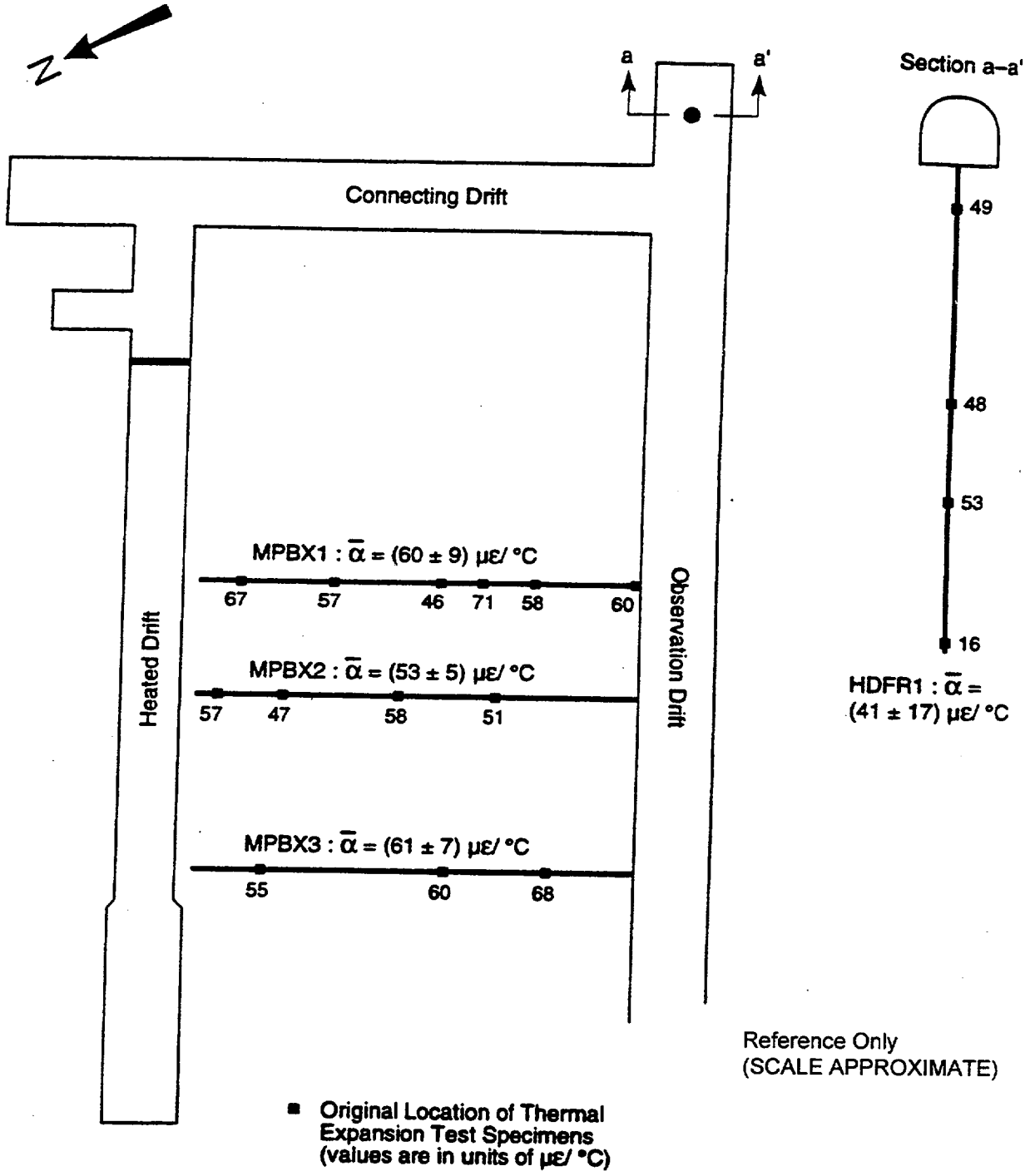

NOTE: Mean values ($\bar{\alpha}$) and standard deviations are given for each borehole.

Figure 3-11. View of the DST Showing Individual Mean Coefficients of Thermal Expansion Calculated Over 275-300°C During the First Heating Cycle

Comparison of DST and SHT Data—Thermal expansion data obtained in this study are compared with values obtained during characterization of the SHT (TDIF #305593) area in Figures 3-12, 3-13, 3-14, and 3-15. The SHT data were generated by Holometrix, Inc., instead of Sandia National Laboratories, but exactly the same equipment was used for both test suites. The results obtained using different data reduction codes compared very favorably. Mean values of MCTE (averaged over all specimens tested) are plotted versus temperature in Figures 3-12 and 3-13 for heating and cooling, respectively. The error bars represent one standard deviation. The DST and SHT data for a given temperature interval are plotted slightly offset from one another on the temperature axis so that the error bars can be viewed easily. There is more variability in the DST data than the SHT data, although the DST study included a much large sampling volume. During heating DST mean values are consistently higher than those for the SHT, and are generally higher during cooling. However, with only one exception, (which occurred at the lowest temperature during cooling) the mean SHT values are within one standard deviation of the mean DST values. A more definitive, statistical evaluation of the agreement between DST and SHT data is being planned to determine if the differences are significant.

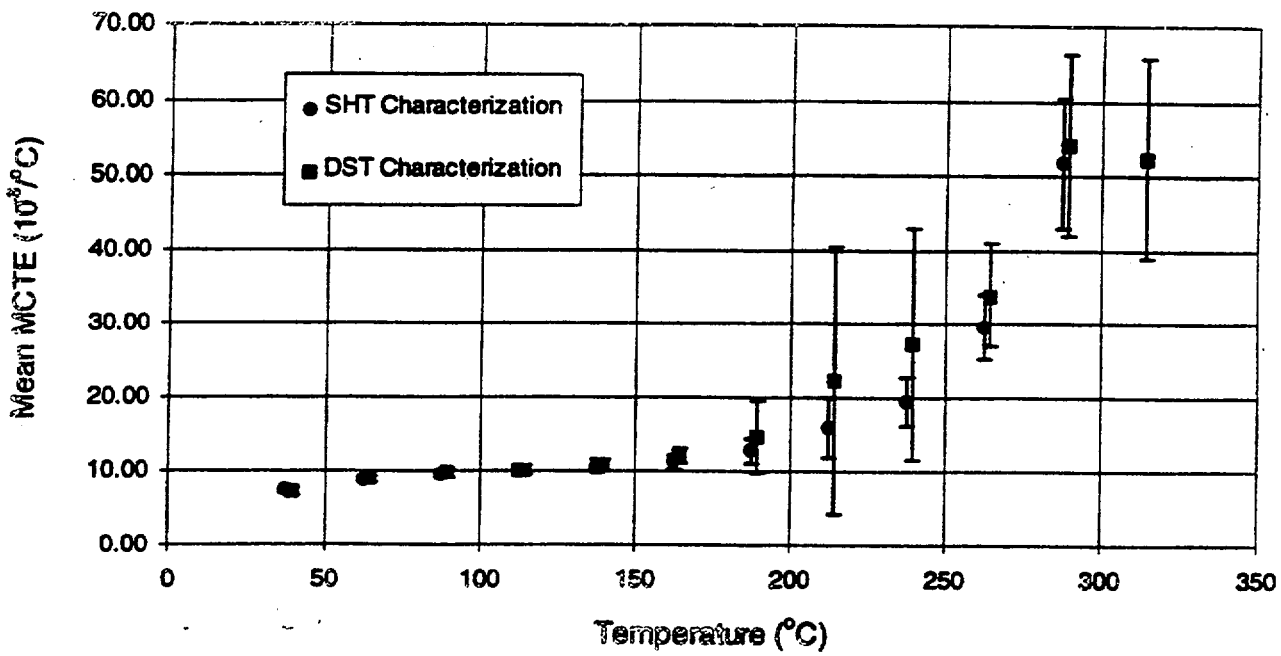

NOTE: Error bars represent ± one standard deviation. Mean MCTEs for the DST data are each plotted 2°C above the mean temperature to offset the two data sets.

Figure 3-12. Mean MCTEs and Standard Deviations Obtained During the First Heating Cycle for 17 DST Specimens and Nine SHT Specimens

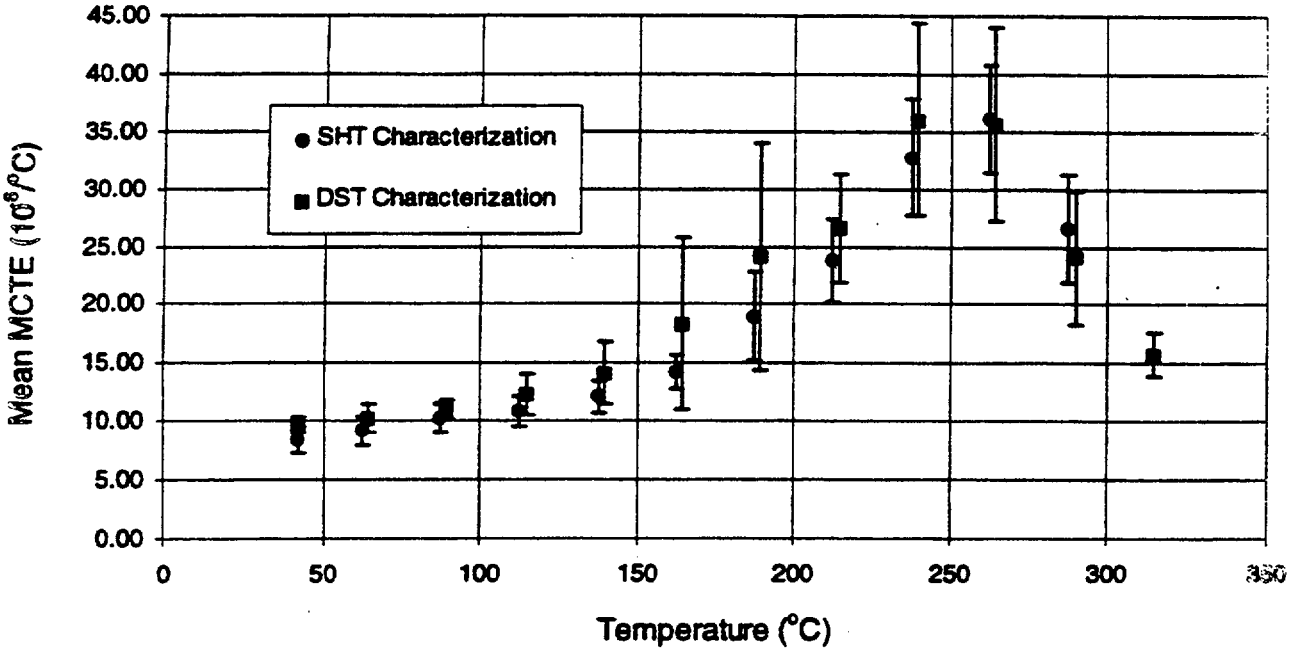

NOTE: Error bars represent ± one standard deviation. Mean MCTEs for the DST data are each plotted 2°C above the mean temperature to offset the two data sets.

Figure 3-13. Mean MCTEs and Standard Deviations Obtained During the First Cooling Cycle for 17 DST Specimens and Nine SHT Specimens

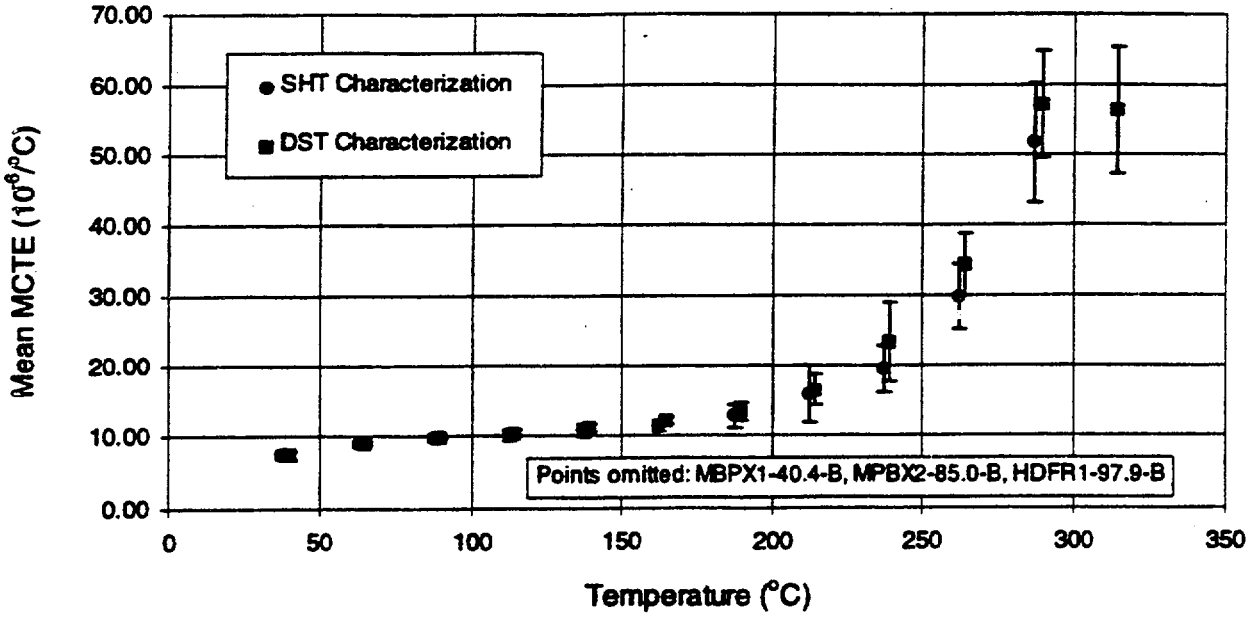

NOTE: Error bars represent ± one standard deviation. Mean MCTEs for the DST data are each plotted 2°C above the mean temperature to offset the two data sets. Three DST specimens that behaved as outliers (MPBX-30.4-B, MPBX2-85.0B, and HDFR1-97.9-B) were eliminated from the calculations.

Figure 3-14. Mean MCTEs and Standard Deviations Obtained During the First Heating Cycle for 14 DST Specimens and Nine SHT Specimens

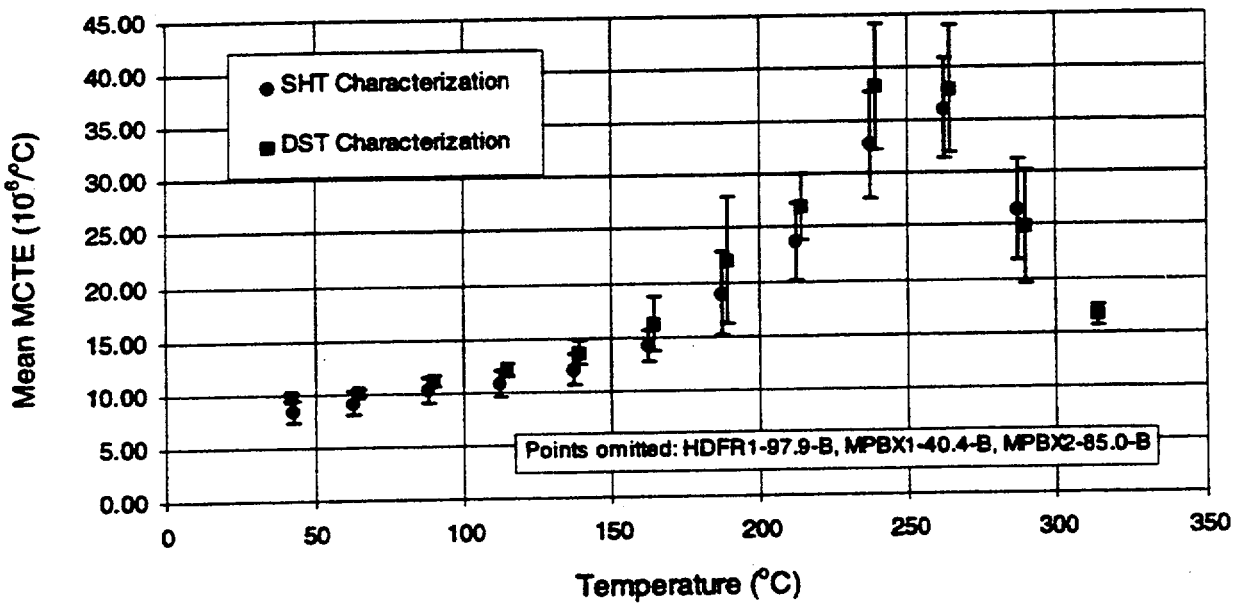

NOTE: Error bars represent ± one standard deviation. Mean MCTEs for the DST data are each plotted 2°C above the mean temperature to offset the two data sets. (Three DST specimens that behaved as outliers (MPBX1-40.4-B, MPBX2-85.0B, and HDFR1-97.9B) were eliminated from the calculations.

Figure 3-15. Mean MCTEs and Standard Deviations Obtained During the First Cooling Cycle for 17 DST Specimens and Nine SHT Specimens

INTENTIONALLY LEFT BLANK

4. LABORATORY TESTING: MECHANICAL PROPERTIES

4.1 OBJECTIVES AND DESCRIPTION

The objective of laboratory testing of mechanical properties was to characterize the intact rock properties in the DST block, including elastic constants and strength parameters, and their spatial distribution and variability. These data are necessary as input to the numerical models used to predict the mechanical response of the local rock mass surrounding the repository.

Unconfined compression tests were performed on sixteen tuff specimens from the Tptpmn lithostratigraphic unit. These laboratory-determined properties of intact rock samples represent upper limit values of the strength and deformability of the in situ rock mass, since rock mass factors such as discontinuities and other defects are not reflected in the intact rock. The reduction of strength and stiffness typically observed in the field is a function of the frequency and nature of existing discontinuities. Testing of intact rock is standard practice for characterizing rock behavior because it provides for more control of specimen and boundary conditions. Laboratory testing compliments field testing of similar rock properties needed to characterize a specific rock block or mass. Discontinuity characteristics in the DST block are discussed in Sections 7 and 8 of this report.

The data in this section have been entered into automated Technical Data Tracking and were submitted to the Records Center under DTN SNL02100196001.001 and TDIF 306126. The procedures used were SNL TP-051, SNL TP-257, and SNL TP-219. The work in this section was completed in partial satisfaction of Level 4 Milestone SP5145M4 (SNL 1997c). The data in this section are considered qualified data.

4.2 SAMPLES

Boreholes were drilled into the observation drift area to accommodate placement of instrumentation, and cores taken from these boreholes were used to prepare specimens for both mechanical and thermal property measurements. Figure 4-1 shows the approximate locations of the four boreholes used for sample acquisition, and Figure 4-2 shows an enlarged view of one section of the DST block with the approximate original locations of the mechanical test specimens. Table 3-1 shows the correlation between borehole number, shown in Figures 4-1 and 4-2, the text of this report, and the full borehole designation.

Test specimens were prepared according to Sandia National Laboratories (SNL) Technical Procedure SNL TP-051, *Preparing Cylindrical Specimens, Including Inspection of Dimension and Shape Tolerances.* All specimens were ground, right-circular-cylinders with nominal specimen dimensions of 38.1 mm in diameter and 76.2 mm in length. Because the raw core was less than 50 mm in diameter, the specimens for this study were slightly smaller than those used in previous studies from the North Ramp geologic and systematic drilling boreholes. This size variation is considered important because of the inverse relationship between sample size and rock strength. All specimens tested were from the Tptpmn lithostratigraphic unit.

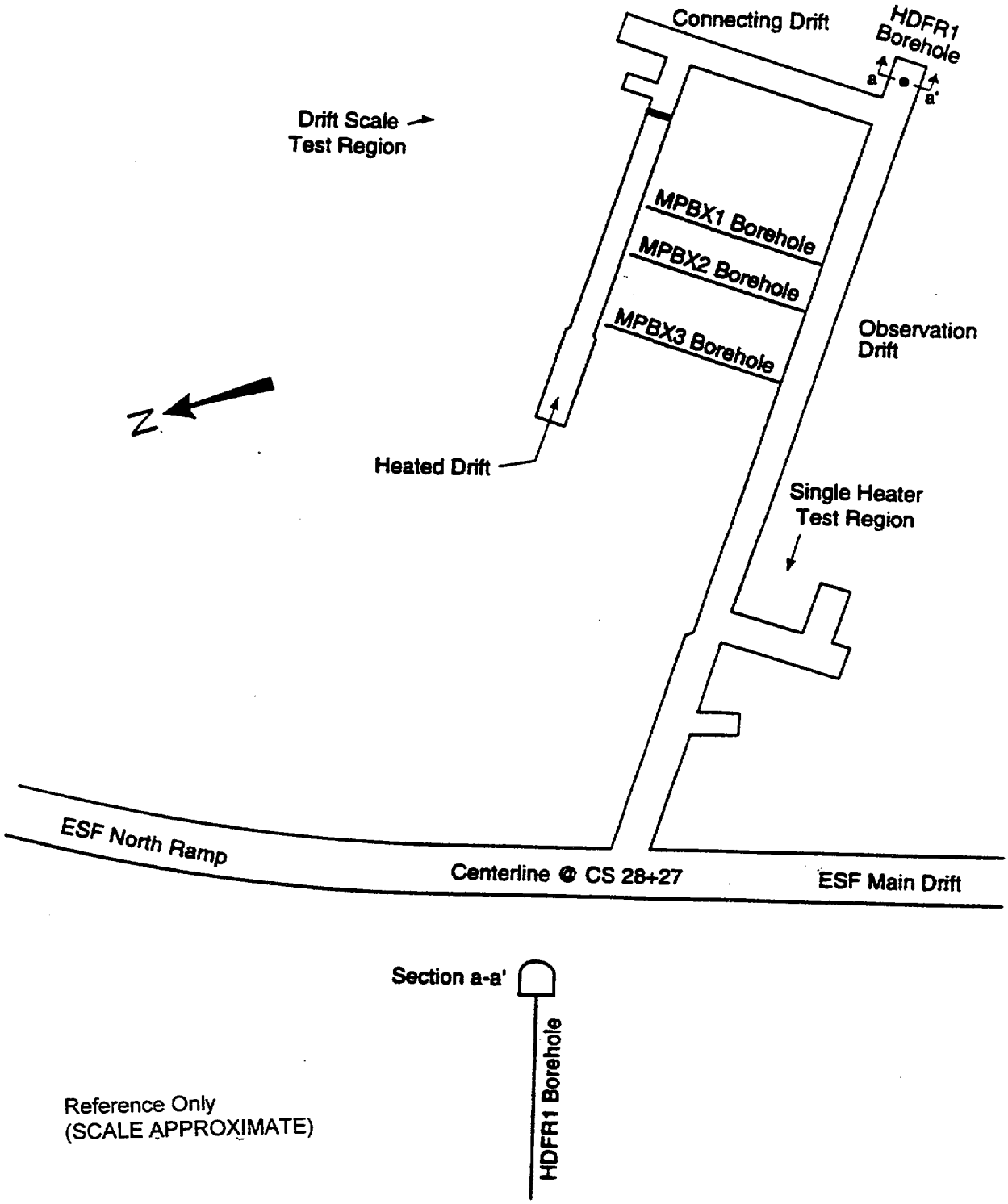

Figure 4-1. Locations of Instrumentation Boreholes Used for Sample Collection

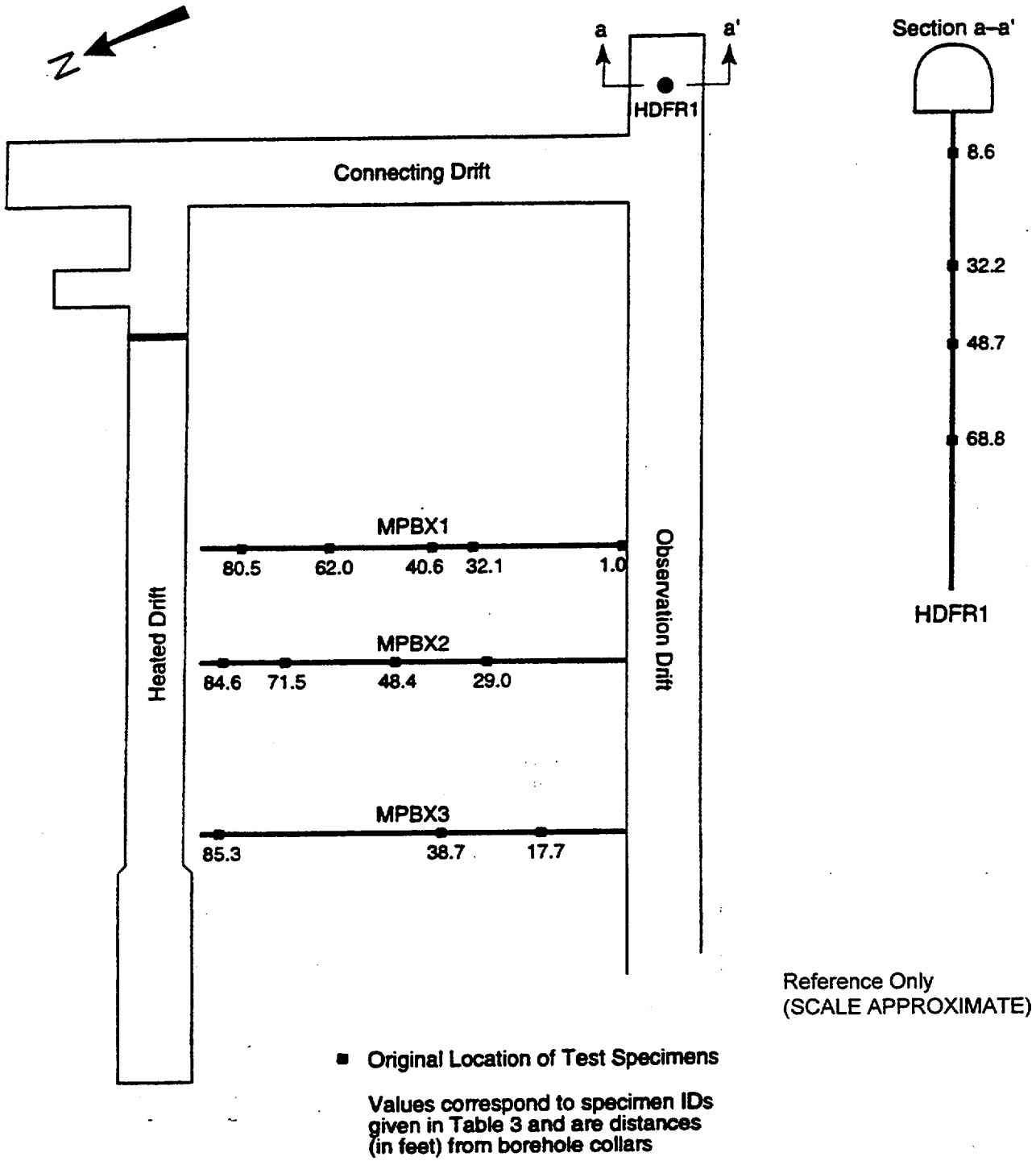

Figure 4-2. Approximate Locations of Unconfined Compressive Test Specimens

Specimens were tested in the air-dried state, that is, in the "as-received" condition with no effort made to preserve or alter the moisture content. The moisture content of these samples during testing was likely substantially different than the moisture content of the samples in situ. After recovery from the ESF, the cores may have dried out at the Sample Management Facility at the Nevada Test Site. They were then machined into specimens, using water as a coolant, and may have dried out somewhat in the laboratory before testing. Immediately after testing, specimen fragments were collected and weighed. They were then dried using the SNL Technical Procedure TP-065, *Drying Geologic Samples to Constant Weight,* to determine moisture contents during testing.

4.3 METHODOLOGY

Before testing tuff specimens, validation tests were performed on 6061 aluminum to validate the test method. Tests were also performed midway through the testing program and after completion of the test suite. For the pretest validation, measurements of Young's modulus and Poisson's ratio were within 9 and 15 percent of the expected values, respectively. For the midtest and posttest validations, measurements of Young's modulus and Poisson's ratio were within 2 and 8 percent of the expected values, respectively.

The specimen assembly used for unconfined compression tests is illustrated in Figure 4-3. The specimen was placed in a flexible jacket to maintain constant moisture content during testing and to contain the specimen fragments during failure. Ports are cut out of the jacket at the requisite locations to accommodate axial and lateral deformation gauges.

The axial displacement gauge consists of two linear variable displacement transducers (LVDTs) located on opposite sides of the specimen. The LVDT barrels are arranged in a ring, which is attached approximately one specimen radius from the upper end of the specimen. The LVDT cores are on extended rods that rest in cups located on a lower ring placed approximately one specimen radius from the lower end of the specimen. The axial displacement gauge therefore measures displacements occurring over the central section of the specimen.

Radial strains were measured across one diameter of the specimen using the radial displacement gauge developed by Holcomb and McNamee (1984). This gauge consists of an LVDT mounted in a ring, which is spring-loaded against the specimen. The barrel of the LVDT is mounted in the ring, and the core of the LVDT is attached to a leaf spring that directly contacts the specimen surface. Changes in specimen diameter directly displace the LVDT core relative to the barrel. The accuracies of calibrations for both the axial and lateral displacement gauges were within ± 2 percent of reading over the verified range of 10 to 100 percent of full scale. (Full scale output for the lateral gauge was 0.635 mm [0.025 in] or 0.0167 strain; for the axial gauge, full scale output was 1.27 mm [0.05 in] or 0.333 strain.) The LVDTs were calibrated while mounted in the rings using SNL Technical Procedure TP-257, *LVDT Calibration at Sandia National Laboratories.*

Tests were conducted in a servo-controlled hydraulic loading frame. The servo-controller was operated in strain-control feedback and force was applied so that a constant axial strain rate of $10^{-5}s^{-1}$ was imposed. The axial force was measured with a load cell calibrated in place by the manufacturer. The calibration constant for the load cell has a standard deviation of 0.02 percent.

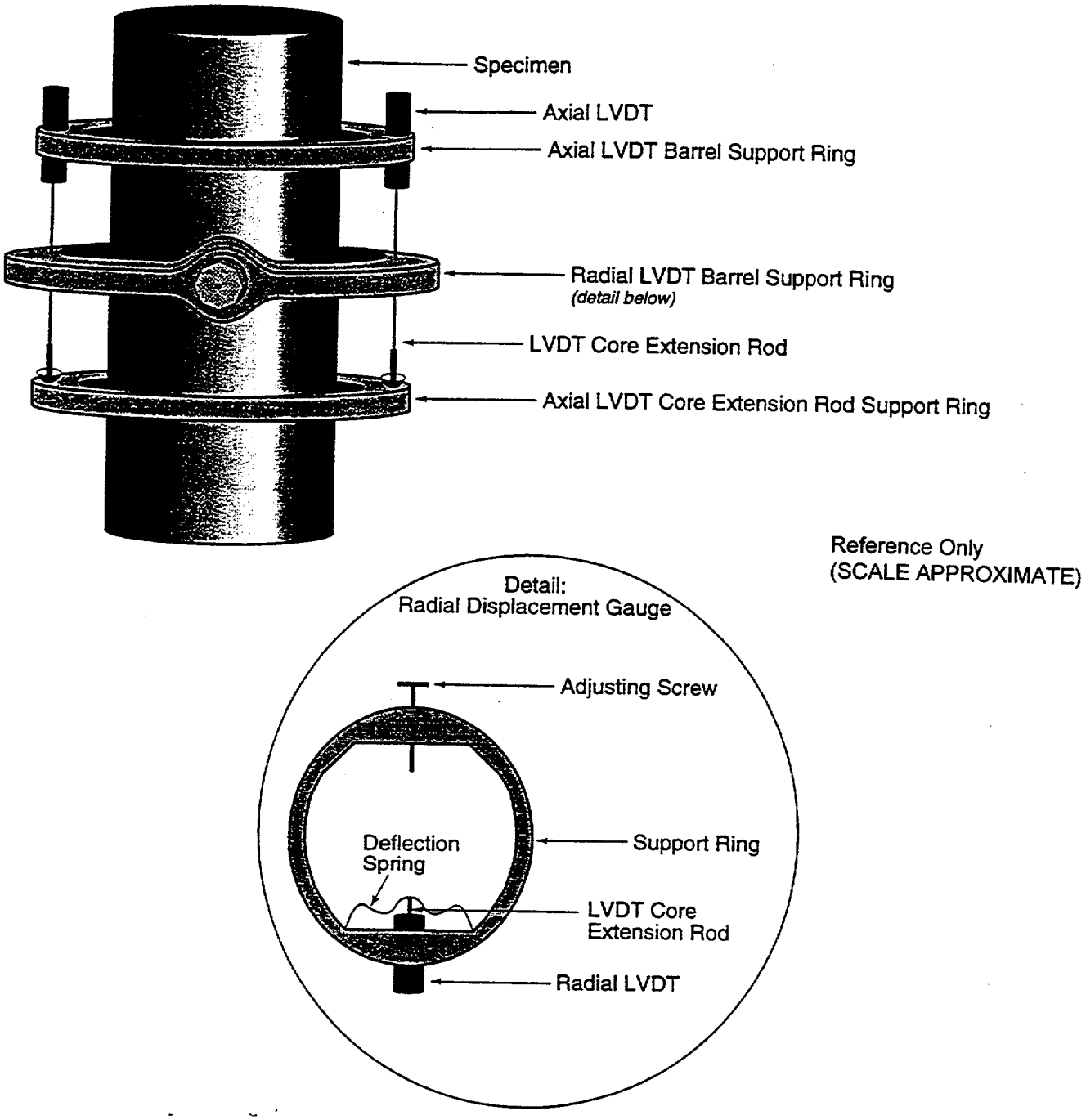

Figure 4-3. Specimen Instrumentation Assembly for Unconfined Compression Tests

Testing was performed in accordance with SNL Technical Procedure TP-219, *Unconfined Compression Experiments at Ambient Conditions and Constant Strain Rate.* Specimens were inspected for surface irregularities, vugs, and preexisting fractures. Samples were not rejected unless gross irregularities existed. Every sample was inspected prior to testing, which can be beneficial for evaluation and explanation of test results. After being jacketed and instrumented, specimens were loaded at a constant strain rate of $10^{-5}s^{-1}$ until peak force was reached. Specimens were unloaded after passing the peak in axial force.

Strains were calculated by dividing the measured axial and lateral displacements by the original gauge separations. The axial gauge consists of two LVDTs, and the average axial strain is reported. Peak stress is the unconfined compressive strength and was obtained by dividing the peak force by the original cross-sectional area of the specimen. The static elastic constants were calculated by performing linear regression to the data collected between 10 and 50 percent of the stress difference at failure. Young's modulus is the slope of the linear fit to the axial strain versus axial stress data, and Poisson's ratio is the slope of the linear fit to the axial strain versus lateral stain data.

4.4 RESULTS

The experimental data for the sixteen specimens tested in unconfined compression are summarized in Table 4-1. Mean values, standard deviations, and 95 percent confidence limits are given in Table 4-1 for Young's modulus, Poisson's ratio, unconfined compressive strength, and axial strain at peak stress. One specimen, MPBX1-1.0-A (test UCDST001), was unloaded after force began to drop at approximately 53 MPa. The specimen was later reloaded (test UCDST017) to a peak stress of 179 MPa. Data from the first loading of this specimen were used to calculate the mean elastic moduli in order to be consistent with the other tests. Data from the second loading were used in calculations of mean unconfined compressive strength and mean axial strain at peak stress. Stress-strain curves for all tests are given in Appendix C.

The distribution of Young's modulus is given in Figure 4-4. Young's us ranged from 28.9 GPa to 43.1 GPa, with a mean value of 36.8 GPa. The standard deviation was ± 3.5 GPa and the 95 percent confidence limit was ±1.7 GPa. The high Young's modulus value (43.1 GPa) corresponds to the first loading of MPBX1-1.0-A. Because this specimen was unloaded at a low stress difference, the modulus was calculated over a lower stress range than for the other specimens.

The distribution of Poisson's ratios is given in Figure 4-5. Poisson's ratio ranged from 0.17 to 0.34, with a mean value of 0.20. The standard deviation was ± 0.04 and the 95 percent confidence limit was ± 0.02. The three specimens with the highest Poisson's ratios (0.34 corresponding to HDFR1-32.2A, 0.22 corresponding to MPBX1-80.5A, and 0.22 corresponding to MPBX3-38.7) were the only specimens that had preexisting open fractures.

The distribution of unconfined compressive strength values is given in Figure 4-6. Strengths ranged from 71 MPa to 324 MPa, with a mean value of 176 MPa. The standard deviation was ± 66 MPa and the 95 percent confidence limits was ± 32 MPa. The highest and lowest strengths were obtained on specimens from MPBX2 that were in relatively close proximity (4 m apart). Neither specimen had notable surface features that might indicate anomalous behavior. The data shown in Figure 4-6 appear to be symmetrically distributed about the mean. No analyses were performed to determine

Table 4-1. Tabulation of Unconfined Compression Tests

Test Identification	UCDST001	UCDST002	UCDST003	UCDST004	UCDST005	UCDST006	UCDST007	UCDST008	UCDST009	UCDST010	UCDST011
Specimen Identification	ESF-SDM-MPBX1-1.0-A	ESF-SDM-MPBX1-32.1-A	ESF-SDM-MPBX1-40.6-A	ESF-SDM-MPBX1-62.0-A	ESF-SDM-MPBX1-80.5-A	ESF-SDM-MPBX2-29.0-A	ESF-SDM-MPBX2-48.4-A	ESF-SDM-MPBX2-71.5-A	ESF-SDM-MPBX2-84.6-AV	ESF-AOD-HDFR1-8.6-A	ESF-AOD-HDFR1-32.2-A
Date Tested	3/28/97	3/28/97	3/31/97	3/31/97	3/31/97	3/31/97	3/31/97	3/31/97	4/1/97	4/1/97	4/1/97
Thermal/Mechanical Unit	TSw2	TSw2	TSw2	TSw2	TSw2	TSw2	TSw2	TSw2	TSw2	TSw2	TSw2
Lithostratigraphic Unit	Tptpmn	Tptpmn	Tptpmn	Tptpmn	Tptpmn	Tptpmn	Tptpmn	Tptpmn	Tptpmn	Tptpmn	Tptpmn
Dry Bulk Density	2.27	2.26	2.27	2.27	2.30	2.26	2.23	2.30	2.31	2.28	2.28
Moisture Content (%)	0.48	0.51	0.60	0.81	0.61	0.45	0.53	0.49	0.56	0.67	0.32
Confining Pressure	0	0	0	0	0	0	0	0	0	0	0
Static Young's Modulus (GPa)	43.1	38.5	38.2	39.3	36.2	37.8	34.5	40.2	37.8	37.4	34.5
Static Poisson's Ratio	0.18	0.21	0.19	0.19	0.22	0.20	0.19	0.17	0.19	0.20	0.34
Unconfined Compressive Strength (MPa)	52.7	201.0	232.6	114.1	97.2	178.0	128.0	71.3	324.1	268.3	123.1
Axial Strain at Peak Stress	0.001267	0.005642	0.006191	0.003016	0.003577	0.005467	0.003877	0.001852	0.009506	0.007966	0.003497
Test Identification	UCSDT012	UCDST013	UCDST014	UCDST015	UCDST016	UCDST017 Reloading		Statistical Summary (a)			
Specimen Identification	ESF-AOD-HDFR1-48.7-A	ESF-AOD-HDFR1-68.8-A	ESF-SDM-MPBX3-17.7-A	ESF-SDM-MPBX3-38.7-A	ESF-SDM-MPBX3-85.3-A	ESF-AOD-MPBX1-1.0-A		Mean	Standard Deviation	Count	95% Confidence Limit
Date Tested	4/1/97	4/1/97	4/1/97	4/2/97	4/2/97	4/1/97					
Thermal/Mechanical Unit	TSw2	TSw2	TSw2	TSw2	TSw2	TSw2					
Lithostratigraphic Unit	Tptpmn	Tptpmn	Tptpmn	Tptpmn	Tptpmn	Tptpmn					
Dry Bulk Density	2.28	2.24	2.24	2.29	2.26	2.27					
Moisture Content (%)	0.46	0.83	0.74	0.42	0.48	0.48					
Confining Pressure	0	0	0	0	0	0					
Static Young's Modulus (GPa)	40.0	31.6	28.9	34.8	35.4	38		36.8	3.5	16	1.7
Static Poisson's Ratio	0.19	0.17	0.18	0.22	0.18	2.06		0.201	0.040	16	0.020
Unconfined Compressive Strength (MPa)	175.6	159.0	172.2	158.6	239.1	179.4		176.4	65.8	16	32.3
Axial Strain at Peak Stress	0.003668	0.005536	0.006551	0.007332	0.006082	0.003582		0.005209	0.002048	16	0.001004

Test Conditions: Nominally 38.1 mm in diameter, 76.2 mm in length, ambient temperature and pressure, nominal strain rate of 10^{-5} s^{-1}.
(a) Test specimen ESF-SDM-MPBX1-1.0-A was tested twice. Mean Young's modulus and mean Poisson's ration were calculated using data from the first loading only (UCDST001). Mean unconfined compressive strength was calculated using data from the second loading only (UCDST017).

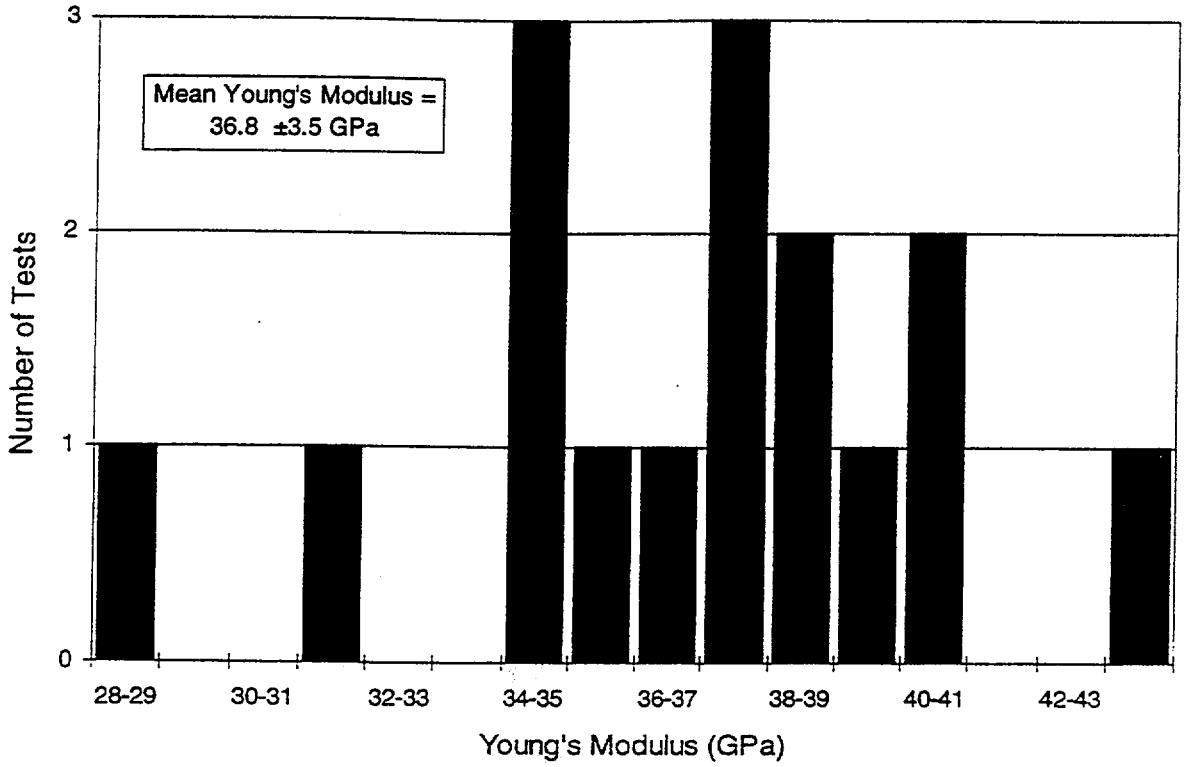

Figure 4-4. Distribution of Young's Modulus

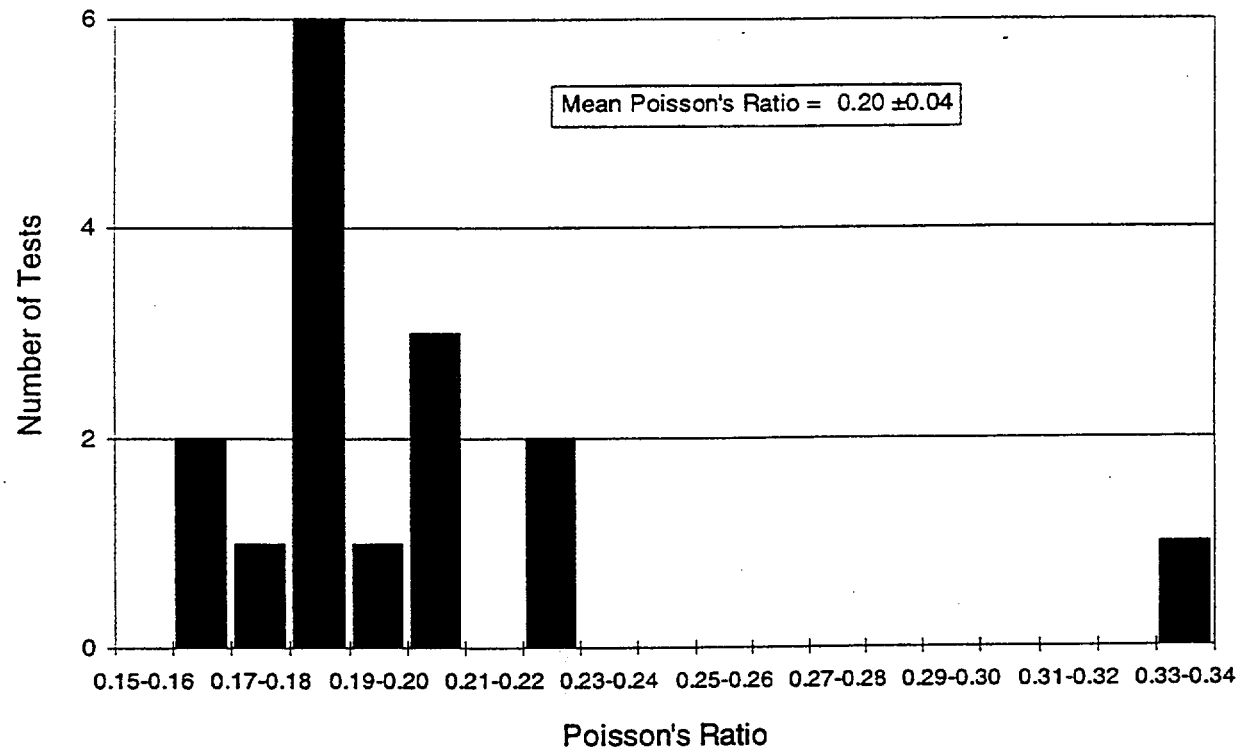

Figure 4-5. Distribution of Poisson's Ratios

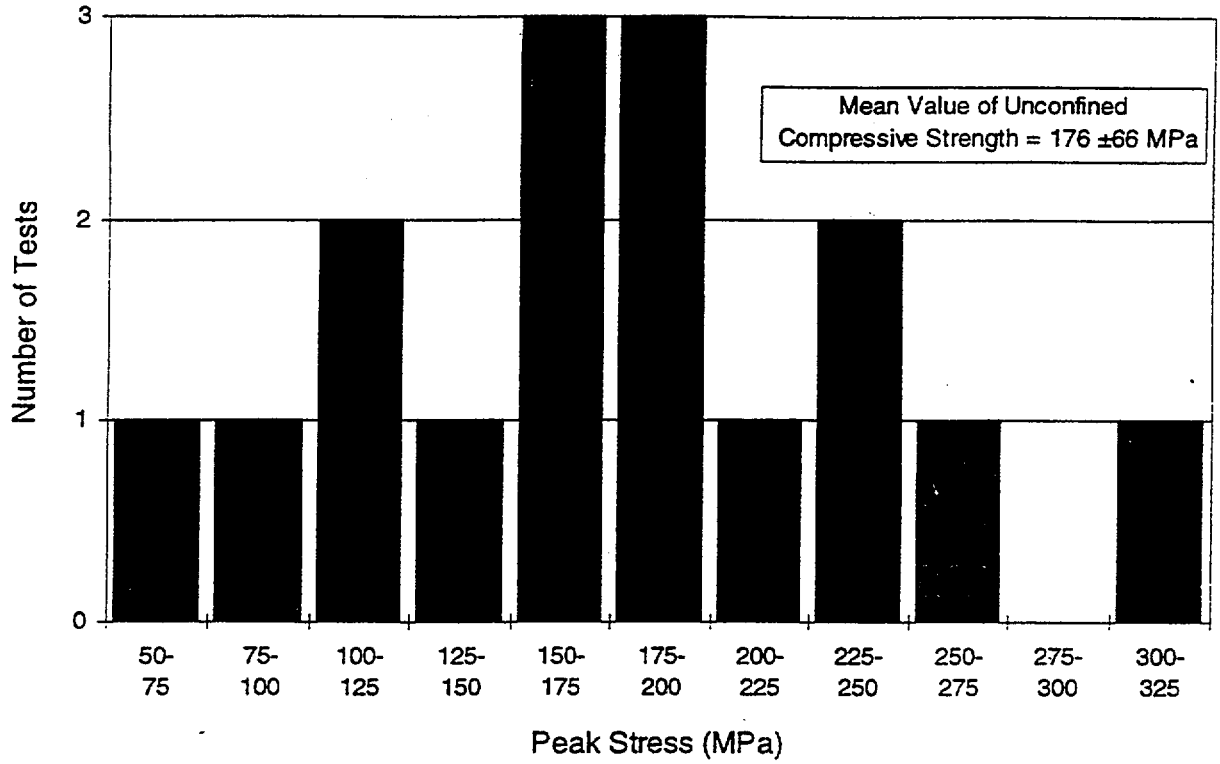

Figure 4-6. Distribution of Unconfined Compressive Strengths

the best fitting distribution curves for Young's modulus, Poisson's ratio, or unconfined compressive strength.

All specimens failed audibly except for MPBX1-1.0-A, which was loaded twice. Most rocks failed explosively. The four rocks with the highest compressive strengths all failed by axial splitting. Three additional rocks, which had average to below average strengths, also failed by axial splitting. The three specimens that failed along shear planes had above average, below average, and well below average strengths. There does not appear to be a significant correlation between the failure mode and the peak stress value, which was also the conclusion from unconfined compressive testing on specimens from the SHT area (TDIF #305602).

Individual determinations of Young's modulus, Poisson's ratios, and unconfined compressive strengths are shown in Figures 4-7, 4-8, and 4-9, respectively, plotted at the locations of the original test specimens. The mean values for each borehole are also shown. Because the data are highly variable and there are very few tests per borehole, caution must be exercised when comparing boreholes. However, the Young's modulus mean for each borehole does decrease with increasing distance from the connecting drift. The mean unconfined compressive strength also systematically increases with distance from the connecting drift (Figure 4-9), although the standard deviations associated with strength data for each borehole are extremely large. The highest compressive strength values were obtained close to the heated drift. No systematic variation in Poisson's ratio is indicated. Data from HDFR1 show no systematic changes in properties with depth. There are insufficient data to assess anisotropy.

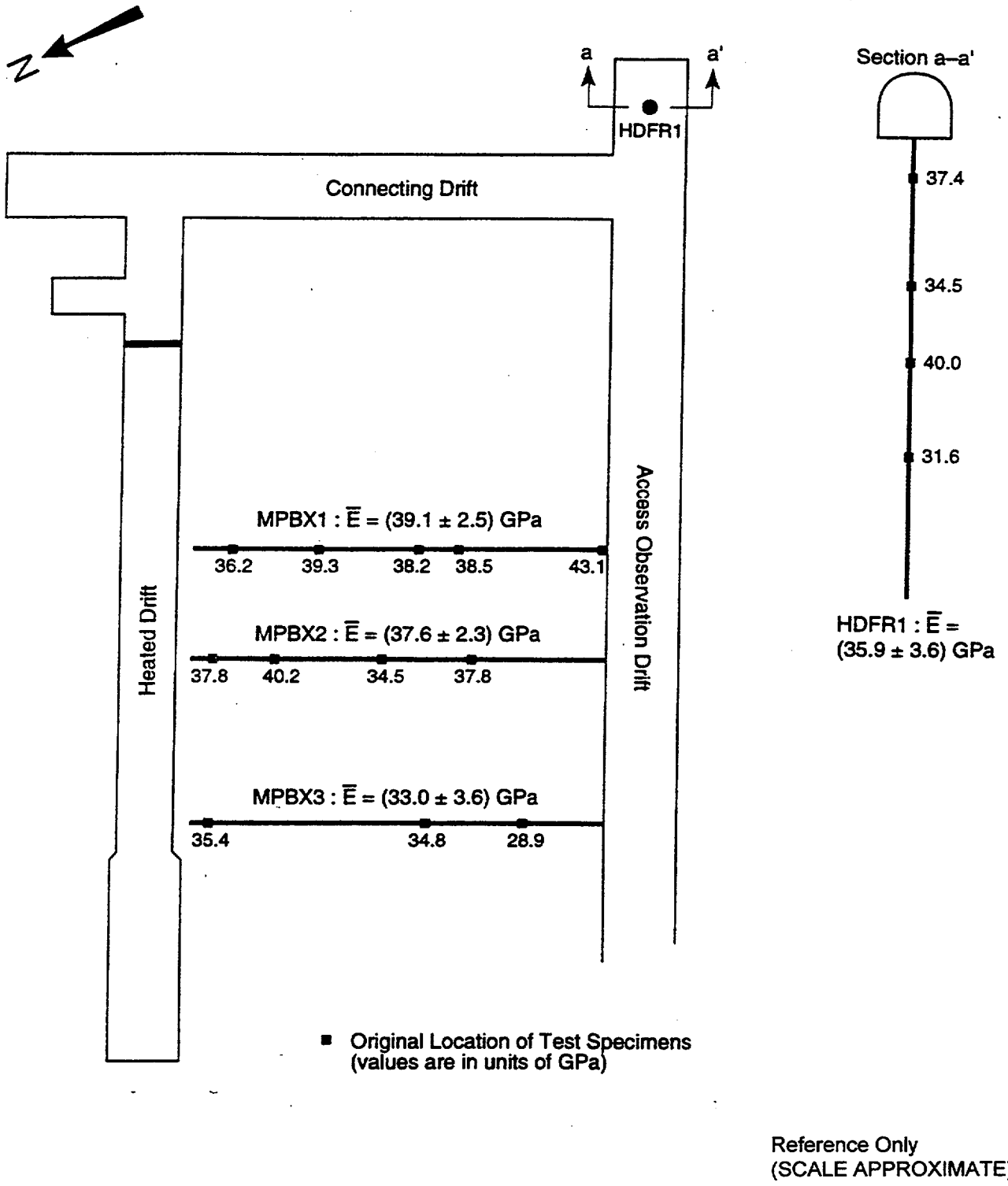

NOTE: $\bar{E}$ is the average Young's modulus for each borehole.

Figure 4-7. View of DST Block Showing Individual Young's Modulus.

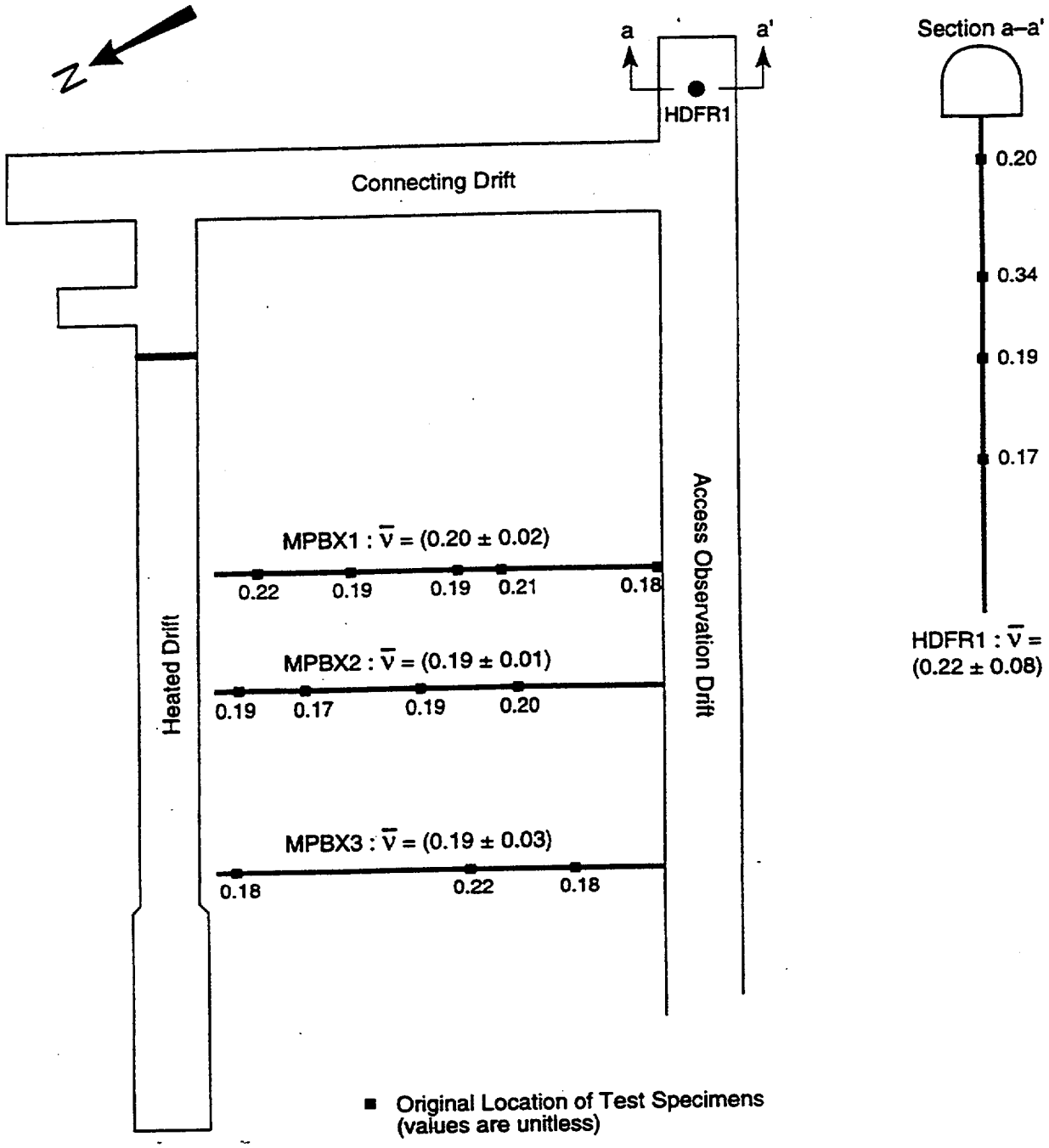

NOTE: $\bar{\nu}$ is the average Poisson's modulus for each borehole.

Figure 4-8. View of DST Block Showing Individual Poisson's Ratio.

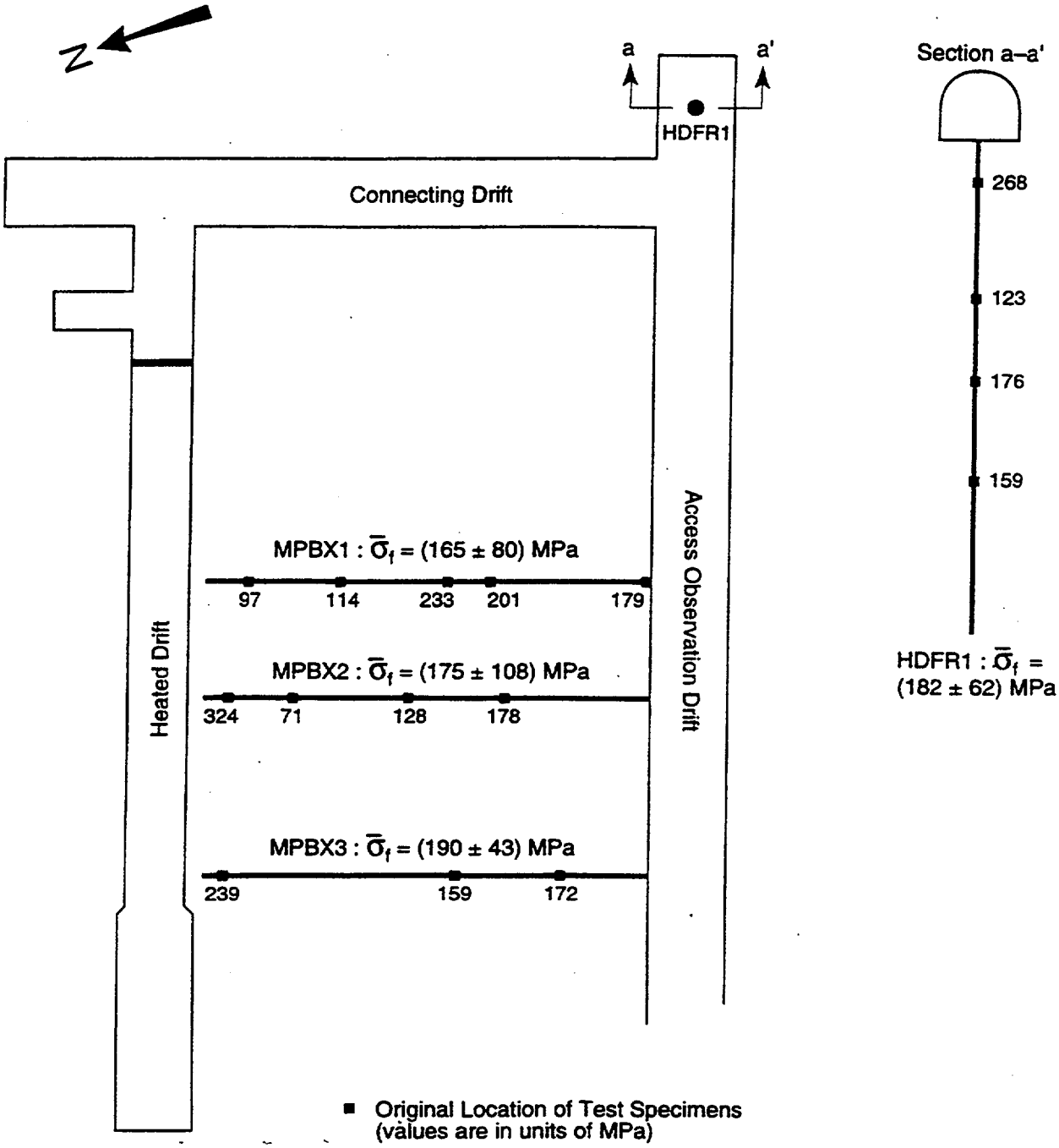

NOTE: $\bar{\sigma}_f$ is the average stress at failure for each borehole.

Figure 4-9. View of DST Block Showing Individual Unconfined Compressive Strength.

The mean values of Young's modulus, Poisson's ratio, and strength are all higher than the values obtained during characterization of the SHT area. Minor differences in the testing programs could account for some differences in test results. First, the SHT test specimens had a length-to-diameter ratio of 2.5, whereas the DST test specimens had an length-to-diameter ratio of 2.0. Work reported in Paterson (1978) indicates that in Westerly granite, unconfined compressive strength increased by 3 percent when the length-to-diameter ratio decreased from 2.5 to 2.0. The same relationship is not necessarily expected in tuff, but the work reported in Paterson (1978) is cited to provide a possible indication of the magnitude of the effect. The increase in observed strengths is approximately 21 percent, so the effect of different length-to-diameter ratios is considered minor. Second, differences in the results of validation tests on aluminum could account for approximately a 4 to 8 percent difference in the Poisson's ratio value. Finally, the moisture content for all DST specimens was less than 1 percent, but two of the SHT specimens were saturated. The remainder of the SHT specimens were tested "as is" (moisture content), similar to the DST tests.

The coefficients of the thermal expansion were also somewhat higher for the DST than for the SHT (TDIF #306127). The differences in properties between the DST and the SHT, and a possible systematic change in Young's modulus with the increasing distance from the connecting drift as shown by the DST data, may be indicative of spatial variability within the TTF.

INTENTIONALLY LEFT BLANK

5. LABORATORY TESTING: HYDROLOGICAL PROPERTIES

5.1 OBJECTIVE AND DESCRIPTION

The objective of the laboratory testing of the hydrological properties was to determine saturation, bulk density, particle density, and gravimetric water content for both dry-drilled cores and wet-drilled cores from the DST block and the SHT block of the TTF of the ESF. Core measurements are part of the hydrological characterization study to determine the amount of pore water available for evaporation and boiling during the heating phase.

Another objective was to determine the moisture imbibition potential of the rock at elevated temperatures. Hydrological properties, including porosity, are determined and then the moisture retention curves of core samples from both the SHT and the DST are determined. This laboratory work is partially complete.

The data in this section have been entered into Automated Technical Data Tracking and were submitted to the Records Center under the DTNs LB970500123142.003 and LL97070904244.035. The Technical Data Information Form (TDIF) numbers are #306135 and #306238, and the scientific notebook numbers are YMP-LBNL-JSW-4-1.0 and YMP-LBNL-JSW-4-1.1. All the measurement and analysis in this study were performed by qualified personnel and the equipment used was calibrated under the Lawrence Berkeley National Laboratory Quality Assurance Program. All data presented are qualified data. The work described in this section was completed in satisfaction of Level 4 Milestone SP5130M4 (Wang and Suarez-Rivera 1997), and SP5110M4 (Lin 1997).

5.2 SAMPLES

Two sets of samples from the DST block were tested: one set from dry-drilled boreholes and one set from wet-drilled boreholes. The dry-drilled set was from cores from three permeability boreholes, from an elevated platform at the end of the connecting drift, as shown in Figure 2-2. The 20 boreholes were drilled toward the east, away from the heated drift. Borehole #183 or ESF-HD-PERM-2 is horizontal, and the other two permeability boreholes are inclined at 20°.

Included in the second set of samples from the DST block, from wet-drilled boreholes, are samples from one 46 m MPBX borehole drilled horizontally toward the west, parallel to the heated drift axis, from the same platform as the PERM boreholes but in the opposite direction. The wet-drilled samples are from three 40 m chemistry boreholes in a plane normal to the heated drift, drilled from the observation drift, at angles of 24°, 14° (above horizontal) and -22° (below horizontal).

During core processing, observations of factors potentially affecting test results were recorded. Some obvious differences in core condition were observed between the samples from the dry-drilled permeability boreholes away from the heated drift and the samples from the wet-drilled MPBX and chemistry boreholes near the heated drift. Samples from the permeability boreholes were less fractured or crumbled, and the core surfaces and the core containers of the dry-drilled permeability boreholes were relatively drier.

Samples from the SHT block were from three wet-drilled boreholes, which were shorter than the DST boreholes. Twenty-four samples were tested for moisture imbibition, including 11 samples from the SHT block and 13 from the DST block.

5.3 METHODOLOGY

The procedure for determining hydrological properties (water content, bulk density, porosity, and particle density of core rocks) consisted of measuring the gravimetric water content, determining bulk density and porosity using the Archimedes water immersion technique, and using the calculated values of dry weight, bulk volume and porosity, to determine the particle density.

Core samples previously stored in sealed packets were placed in containers with tight-fitting lids and immediately weighed. The samples were subsequently placed in a drying oven at a temperature between 100°C to 110°C, until they reached a constant weight. Samples were then placed in a desiccator, cooled, and weighed to determine the gravimetric water content. This procedure ensures that samples are dried at a specified temperature to a constant weight, with nothing lost during the process but water.

The samples were then water-saturated in a vacuum chamber and weighed following the Archimedes method (i.e., immersed in air and water) to determine volume and weight under conditions of full saturation. Knowledge of the dry weight, saturated weight and sample bulk volume were used to calculate bulk density, porosity, and particle density.

Moisture imbibition potential was determined as follows. After determining the effective porosities of the individual samples, the moisture retention curves were determined for each sample. The samples for which the porosities had been determined were placed in a relative humidity chamber where both temperature and humidity were maintained at a constant level during each phase of the testing. The measurements were made by first setting the temperature and relative humidity of the chamber to their initial levels. The samples' dry and fully saturated densities are needed to calculate porosities, and the moisture retention curves can be determined using either initially dry or saturated samples. For convenience, initially dry samples were used. It is not known whether there is a difference in the results dependent on whether initially wet or dry samples are used. However, moisture retention curves for both wetting and drying cycles were determined. Expectedly, the moisture retention curves are affected by the moisture content of the sample in that the response will vary depending on whether moisture content is decreasing or increasing (hysterisis).

Dry samples were placed in the humidity chamber. All samples were wrapped immediately after coring to maintain moisture control. The sample weights were determined periodically until they remained unchanged for a few days. Then the humidity level in the chamber was increased to a higher level, and the measurement repeated. When the relative humidity in the chamber reached 95% and the sample weights reached equilibrium, the measurement in the wetting phase was complete, and the measurements in the draining phase were started by repeating the measurements at gradually decreased relative humidity levels. Then, the entire process was repeated for higher temperature levels.

5.4 RESULTS

The data from the two sets of measurements for the DST block are tabulated in Table 5-1 for the dry-drilled cores and Table 5-2 for the wet-drilled cores. Summaries of the averages and standard deviations of the measured values are presented at the end of each table. Data from both sets are also presented graphically in Appendix D, Figures D-1 through D-5, for saturation, porosity, bulk density, particle density, and gravimetric water content, respectively. Property data points are plotted against borehole depths. Data points are connected or not, based on a subjective determination of reliability of measurement.

The average saturation for DST samples from the dry-drilled boreholes was 84 percent, and the average saturation for DST samples from the wet-drilled boreholes was 93 percent. This discrepancy may in part arise from spatial heterogeneity, and in part from the different drilling methods. For comparison, the saturation value compiled from all surface-based boreholes for the Tptpmn lithostratigraphic unit (266 samples) is 85 ± 12 percent (Flint 1996). The corresponding borehole porosity value is 11 ± 2 percent, as compared to the average values from 11 percent for dry cores to 13 percent for wet cores.

The results of testing on samples from the SHT block boreholes are presented in Table 5-3 and Figures D-5 through D-10. Saturation values were in the 95 percent range, and the variability of rock properties is comparable in magnitude to the DST HD data set. Table 5-4 presents previously reported laboratory measurements of five grab samples from wet excavation of the observation drift (CRWMS M&O 1996). One grab sample subsample had a saturation value of 81 percent, while the saturation of the other four subsamples were all above 94 percent.

The 10 percent difference in the mean saturation between the dry-drilled and the wet-drilled data sets in the TTF is within the standard deviation of 12 percent for all the surface-based samples. An analysis of this core may indicate whether the mean saturation difference is because of the drilling method or because of the local rock conditions.

Although laboratory work for determining the moisture imbibition potential is not yet complete, the determination of effective porosities has been completed for both the SHT and DST samples. The sample identification, location, and effective porosity are listed in Table 5-5 for the SHT samples and in Table 5-6 for the DST samples. The drying and wetting phase of the measurements for the SHT samples at room temperature have been completed. The results are shown in Tables 5-7 and 5-8 and Figure 5-1.

The DST samples were placed in the constant humidity camber. The samples were at 80% relative humidity and room temperature, in the wetting phase of the measurement. The data obtained so far are listed in Table 5-9 and shown in Figure 5-2.

Table 5-1. Laboratory Hydrological Measurements of Dry-Drilled Cores from DST Permeability Boreholes

Borehole #182, ESF-HD-PERM-1					
Sample Location (m)	Saturation (%)	Porosity (%)	Bulk Density (g/cc)	Particle Density (g/cc)	Gravimetric Water Content (g/g)
5.5	86.67	9.61	2.27	2.51	0.037
9.9	89.67	11.02	2.24	2.52	0.044
15.5	85.08	10.27	2.25	2.51	0.039
19.8	86.72	10.27	2.25	2.51	0.039
Borehole #183, ESF-HD-PERM-2					
Sample Location (m)	Saturation (%)	Porosity (%)	Bulk Density (g/cc)	Particle Density (g/cc)	Gravimetric Water Content (g/g)
5.2	83.84	9.62	2.27	2.51	0.035
10.1	82.86	12.02	2.21	2.51	0.045
15.3	76.61	13.35	2.19	2.53	0.046
19.9	79.21	10.89	2.24	2.51	0.038
Borehole #184, ESF-HD-PERM-3					
Sample Location (m)	Saturation (%)	Porosity (%)	Bulk Density (g/cc)	Particle Density (g/cc)	Gravimetric Water Content (g/g)
5.1	81.40	9.87	2.25	2.50	0.035
10.0	86.61	10.91	2.24	2.51	0.042
15.5	85.80	9.43	2.27	2.51	0.035
18.9	81.76	10.17	2.26	2.52	0.037
DST PERM Borehole Summary					
	Saturation (%)	Porosity (%)	Bulk Density (g/cc)	Particle Density (g/cc)	Gravimetric Water Content (g/g)
DST PERM average; standard deviation	83.85 3.67	10.62 1.14	2.25 0.02	2.51 0.01	0.039 0.004

Table 5-2. Laboratory Hydrological Measurements of Wet-Drilled Cores from DST Boreholes

Borehole #81, ESF-HD-MPBX-1					
Sample Location (m)	Saturation (%)	Porosity (%)	Bulk Density (g/cc)	Particle Density (g/cc)	Gravimetric Water Content (g/g)
4.6[1]	96.43	10.15	2.25	2.50	0.043
6.8	84.97	9.73	2.27	2.51	0.036
12.3[2]	96.02	10.16	2.26	2.52	0.043
17.8[3]	96.80	9.46	2.26	2.49	0.040
20.8[4]	103.77	15.34	2.14	2.53	0.073
24.1	94.10	8.77	2.28	2.50	0.036
32.0	95.42	9.67	2.28	2.52	0.040
35.1[5]	92.97	11.81	2.21	2.51	0.050
39.4	92.82	10.31	2.26	2.52	0.042
45.3	94.57	9.27	2.28	2.51	0.038
Borehole #52, ESF-HD-CHE-1					
Sample Location (m)	Saturation (%)	Porosity (%)	Bulk Density (g/cc)	Particle Density (g/cc)	Gravimetric Water Content (g/g)
15.3[6]	87.56	11.73	2.22	2.52	0.046
18[7]	95.91	17.32	2.09	2.52	0.079
26.5[6]	87.89	11.04	2.24	2.51	0.043
29.9[8]	97.32	13.98	2.16	2.51	0.063
35.0	96.98	18.19	2.07	2.53	0.085
38.2[9]	98.58	16.57	2.11	2.53	0.077
Borehole #53, ESF-HD-CHE-2					
Sample Location (m)	Saturation (%)	Porosity (%)	Bulk Density (g/cc)	Particle Density (g/cc)	Gravimetric Water Content (g/g)
10.7[9]	95.31	11.67	2.22	2.51	0.050
16.7[9]	96.84	12.94	2.19	2.51	0.057
22.2	94.96	11.52	2.22	2.51	0.049
28.2[10]	74.03	15.62	2.11	2.50	0.055
36.5[10]	95.47	12.80	2.21	2.53	0.055

Table 5-2. Laboratory Hydrological Measurements of Wet-Drilled Cores from DST Boreholes (continued)

Borehole #56, ESF-HD-CHE-5					
Sample Location (m)	**Saturation (%)**	**Porosity (%)**	**Bulk Density (g/cc)**	**Particle Density (g/cc)**	**Gravimetric Water Content (g/g)**
10.6	94.99	14.57	2.15	2.52	0.064
18.0[9]	94.34	12.33	2.20	2.51	0.053
23.2	95.58	16.02	2.11	2.51	0.072
29.6	92.79	15.91	2.14	2.54	0.069
35.7	86.21	11.65	2.21	2.51	0.045
38.9	82.40	10.09	2.25	2.51	0.037
DST Heated Drift Borehole Summary					
	Saturation (%)	**Porosity (%)**	**Bulk Density (g/cc)**	**Particle Density (g/cc)**	**Gravimetric Water Content (g/g)**
DST heated drift average:	93.15	12.54	2.20	2.51	0.053
standard deviation	5.93	2.75	0.06	0.01	0.015

[1] entire surface of core was wet
[2] closed vertical fracture along core axis
[3] two fractures with small aperture
[4] two open fractures + "crushed zone" + porous-looking calcite inclusion
[5] large open fracture down center of upper half
[6] water drop loss during transfer
[7] large fracture exposed on surface
[8] contains large open vug on side surface
[9] contains fracture on side surface
[10] large amount of water condensed in container

Table 5-3. Laboratory Hydrological Measurements of Wet-Drilled Cores from SHT Boreholes

Borehole #1, ESF-TMA-H-1					
Sample Location (m)	Saturation (%)	Porosity (%)	Bulk Density (g/cc)	Particle Density (g/cc)	Gravimetric Water Content (g/g)
1.0	89.46	10.66	2.25	2.51	0.043
2.5[1]	88.04	13.30	2.18	2.52	0.054
3.7	93.60	8.87	2.29	2.52	0.036
4.7	97.27	11.83	2.22	2.51	0.051
5.7	93.97	13.83	2.16	2.51	0.061
6.7	96.03	11.89	2.21	2.51	0.052
Borehole #6, ESF-TMA-OMPBX-1					
Sample Location (m)	Saturation (%)	Porosity (%)	Bulk Density (g/cc)	Particle Density (g/cc)	Gravimetric Water Content (g/g)
0.2	94.82	11.00	2.24	2.51	0.047
2.4	94.75	10.43	2.25	2.51	0.044
4.4	93.58	10.18	2.26	2.51	0.042
7.5[2]	96.87	23.62	1.96	2.57	0.104
subcore		20.44	2.02	2.53	
9.3	96.17	11.55	2.22	2.52	0.050
11.3	93.07	9.74	2.27	2.51	0.040
Borehole #5, ESF-TMA-MPBX-4					
Sample Location (m)	Saturation (%)	Porosity (%)	Bulk Density (g/cc)	Particle Density (g/cc)	Gravimetric Water Content (g/g)
0.7[3]	95.85	17.03	2.05	2.48	0.079
2.1[4]	101.61	9.69	2.25	2.49	0.044
2.6	102.17	13.33	2.17	2.50	0.063
3.8	96.74	10.58	2.24	2.50	0.046
subcore		10.44	2.24	2.50	
5.4	97.65	9.60	2.27	2.51	0.040
SHT Borehole Summary					
	Saturation (%)	Porosity (%)	Bulk Density (g/cc)	Particle Density (g/cc)	Gravimetric Water Content (g/g)
SHT average; standard deviation	95.39 3.56	12.53 3.89	2.20 0.09	2.51 0.02	0.053 0.017

[1] contains small voids
[2] split along axis during oven drying
[3] contains open fractures and large vugs
[4] received in fragments

Table 5-4. Laboratory Hydrological Measurements of Grab Samples from Wet Excavation of the Observation Drift

Observation Drift Grab Samples					
CS Location (m)	**Saturation (%)**	**Porosity (%)**	**Bulk Density (g/cc)**	**Particle Density (g/cc)**	**Gravimetric Water Content (g/g)**
30.0	99.00	8.60	2.26	2.47	0.038
sub-sample	94.90	8.30	2.27	2.47	0.035
40.0	95.40	9.30	2.27	2.50	0.039
sub-sample	93.80	10.10	2.24	2.49	0.042
sub-sample	80.50	10.40	2.24	2.50	0.037
Observation Drift Grab Sample Summary					
	Saturation (%)	**Porosity (%)**	**Bulk Density (g/cc)**	**Particle Density (g/cc)**	**Gravimetric Water Content (g/g)**
Observation Drift average;	92.72	9.34	2.26	2.49	0.038
standard deviation	7.10	0.91	0.02	0.02	0.003

Table 5-5. Effective Porosities for Moisture Imbibition Potential Determination in the SHT Block

Sample Identification	Borehole Number	Depth (ft)	Effective Porosity (%)
0047525.2	CHE-1	2.2	10.2
0047525.2A	CHE-1	2.3	10.2
0047526.2	CHE-1	4.6	10.9
0047527.2	CHE-1	8.2	9.98
0047528.2	CHE-1	12.5	10.7
0047529.2	CHE-1	14.0	10.9
0047530.2A	CHE-2	14.8	12.7
0047531.2	CHE-2	5.0	11.1
0047533.2	CHE-2	12.7	13.5
0047534.2	CHE-2	15.2	10.3
0047535.2	CHE-2	17.6	11.9

Table 5-6. Effective Porosities for Moisture Imbibition Potential Determination in the DST Block

Sample Identification	Borehole Number	Depth (ft)	Effective Porosity (%)
01002163-1	CHE-1	92.3 - 93.2	8.53
01002176-1	CHE-2	128.9 - 129.6	11.10
01002179-1	CHE-5	39.4 - 40.1	8.31
01002189-1	CHE-6	43.4 - 44.1	9.14
01002190-1	CHE-6	63.9 - 64.6	8.35
01002194-1	CHE-6	99.7 - 100.4	10.6
01002199-2	CHE-7	51.9 - 52.6	12.7
01002200-1	CHE-7	80.0 - 80.7	8.95
01002206-2	CHE-10	15.7 - 16.3	10.2
01002207-2	CHE-10	27.3 - 28.0	8.91
01002209-2	CHE-10	75.6 - 76.3	12.5
01002212-1	CHE-10	91.6 - 92.3	12.4
01002215-1	CHE-10	124.0 - 124.7	7.96

Table 5-7. Relative Humidity and Water Saturation of SHT Samples in Wetting Phase at Room Temperature

Relative Humidity	Matric Potential (MPa)	Average Water Saturation (%)	Error for Water Saturation (%)
0.224	-205.22	18.5	3.29
0.316	-158.23	20.6	3.68
0.479	-101.07	22.9	4.10
0.650	-59.15	24.8	4.44
0.801	-30.48	27.2	4.96
0.954	-6.47	36.9	5.85
1.0	0.00	100.0	

Table 5-8. Relative Humidity and Water Saturation of SHT Samples in Drying Phase at Room Temperature

Relative Humidity	Matric Potential (MPa)	Average Water Saturation (%)	Error for Water Saturation (%)
1.0	0.00	100.0	-
0.954	-6.47	36.9	5.85
0.809	-29.10	28.7	5.02
0.656	-57.91	25.9	4.55
0.485	-99.36	23.5	4.15
0.296	-167.16	20.5	3.66
0.208	-215.82	18.3	3.23

Table 5-9. Matric Potential and Water Saturation of the DST Samples at Room Temperature in the Wetting Phase

Relative Humidity Measurement	Matric Potential (MPa)	Average Water Saturation (%)	Error for Water Saturation (%)
0.237	-197.7	14.3	2.27
0.452	-109.1	17.8	2.82

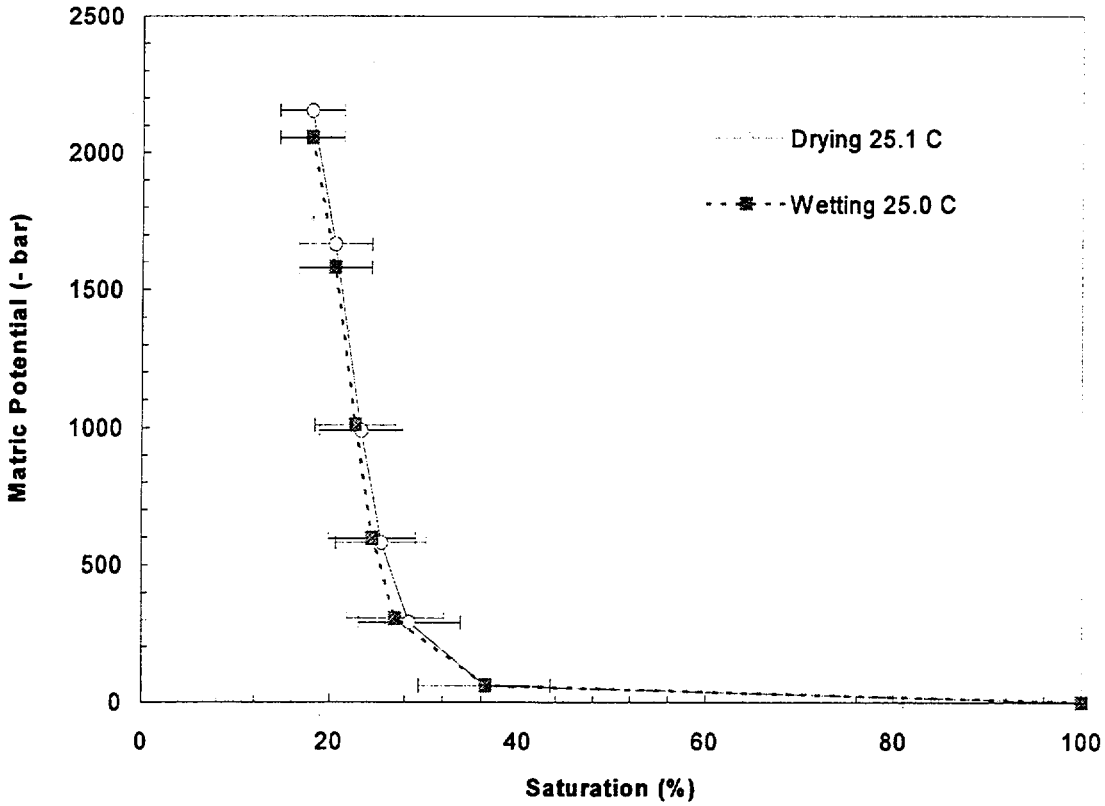

Figure 5-1. Matric Potential and Water Saturation of the SHT Samples at Room Temperature During Drying and Wetting Phases.

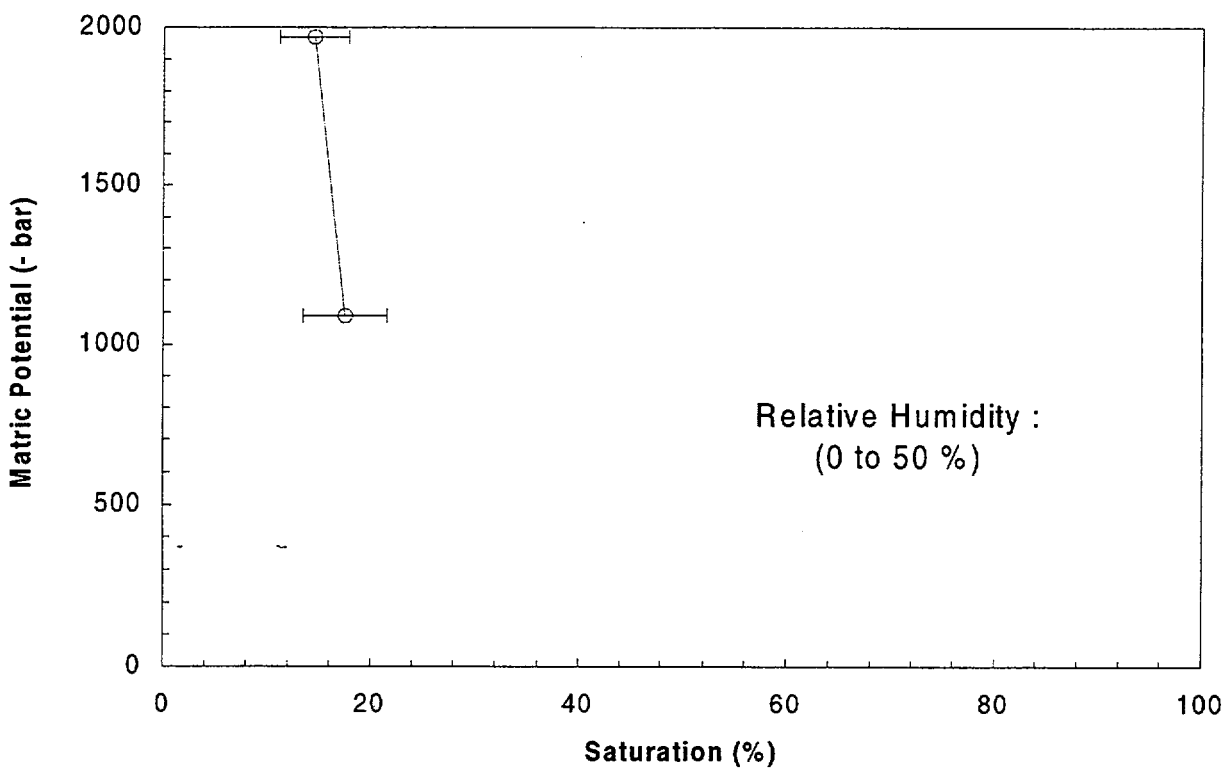

Figure 5-2. Matric Potential and Water Saturation of the DST Samples at Room Temperature During the Wetting Phase up to 50% Relative Humidity.

INTENTIONALLY LEFT BLANK

6. LABORATORY TESTING: CHEMICAL PROPERTIES

6.1 MINERALOGY AND PETROLOGY

6.1.1 Objective and Description

The objective of the laboratory testing of the mineralogy was to characterize, by X-ray diffraction, the relative mineral abundances of seventeen subsamples from cores collected from instrumentation boreholes in the DST block.

Because other sub-samples from these cores are being used for thermal expansion measurements, the abundance of minerals that could affect the thermal/mechanical behavior of the rock at elevated temperatures is of particular interest.

Previous X-ray diffraction analyses of samples from the ESF (Roberts and Viani 1997b, Viani and Roberts 1996) utilized the matrix flushing method of Chung (1974) and an internal intensity standard (corundum) to quantify the phases present. Although this method is adequate for obtaining relative abundances, its accuracy and precision is limited by the inherent differences between the external standards used to compute the reference intensity ratio and the phases in the samples. The mineral abundances reported here (Table 6-1) were estimated using the Rietveld method of whole X-ray pattern fitting (Snyder and Bish 1989; Young 1993). The Rietveld method of quantification avoids the use of external standards. This method is based on fitting a calculated X-ray diffraction pattern to the observed pattern over the entire angular range over which data is collected. The calculated pattern is refined by adjusting the quantity of the phases included in the calculation, as well as their crystallographic properties. The method requires identification of all the phases in the sample, as the refined abundances are normalized to 100 percent. In order to assess the overall accuracy of the method, a known quantity of corundum was added to each sample analyzed.

The data for this section have been entered into automated Technical Data Tracking and will be submitted to the Records Center under DTN LL970600304244.032 and TDIF #306139. The Lawrence Livermore National Laboratory Yucca Mountain Project controlled Scientific Notebook No. 269. This work was performed in satisfaction of Level 4 Milestone SPAS11M4 (Roberts and Viani 1997a).

6.1.2 Samples

The samples received were the annular region of cores which are approximately 3 inches in length (the center sections were used for thermal expansion tests at Sandia National Laboratories). Each sample was crushed using an hydraulic press to < 1/4 inch, then processed through a flat-plate pulverizer until the entire sample passed a 250-μm sieve. After crushing, the samples were placed in a homogenizer for a period of at least 8 hours. A sub-sample of each was then further ground in a vibratory micro-mill (Fritsch) with a sintered corundum mortar and ball for 30 minutes at ~1/3 full power using an intermittent power cycle. Particle sizes determined optically by this method were approximately 10μm or less. The corundum internal standard used in the quantitative analyses (Buehler, 1.0-μm AL_20_3) was not ground because of its small size. The ground samples were mixed

Table 6-1. Mineral Abundances[1] for Samples from the Drift Scale Test Block

Sample #	Quartz	Cristobalite	Albite	Sanidine	Tridymite	Zeolite Phase	Data File [2]
SDM-MPBX1-1.0-1.2-D	12	23	34	32	nd[3]	nd[3]	YMP070A
SDM-MPBX1-21.0-21.2-D	10	27	25	35	3	nd[3]	YMP072A
SDM-MPBX1-21.0-21.2-D dup	9	27	25	35	4	nd[3]	YMP072B
SDM-MPBX1-31.9-32.1-D	4	31	32	33	nd[3]	nd[3]	YMP071A
SDM-MPBX1-40.4-40.6-D	20	14	31	29	7	nd[3]	YMP073A
SDM-MPBX1-62.0-D	11	26	27	36	nd[3]	nd[3]	YMP074A
SDM-MPBX1-80.7-80.9-D	12	24	31	33	nd[3]	nd[3]	YMP075A
SDM-MPBX2-29.0-29.2-D	4	31	33	32	nd[3]	nd[3]	YMP076A
SDM-MPBX2-29.0-29.2-D dup	4	29	34	33	nd[3]	nd[3]	YMP076B
SDM-MPBX2-48.6-D	18	18	30	34	nd[3]	nd[3]	YMP077A
SDM-MPBX2-72.0-D	6	28	34	32	nd[3]	nd[3]	YMP078A
SDM-MPBX2-85.0-D	7	26	34	33	nd[3]	nd[3]	YMP080A
SDM-MPBX3-17.5-17.7-D	8	25	33	34	nd[3]	nd[3]	YMP079A
SDM-MPBX3-38.5-38.7-D	5	31	24	40	nd[3]	nd[3]	YMP081A
SDM-MPBX3-85.6-D	11	22	30	34	nd[3]	3 - stilbite	YMP082A
AOD-HDFR#1-9.0-D	13	20	32	34	nd[3]	2 - clinoptilolite	YMP083A
AOD-HDFR#1-9.0-D dup	15	20	31	35	nd[3]	Trace - clinoptilolite	YMP083C
AOD-HDFR#1-48.5-D	12	25	26	37	nd[3]	nd[3]	YMP085A
AOD-HDFR#1-68.6-D	12	25	24	39	nd[3]	nd[3]	YMP086A
AOD-HDFR#1-98.0-D	37	4	29	30	nd[3]	nd[3]	YMP084A

[1] Mineral abundances were normalized to 100% after subtracting out the estimated abundance of the corundum standard. Sums may differ from 100% due to roundoff error.
[2] The identification YMP### refers to computer filenames associated with the diffraction pattern data.
[3] nd - not detected.

with corundum in a 4:1 ratio, and again placed in the micro-mill for 30 minutes using the power cycles described above. Samples were packed into stainless steel side-mount holders having a sample length of 18mm and width of 13mm.

6.1.3 Methodology

Mineral quantification involved two steps. First, the phases present in each sample were identified using an X-ray diffraction pattern processing software program (Jade version 3.0, Materials Data, Inc., Livermore, California) which utilizes data from the Joint Committee on Powder Diffraction Standards-Power Diffraction File. After the mineral phases were identified, then the Rietveld method of quantification was employed. A least squares refinement is carried out until the best fit is obtained between the entire observed powder diffraction pattern and the entire calculated pattern based on the crystal structures and lattice parameters of phases that are present. The Rietveld analyses were performed using quantitative X-ray diffraction software (Siroquant, version 2.0, Sietronics, Australia).

X-ray scans were collected using a Scintag PAD-V generator equipped with a Cu X-ray tube operated at 45 kV and 35 mA, and a Sieffert goniometer with a solid state detector. Diffraction patterns were collected in step scan mode at 2 seconds per 0.02° 2θ. Collimation was provided by a 1° divergence and 2° scatter slit on the X-ray tube and a 0.3 mm scatter and 0.2mm registration slit on the detector. Samples were scanned from 2-72° 2θ.

Prior to mineral phase identification and Rietveld analysis, the observed diffraction pattern was corrected for instrumental error based on a calibration curve determined using standard phases. The calibration correction used to correct data from this report was derived by scanning two standards: a fluorophlogopite mica for the low angle peaks (NBS traceable), and a mixture of silicon (NBS traceable)-tungsten-silver metals (SiWAg) for the high angle peaks. Both standards were scanned with the same instrumental parameters listed in the above section, the mica from 2-72° 2θ, and the SiWAg from 20-110° 2θ. The two scans were merged into one and a calibration curve built on observed versus the National Bureau of Standards and probability distribution or density function (Power Diffraction File) 2θ angles.

The Jade Pattern Processing Program was used to identify major and minor mineral phases present in each sample. The Jade program searches located peaks only, and compares them with the strongest lines of a potential phase in the Power Diffraction File database. The selected peaks are checked visually to confirm realistic phase identification.

The data in Table 6-1 were derived from the quantitative analysis results by subtracting out the estimated abundance of corundum, and normalizing the other phases to the remainder. The estimated abundance of corundum varied between 21.0 and 24.8 percent with a mean of 23.1 ± 1.0 percent. This suggests that there is a systematic overestimate of the corundum abundances by ~3 percent. However, the agreement between the calculated and observed patterns is good.

6.1.4 Results

Mineral abundances for 17 samples (plus duplicate scans) are shown in Table 6-1. In most samples, albite, sanidine, and cristobalite are the dominant phases, with lesser amounts of quartz. Tridymite is significant in 3 samples, with cristobalite being less abundant in these samples. Zeolite phases were observed in 3 samples, clinoptilolite in two samples, and stilbite in one sample. Compared to results of previous analyses of ESF TTF samples (Roberts and Viani 1997b, Viani and Roberts 1996), these samples show similar composition with regard to total silica polymorph content (between 33 and 41 weight percent). The quartz and cristobalite contents appear to be inversely related. No samples contained detectable mica phases. Duplicate scans show excellent reproducibility, the method appears to yield better precision than the matrix flushing method of Chung (1974).

As mentioned above, the total abundance of the silica polymorphs is quite uniform. However, the cristobalite component varies from 4 to 31 percent. Hence, the thermal/mechanical properties of these samples might be expected to differ significantly at the temperatures over which cristobalite undergoes a phase change.

6.2 PORE WATER ANALYSES

6.2.1 Objective and Description

The objective of analyses conducted on pore water and pore water salts extracted from dry-drilled core samples obtained from the DST block was to characterize in situ pore water in rock and to compare results with previous results from other data sets.

This data has been entered into Automated Technical Data Tracking and was submitted to the Records Center under the following DTNs and TDIF numbers: for strontium isotopes: DTN GS970508312272.002, TDIF 3060137; for uranium isotopes: DTN GS970508312272.001, TDIF 306136; for stable isotopes: DTN GS970608312272.004, TDIF 306141; for tritium analysis: DTN GS970608312272.005, TDIF 306145; and for sodium and potassium ratios: DTN GS970508312272.003, TDIF 3060138. Sample preparation procedures are summarized in Table 6-2. The following procedures were used: USGS TP GCP-12, USGS TP GCP-03, USGS TP HP-126, USGS TP GCP-17, and USGS TP HP-204. Scientific Notebook SN-0058 was also used for stable isotope analyses. The work in this section was completed in satisfaction of Level 4 Milestone SPH37DM4 (Yang et al. 1997). All data presented are qualified data.

6.2.2 Method

Strontium Isotopes—Borehole core samples from the DST block submitted for strontium and uranium analyses were cleaned with stainless steel wire brushes to remove fine cuttings, coarsely crushed in a laboratory jaw crusher, pulverized in a vertical rotary pulverizer, and sieved to obtain a sized fraction between 8-mesh and 60-mesh. Prior to crushing, each sample (composed of whole core and and pieces of core) was weighed: 10-3 (519g), 10-4 (470g), 14-2 (452g), 16-1 (297g), 20-1 (329g), and 21-5 (364g).

Table 6-2. Sample Preparation Procedures

Sample Name	SMF[1] Bar Code Number	Starting Material	Sieve Fraction (mesh size)	Additional Cleaning	Leach Procedure	Centrifugation	Filtration Time
UZ14-843'(-8+60) L1	SPC00035325	Borehole cuttings	<8, >60	none	10 min DI[2] H_2O in ultrasonic bath	no	~8 hrs
UZ14-843'(-8+60) L2	SPC00035325	Borehole cuttings	<8, >60	none	30 min DI H_2O leach w/ 15 min ultrasonic bath	yes	~30 min
UZ14-843'(-8+60) L3	SPC00035325	Borehole cuttings	<8, >60	none	15 hr DI H_2O leach w/ 15 min ultrasonic bath	yes	~1 hr
TA(433) 10-3a L	SPC01002487	Crushed core	<8, >60	none	5 min DI H_2O leach in ultrasonic bath	no	~15 min
TA(433) 10-3b L	SPC01002487	Crushed core	<8, >60	none	5 min DI H_2O leach in ultrasonic bath	yes	~5 min
TA(433) 16-1 L	SPC01002499	Crushed core	<8, >60	< 100 fraction removed with air	5 min DI H_2O leach (hand shaking)	4000 rpm for 6 min	~5 min
TA(433) 20-1 L	SPC01002507	Crushed core	<8, >60	< 100 fraction removed with air	5 min DI H_2O leach (hand shaking)	4000 rpm for 6 min	~5 min
TA(435) 10-4 L	SPC01002518	Crushed core	<8, >60	< 100 fraction removed with air	5 min DI H_2O leach (hand shaking)	4000 rpm for 6 min	~5 min
TA(435) 14-2 L	SPC01002526	Crushed core	<8, >60	< 100 fraction removed with air	5 min DI H_2O leach (hand shaking)	4000 rpm for 6 min	~5 min
TA(435) 14-2 (dust) L	SPC01002526	Crushed core		< 100 fraction removed with air	5 min DI H_2O leach (hand shaking)	4000 rpm for 6 min	~5 min
TA(435) 21-2 L	SPC01002538	Crushed core	<8, >60		5 min DI H_2O leach (hand shaking)	4000 rpm for 6 min	~5 min

[1]SMF Sample Management Facility
[2]DI deionized

Approximately 30g of the 20- to 60-mesh fraction were weighed into a teflon beaker and approximately 30g of high-purity, de-ionized water were introduced. The samples were placed into an ultrasonic bath for 15 minutes, then allowed to settle. The leachate was decanted into a 50ml centrifuge tube and after centrifuging for 10 minutes was transferred to a syringe tube with a 0.45 micron filter. The leachate was passed through a syringe filter into a teflon container and evaporated to dryness. The residue was brought into solution with 5ml of 1N HC1, and standard separation procedures were used to separate Sr from most elements. Sr mass spectrometric analyses were performed on a Finnigan MAT 262 mass spectrometer. The procedure followed was USGS Technical Procedure GCP-12, Rev. 4, *Rubidium - Strontium Isotope Geochemistry*. Comparable leaching studies of uncrushed cuttings of high-silica rhyolite from UZ-14 yielded comparable Sr isotopic ratios.

Uranium Isotopes—In preparation for determining uranium isotopic compositions of pore-water salts from core samples obtained in the Thermal Alcove, three separate leaching and analysis experiments were conducted on sieved cuttings from UZ-14. Borehole UZ-14 was used for comparison purposes. Cuttings were sieved to between an 8- and 60-mesh size and were subjected to deionized water leaches for 15 minute, 45 minute, and overnight durations. Measured $^{234}U/^{238}U$ activity ratios suggest that there are small but significant differences between the timed leaches, with the longest exposures able to extract additional ^{234}U from rock-surface sites. These results indicate that the shortest leach times that give adequate amounts of uranium for analysis yield isotopic compositions that are closest to readily-dissolved salts on pore-surfaces. (Note: $^{230}Th/^{238}U$ ratios were not measured since Th is insoluble.)

Six core samples from two DST block boreholes (numbers 182 and 184, ESF-HD-PERM-1 and -3) were analyzed for uranium isotopic compositions by thermal ionization mass spectrometry. Cores were crushed, sieved (between 8- and 60-mesh size), air-cleaned of fines, and leached in deionized water for 5 minutes. The procedure followed was USGS Technical Procedure GCP-03, Rev. 3, *Uranium-Thorium Disequilibrium Studies*.

Stable Isotopes—The stable hydrogen (δ^2-H) and oxygen ($\delta^{18}O$) isotopic compositions were determined for four water samples from the TTF with a VSMOW reference standard. These are pore waters distilled from core samples. The procedures followed were USGS Technical Procedure HP-126, Rev. 1, *Extraction of Residual Water for Tuff Samples by Vacuum Distillation*, and GCP-17, Rev. 3, *Determination of the Isotopic Ratio of H/D in H_20*. Scientific Notebook SN-0058 was also used.

Tritium Analyses—Tritium concentrations were determined for four pore-water samples extracted from cores for the ESF TTF. Water was vacuum-distilled and counted with a liquid scintillation counter to assay for the concentration of tritium. The procedures followed were USGS Technical Procedure HP-126, Rev. 1, *Extraction of Residual Water for Tuff Samples by Vacuum Distillation*, and HP-204, Rev. 0, *Liquid Scintillation Spectrometry Method for Tritium Measurement of Water Samples*.

Sodium-Potassium Ratios—Following the protocol used for dissolving pore-water salts for Sr-isotope analyses, leachates (approximately 30ml on approximately 30g of rock) were obtained for sodium and potassium analyses. These concentrations cannot be converted to the actual concentrations of the pore water, but the ratios of Na to K should be the same as those of the parent pore waters. High abundance of Na and K in pore-water makes the release of ions during crushing a comparatively minor influence. The procedure followed was USGS Technical Procedure HP-126, Rev. 1, *Extraction of Residual Water for Tuff Samples by Vacuum Distillation*.

6.2.3 Results

Strontium Isotopes—The $^{87}Sr/^{86}Sr$ ratios of 0.71238 to 0.71249 (see Table 6-3) for the pore-water salts are similar to values obtained for pore-water salts from samples of the crystal-poor zone of the Topopah Spring Tuff from borehole USW SD-7 and to values for perched water encountered in USW UZ-14. Samples from which the pore-water salts were analyzed represent distances into the rock mass of 6.4 to 16.4 m (21 to 54 feet). The nearly constant $^{87}Sr/^{86}Sr$ ratios for the pore water salts indicate that the pore waters are relatively homogeneous in composition over this scale. However, the $^{87}Sr/^{86}Sr$ values of the pore water salts are not in isotopic equilibrium with the bulk-rock which, on the basis of published analyses, is expected to have values in the range of 0.717 to 0.720. Strontium isotopic analyses of these particular bulk-rock samples will be completed in the future. These isotopic differences will allow minimum estimates of water flux through the matrix based on a reaction model developed by Johnson and DePaolo (1997) subject to the limitations of that model.

Uranium Isotopes—As shown in Table 6-4 and Figure 6-1, leachate U abundances were low (1 to 3ng from 100 to 200g of crushed rock) with measured $^{234}U/^{238}U$ activity ratios between 1.0 and 2.4. These values do show a dispersion outside of analytical uncertainties.

Stable Isotopes—As shown in Table 6-5, for all samples, the $\delta^{18}O$ values range from -13.3 to -12.3 per mil and the $\delta^{2}H$ values from -95 to -89 per mil relative to VSMOW. When compared to the ground water stable $\delta^{2}H$ and $\delta^{18}O$ isotopic compositions reported by Benson and McKinley in 1985, the TTF waters fall near the heavy isotope enriched part of that trend. These are also the ground waters with the youngest ^{14}C ages, which appear to represent recent recharge of the Fortymile Wash drainage system. The TTF water $\delta^{18}O$ values are comparable to those reported by Yang and others in 1996 for Topopah Spring Tuff pore waters from borehole USW UZ-14 and for perched waters. The $\delta^{2}H$ values of the ESF waters, however, are slightly heavier (several per mil) than those of either the UZ-14 pore water or the perched water data sets.

Tritium Analyses—Tritium concentrations of four pore-water samples extracted from cores from the ESF TTF are between 0 and 10.4 tritium unit (TU) (see Table 6-6). These values are significantly smaller than the values of 40 to 150 TU measured in the borehole-core samples of the Paintbrush nonwelded unit at Yucca Mountain which clearly establish the presence of post-bomb test tritium. Prior to 1952, natural tritium incorporated into ground water was produced only from cosmic radiation interacting with the nitrogen in the upper atmosphere. Historical concentrations in rain water in the middle latitudes were on the order of 10 TU, one TU being equal to one tritium atom per 10^{18} atoms of ^{1}H. Between 1952 and 1963 nuclear tests in the northern hemisphere produced significant amounts of tritium in the Earth's atmosphere. In 1963, a yearly average value of 2,700 TU in precipitation near Salt Lake City, Utah was reported. Considering the analytical uncertainties (1 sigma in the table), the low tritium values obtained for the pore-water samples from the TTF must be considered to be at or below detection limits. Therefore, it is likely that these waters are of the pre-bomb pulse age.

Table 6-3. $^{87}Sr/^{86}Sr$ Ratios[a]

Date of Analysis	SMF[b] Identification	Sample Coordinates	Machine	Raw $^{87}Sr/^{86}Sr$	Corrected $^{87}Sr/^{86}Sr$
7.05.06	1002487	(433) ESF-HD-PERM-1, 22.7 ft.	Finnigan MAT262	0.71235	0.71244 ± 0.00001
7.05.07	1002518	(435) ESF-HD-PERM-3, 23 ft.	Finnigan MAT262	0.71240	0.71249 ± 0.00003
7.05.07	1002499	(433) ESF-HD-PERM-1, 40.7 ft.	Finnigan MAT262	0.71233	0.71242 ± 0.00001
7.05.07	1002507	(433) ESF-HD-PERM-1, 54 ft.	Finnigan MAT262	0.71229	0.71238 ± 0.00001
7.05.07	1002538	(435) ESF-HD-PERM-3, 53 ft.	Finnigan MAT262	0.71233	0.71242 ± 0.00001
7.05.08	1002526	(435) ESF-HD-PERM-3, 35.1 ft.	Finnigan MAT262	0.71235	0.71244 ± 0.00001

[a]Raw ratios are corrected for mass fractionation using a value for $^{88}Sr/^{86}Sr$ of 0.1194. Corrected ratios are adjusted to a sea water value of $^{87}Sr/^{86}Sr$ of 0.7092.
[b] SMF: Sample Management Facility

Table 6-4. Summary of Uranium Isotopic Data on Pore-Water Leaches from Borehole Cuttings, Crushed Core, and Fracture Water[a]

Sample Name	Borehole Identification	Footage	Rock/water wt. (g)	Leach wt.[b] (g)	U Abundance (ng)	U Concentration[c] (ppb)	$^{234}U/^{238}U$ Activity (2σ)
UZ14-843' (-8+60) L1	USW UZ-14	843'	214.22	0.19	7.37	39	1.403 (0.028)
UZ14-843' (-8+60) L2	USW UZ-14	843'	215.40	0.17	2.99	18	2.046 (0.087)
UZ14-843' (-8+60) L3	USW UZ-14	843'	212.52	0.25	0.79	3.2	2.60 (0.23)
TA(433) 10-3aL	Thermal Alcove Borehole (433) ESF-HD-PERM-1	22.7'-23.1'	140.45	2.29	1.13	0.49	1.60 (0.11)
TA(433) 10-3bL	Thermal Alcove Borehole (433) ESF-HD-PERM-1	22.7'-23.1'	178.71	3.18	1.22	0.38	2.12 (0.13)
TA(433) 16-1 L	Thermal Alcove Borehole (433) ESF-HD-PERM-1	40.7'-41.1'	111.49	0.42	1.13	2.7	1.035 (0.085)
TA (433) 20-1 L	Thermal Alcove Borehole (433) ESF-HD-PERM-1	54.0'-54.4'	95.96	0.32	2.36	7.4	1.156 (0.052)
TA(435) 10-4 L	Thermal Alcove Borehole (435) ESF-HD-PERM-3	23.0'-23.5'	244.44	1.17	1.17	1.00	2.37 (0.15)
TA(435) 14-2 L	Thermal Alcove Borehole (435) ESF-HD-PERM-3	35.1'-35.6'	206.55	0.83	2.78	3.4	1.761 (0.057)
TA(435) 14-2 (dust) L	Thermal Alcove Borehole (435) ESF-HD-PERM-3	35.1'-35.6'	19.48	0.05	1.11	22	1.437 (0.102)
TA(435) 21-21	Thermal Alcove Borehole (435) ESF-HD-PERM-3	53.0'-53.4'	148.86	0.36	2.21	6.1	1.694 (0.065)
SPC00520853	ESF TTF: SHT, Borehole 16, Interval 4	Water	349.15		35.37	0.101	8.032 (0.111)

[a] Uranium isotopic data obtained by mass spectrometry at U.S. Geological Survey, Denver, Colorado.
[b] Leach weight represents total weight of all dissolved materials (weight of rock after leaching subtracted from the weight of rock before leaching).
[c] U Concentration represents the concentration of U relative to the weight of the total dissolved materials (leach wt.) except the SPC00520853 water sample where the U concentration represents the concentration of U relative to the weight of water used.

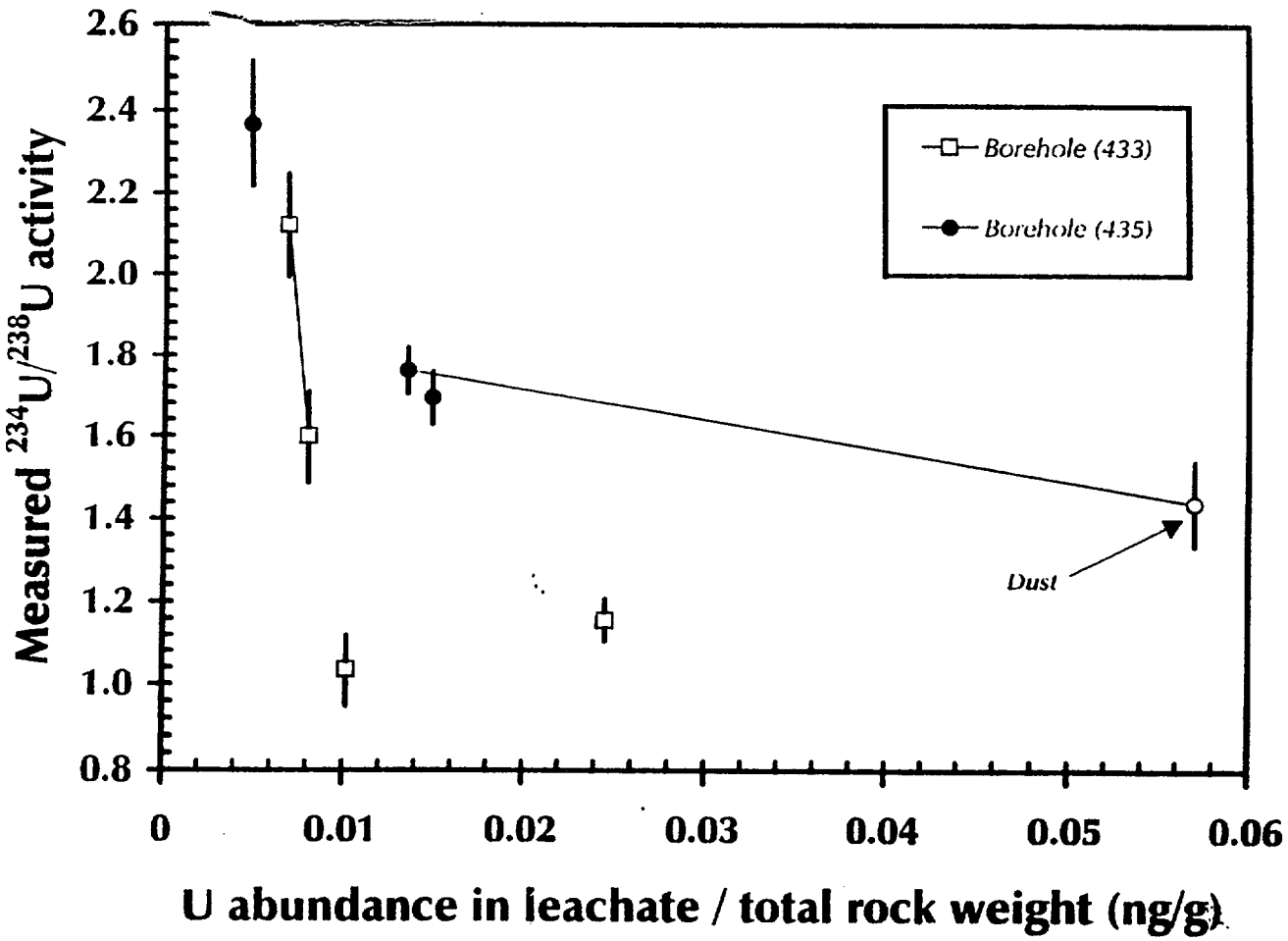

Figure 6-1. U Abundance in Pore-Water Leachates

Sodium-Potassium Ratios—The Na/K ratios of the pore-water salts, presented in Table 6-7, show substantial apparent scatter from 4.9 to 6.4 (weight ratios). However, most of this variation can be attributed to a ±0.1mg/L uncertainty in the atomic adsorption analyses of K. Thus, within the sensitivity of the method, the Na/K ratios can be considered to be uniform among the samples, with an average value of 5.6. The native waters from the perched and saturated zones are characteristically sodium-rich relative to potassium. Thus, the pore waters are similar in this parameter.

Table 6-5. Stable δ^2H and $S^{18}O$ Values

Sample Number	Log Number	$\delta^{18}O_{smow}$ [a]	δ^2H_{smow}
ESF-HD/PERM-1/35.0-35/6/A/D	227-H-7		-91.6
ESF-HD/PERM-1/35.0-35.6/A/D	227-H-8		-94.3
ESF-HD/PERM-1/35.0-35.6/A/D	169-W-6	-12.7	
ESF-HD/PERM-1/37.5-38.1/A/D	227-H-5		-93.0
ESF-HD/PERM-1/37.5-38.1/A/D	227-H-6		-94.0
ESF-HD/PERM-1/37.5-38.1/A/D	169-W-7	-12.7	
ESF-HD/PERM-1/41.1-41/3/A/D	227-H-1		-89.7
ESF-HD/PERM-1/41.1-41.3/A/D	227-H-2		-88.9
ESF-HD/PERM-1/41.1-41/3/A/D	169-W-8	-12.3	
ESF-HD/PERM-1/43.9-44.4/A/D	227-H-3		-94.6
ESF-HD/PERM-1/43.9-44.4/A/D	227-H-4		-95.2
ESF-HD/PERM-1/43.9-44.4/A/D	169-W-9	-13.5	
ESF-HD/PERM-1/43.9-44.4/A/D	169-W-10	-13.1	
SLAP[b] #158 SPL3	226-H-11		-427.0
SLAP #158 SPL3	226-H-12		-429.0
SLAP #158 SPL3	169-W-4	-55.9	
SLAP #158 SPL3	169-W-5	-55.1	
SLAP #158 SPL3 4-17-97	NA		-431.2
SLAP #158 SPL3 4-17-97	NA		-424.8
VSMOW[c]	226-H-13		0.2
VSMOW	226-H-14		-0.2
VSMOW	169-W-2	-0.1	
VSMOW	169-W-3	0.1	
VSMOW 4-17-97	NA		-0.1
VSMOW 4-17-97	NA		0.1

[a] Standard Mean Ocean Water
[b] Standard Light Anarctic Precipitation
[c] Vienna Standard Mean Ocean Water

NOTE: Values are corrected for SMOW/SLAP stretching.

Table 6-6. Tritium Data

Sample Identification	Collection Date	Analysis Date	CPM*	TU
ESF/PERM-1/35.0-35.6	04/01/97	06/01/97	1.355	-4.7 ± 4.1
ESF/PERM-1.37.5-38.1	04/01/97	06/01/97	1.422	0.5 ± 4.1
ESF/PERM-1/41.1-41.3	04/01/97	06/01/97	1.480	4.9 ± 4.2
ESF/PERM-1/43.9-44.4	04/01/97	06/01/97	1.552	10.4 ± 4.2
Background/Arvada Well Water	04/01/97	06/01/97	1.416	

* Counts per Minute

NOTE: All uncertainties are 1 sigma. Negative TU values can occur because the net tritium count rate is the difference between the count rate of the sample and that of a tritium-free sample (background sample). Given a set of "unknown" samples with no tritum, the distribution of net results should become symmetrical around 0 TU. The negative values are reported here for the benefit of allowing the user unbiased statistical treatment of the data. For other applications, 0 TU should be used.

Table 6-7. Sodium-Potassium Ratios

SEQUENCE/ SAMPLE NUMBER	ANALYSIS			
	POTASSIUM-ICP[a] (mg/L)	POTASSIUM-AA[b] (mg/L)	SODIUM-ICP[a] (mg/L)	SODIUM-AA[b] (mg/L)
03/13.8 21.2-22.4	2	2.2	31.0	3.2
01/10.3 22.7-23.1	<1	0.8	3.9	4.3
02/10.4 23.0-23.5	<1	0.8	4.4	4.8
04/14.2 35.1-35.6	1	0.8	4.3	4.8
05/16.1- 47.7-41.1	<1	0.7	4.0	4.5
06/20.1 54.0-54.4	<1	0.8	3.7	4.0
07/20.2 53.0-53.4	<1	0.8	3.6	3.9

[a] Inductively-Coupled Plasma
[b] Atomic Absorption

NOTE: Sample 03/13.8 21.2-22.4 is a QA sample. The USGS reference number is M-138 which has potassium (K) and sodium (Na) concentrations of 1.82 and 31.6 mg/L respectively.

7. FIELD MEASUREMENTS: FRACTURE MAPPING

7.1 OBJECTIVE AND DESCRIPTION

The objective of the geologic mapping in the DST block was to determine the vertical and horizontal variability of fracture networks and lithophysal zones and to identify values for parameters to be used for rock mass classification.

The data in this section have been entered into automated Technical Data Tracking and were submitted to the Records Center under DTN GS970608314224.007 and GS970608314224.006 and TIDF 306177 and 306176. The procedure used was USGS TP GP-32. The work in this section was completed in satisfaction of Level 4 Milestone SPG42FM4 (Steighner and Singleton 1997). The data in this section are considered qualified data.

7.2 METHODOLOGY

Mapping in the TTF was done essentially to the same standards used in the ESF Main Drift, using technical procedure NWM-USGS-G-32. From these procedures, the U.S. Geological Survey/U.S. Bureau of Reclamation (USGS/USBR) used full-periphery mapping techniques and detailed line surveys (DLSs) to characterize the rock and fractures in the TTF.

The following line survey procedure was used.

General—Geologic mapping in the thermal test alcove included recording lithostratigraphic and structural features on 1:125 scale drawings. Maps were developed in the full-periphery style in which the tunnel walls were "unrolled" to produce a flat map of the tunnel periphery. Discontinuities and lithostratigraphic contacts with trace lengths longer than 1m were recorded on the field sheets. The orientation of geologic features was determined using a goniometer for strike azimuth and a clinometer for dip values. Discontinuity orientations were recorded using the right-hand rule, where dip direction is 90° to the right (clockwise) of strike. Traces of lithostratigraphic and structural features were sketched onto the geologic drawings and later digitized with AutoCAD.

DLSs were generally conducted along the right wall, approximately one meter below the springline. A metric measuring tape was affixed to the wall and discontinuities with trace lengths longer than 30 cm were reported on the survey. Discontinuities that intersected the wall within 30 cm above and below the tape area were also considered. Strike azimuth, dip, discontinuity type, trace length, number of visible fracture terminations and types of terminations, aperture, roughness, infilling type, and thickness were recorded in the DLS notebook in tabular form. These data were then transferred to a database.

Fractured Wedge—Fractures along a wedge were projected along the strike to the DLS tape. The fracture stations were recorded, and the RQD (Deere 1963; Deere and Deere 1988) was calculated normally using only the fracture stations. The notation fw for fractured wedge and dw for deep wedge were optionally noted on the RQD scanline form. Fracture stations did not necessarily project to the DLS tape in numerical order, so data was sorted and entered into the spreadsheet in increasing station order.

Subparallel Fractures—Fractures which strike nearly parallel to the hypothetical borehole, or low angle fractures, produce a theoretical longitudinal fracture of the core. For this condition, the length of fracturing was assigned a zero RQD value. The beginning station was recorded and identified with the notation pf. The ending station was recorded and identified with the notation EZ. This RQD value represents the most conservative approach. This procedure differs slightly from Deere's (1963) procedure which states that subparallel fractures should be treated the same way as any other fracture, by determining where it intersects the centerline of the core.

Fractures Behind Steel Sets—In areas supported by steel sets, an accurate station for fractures behind the set can be recorded. Where fracturing on either side of the steel sets suggests fracturing behind the steel sets, an estimated station for the inferred fractures was recorded and an RQD was calculated using these fractures.

Lithophysal—Lithophysae encountered in core drilling would produce a length of borehole with no core recovery. For reaches through lithophysal zones, cavities larger than about 50 mm were excluded from the theoretical length of intact rock. The notation lith and EZ were used on the scanline forms either to identify the location of lithophysae cavities or to estimate an overall length reduction due to the cavities. This procedure of "zeroing out" lithophysae zones produces a more conservative or lower RQD value. Lithophysae might not produce sliding planes, which affect stability. This particular issue is not addressed by Deere (1963) or in any other current publications.

Fracture stations and notations on the Scanline RQD field form were entered into a spreadsheet to calculate a line survey RQD. The same tape was used to determine the RQD. For the RQD, all natural fractures were considered, thereby ignoring mechanical breaks, which can be determined from natural fractures, as a result of drilling or blasting. Either the station of each individual fracture was recorded, or the beginning and ending stations of zones with zero RQDs were recorded.

The fundamental assumption for the calculation of a RQD using the scanline data is that the length of rock between recorded fractures is intact rock. From that assumption, the total of intact rock pieces which are longer than 10cm are determined from the fracture spacing. That length, expressed as a percentage of the total length, is the line survey RQD. Note: This technique does not depend on an assumed fracture spacing distribution. In fact, the fracture-spacing distribution may be deduced from the RQD data collected in this procedure. The directional bias associated with a line survey in one direction is not eliminated.

The paragraphs below list several details applied to standardize the line survey RQD procedure.

Fracture Zones—An area of closely spaced fractures was described by noting the beginning and ending stations of the zone. Individual fractures were not recorded. The average fracture spacing was estimated. On the RQD Scanline form, the notations fz and EZ were used to identify the beginning and ending stations of a fracture zone. The calculated length of intact rock was zero through these zones.

Shallow Wedge—Generally, this wedge will result from the intersection of two fractures subparallel to the scanline. This shallow wedge appears to fracture the hypothetical core so that the shortest side of the core is less than 100mm. The length between beginning and ending fractures was not counted

as intact rock for calculation for the RQD. The beginning and ending stations of this zero RQD zone were identified on the scanline form as sw and EZ.

7.3 RESULTS

Full periphery geotechnical maps for the DST connecting drift are presented in Figures 7-1 through 7-3, and Figures 7-4 through 7-6 for the DST heated drift.

The lithology of the unit consists of densely welded, devitrified tuff of rhyolitic composition, containing vapor phase minerals and about 1 percent phenochrysts, chiefly feldspar and biotite (Geslin et al. 1995). Matrix colors are a variable mixture of reddish purple (5RP5/2), or pale red (5R4/2) and light brown (5YR5/6) with wisps of very light gray (N8). Pumice (less than 5%) is mostly less than 20 mm, spherulitic, and grayish brown (5YR3/2) to very light gray (N8). Volcanic lithics (1 - 2%) are light gray (N8), less than 10 mm in size, and locally have very light gray (N8) rims. Lithophysae are rare (less than 1%), and range in size up to 80 mm, with vapor-phase minerals and very light gray (N8) rims and spots. Short (10 - 20 cm), discontinuous, subhorizontal vapor phase partings are present throughout the unit, while the more developed subhorizontal partings from bedding plane features are on the order of meters apart.

Begin Station: 0 **End Station:** 20 **Date:** 04 Apr 97
Rated by: John Steighner

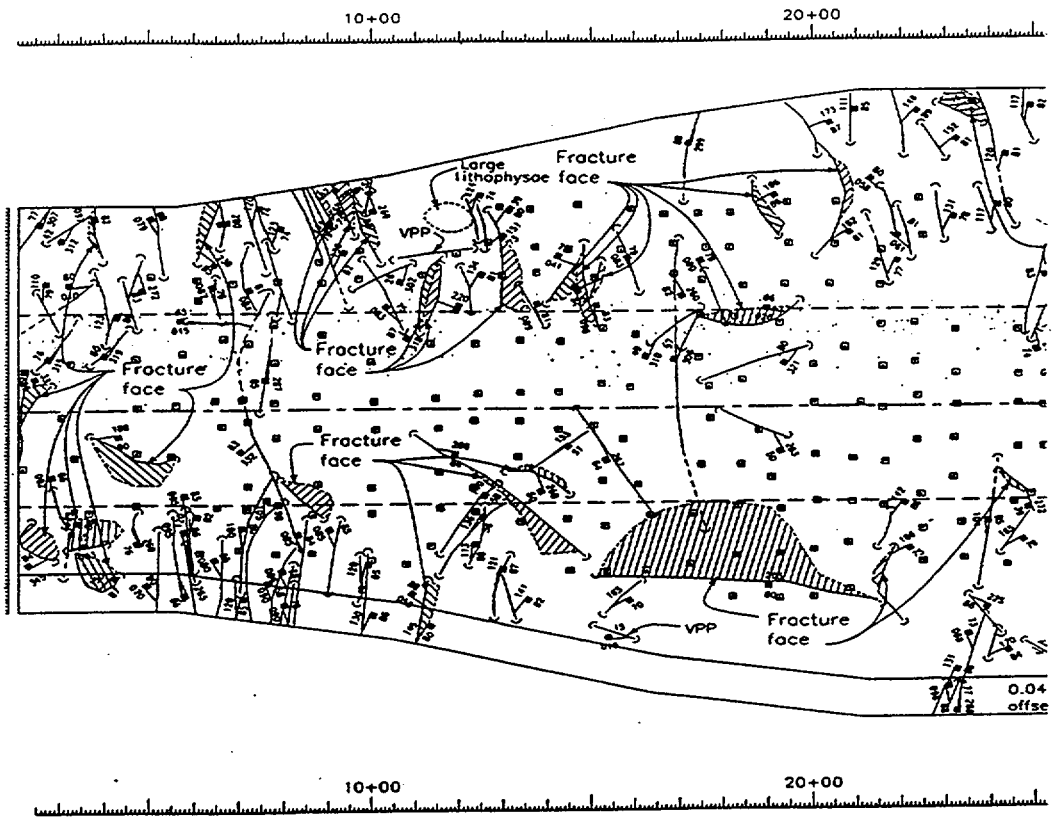

DST Connecting Drift

Q Rating Parameters				
Begin Station	0	5	10	15
End Station	5	10	15	20
Mapped RQD*	86	73	79	71
Jn*	9	9	9	9
Jr*	3	2	3	3
Ja*	2	2	2	2
Jw*	1	1	1	1
SRF*	1	1	1	1
Q-rating*	14	8.1	13	12
Qualitative Description	Good	Fair	Good	Good
Initiated Ground Support Category	1	1	1	1

*see acronym list

RMR Rating Parameters				
Begin Station	0	5	10	15
End Station	5	10	15	20
Mapped RQD*	86	73	79	71
RQD Index*	17	13	17	13
C*	12	12	12	12
Js*	15	10	10	10
Jc*	24	22	25	22
Jw*	15	15	15	16
JOA*	-12	-5	-12	-5
RMR rating*	71	67	67	67
Qualitative Description	Good	Good	Good	Good

Figure 7-1. Rock Mass Classification of the DST Connecting Drift from Station 0+00 to 20+00 m

Begin Station: 20 **End Station:** 40 **Date:** 04 Apr 97
Rated by: John Steighner

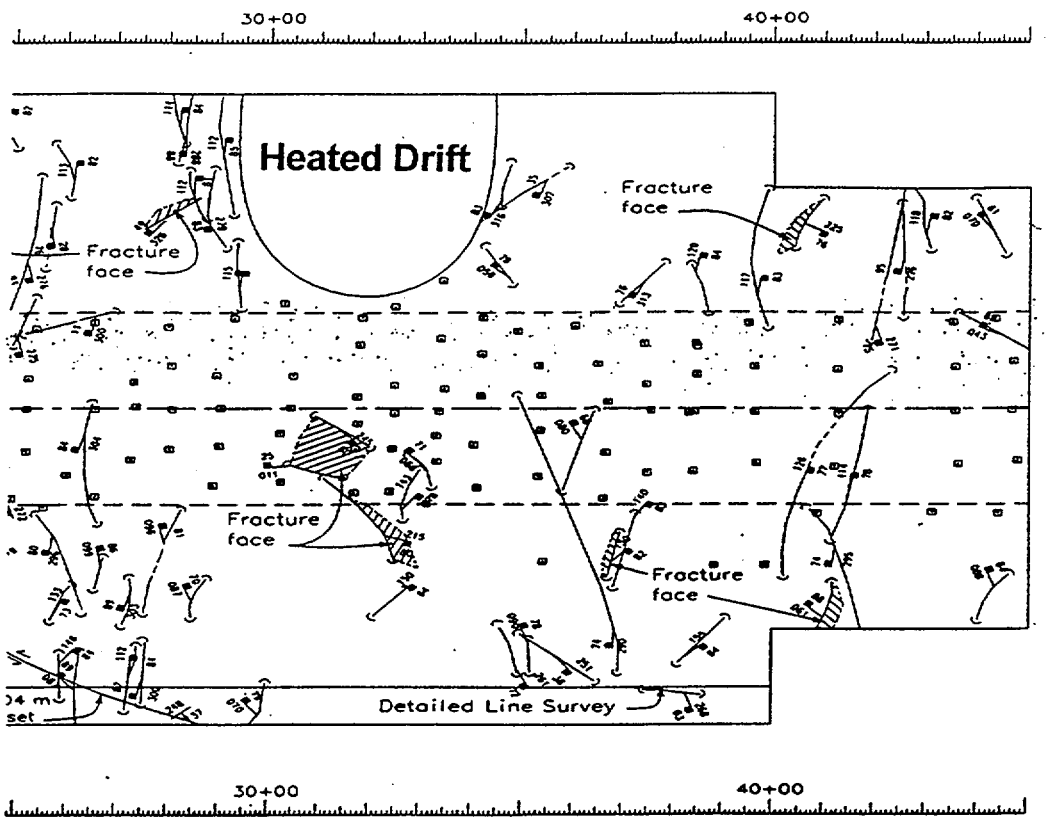

DST Connecting Drift

Q Rating Parameters				
Begin Station	20	25	30	35
End Station	25	30	35	40
Mapped RQD*	70	54	74	62
Jn*	9	9	12	12
Jr*	2	2	2	2
Ja*	2	2	2	2
Jw*	1	1	1	1
SRF*	1	1	1	1
Q-rating*	7.8	6	6.2	5.2
Qualitative Description	Fair	Fair	Fair	Fair
Initiated Ground Support Category	1	1	1	1

*see acronym list

RMR Rating Parameters				
Begin Station	20	25	30	35
End Station	25	30	35	40
Mapped RQD*	70	54	74	62
RQD Index*	13	13	13	13
C*	12	12	12	12
Js*	15	15	15	0
Jc*	20	22	23	18
Jw*	15	15	15	15
JOA*	-12	-12	-12	0
RMR rating*	63	65	66	58
Qualitative Description	Good	Good	Good	Fair

Figure 7-2. Rock Mass Classification of the DST Connecting Drift from Station 20+00 to 40+00 m

Begin Station: 40 **End Station:** 45 **Date:** 07 May 97
Rated by: Bill Singleton

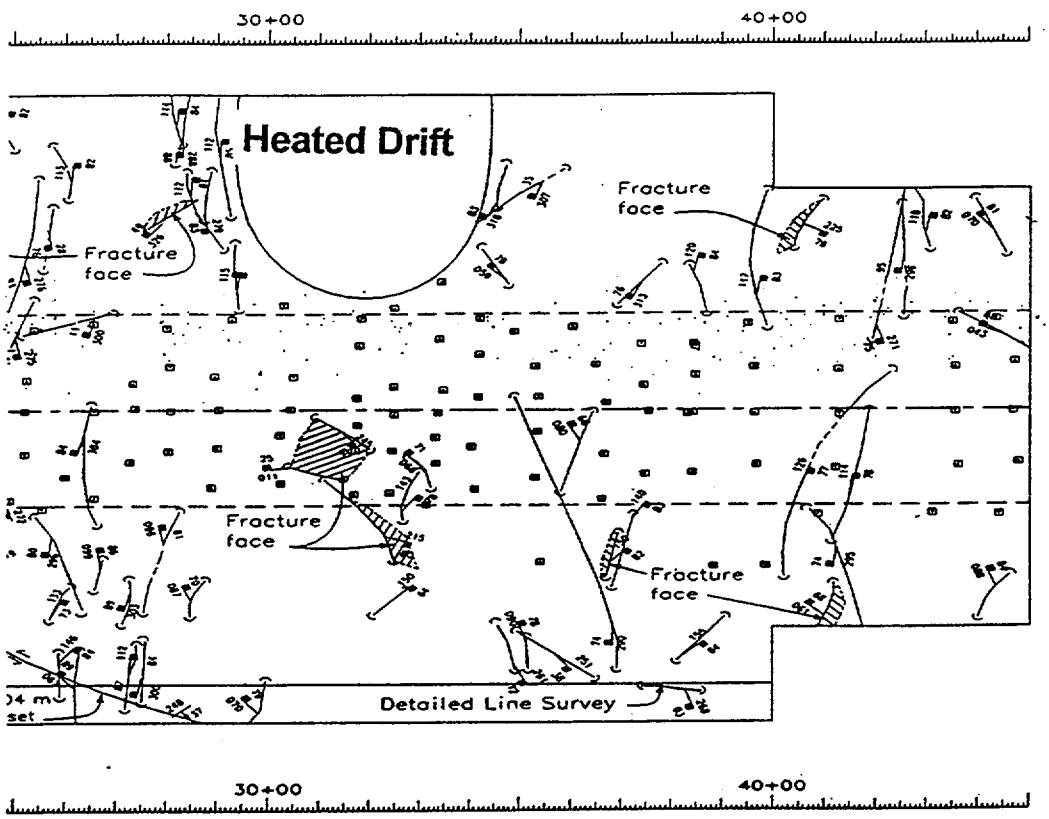

DST Connecting Drift

Q Rating Parameters				
Begin Station	40			
End Station	45			
Mapped RQD*	64			
Jn*	12			
Jr*	2			
Ja*	2			
Jw*	1			
SRF*	2.5			
Q-rating*	2.1			
Qualitative Description	Poor			
Initiated Ground Support Category	1			

RMR Rating Parameters				
Begin Station	40			
End Station	45			
Mapped RQD*	64			
RQD Index*	13			
C*	12			
Js*	8			
Jc*	16			
Jw*	15			
JOA*	-12			
RMR rating*	52			
Qualitative Description	Fair			

*see acronym list

Figure 7-3. Rock Mass Classification of the DST Connecting Drift from Station 40+00 to 45+00 m

Begin Station: 0 **End Station:** 20 **Date:** 07 May 97
Rated by: Bill Singleton

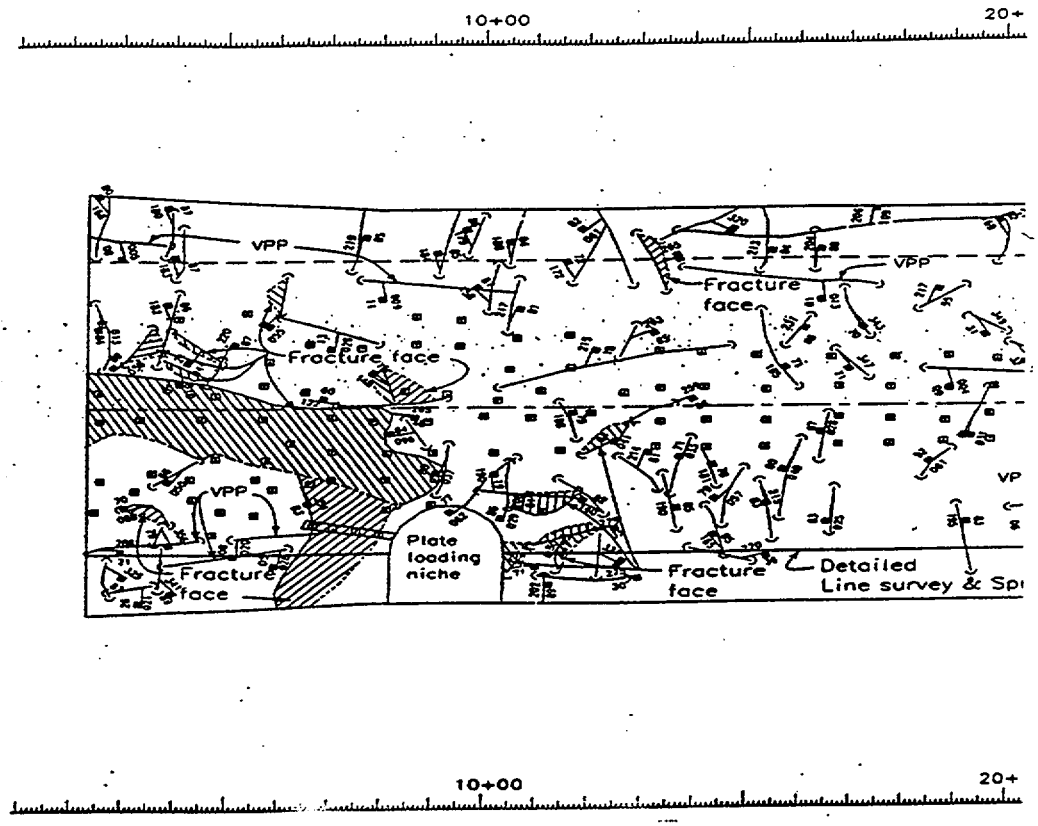

DST Heated Drift

Q Rating Parameters				
Begin Station	0	5	10	15
End Station	5	10	15	20
Mapped RQD*	80	NR	78	69
Jn*	12	NR	9	12
Jr*	3	NR	1	1
Ja*	2	NR	2	2
Jw*	1	NR	1	1
SRF*	2.5	NR	1	1
Q-rating*	4	NR	4.3	2.9
Qualitative Description	Fair	NR	Fair	Poor
Initiated Ground Support Category	1	1	1	1

RMR Rating Parameters				
Begin Station	0	5	10	15
End Station	5	10	15	20
Mapped RQD*	80	NR	78	69
RQD Index*	17	NR	17	13
C*	12	NR	12	12
Js*	8	NR	8	8
Jc*	18	NR	18	18
Jw*	15	NR	15	15
JOA*	-12	NR	-5	-5
RMR rating	58	NR	65	61
Qualitative Description	Fair	NR	Good	Good

*see acronym list

NOTE: The section from station 5 to 10 was **Not Rated (NR)** because the plate loading niche didn't allow for accurate data gathering.

Figure 7-4. Rock Mass Classification of the DST Heated Drift from Station 0+00 to 20+00 m

Begin Station: 20 End Station: 40 Date: 10 Apr 97
Rated by: Bill Singleton

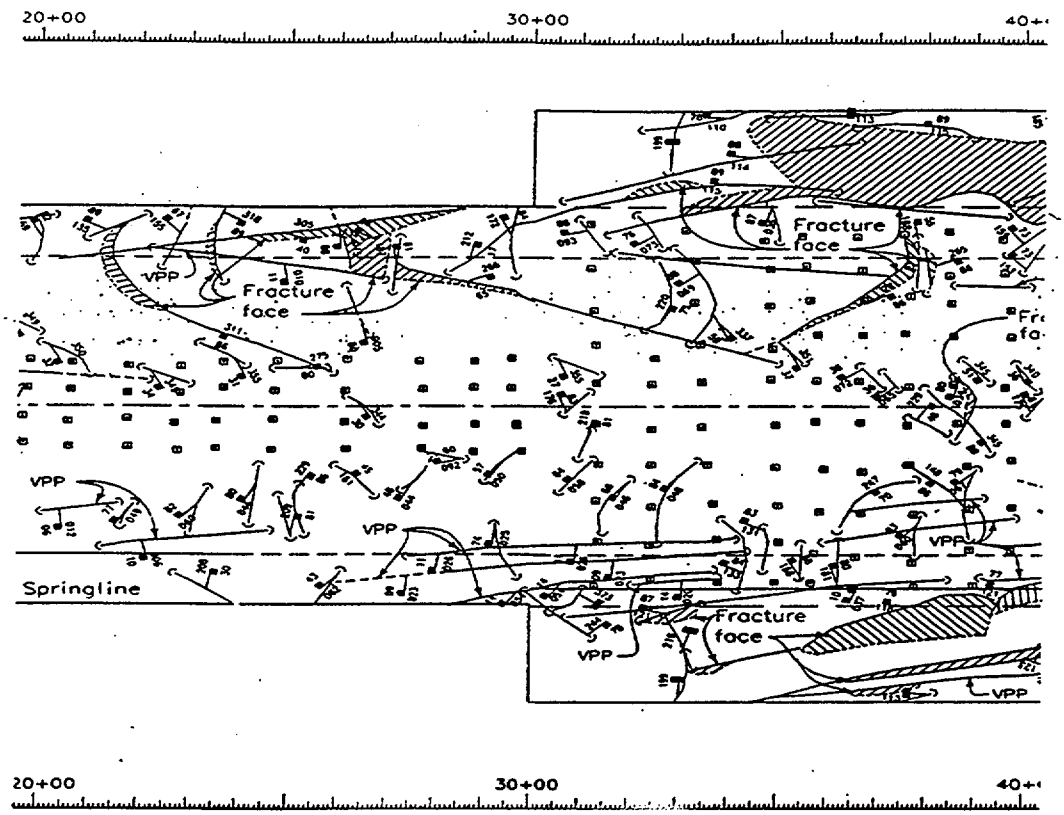

DST Heated Drift

Q Rating Parameters				
Begin Station	20	25	30	35
End Station	25	30	35	40
Mapped RQD*	90	76	77	67
Jn*	12	9	9	9
Jr*	3	3	3	3
Ja*	2	2	2	2
Jw*	1	1	1	1
SRF*	1	1	1	1
Q-rating*	11	13	13	11
Qualitative Description	Good	Good	Good	Good
Initiated Ground Support Category	1	1	1	1

RMR Rating Parameters				
Begin Station	20	25	30	35
End Station	25	30	35	40
Mapped RQD*	90	76	77	67
RQD Index*	20	17	17	13
C*	12	12	12	12
Js*	10	8	15	15
Jc*	23	23	22	22
Jw*	15	15	15	15
JOA*	-5	-5	-12	-12
RMR rating*	75	70	69	65
Qualitative Description	Good	Good	Good	Good

*see acronym list

Figure 7-5. Rock Mass Classification of the DST Heated Drift from Station 20+00 to 40+00 m

Begin Station: 40 **End Station:** 60 **Date:** 24 Feb 97
Rated by: Bill Singleton

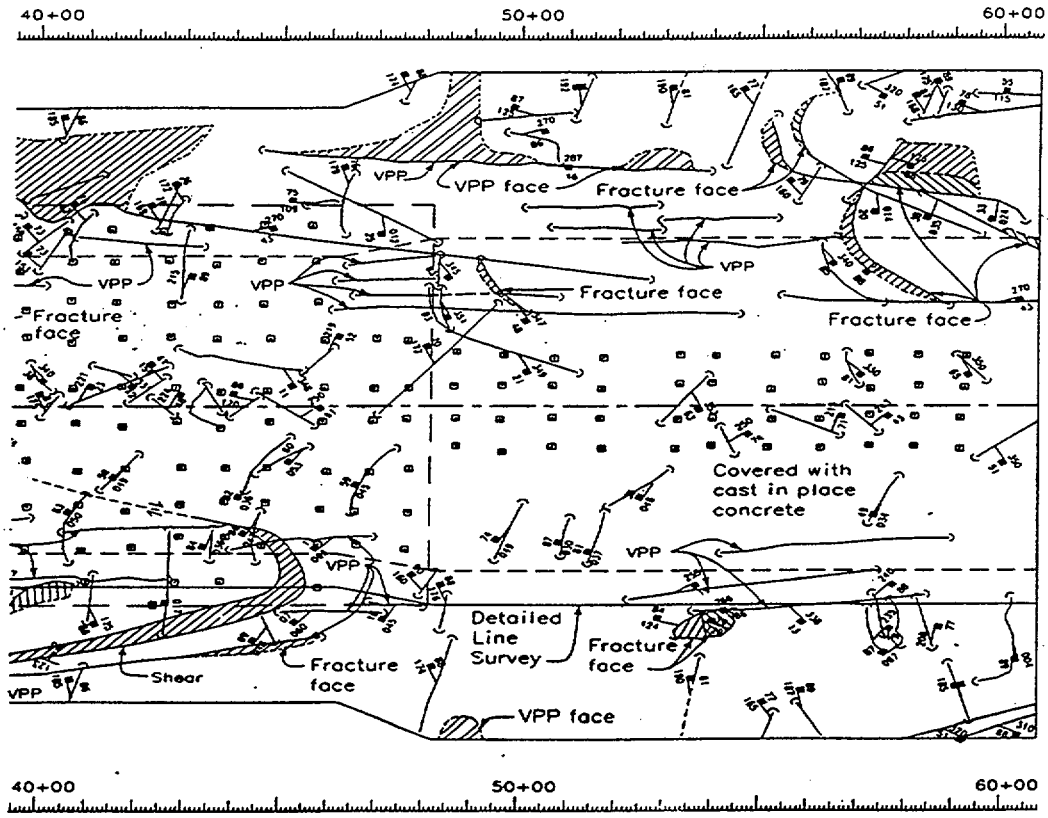

DST Heated Drift

Q Rating Parameters				
Begin Station	40	45	50	55
End Station	45	50	55	60
Mapped RQD*	83	58	59	54
Jn*	15	15	15	15
Jr*	3	3	2	2
Ja*	2	2	2	2
Jw*	1	1	1	1
SRF*	2.5	1	1	1
Q-rating*	3.3	5.8	3.9	3.6
Qualitative Description	Poor	Fair	Poor	Poor
Initiated Ground Support Category	1	1	1	1

RMR Rating Parameters				
Begin Station	40	45	50	55
End Station	45	50	55	60
Mapped RQD*	83	58	59	54
RQD Index*	17	13	13	13
C*	12	12	12	12
Js*	15	8	8	8
Jc*	24	23	23	23
Jw*	15	15	15	15
JOA*	-12	-5	-12	-12
RMR rating*	71	66	59	59
Qualitative Description	Good	Good	Fair	Fair

*see acronym list

Figure 7-6. Rock Mass Classification of the DST Heated Drift from Station 40+00 to 60+00 m

INTENTIONALLY LEFT BLANK

8. FIELD MEASUREMENTS: ROCK MASS CLASSIFICATION

8.1 OBJECTIVE AND DESCRIPTION

The objective of rock mass quality assessments in the TTF was to assess the stability of the local rock mass, to assist in the location for instrument placement, and to provide estimates of the representativeness of test locations. Rock mass quality assessments were performed in all of the thermal testing excavations using line mapping surveys and are reported in both the Q rating system (Barton et al. 1974) and the RMR system (Bieniawski 1974), and using Schmidt Hammer Rebound Index Testing as a non-qualified activity.

Rock mass quality indices were collected following Sandia National Laboratories Technical Procedure-234 Revision 01, utilizing the data reduction program TBM.exe Version 4.5 and 4.51, under Work Agreement-0065 Revision 04. The data concerning the DST have been submitted under TDIF 306063 (DTN SNF32020196001.015). Related data surrounding the SHT have been submitted under TDIF 305579 (DTN SNF32020196001.010). Rock mass quality assessment was performed in satisfaction of Level 4 Milestone SP5140M4 (Lum 1997). All data in this section are qualified.

8.2 METHODOLOGY

Both the Q rating and RMR systems empirically relate rock mass properties such as fracture characteristics, intact rock strength, and geometry to predictions of stability and ground support requirements. Both systems broadly categorize the quality of the rock mass as either very poor, poor, fair, good, very good. These qualities are related to ground support classes with a range of ratings from 1 to 5. RMR and Q ratings correspond to the following categories:

RMR Rating				Q Rating			
0	-	20	very poor	0.001	-	1.0	very poor or worse
21	-	40	poor	1	-	4	poor
41	-	60	fair	4	-	10	fair
61	-	80	good	10	-	40	good
81	-	100	very good	40	-	1000	very good or better

Schmidt Hammer Rebound Index testing, performed as a non-qualified activity, provides empirical information on intact rock strength and modulus. Schmidt Hammer Rebound Index testing will be conducted throughout the repository to provide information on the spatial variability of rock matrix mechanical properties.

RMR and Q indices are calculated from parameters related to degree of jointing, interaction of joint orientations to form blocks, joint frictional strength versus active stress, and hydraulic conditions. Because of the parameters used in their derivation, RMR and Q indices are also useful as indicators of general structural conditions.

RMR and Q indices were determined on 5-meter intervals, through the main drift of the ESF and the TTF. The TTF is located at station 28 + 27 m in the main drift and is entirely contained in the Tptpmn lithostratographic unit which forms the upper portion of the thermal/mechanical unit Topopah Spring Welded Unit Lithophysal-Poor (TSw2). The RMR and Q indices were measured from station 00 + 60 to 01 + 35 m in the observation drift, from station 00 + 03 to 00 + 45 m in the connecting drift, and station 00 + 03 to 00 + 60 m in the heated drift (Figure 1-1).

8.3 RESULTS

While some structural variations within the heated drift were observed, the Q and RMR indices were found to be relatively consistent with those found from the repository horizon TSw2 and did not display any significant systematic variation relative to location. The Q and RMR indices are presented in Tables 8-1 and 8-2, respectively, and in Figures 8-1 through 8-4. Note that these tables and figures include data that were previously presented as part of the SHT block characterization (CRWMS M&O 1996), specifically the observation drift from station 5 to station 60, the thermomechanical alcove/SHT, and the thermomechanical alcove extension.

Surrounding the DST block, Q indices ranged from 0.761 to 621.875, while RMR indices ranged from 51.1 to 97.0 (Figure 8-1, and 8-2; Table 8-1 and 8-2). Both Q and RMR indices were relatively constant through the TTF, with relatively little scatter in values. The range in Q and RMR indices from the TTF was relatively limited compared to that observed from the main drift (Figures 8-3 and 8-4).

During data collection, several observations of the existing geologic and structural conditions were made. These observations are summarized below:

- The rock faces exposed throughout the connecting drift alcove are massive with little jointing and no brecciation. This is reflected in the slightly elevated Q and RMR values from the connecting drift when compared to the values from adjacent drifts (Figure 8-1 and 8-2).

- Within the heated drift, at approximately 12.5 m, there was a change in excavation technique from drill and blast to the alpine miner. Compared to drill and blast, the alpine miner tends to produce a much smoother excavated surface, homogenizes the texture of the exposed face, and minimizes the exposed joint faces. Because the alpine miner tends to minimize the joint face exposure, areas excavated by this method will have elevated Q and RMR values when compared to areas excavated by drill and blast. However, in the interval of the heated drift excavated by the alpine miner (12.5 to 60 m), the invert section was excavated by drill and blast, and this exposure was included in the rock mass quality assessment evaluation.

- Approximately, from station 40 to 60 m in the heated drift, the matrix has been moderately affected by vapor phase alteration and low angle vapor phase partings are present.

Table 8-1. Rock Mass Rating Q for the Thermal Test Facility

Start Station	End Station	Record Number	Revision Number	Stratigraphic Unit	RQD	Jn	Jr	Ja	Jw	SRF	Q	
Observation Drift												
5	10	1	0	Tptpmn	88.6	12	4.0	1.0	1	5.0	5.907	
10	15	11	0	Tptpmn	81.8	12	4.0	1.0	1	5.0	5.453	
15	20	2	0	Tptpmn	89.1	12	4.0	1.0	1	5.0	5.940	
20	25	3	0	Tptpmn	87.7	6	4.0	1.0	1	5.0	11.693	
25	30	4	0	Tptpmn	95.7	12	4.0	1.0	1	1.0	31.900	
30	35	5	0	Tptpmn	71.2	12	4.0	4.0	1	5.0	1.187	
35	40	6	0	Tptpmn	73.9	12	4.0	4.0	1.	5.0	1.232	
40	45	7	0	Tptpmn	63.8	12	4.0	1.0	1	5.0	4.253	*
45	50	8	0	Tptpmn	92.6	12	4.0	3.0	1	5.0	2.058	*
50	55	9	0	Tptpmn	94.3	12	4.0	3.0	1	5.0	2.096	*
55	60	10	0	Tptpmn	92.7	12	4.0	3.0	1	5.0	2.060	*
60	65	12	0	Tptpmn	85.6	12	4.0	3.0	1	5.0	1.902	
65	70	13	0	Tptpmn	87.6	12	4.0	3.0	1	5.0	1.947	
70	75	14	0	Tptpmn	91.7	15	3.3	3.0	1	5.0	1.345	**
75	80	15	0	Tptpmn	75.7	12	4.0	3.0	1	5.0	1.682	**
80	85	16	0	Tptpmn	97.6	6	2.3	3.0	1	5.0	2.494	**
85	90	17	0	Tptpmn	73.0	12	4.0	3.0	1	5.0	1.622	**
90	95	18	0	Tptpmn	83.7	20	4.0	3.0	1	5.0	1.116	**
95	100	19	0	Tptpmn	99.0	20	4.0	3.0	1	5.0	1.320	**
100	105	20	0	Tptpmn	92.7	12	4.0	3.0	1	7.5	1.373	**
105	110	21	0	Tptpmn	49.5	6	4.0	3.0	1	7.5	1.467	**
110	115	22	0	Tptpmn	79.5	12	2.4	3.0	1	7.5	0.707	**
115	120	23	0	Tptpmn	87.2	12	4.0	3.0	1	7.5	1.292	**
120	125	24	0	Tptpmn	88.7	20	4.0	3.0	1	7.5	0.788	**
125	130	~25	0	Tptpmn	67.7	6	4.0	3.0	1	7.5	2.006	**
130	135	26	0	Tptpmn	51.4	12	4.0	3.0	1	7.5	0.761	

Table 8-1. Rock Mass Rating Q for the Thermal Test Facility (continued)

Start Station	End Station	Record Number	Revision Number	Stratigraphic Unit	RQD	Jn	Jr	Ja	Jw	SRF	Q	
Thermomechanical Alcove/Single Heater Test												
3	5	1	0	Tptpmn	86.2	12	4.0	3.0	1	5.0	1.916	*
5	10	2	0	Tptpmn	94.6	12	4.0	4.0	1	5.0	1.577	*
10	15	3	0	Tptpmn	98.5	12	2.1	3.0	1	1.0	5.746	*
15	20	4	0	Tptpmn	78.9	12	4.0	3.0	1	7.5	1.169	*
20	25	5	0	Tptpmn	74.8	12	4.0	3.0	1	7.5	1.108	*
Thermomechanical Alcove Extension												
3	5	1	0	Tptpmn	96.6	6	4.0	3.0	1	5.0	4.293	*
5	10	2	0	Tptpmn	97.8	6	4.0	3.0	1	1.0	21.733	*
10	12	3	0	Tptpmn	93.4	12	4.0	3.0	1	5.0	2.076	*
Connecting Drift												
3	5	1	0	Tptpmn	99.5	6	4.0	3.0	1	1.0	22.111	**
5	10	2	0	Tptpmn	99.5	6	4.0	3.0	1	1.0	22.111	**
10	15	3	0	Tptpmn	99.2	12	4.0	3.0	1	1.0	11.022	**
15	20	4	0	Tptpmn	97.6	12	2.4	3.0	1	1.0	6.507	**
20	25	5	0	Tptpmn	96.9	12	4.0	4.0	1	1.0	8.075	**
25	30	6	0	Tptpmn	84.3	6	2.4	3.0	1	5.0	2.248	**
30	35	7	0	Tptpmn	99.2	6	4.0	3.0	1	1.0	22.044	**
35	40	8	0	Tptpmn	99.8	6	4.0	3.0	1	1.0	22.178	**
40	45	9	0	Tptpmn	99.7	12	4.0	3.0	1	1.0	11.078	**

Table 8-1. Rock Mass Rating Q for the Thermal Test Facility (continued)

Start Station	End Station	Record Number	Revision Number	Stratigraphic Unit	RQD	Jn	Jr	Ja	Jw	SRF	Q	
Heated Drift												
3	5	1	0	Tptpmn	75.9	12	4.0	3.0	1	5.0	1.687	**
5	10	2	0	Tptpmn	89.7	12	4.0	3.0	1	5.0	1.993	**
10	15	3	0	Tptpmn	84.4	6	4.0	3.0	1	5.0	3.751	**
15	20	4	0	Tptpmn	98.4	6	4.0	3.0	1	5.0	4.373	**
20	25	5	0	Tptpmn	80.8	6	4.0	3.0	1	5.0	3.591	**
25	30	6	0	Tptpmn	99.0	12	4.0	3.0	1	1.0	11.000	**
30	35	7	0	Tptpmn	99.5	6	4.0	3.0	1	1.0	22.111	**
35	40	8	0	Tptpmn	99.1	12	4.0	3.0	1	1.0	11.011	**
40	45	9	0	Tptpmn	96.9	6	4.0	3.0	1	5.0	4.307	**
45	50	10	0	Tptpmn	99.5	1	5.0	0.8	1	1.0	621.875	**
50	55	11	0	Tptpmn	96.0	12	4.0	3.0	1	1.0	10.667	**
55	60	12	0	Tptpmn	95.5	6	4.0	3.0	1	5.0	4.244	**
	*	Interval adjacent to the single heater block.										
	**	Interval adjacent to the heated drift.										
	RQD	Rock Quality Designation										
	Jn	Joint Set Number										
	Jr	Joint Roughness Number										
	Ja	Joint Alteration Number										
	Jw	Joint Water Reduction Factor										
	SRF	Stress Reduction Factor										
	Q	Rock Mass Quality Indices										

Table 8-2. Rock Mass Rating RMR for the Thermal Test Facility

Start Station	End Station	Record Number	Revision Number	Stratigraphic Unit	RQD-1	C	Js	Jc	Jw	JOA	RMR	
Observation Drift												
5	10	1	0	Tptpmn	17	12	15	21.1	15	-5	75.1	
10	15	11	0	Tptpmn	17	12	15	21.1	15	-5	75.1	
15	20	2	0	Tptpmn	17	12	15	22.4	15	-5	76.4	
20	25	3	0	Tptpmn	17	12	15	23.6	15	-5	77.6	
25	30	4	0	Tptpmn	20	12	15	23.6	15	-5	80.6	
30	35	5	0	Tptpmn	13	12	8	24.9	15	-5	67.9	
35	40	6	0	Tptpmn	13	12	8	23.6	15	-5	66.6	
40	45	7	0	Tptpmn	13	12	15	21.1	15	-5	71.1	*
45	50	8	0	Tptpmn	20	12	10	22.4	15	-5	74.4	*
50	55	9	0	Tptpmn	20	12	10	22.4	15	-5	74.4	*
55	60	10	0	Tptpmn	20	12	15	22.4	15	-5	79.4	*
60	65	12	0	Tptpmn	17	12	15	21.1	15	-5	75.1	
65	70	13	0	Tptpmn	17	12	15	22.4	15	-5	76.4	
70	75	14	0	Tptpmn	20	12	20	20.1	15	-12	75.1	**
75	80	15	0	Tptpmn	17	12	15	21.1	15	-5	75.1	**
80	85	16	0	Tptpmn	20	12	20	20.1	15	-12	75.1	**
85	90	17	0	Tptpmn	13	12	10	22.4	15	-12	60.4	**
90	95	18	0	Tptpmn	17	12	15	21.1	15	-5	75.1	**
95	100	19	0	Tptpmn	20	12	20	21.1	15	-12	76.1	**
100	105	20	0	Tptpmn	20	12	8	20.1	15	-12	63.1	**
105	110	21	0	Tptpmn	8	12	8	20.1	15	-12	51.1	**
110	115	22	0	Tptpmn	17	12	8	21.3	15	-12	61.3	**
115	120	23	0	Tptpmn	17	12	15	20.1	15	-5	74.1	**
120	125	24	0	Tptpmn	17	12	15	21.1	15	-5	75.1	**
125	130	25	0	Tptpmn	13	12	5	22.4	15	-12	55.4	**
130	135	26	0	Tptpmn	13	12	10	21.1	15	-5	66.1	

Table 8-2. Rock Mass Rating RMR for the Thermal Test Facility (continued)

Start Station	End Station	Record Number	Revision Number	Stratigraphic Unit	RQD-1	C	Js	Jc	Jw	JOA	RMR	
Thermomechanical Alcove/Single Heater Test												
3	5	1	0	Tptpmn	17	12	8	17.1	15	-10	59.1	*
5	10	2	0	Tptpmn	20	12	10	27.4	15	-5	79.4	*
10	15	3	0	Tptpmn	20	12	15	18.9	15	-10	70.9	*
15	20	4	0	Tptpmn	17	12	15	23.6	15	-5	77.6	*
20	25	5	0	Tptpmn	13	12	15	23.6	15	-5	73.6	*
Thermomechanical Alcove Extension												
3	5	1	0	Tptpmn	20	12	10	21.3	15	-5	73.3	*
5	10	2	0	Tptpmn	20	12	15	21.3	15	-5	78.3	*
10	12	3	0	Tptpmn	20	12	10	18.5	15	-10	65.5	*
Connecting Drift												
3	5	1	0	Tptpmn	20	12	10	22.4	15	-12	67.4	**
5	10	2	0	Tptpmn	20	12	15	21.3	15	-5	78.3	**
10	15	3	0	Tptpmn	20	12	20	21.3	15	-5	83.3	**
15	20	4	0	Tptpmn	20	12	20	21.3	15	-5	83.3	**
20	25	5	0	Tptpmn	20	12	15	27.4	15	-2	87.4	**
25	25	6	0	Tptpmn	17	12	15	21.3	15	-2	78.3	**
30	35	7	0	Tptpmn	20	12	15	22.4	15	-5	79.4	**
35	40	8	0	Tptpmn	20	12	15	22.4	15	-5	79.4	**
40	45	9	0	Tptpmn	20	12	15	21.3	15	-5	78.3	**

Table 8-2. Rock Mass Rating RMR for the Thermal Test Facility (continued)

Start Station	End Station	Record Number	Revision Number	Stratigraphic Unit	RQD-1	C	Js	Jc	Jw	JOA	RMR	
Heated Drift												
3	5	1	0	Tptpmn	17	12	15	21.3	15	-5	75.3	**
5	10	2	0	Tptpmn	17	12	15	22.4	15	-12	69.4	**
10	15	3	0	Tptpmn	17	12	10	22.4	15	-12	64.4	**
15	20	4	0	Tptpmn	20	12	15	22.4	15	-5	79.4	**
20	25	5	0	Tptpmn	17	12	15	22.4	15	-5	76.4	**
25	30	6	0	Tptpmn	20	12	15	22.4	15	-12	72.4	**
30	35	7	0	Tptpmn	20	12	15	21.3	15	-10	73.3	**
35	40	8	0	Tptpmn	20	12	15	21.3	15	-10	73.3	**
40	45	9	0	Tptpmn	20	12	15	22.4	15	-10	74.4	**
45	50	10	0	Tptpmn	20	12	20	30	15	0	97	**
50	55	11	0	Tptpmn	20	12	15	23.6	15	-2	83.6	**
55	60	12	0	Tptpmn	20	12	8	23.6	15	-5	73.6	**
	*	Interval adjacent to the single heater block.										
	**	Interval adjacent to the heated drift.										
	RQD	Rock Quality Designation Rating										
	C	Intact Rock Strength Rating										
	Js	Joint Spacing Rating										
	Jc	Joint Condition Rating										
	Jw	Ground Water Rating										
	JOA	Joint Orientation Adjustment										
	RMR	Rock Mass Rating										

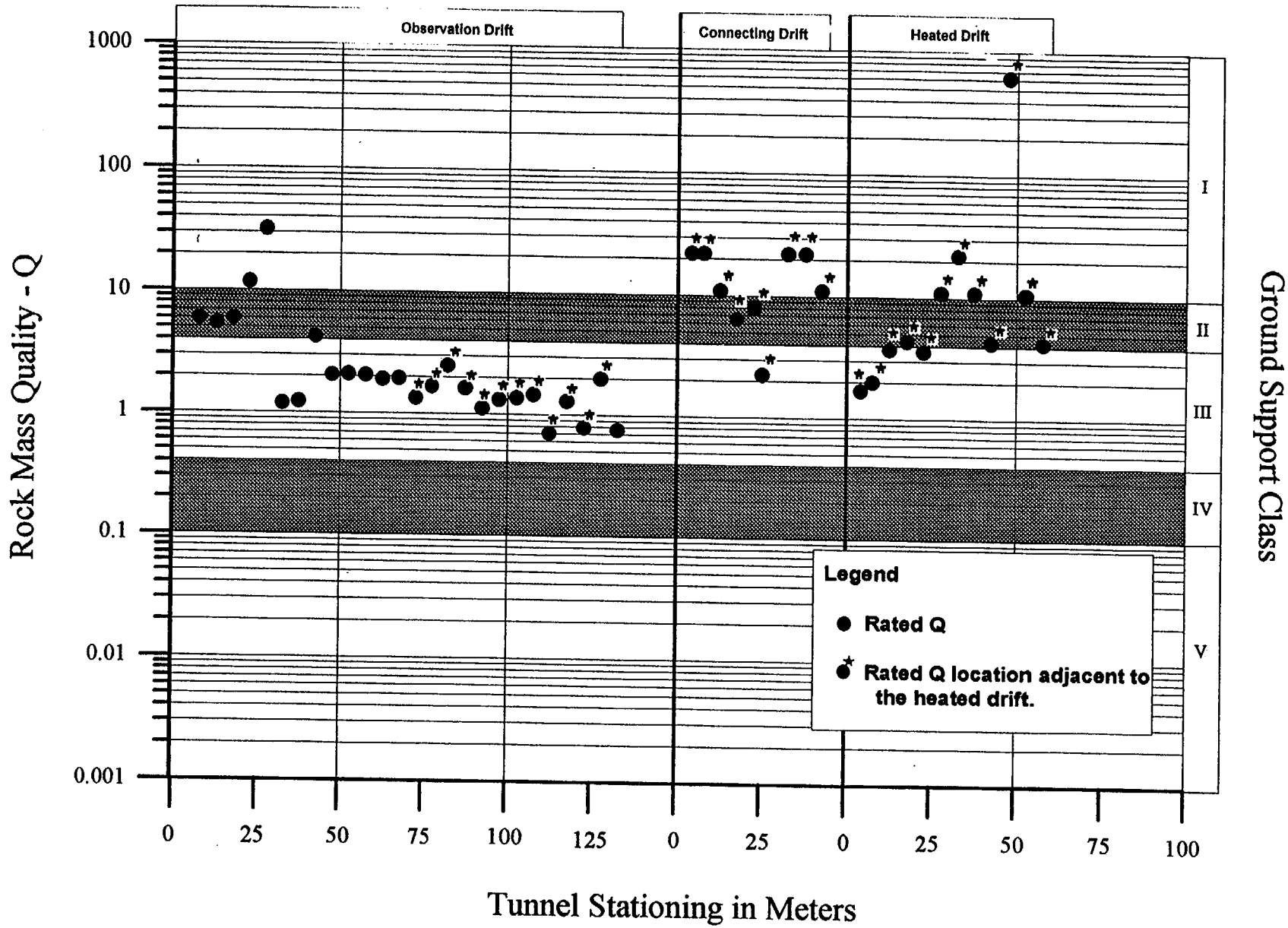

Figure 8-1. Q Values from the Thermal Test Facility Surrounding the Drift Scale Test

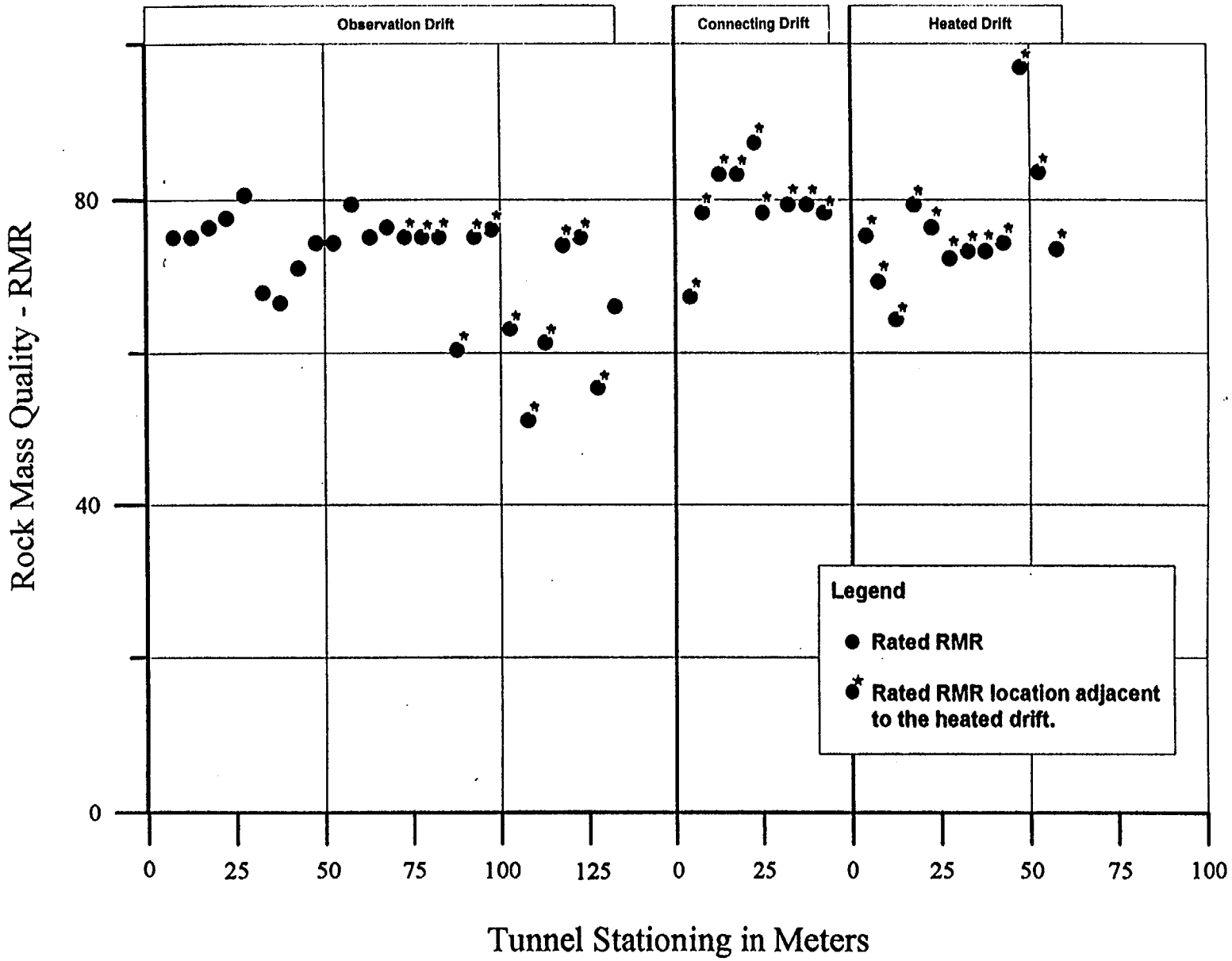

Figure 8-2. RMR Values from the Thermal Test Facility Surrounding the Heated Drift

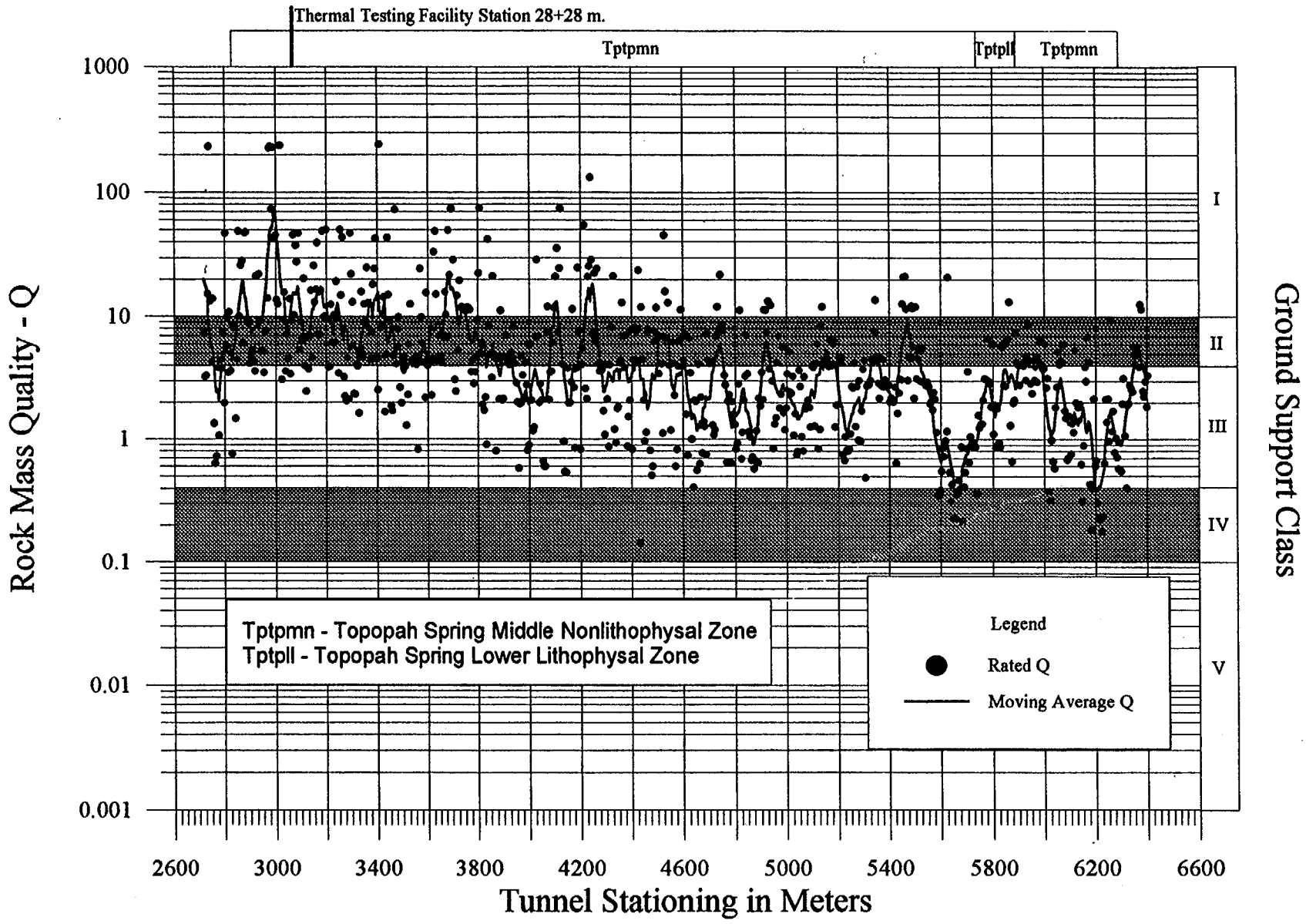

Figure 8-3. Q Values for TSw2 (Tptpmn and Tptpll) for the Main Drift at Station 27+15 to 63+05 m

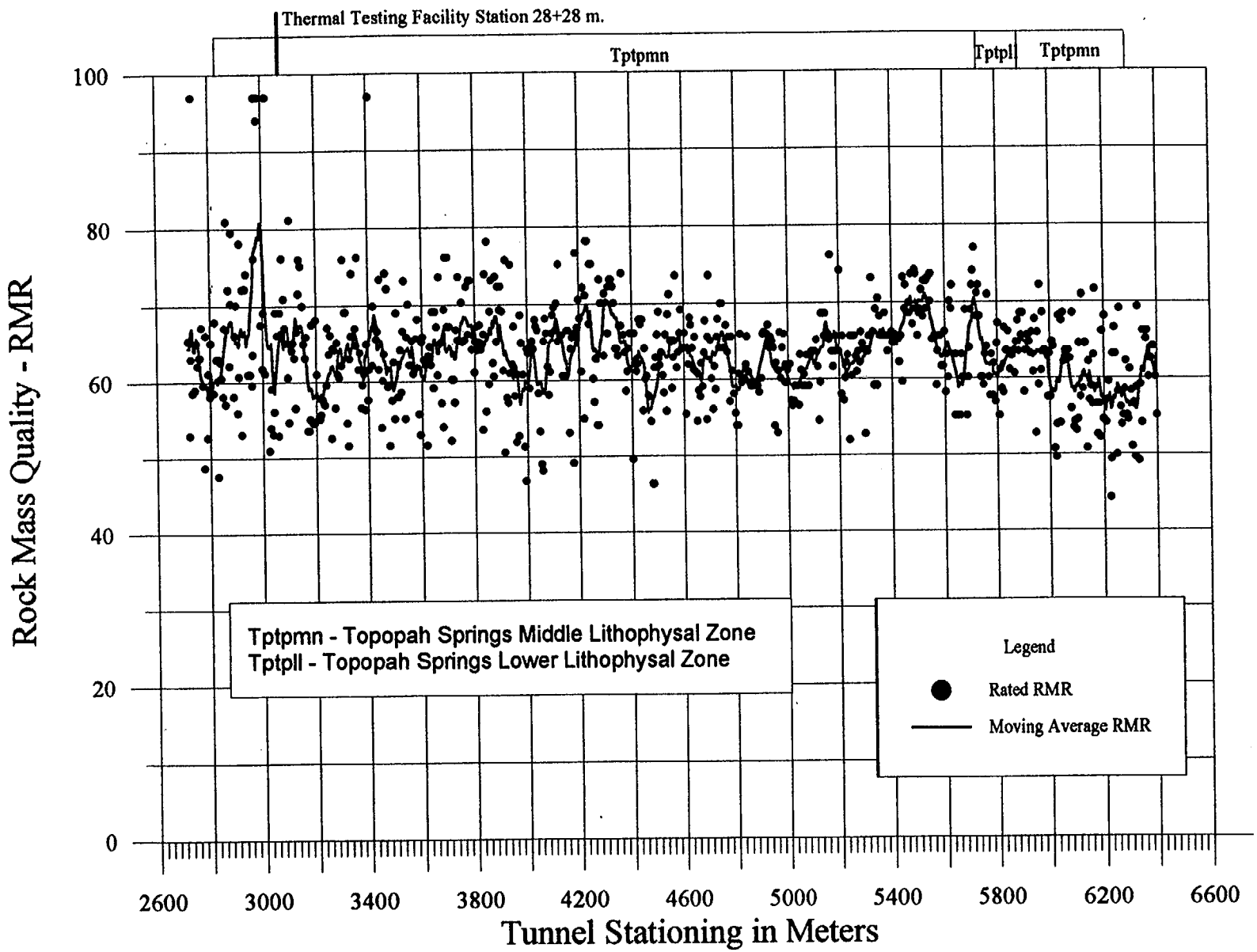

Figure 8-4. RMR Values for TSw2 (Tptpmn and Tptpll) for the Main Drift at Station 27+15 to 63+05 m

- Schmidt Hammer values have been collected throughout the TTF as a non-qualified activity. Despite the massive texture observed in the connecting drift and the vapor phase alteration observed at the terminus of the heated drift, Schmidt Hammer values through the heated drift test area are relatively constant and range from 58.8 to 61.8 with an average value of 59.9 ± 1.1, n=6 (Internal Memorandum from Moo Lee, SNL, to Dick Kovack, LANL, Subject Schmidt Hammer Test Results, March 14, 1996.)

There are three prominent joint sets observed in the TTF. These joint sets are also observed in the Tptpmn in the main drift. Joint Set 1 (JS1) and Joint Set 2 (JS2) are both nearly vertical, moderately long joints (1 to 3 m), have relatively smooth surfaces [Joint Roughness Coefficient (JRC) 8 to 10, Brown 1981], and have relatively small variations in amplitudes normal to the joint surfaces (0.1 to 0.2 m). Joint apertures are typically 1 to 2 mm, open, with little or no infilling. JS1 has a dip direction of approximately 30° and a dip angle from 70° to 85° while JS2 has a dip direction of approximately 110° and a dip angle of 70° to 85°.

Joint Set 3 (JS3) is a relatively low angle (20° to 40° dip) joint set with a dip direction of 30 degrees. In the heated drift alcove from station 40 to 60 m this joint set appears to have been altered to a vapor phase parting surface with infillings of calcite and quartz. Compared to JS1 and JS2, the joint surfaces of JS3 are generally shorter (1 - 2 m), have a slightly more irregular surfaces (JRC 10 to 12, Brown 1981), and have larger variations in amplitudes normal to the joint surfaces (0.2 to 0.3 m). The apertures for JS3 are generally small (1 - 2 mm) and are typically open and unfilled.

Rock Mass Indices Q and RMR for the thermal/mechanical unit TSw2 from the main drift are plotted in Figures 8-3 and 8-4. Examining the Q and RMR values from the DST block shows that the observed variation falls within the range observed for TSw2 in the main drift (Figures 8-1 through 8-4). Comparing average and standard deviation for RMR between the DST block and main drift, it is apparent that the indices from the DST block fall within the observed norm for the main drift, as shown in Table 8-3.

The average RMR and standard deviation for the DST block is 74.1 ± 9.1, as compared to 63.7 ± 7.0 for the TSw2 unit in the main drift. This indicates that no significant difference exists in RMR values determined from the DST block and TSw2 main drift. Similarly, Q and RMR indices calculated for the SHT block also fall within the range observed for TSw2 main drift (TDIF 305579/DTN SNF32020196001.010 and TDIF 305970/DTN SNF32070996001.005).

Table 8-3. RMR Indices for Topopah Spring Middle Non-Lithophysal Zone (TSw2)

	X_{RMR}	σ_{RMR}	N
Thermal Test Facility	74.1	9.1	33
Main Drift	63.7	7.0	718

X_{RMR} = Average
σ_{RMR} = Standard Deviation
N = Number of Samples

INTENTIONALLY LEFT BLANK

9. FIELD MEASUREMENTS: AIR PERMEABILITY TESTING

9.1 OBJECTIVE AND DESCRIPTION

The objective of hydrological characterization by air permeability testing of the DST block prior to heating was to define the initial conditions of the test block. It is essential for the interpretation and analysis of the coupled thermo-hydrological-mechanical-chemical processes associated with the in-site DST in the ESF.

The test results provide an estimate of the three-dimensional heterogeneous gas phase permeability structure and fracture connectivity in the block. Since the dominant thermal-hydrological response of the rock mass to the applied heat is the vaporization of pore water near the heat source, and the redistribution of moisture through vapor transport, it is important to develop an understanding of the potential pathways for fluids and gases in the DST block. Characterization by air permeability tests, prior to the onset of heating, provides this information and allows predictive calculations to be made regarding fluid, heat, and flow in the block during both the heating and cooling phases of the thermal test. The pre-test characterization data will also serve as a basis for post-test comparison to observe where and what changes in permeability have occurred due to heating and possible thermo-hydrologic-chemical coupling.

All field and laboratory measurements were performed by qualified personnel, with calibrated equipment, under the Lawrence Berkeley National Laboratory (LBNL) QA program. Therefore, all data presented in this section are qualified data. The Data Tracking Number for the air permeability tests is DTN: LB970600123142.001, and the TDIF is 306164. Scientific Notebook YMP-LBNL-YWT-1.3 was used. Work in this section was performed in satisfaction of Level 4 Milestone SP9512M4 (Tsang and Cook 1997).

9.2 METHODOLOGY

Air permeability tests were carried out in the DST block from 14 boreholes collared on the observation drift.

Air permeability tests for the DST were carried out in November and December of 1996, and again in February and March of 1997, in available boreholes; that is, those which were drilled and logged by video, but not yet permanently installed with instrumentation for the heater test proper. During this period, the heated drift of the DST was still under construction, and therefore, the majority of the instrumental boreholes and wing heater boreholes originating from the heated drift were not yet drilled. There were fourteen boreholes available for the air permeability test, each 40 m in length, all originating from the observation drift that runs parallel to the heated drift. They are separated from the heated drift by 30 m. These boreholes are oriented approximately south/north toward the heated drift, with incline angles ranging from 24° to -22° from the horizontal, forming a fan and bracketing the heated drift. The fourteen holes form two spatial clusters approximately 20 m apart at their collars along the observation drift wall. Within each cluster, the separation of some adjacent boreholes at their collars can be less than one meter. However, since these boreholes form divergent fans from their collars on the rock surface, the separation distances between boreholes increases to

30 to 40 m at the bottom of the boreholes. Figure 9-1 shows the layout of the DST area and the location of the 14 boreholes used for characterization by air permeability tests. The 14 boreholes are identified by bold letter and underlined. Figure 9-1 is the plan view (note that the true north makes an angle of 18° with the horizontal, which is generally referred to as the local north in the heater test. Figure 9-2 shows an approximately E-W section and the positions of the boreholes at their collars, and Figure 9-3 shows two N-S sections. Again, only those boreholes in bold letters and underlined have been drilled during the air permeability testing.

For the permeability tests, each borehole was separated by three inflatable packers into approximately 12 m sections. Each packed-off zone within the boreholes was instrumented with a sensor to monitor the pressure response. A typical test consisted of injecting air at a constant flow rate in one chosen section, while the pressure response(s) in this and all other packed off sections were monitored. The pressure response in the injection section is used to calculate the local permeability, averaged over the length of the packed-off zone. The response of pressure in all other packed-off sections will yield information on the connectivity of pneumatic pathways between these sections and the injection section.

The air permeability testing equipment consisted of pneumatic packers, pressure sensors, air supply and control equipment, a flow control unit, and different components were connected via electronic cabling and flexible tubing. The air supply and control equipment was responsible for providing dry, clean air under pressure to the flow control unit. The integrated flow control and acquisition system unit used a centralized set of manifolds for injecting and with drawing gas from packed off zones of interest, and for the monitoring of zone pressure. The electronic control system was run using a laptop personal computer with Labview for Windows® for both control and data collection. The instrumentation interface and software control allowed the user to rapidly reconfigure the system in the field for conducting a varied testing program.

Pneumatically inflated packers were custom designed for the purpose of characterizing the DST area by air injection tests. The design was such that up to four packers could be placed in a single borehole to separate the borehole into four independently observable injection zones. The packers consisted of a 1/4-in thick natural gum rubber gland applied over a stainless steel packer body. The length of the packer bodies is 0.61 m giving a sealing surface of approximately 0.55 m in length. To allow air injection into, and pressure monitoring for each zone requires multiple feedthroughs of stainless tube for each packer: for air injection (½-inch outside diameter), packer inflation (1/8-inch outside diameter) and pressure sensor (1/4-inch outside diameter). One of the ½-inch feedthroughs also serves as a structural backbone for the packer string. The innermost of the four packers, that is, the one closest to the bottom of the borehole, would have a minimum of three feedthroughs, while the fourth packer, placed closest to the collar, would have a maximum of twelve feedthroughs. A schematic diagram of a packer string consisting of only two packers is shown in Figure 9-4. The packers were fabricated in two standard sizes, nominally referred to as 3-inch and 4-inch packers to accommodate the two standard-size borings, 7.57 cm and 9.60 cm in diameter. To isolate zones in the wellbore, packers were typically inflated to 35 Psig (2.41×10^5 Pa).

Pressure measurements were made using Setra pressure transducers (models C204 and 280) mounted near the collar of each borehole. The transducers monitored the zone of interest through a polyethylene tube connected to a 1/4-inch feedthrough.

Measurements were made using a Keithley 2001 digital multimeter (DMM)®. All data channels were scanned through a Keithley 7002 Switch System®. Data was dumped across an IEEE-488 bus to a personal computer laptop. To control and measure the rate at which compressed air was injected, Sierra Instruments Series 840® mass flow controllers were used for three flow ranges, 0-10 standard liter per minute (SLPM), 0-100 SLPM and two 0-500 SLPM connected in parallel. The Series 840 mass flow controllers were controlled by a Hewlett Packard E3631 programmable power supply and monitored using the Keithley DMM. Ambient conditions in the drift were continuously monitored using a Vaisala HMP 132Y humidity/temperature probe and an extra Setra pressure transducer. The as-built Cartesian collar coordinates of the fourteen boreholes available for air-injection test boreholes (ESF As Built Survey, personal communication, LANL, Douglas Weaver to Yvonne Tsang, November 1996) are shown in Table 9-1. The borehole Identification numbers are in accordance with the Field Work Package FWP-ESF-96-003, Revision 3, for thermal testing in the ESF. The as-built coordinates convention is that the +Y-axis is along the heated drift (parallel to the observation drift), toward west. The +X-axis runs toward the north away from the observation drift, and the origin (0,0,0) is at the center of the heated drift on the hot side of the bulkhead.

Table 9-1. As-Built Coordinates of the Collar and Diameter of Air Permeability Boreholes*

Borehole Identification	X (m)	Y (m)	Z (m)	Borehole Diameter (cm)
45 ESF-HD-ERT-1	-28.875	4.577	4.118	7.57
46 ESF-HD-ERT-2	-27.408	4.572	1.533	7.57
47 ESF-HD-NEU-1	-29.114	6.385	4.636	7.57
48 ESF-HD-NEU-2	-29.051	6.391	4.042	7.57
51 ESF-HD-NEU-5	-28.993	6.414	2.254	7.57
52 ESF-HD-CHE-1	-29.211	8.247	4.540	9.6
53 ESF-HD-CHE-2	-29.232	8.258	4.014	9.6
56 ESF-HD-CHE-5	-29.223	8.248	2.322	9.6
57 ESF-HD-HYD-1	-28.841	10.054	4.748	7.57
69 ESF-HD-CHE-6	-29.199	28.368	6.842	7.57
70 ESF-HD-CHE-7	-29.261	28.373	6.315	7.57
73 ESF-HD-CHE-10	-29.062	28.375	4.546	7.57
75 ESF-HD-HYD-7	-29.306	30.215	6.303	7.57
78 ESF-HD-HYD-10	-29.376	30.191	4.702	7.57

*Coordinates are 0, 0, 0 at the center of the heated drift bulkhead.

The Y coordinates of the boreholes indicate that the fourteen boreholes form two spatial clusters at their collars along the observation drift wall: one cluster of nine including boreholes 45, 46, 47, 48, 51, 52, 53, 56, 57, centered around Y = 7 m; and another cluster of five including boreholes 69, 70, 73, 75, 78, centered around Y = 28 m. The video logs of all boreholes in the single heater block were reviewed, and the fracture characteristics in each borehole were noted.

The original test plan for the ambient temperature bulk permeability measurements to estimate the three-dimensional heterogeneity in the DST block consisted of two phases. The first phase was to use two packers to divide each borehole into approximately two equal zones of 20 m in length. The intention was that data from this first phase testing would probe the heterogeneous permeability structure on a large scale, and would guide in the design of the second phase testing, where four packers would be used for each borehole to provide information on a smaller scale about the permeability structure.

The test plan was modified after viewing of the borehole video logs because they showed very extensive sections of voids and fractures, so much so that it was difficult to identify the locations of intact rock suitable for placement of inflatable packers. Thus it was decided that each borehole should only be isolated by packers in thirds, with the third packer placed as close to the collar as feasible.

The modified test plan was as follows: the first phase of testing would involve air injection and pressure response in the two zones closest to the bottom of the boreholes (the zones over the wing heater and the heater drift); and the second phase of testing would involve air injection into the zone nearest the collar, separated by the second and third packer. This zone would also be the farthest from the region of applied heat during the thermal test. Each packed zone is on the order of 12 m; the actual depth of each packer was adjusted to avoid overlay onto fractured borehole walls.

Figure 9-5 shows the packer positions in the 14 boreholes. The 3-D view is that of facing east away from the ESF main drift so the heated drift centered at X = 0 is to the left and the observation drift wall at x ≅ -29 m is to the right. The lengths of the air injection zones L, as isolated by packers, are tabulated in Table 9-2. L is determined from the borehole lengths (ESF As Built Survey, personal communication, LANL, Douglas Weaver to Yvonne Tsang, November 1996) and the depth setting of the packers, as measured in the field and recorded in the field notebook. The nomenclature is such that zone 1 refers to the zone closest to and including the bottom of the borehole, and zone 3 refers to the zone closest to the collar of the borehole. A shorthand notation consisting of the borehole number plus zone will be used, for example, 45-3 will denote zone 3 in borehole 45.

In borehole 53, only two packers were installed because of an obstruction by rocks, and for the same reason, the zone closest to the bottom of the borehole for boreholes 47 and 57 are exceptionally long. There are two entries for borehole 75. The first is applicable for tests carried out in November and December of 1996. Two packers were installed, and due to obstruction by rocks in the borehole, the first zone closest to the bottom of the borehole is 23.4 m. The second entry for borehole 75 is applicable for tests conducted in February and March of 1997. The obstruction was cleared, the packer string was moved down the borehole and a third packer was installed near the collar.

Table 9-2. Lengths of Packed-Off Zones for Air Permeability Tests

Borehole Identification	Length of Zone 1 (m)	Length of Zone 2 (m)	Length of Zone 3 (m)
45 ESF-HD-ERT-1	10.9	11.6	15.4
46 ESF-HD-ERT-2	13.9	11.6	9.1
47 ESF-HD-NEU-1	18.5	11.6	7.6
48 ESF-HD-NEU-2	12.9	14.6	9.1
51 ESF-HD-NEU-5	14.1	13.1	9.3
52 ESF-HD-CHE-1	13.1	11.6	12.3
53 ESF-HD-CHE-2	25.3	11.6	0.0
56 ESF-HD-CHE-5	15.8	10.1	10.6
57 ESF-HD-HYD-1	22.5	11.6	3.2
69 ESF-HD-CHE-6	12.0	11.6	14.2
70 ESF-HD-CHE-7	15.2	11.6	11.2
73 ESF-HD-CHE-10	14.9	11.6	11.1
75 ESF-HD-HYD-7	23.4	11.6	0.0
75 ESF-HD-HYD-7	14.0	11.6	11.9
78 ESF-HD-HYD-10	13.7	11.6	11.9

All the fittings on the feedthroughs on the packer strings were checked for leaks during packer string installation. To isolate zones in the wellbore, the packers were typically inflated to a pressure of 35 psig (2.41×10^5 Pa). The pressure within the packers was monitored periodically throughout testing. All sensors and equipment such as flow control unit and air supply and control equipment were installed and linked to be controlled by the laptop personal computer running Labview. Prior to actual data logging, the whole acquisition and control system was tested for proper functions with all the electronics attached.

In a typical injection test, the injection line to the selected injection zone is connected to the flow control unit. An injection test consists of a period of background monitoring before injection, followed by an injection at constant mass flux, maintained by the mass flow controller. After either a predetermined interval of time, or a steady state response is reached, the injection is halted and the recovery is monitored. The pressure sensor is sampled every five seconds during the early part of the injection and recovery. The sampling rate is decreased with increasing test duration to a minimum of once every ten minutes for overnight tests or continuous background monitoring. The Labview code used in the data acquisition system allows for a real time display of parameters during testing. Viewing the pressure response of the sensors in different zones of the different boreholes during each injection test allows preliminary interpretation of the air permeability structure in the test block, and guides the tester in configuring subsequent tests.

Local permeability was estimated from the steady state pressure response to the air injection test. The analytical solution for the steady state pressure response of a constant flow rate injection in a finite line source is as follows:

$$k = \frac{P_{sc}\, Q_{sc} \mu \ln\left(\frac{L}{r_w}\right) T_f}{\pi L \left(P_2^2 - P_1^2\right) T_{sc}} = \frac{P_{sc}\, Q_{sc} \mu \ln\left(\frac{L}{r_w}\right) T_f}{\pi L \left(2P_1 + \Delta P\right) \Delta P T_{sc}} \qquad (9\text{-}1)$$

where

k	=	permeability, m^2
P_{sc}	=	Pressure at standard conditions, 1.013×10^5 Pa
Q_{sc}	=	flowrate at standard conditions, m^3/s
μ	=	dynamic viscosity of air, 1.81×10^{-5} Pa-s at 20° C
L	=	Length of air injection zone, m
r_w	=	radius of borehole, m
T_f	=	temperature of formation, K (an average of 24.6° C was assumed for all tests)
P_2	=	steady-state pressure, Pa
P_1	=	ambient pressure, Pa
ΔP	=	$(P_2 - P_1)$, Pa
T_{sc}	=	temperature at standard conditions, 293.16 K

Equation (9-1) has been used by both LeCain (1995) and Guzman et al. (1996) for the analysis of single borehole injection tests in fractured tuff at Apache Leap Research Site, Arizona. It was adapted from the steady-state analytical solution for ellipsoidal flow of incompressible fluid from a finite line source (Hvorslev 1951), where $L/r_w > 1$ in an infinite medium. The derivation of Equation (9-1) requires the assumption that air is the only mobile phase within the rock near the test interval, and that it obeys the ideal gas law so that the compressibility is inversely proportional to pressure. A detailed derivation of Equation (9-1) can be found in LeCain (1995). The same equation has also been applied for the air injection tests for surface-based boreholes at Yucca Mountain (Rousseau et al. 1996). Equation (9-1) has its origin in well test analysis for a homogeneous porous medium. The welded tuff DST test block is a fractured medium and may not be well represented conceptually by a homogeneous porous medium. Furthermore, the proximity of the drifts implies that the finite line source is not in an infinite medium. Nevertheless, Equation (9-1) is still valuable as a simple tool to obtain an order of magnitude estimate of the average permeability values around each borehole, thus providing an initial estimate of the spatial variability of permeability in the test block. In addition, the limitations should be similar for zones within the same unit, so comparative values, although not absolute, are adequate for characterization purposes. This approach was also used in the analysis for the air permeability measurements for the SHT (Tsang et al. 1996).

In many zones, more than one injection test was carried out to investigate the sensitivity of the derived permeability values to different test conditions. Injection tests in some zones were carried out on different dates to investigate the repeatability of the test. The sensitivity of the derived permeability values to different mass flow rates injected into the same isolated zone were

investigated in several tests. These were sometimes carried out in separate tests, each with its own constant flowrate, and sometimes within the same test by increasing the constant air flowrate in discrete steps, so that permeability could be estimated from multiple sets of steady state pressure responses to the different flowrates. In addition to injecting air into isolated zones, injection tests were also carried out in longer zones by selectively deflating packers in a borehole. Specifically, Packer 1 was deflated in borehole 45 so that the effective length of the borehole tested was 22.6 m. Similarly, when both Packers 1 and 2 were deflated, Packer 3 (near the collar), was tested. This was a zone of 38.5 m; almost the entire length of borehole 45, which was isolated by just one packer.

9.3 RESULTS

9.3.1 Air Permeability Estimation

Estimates of permeability values from steady-state pressure response show a range from 8.8×10^{-16} m^2 to 2.0×10^{-12} m^2. These are of the same order of magnitude as those obtained from the SHT area (Tsang et al. 1996), as well as those obtained from surface-based air-injection tests in vertical boreholes for the Topopah middle non-lithophysal stratigraphic unit (Rousseau et al. 1996).

One complete set of estimated permeability values for all the zones of the 14 boreholes is shown in 3-D in Figure 9-6. The logarithm of permeability, normalized to the highest value of 2.0×10^{-12} m^2 in borehole 52, zone 3, is coded in rainbow color. The same set of estimated permeability values are tabulated in Table 9-3.

Table 9-3. Estimated Local Permeability for the 41 Packed-Off Zones in 14 Boreholes

Borehole Identification	Permeability (m^2)		
	Zone 1	Zone 2	Zone 3
45 ESF-HD-ERT-1	5.8E-14	2.4E-14	4.5E-13
46 ESF-HD-ERT-2	4.1E-15	6.2E-15	9.0E-14
47 ESF-HD-NEU-1	6.1E-14	4.4E-13	4.7E-13
48 ESF-HD-NEU-2	2.4E-14	3.5E-14	3.4E-13
51 ESF-HD-NEU-5	8.8E-16	4.4E-13	4.1E-14
52 ESF-HD-CHE-1	1.0E-13	1.2E-13	2.0E-12
53 ESF-HD-CHE-2	1.1E-13	1.3E-12	N/A
56 ESF-HD-CHE-5	1.9E-15	3.4E-14	4.8E-13
57 ESF-HD-HYD-1	2.7E-13	6.1E-14	1.4E-13
69 ESF-HD-CHE-6	2.1E-13	9.5E-15	4.9E-13
70 ESF-HD-CHE-7	1.9E-14	4.5E-14	4.2E-13
73 ESF-HD-CHE-10	6.6E-14	6.8E-15	1.0E-13
75 ESF-HD-HYD-7	4.9E-13	1.4E-13	3.0E-13
78 ESF-HD-HYD-10	5.5E-14	1.1E-14	7.8E-14

The estimated values of permeability for all tests are summarized in Table 9-4. The test data file in the first column is identified by first the borehole number and zone number, then the date of the test, and then the order of the test during that day.

The results in Table 9-4 show that typically the estimated permeability of the same zone does not differ by more than 30 percent under different test conditions. This is on the same order of magnitude as the coefficient of variation of the permeability value estimated from Equation (9-1) derived from an error analysis (Tsang et al. 1996), where permeability estimates under similar test conditions were performed for the SHT. For the SHT, the coefficient of variation (ratio of the standard error of the calculated permeability to the calculated permeability) was 23 percent.

The results shown in Table 9-4 for the air injection into the entire length of borehole 45 are interesting. This is the case where Packers 1 and 2 were deflated, while the pressure sensors of all three zones remained in the same position as when the three zones were isolated by all inflated packers. The readings indicated that within the borehole, there was dynamic movement of air from zone 2 and zone 1 toward zone 3, confirming that in a heterogeneous formation, the fluid tends to flow toward the least resistive path in the rock formation. Hence in each injection test, flow out into the rock formation most probably occurred through only a fraction of the packed off zone. Therefore, for zones intersecting very conductive features, Equation (9-1) would tend to underestimate the permeability, and the greater the length of the zone tested, the greater the underestimation.

The frequency distributions of the local permeability values as tabulated in Tables 9-3 and 9-4 are shown in Figure 9-7 in the top and middle graphs. For comparison, the distribution for the air permeability values from the SHT block are also shown in Figure 9-7 in the bottom graph. Note that the range of air permeability values are quite similar in the DST and SHT. The variance in the permeability distribution from the SHT characterization is considerably larger than that from the DST, because the packed zones in the DST characterization are on the order of 12 m or longer, while the injection zones in the characterization for the SHT block are typically 5 to 8 inches. The longer the injection zones, the more averaging that occurs, therefore, the narrower the distribution or the smaller the variance. The statistics of the permeability values from the 14 boreholes from the DST are: minimum, 8.8×10^{-16} m^2; maximum, 2.0×10^{-12} m^2; arithmetic mean, 2.4×10^{-13} m^2; median, 1.4×10^{-13} m^2 and geometric mean, 1.0×10^{-13} m^2.

9.3.2 Interference Pressure Responses and Conceptual Model for Gas Flow in the DST Block

While in Section 9.3.1 the focus was on estimates of local permeability from the steady state pressure response in the zone into which air was injected, in this section the focus is on the pressure response from all the monitoring zones. Figures 9-8 through 9-16 show the pressure response from a selection of injection tests. A complete set of pressure responses from all injection tests will be submitted electronically and tracked through a TDIF. Figure 9-8 for example, shows the injection into the most permeable zone 52-3 with a local permeability of 2×10^{-12} m^2. For all these figures, the horizontal axis denotes time, the right vertical axis denotes injection flow rate in standard liters per minute, and the left axis denotes the pressure increase from ambient, ΔP, in kPa. The legend on each graph denotes those zones where pressure response is measured. The list is manually sorted, in descending

Table 9-4. Estimated Permeability Values from All Injection Tests Conducted in the 14 Boreholes

Test Identification	Injection Flow Rate Q (Standard Liters Per Minute)	Permeability (m^2)
45 Zone 1 (11-21-96 01)	200	4.46E-14
45 Zone 1 (3-05-97 03)	80	5.83E-14
45 Zone 2 (12-18-07)	80	2.41E-14
45 Zone 3 (3-05-97 04)	80	4.52E-13
45 Zone 3 (3-05-97 04)	160	3.17E-13
45 Zone 3 (3-05-97 04)	80	2.39E-13
45 Zone 3 (2-28-06)	50	5.35E-13
45 Zone 1,2 (3-05-97 05) 1	80	5.58E-14
45 Zone 1,2 (3-05-97 05) 2	80	5.48E-14
45 Zone 1,2,3 (3-05-97 08) 3	160	1.90E-13
45 Zone 1,2,3 (3-05-97 08) 1	80	2.43E-13
45 Zone 1,2,3 (3-05-97 08) 1	160	1.80E-13
45 Zone 1,2,3 (3-05-97 08) 1	80	1.43E-13
45 Zone 1,2,3 (3-05-97 08) 2	80	2.21E-13
45 Zone 1,2,3 (3-05-97 08) 2	160	1.63E-13
45 Zone 1,2,3 (3-05-97 08) 2	80	1.29E-13
45 Zone 1,2,3 (3-05-97 08) 3	80	2.53E-13
45 Zone 1,2,3 (3-05-97 08) 3	80	1.54E-13
46 Zone 1 (11-21-96 02)	10	4.05E-15
46 Zone 2 (12-18-02)	20	6.21E-15
46 Zone 3 (2-27-05)	30	9.04E-14
47 Zone 1 (11-21-96 05)	300	6.11E-14
47 Zone 2 (12-18-06)	100	4.35E-13
47 Zone 3 (2-28-04)	50	4.65E-13
48 Zone 2 (12-18-10)	80	3.52E-14
48 Zone 1 (11-22-96 03)	200	2.42E-14
48 Zone 3 (2-28-10)	50	3.35E-13
51 Zone 1 (11-21-96 03)	5.00	8.81E-16
51 Zone 2 (11-22-96 05)	10	4.43E-13
51 Zone 2 (3-05-97 02)	50	3.87E-13
51 Zone 2 (2-27-03)	100	2.42E-13

Table 9-4. Estimated Permeability Values from All Injection Tests Conducted in the 14 Boreholes (continued)

Test Identification	Injection Flow Rate Q (Standard Liters Per Minute)	Permeability (m^2)
51 Zone 2 (2-28-02)	90	4.06E-14
52 Zone 1 (11-20-96 02)	400	1.04E-13
52 Zone 2 (12-18-11)	100	1.16E-13
52 Zone 3 (3-05-97 01)	200	1.59E-12
52 Zone 3 (2-28-08)	50	2.02E-12
53 Zone 1 (11-22-96 02)	200	1.12E-13
53 Zone 1 (11-22-96 02)	400	8.87E-14
53 Zone 1 (11-22-96 02)	200	7.30E-14
53 Zone 2 (11-22-96 04)	400	6.12E-12*
53 Zone 2 (3-05-97 09)	400	1.27E-12
53 Zone 2 (12-19-03)	410	6.23E-12*
56 Zone 1 (11-21-96 04)	3.00	1.94E-15
56 Zone 2 (12-18-04)	10	3.42E-14
56 Zone 3 (2-28-09)	50	4.79E-13
57 Zone 1 (11-22-96 01)	500	2.69E-13
57 Zone 2 (12-18-08)	80	6.13E-14
57 Zone 2 (12-19-02)	40	7.63E-14
57 Zone 3 (2-27-01)	100	1.40E-13
69 Zone 1 (11-20-96 01)	400	2.12E-13
69 Zone 2 (12-18-03)	50	9.51E-15
69 Zone 3 (3-05-97 07)	150	3.82E-13
69 Zone 3 (2-27-06)	60	4.88E-13
70 Zone 1 (11-19-96 02)	200	1.85E-14
70 Zone 2 (12-18-05)	50	4.51E-14
70 Zone 3 (3-05-97 06)	150	2.72E-13
70 Zone 3 (2-28-05)	50	4.20E-13
73 Zone 1 (11-19-96 03)	200	6.64E-14

*The permeability value of over 6×10^{-12} m^2 for 53-2 measured in November and December 1996 is not a reliable estimation of the permeability of the formation surrounding zone 53-2. During November and December 1996, two packers were installed in the 14 boreholes to nominally isolate the last 2/3 length of each boreholes. Due to obstruction by rock in borehole 53, the second packer in borehole 53 is set at about 2 meters from the hole collar. As a result, the injection zone 53-2 was surrounded by open sections of boreholes from which injected air could escape, which led to an erroneously large estimate of the permeability. The situation was rectified in February 1997 when a third packer was placed near the collar of all boreholes, then the pressure response in 53-2 from air injected in 53-2 correctly reflected the permeability of the rock formation.

Table 9-4. Estimated Permeability Values from All Injection Tests Conducted in the 14 Boreholes (continued)

Test Identification	Injection Flow Rate Q (Standard Liters Per Minute)	Permeability (m^2)
73 Zone 2 (11-22-96 07)	24	6.79E-15
73 Zone 2 (12-19-01)	6	5.76E-15
73 Zone 3 (2-28-07)	50	1.00E-13
75 Zone 1 (11-21-96 06)	500	3.59E-13
75 Zone 1 (2-28-01)	200	4.89E-13
75 Zone 2 (12-18-01)	100	2.85E-13
75 Zone 2 (2-28-03)	100	1.37E-13
75 Zone 3 (2-27-02)	100	3.03E-13
78 Zone 1 (11-19-96 01)	200	5.45E-14
78 Zone 2 (11-22-96 06)	60	1.14E-14
78 Zone 3 (2-27-04)	60	7.79E-14

order of steady-state pressure rise, so that the injection zone will always be at the top of the list. Figure 9-8a shows that the pressure in the majority of the boreholes rises and falls in response to the constant-flow air injection in 52-3.

In general, the largest pressure responses were in those monitoring zones that are relatively close to the injection zone 52-3. These are represented in Figure 9-8b. Figure 9-8d shows that even those zones that are tens of meters away from the injection zone communicated with 53-2, although the magnitude of the response was small. Thus, there is the general trend that the farther apart the injection and monitored zone, the smaller the magnitude of pressure response. However, note that 57-3, which is in close physical proximity to 52-3, is listed in Figure 9-8d, the group of smallest measurable steady state ΔP's. This indicates the presence of a low permeability barrier between 52-3 and 57-3.

Figure 9-9 shows the pressure response from injection into 51-1, which was the most impermeable zone tested (with an estimated local permeability of 8.8×10^{-16} m^2). The contrast between Figure 9-9a and 9-8a is apparent. The pressure built up in 51-1 almost linearly to 120 kPa, even with a small injection rate of 10 liters per minute. This indicates a highly impermeable rock formation. A pressure response down to 0.5 percent of the maximum ΔP was not detected in any other monitored zone. Figure 9-9b plots those responses that are smaller than 0.5 percent of the maximum ΔP's, and only two zones can be picked out: in 56-1, which is adjacent and parallel to 51-1, and perhaps in 70-2.

Figure 9-10 shows the injection test in another relatively low permeability zone, 78-2 ($k = 1.14 \times 10^{-14}$ m^2). Note again the steep pressure rise in 78-2 with the initial injection flowrate of 100 SLPM. Consequently, the flowrate was adjusted down in two steps to the final constant rate of 60 SLPM. A steady state ΔP was reached in 78-2. Again, no other interference pressure rise was

observed until the left vertical axis in Figure 9-10 was reduced to read ΔP less than 2 percent of the maximum; then, two pressure response curves from monitored zones 73-2 and 75-2 appeared. There was a larger response in 73-2 due to the proximity of the two adjacent and parallel zones of 78-2 and 73-2.

Figures 9-11a and 9-11b show the injection test in a reasonably permeable zone, 75-1 ($k = 4.9 \times 10^{-13}$ m^2). While most of the monitored zones that registered a pressure response were from boreholes within the same spatial cluster centered around $y = 28$ m, there was one exception: Figure 9-11b shows that zone 46-2 in the other cluster, tens of meters away, also responded to the air injection in 75-1.

Figure 9-12 shows the pressure injection test in zone 69-3 on two different dates with different constant flow rates. The data demonstrate that the injection test is repeatable. The local permeability of 69-3 is similar to that of 75-1 shown in Figure 9-11.

The next example is from the injection into 51-2 ($k = 2$ to 4×10^{-13} m^2), shown in Figure 9-13. Note that in Figure 9-13a, the zones which responded to 51-2 with respective steady-state ΔP within 10 percent of the injection zone, are parallel zones and therefore in close proximity to 51-2. In addition, more zones within the same spatial cluster as 51 (collar centered around $7 = 7$ m) responded with smaller ΔP (less than 10 percent but greater than 3 percent of the ΔP from injection zone 51-2), as shown in Figure 9-13b. Figure 9-13c shows those pressure responses where the steady-state ΔP is less than 3 percent of the maximum ΔP in the injection zone 51-2. Note that the distant boreholes 73, 75, 78 in the other spatial cluster (borehole collars centered around $Y = 28$ m) also registered pressure rises in response to the injection test.

Figure 9-14 shows the interference pressure data for air injection tests into zone 48-3 (local permeability 3×10^{-13} m^2). While there were very few zones with a pressure response within 8 percent of the maximum in the injection zone (Figure 9-14a), numerous zones responded to the injection with ΔP less than 8 percent of the maximum ΔP for zone 48-3.

Figure 9-15 shows the interference pressure data from the injection tests into 69-1, which had a local permeability of 2×10^{-13} m^2. Note again that while the largest steady-state ΔP's shown in Figure 9-15a were from boreholes within the same spatial cluster as, and parallel to, 69-1. Distant zones tens of meters away also showed a pressure response when the vertical axis was scaled down to less than 1 percent of the maximum ΔP in Figure 9-15b. The pressure sensor for 69-1 demonstrated instability as shown in Figure 9-15b. The sensor was replaced for tests carried out in February and March of 1997.

Lastly, in Figure 9-16, interference pressure data from the air injection into zone 53-1 are presented. Zone 53-1 has a local permeability of 0.7 to 1×10^{-13} m^2, on the order of the geometric mean of all the permeabilities measured. The constant flow rate doubled from 200 to 400 SLPM during the same test. Again, similar to the previous cases discussed, a large number of zones responded and were not limited to those zones that were in close proximity to the injection zone, though the ΔP was typically small compared to that of the injection zone.

The interference pressure data from the 14 boreholes tested demonstrates that on a scale from 1 to 30 meters, the fractures appeared to be connected pneumatically, and the air flow in the fractures resembled more that of flow through a continuum than flow through a discrete fracture network. Though the local permeability values of the zones ranges over several orders of magnitude, most of the flow seems to be taking place through a medium with an average permeability on the order of a fraction of a darcy, and there is no evidence of a large permeability feature that formed a direct connection between zones.

This is in contrast to the SHT block, where there was evidence of a large permeability fracture zone about 4 m in extent. To illustrate, the pressure responses for an air injection test in borehole 11 in the SHT block are shown in Figure 9-17 and Figure 9-18. Figure 9-17 shows the pressure responses from the injection tests into borehole 11 and three nearby monitoring boreholes (28, 29, 31), which are all parallel to and within a meter of borehole 11. Figure 9-18 shows the pressure responses of five more distant boreholes: boreholes 6, 8 and 12 which are parallel to 11, and boreholes 7 and 13 which are orthogonal to 11. The pressure data shown in Figure 9-17 reveal the presence of a direct flow path from borehole 11 to borehole 6 and 7. In other words, a steady-state pressure response of an almost identical magnitude as that from borehole 11 was observed in boreholes 6 and 7, even though these boreholes are not spatially close to 11. On the other hand, boreholes 28, 29, and 31, which are spatially closest to borehole 11, registered much smaller pressure increases in response to air injection into borehole 11.

Based on the air injection data, borehole video logs, and fracture mapping data, it was determined that there is a vertical high permeability feature (permeability values of darcies) about 4 m in extent, which intersects the boreholes 11, 2, 6, 8, 12, 7, and 13, while the rest of the SHT block exhibited a lower permeability background (Birkholzer and Tsang 1996). The pressure response in boreholes 28, 29, 31 were through the lower permeability background.

For injection and monitored zones that are closely spaced, the characterization data of the DST show the same kind of response exhibited by boreholes 28, 29, 31 in the SHT. When the measured distance between injection and monitoring sections increases to tens of meters, the DST characterization data show a pressure rise of a much smaller magnitude. None of the DST data collected have the same characteristics as those pressure responses shown in Figure 9-18, where distant boreholes showed a pressure response similar in magnitude to that of the injection zone. The characterization data from the 14 boreholes in the observation drift therefore do not reveal a direct connection on the scale of tens of meters. Rather, the data support the concept that the fractures are a heterogeneous continuum.

In summary, the interference air permeability data indicate that the fractures are well connected, in that a pressure response to air injection was obtained in most monitoring zones. However, the magnitude of the pressure response was typically small in monitored zones as compared to the response from the injection zone. A direct connection between the two zones by a large fracture such as that found in the SHT block (Birkholzer and Tsang 1996) was not evidenced here. This is not inconsistent with the fracture mapping of a DLS performed by the USGS/USBR in the ESF. A review and analysis of that data by Sonnenthal and Ahlers (1997) indicates that more than half of the mapped fractures have lengths less than 1 m and an average spacing of 0.5 m; and the lengths of the fractures range from less than 1 m to greater than 18 m, the spacing of the fractures increases

with length. Therefore, the DST block may be conceptualized as a fracture continuum formed by well-connected, mostly "short" fractures (less than 1 m long).

As stated in Section 9.3.1 above, the estimated local permeability values have a geometric mean of 1×10^{-13} m^2 and median value of 1.4×10^{-13} m^{-2}. Since a discrete large permeability feature was not found in the set of 14 boreholes tested, and since, in a continuum, the fluid flow will seek out the least resistive path while avoiding low permeability regions, the fractures in the DST block are well approximated by a continuum with an average permeability on an order of 10^{-13} m^2.

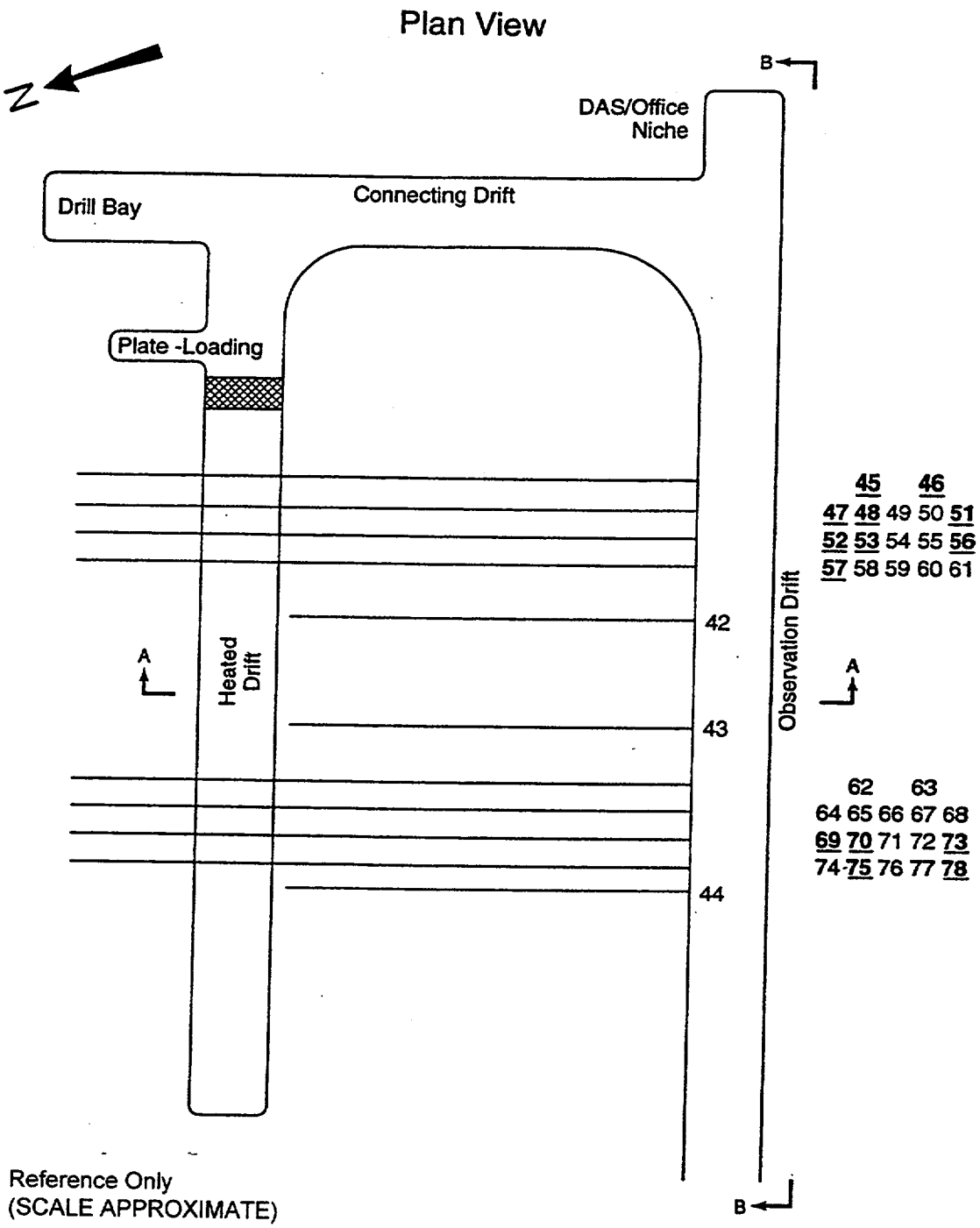

Figure 9-1. Plan View of DST Block

Section B-B

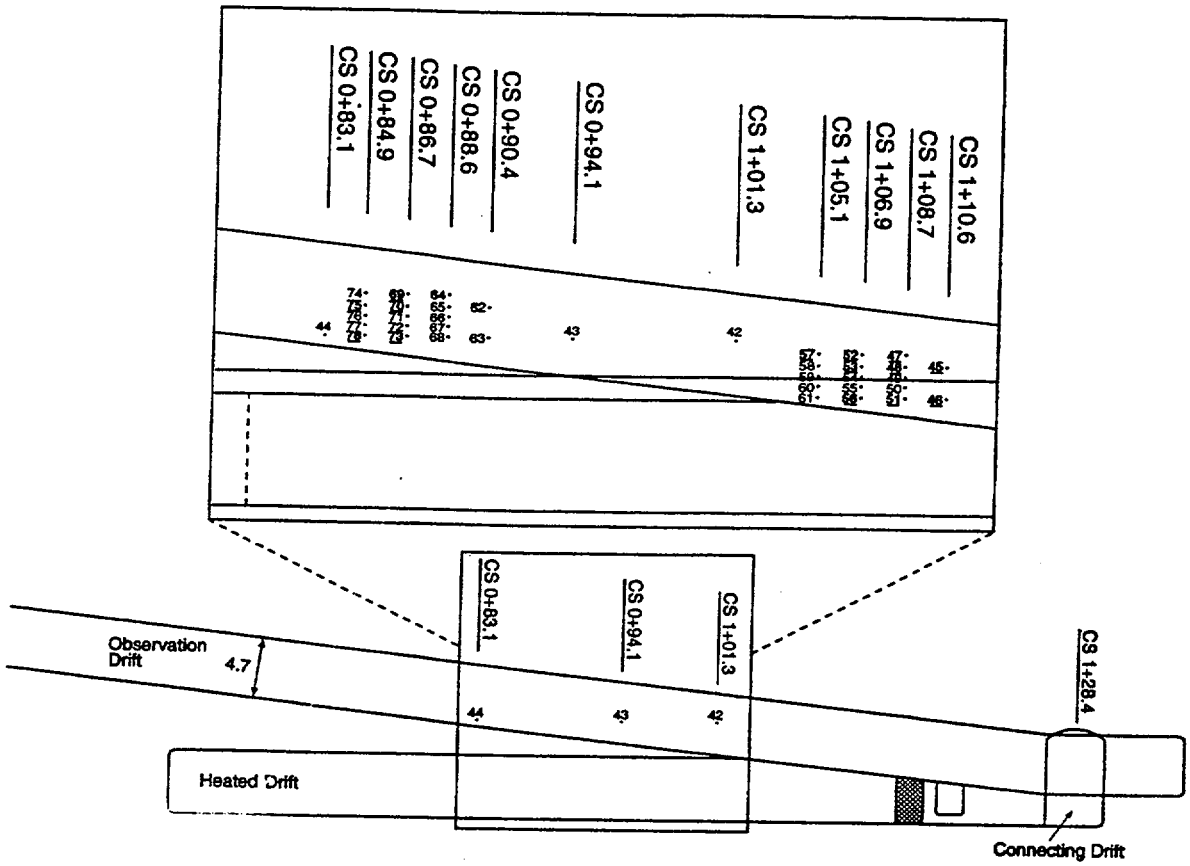

Reference Only
(SCALE APPROXIMATE)

Figure 9-2. E-W Cross-Section of DST Block

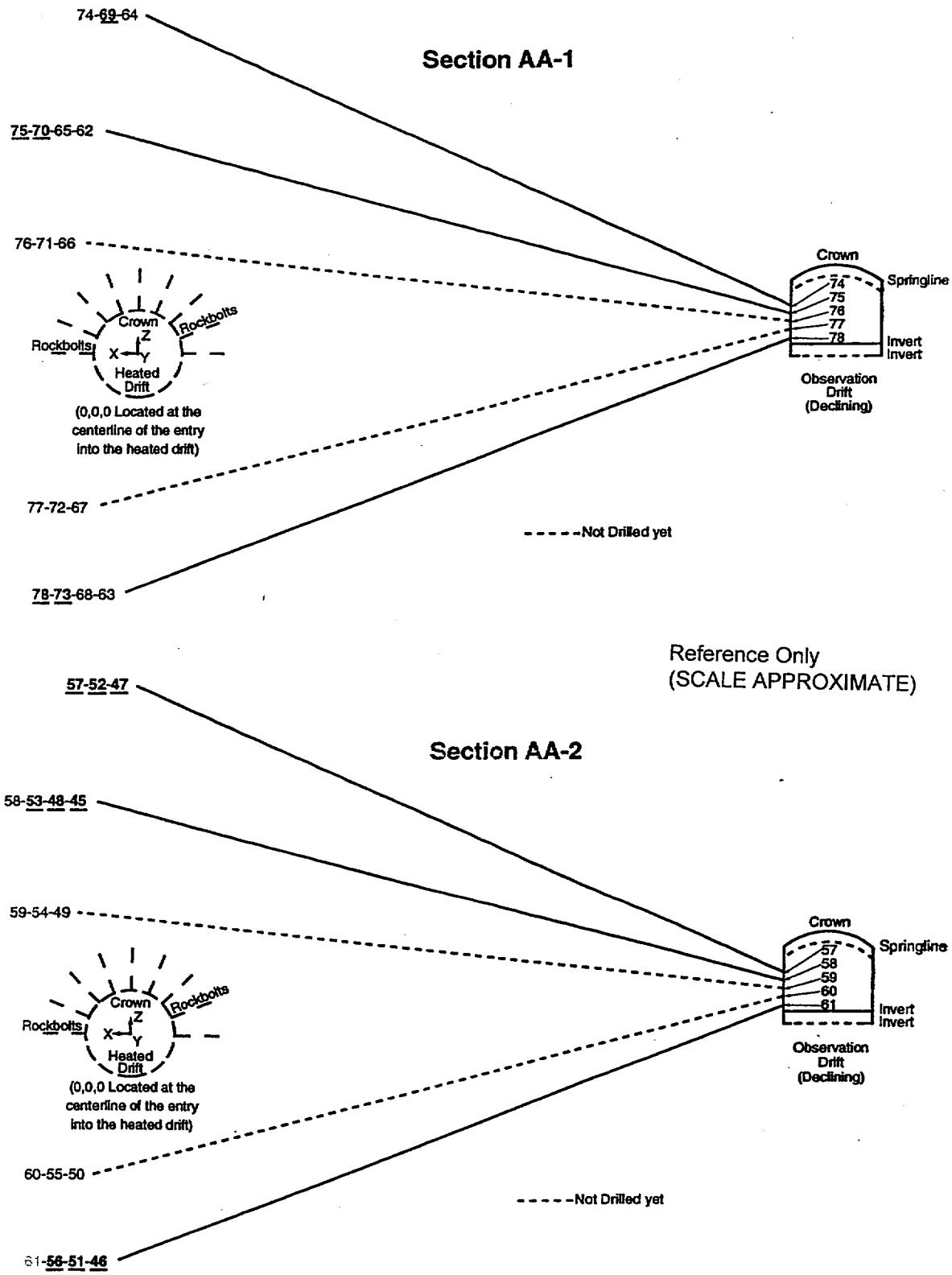

Figure 9-3. Two N-S Cross-Sections of DST Block

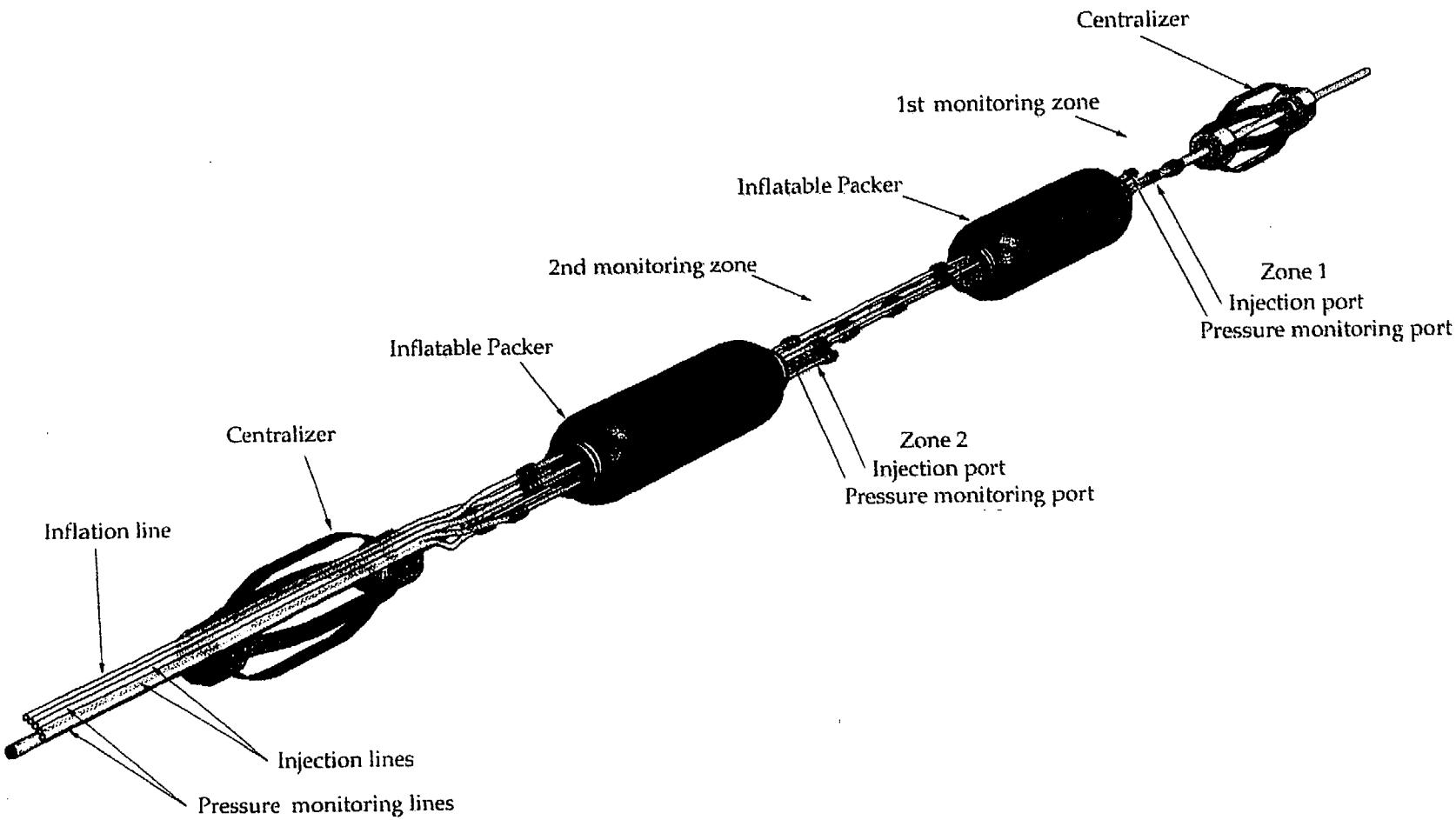

Figure 9-4. Schematic Diagram of a Packer String with Two Packers

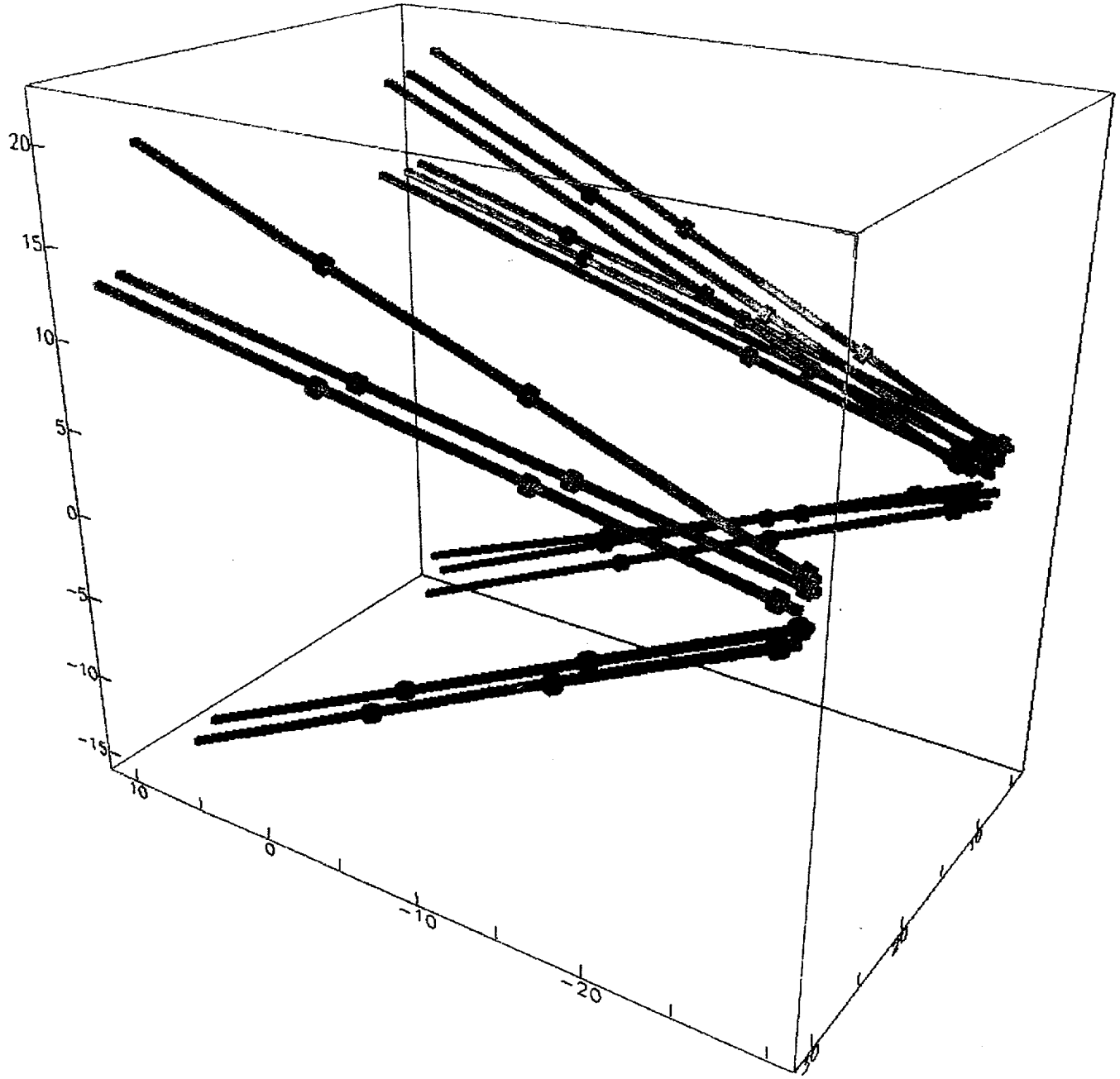

NOTE: Characterization of the DST area packer positions in 14 observation drift boreholes.

Figure 9-5. Packer Positions for Air Permeability Tests

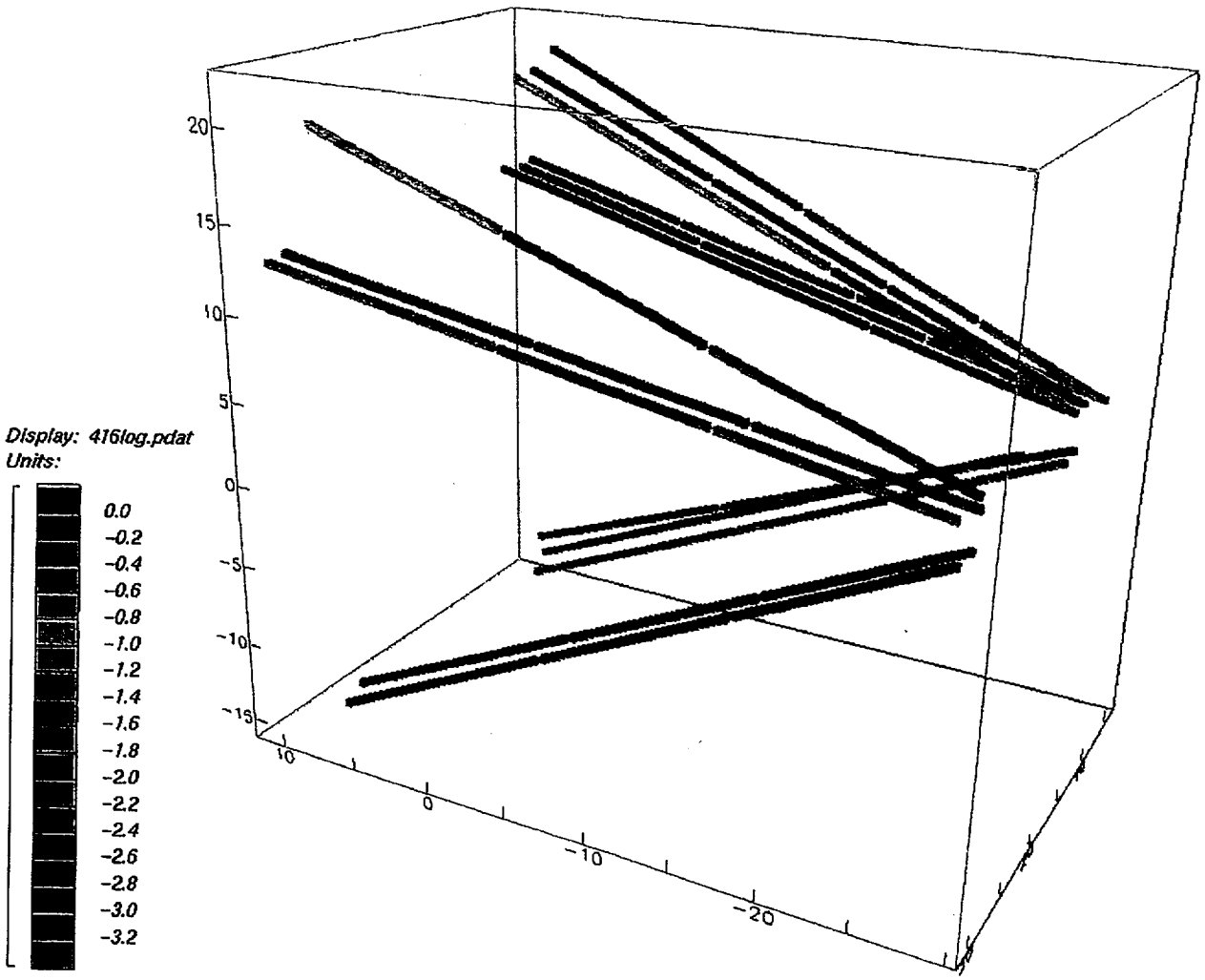

NOTE: Air permeability estimates are normalized to two darcies, color code in logarithm scale.

Figure 9-6. Local Permeability Estimates in 41 Cross-Sections of the 14 Observation Drift Boreholes

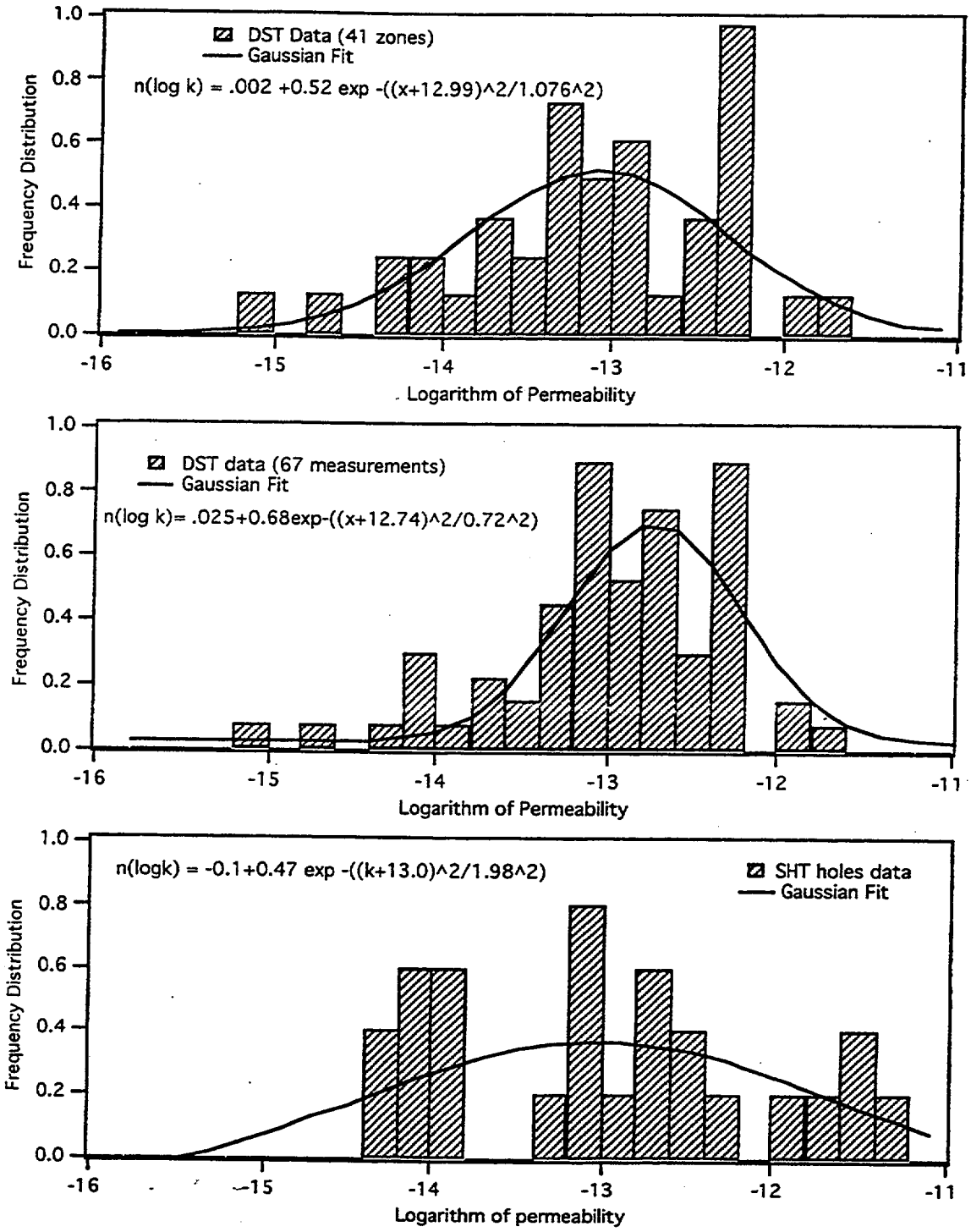

Figure 9-7. Frequency Distribution of Permeability Values from the DST and SHT Blocks

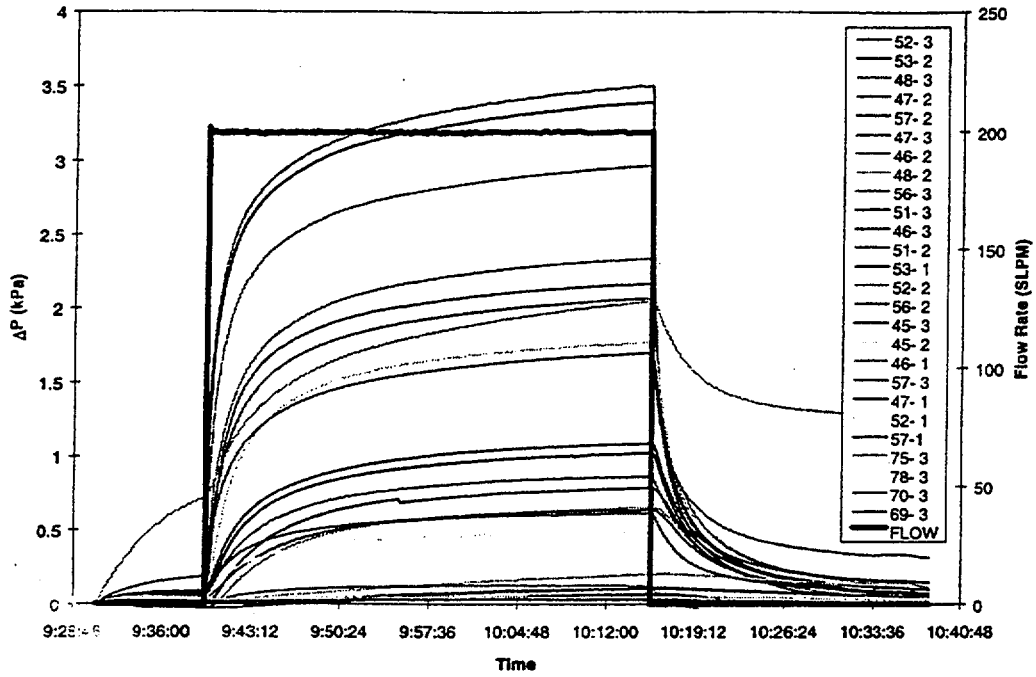

(a) Generic: March 5, 1997

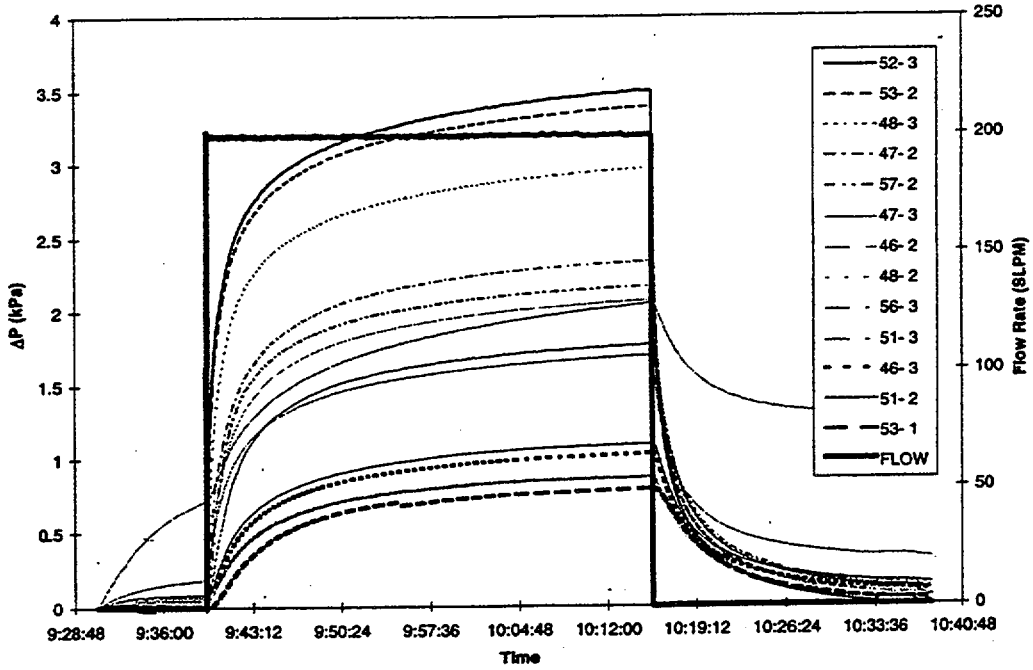

(b) ΔP > 10% (> 20% of Maximum ΔP): March 5, 1997

Figure 9-8. Interference Pressure Data From Injection in 52-3

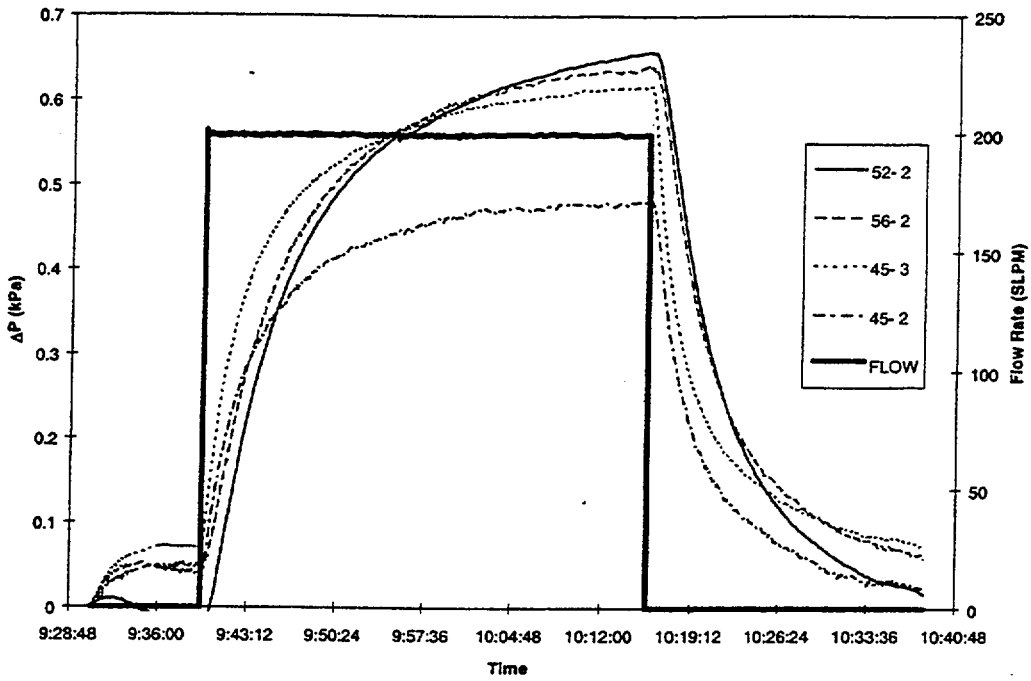

(c) 20% > ΔP > 6%: March 5, 1997

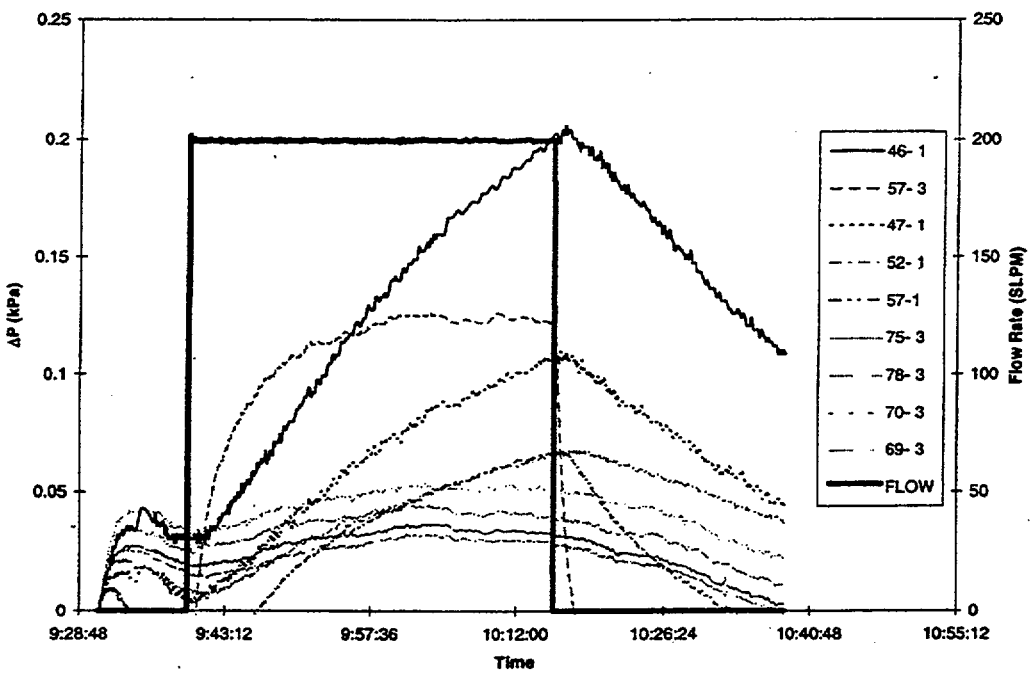

(d) ΔP ≤ 6%: March 5, 1997

Figure 9-8. Interference Pressure Data From Injection in 52-3 (continued)

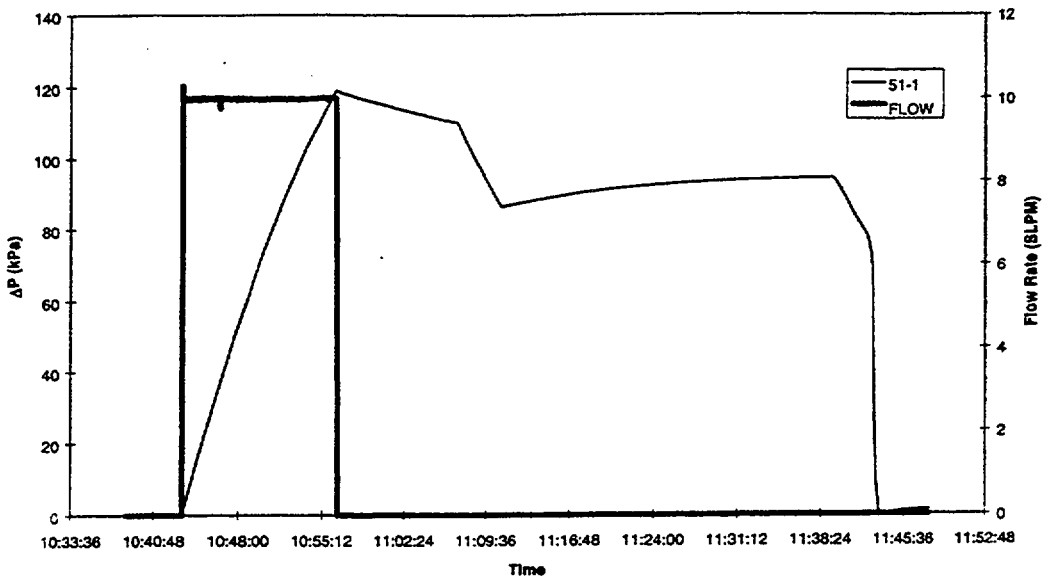

(a) ΔP > 0.5%: November 21,1996

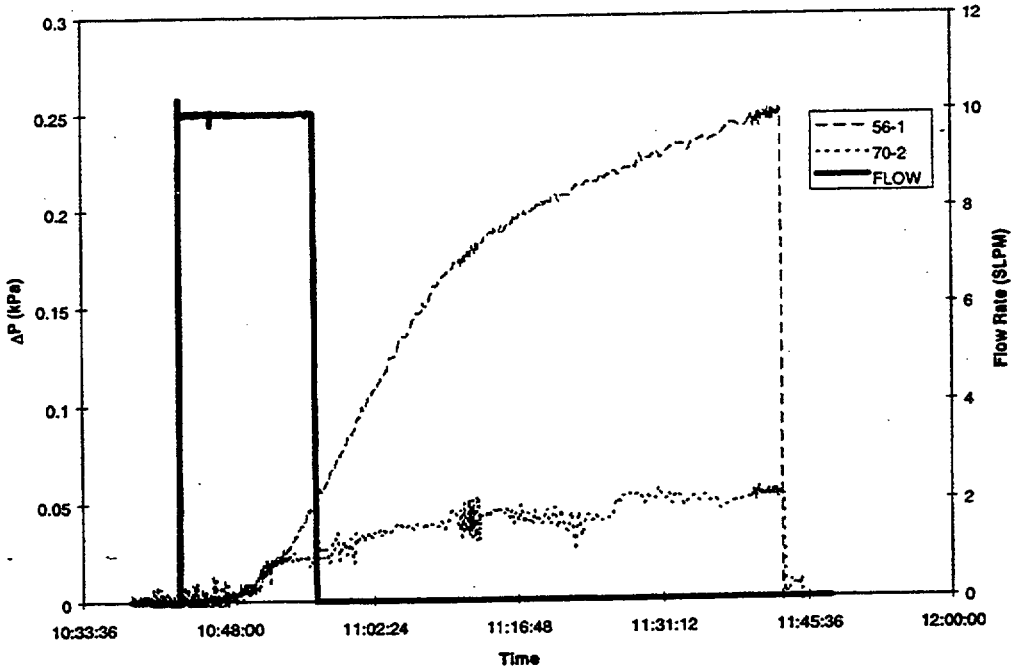

(b) ΔP < 0.5%: November 21, 1996

Figure 9-9. Interference Pressure Data From Injection in 51-1

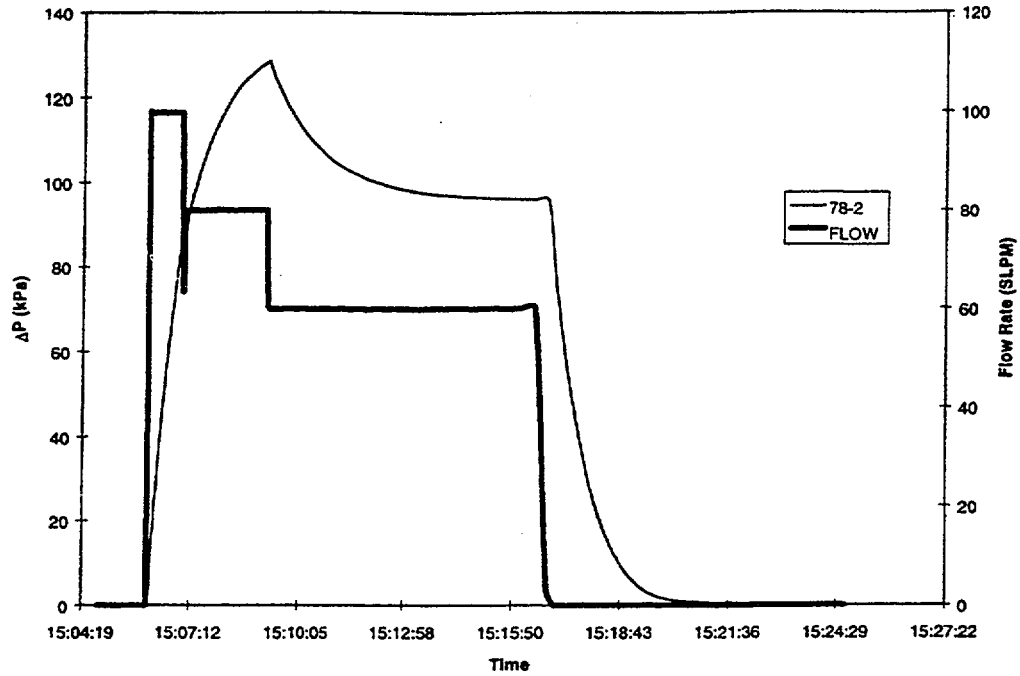

(a) ΔP > 2%: November 22, 1996

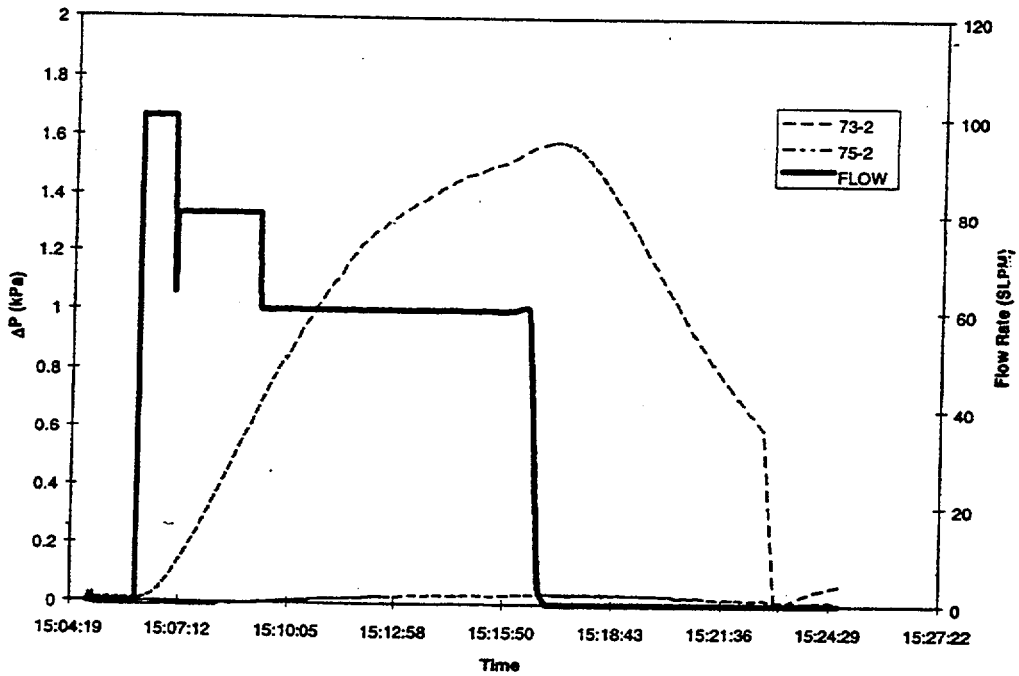

(b) ΔP < 2%: November 22, 1996

Figure 9-10. Interference Pressure Data From Injection in 78-2

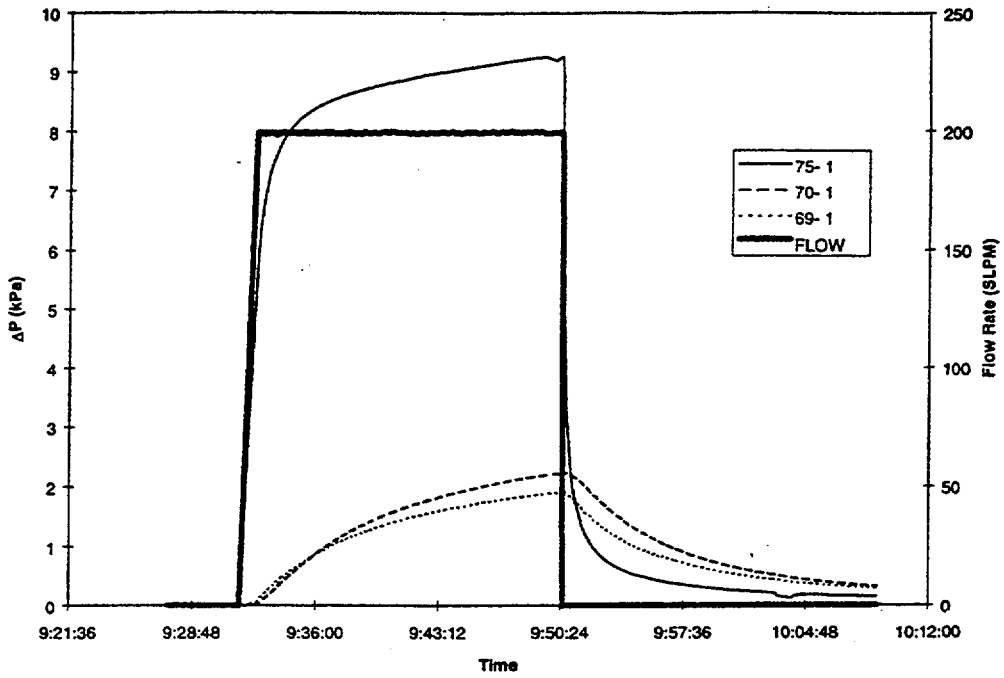

(a) ΔP > 5%: February 28, 1997

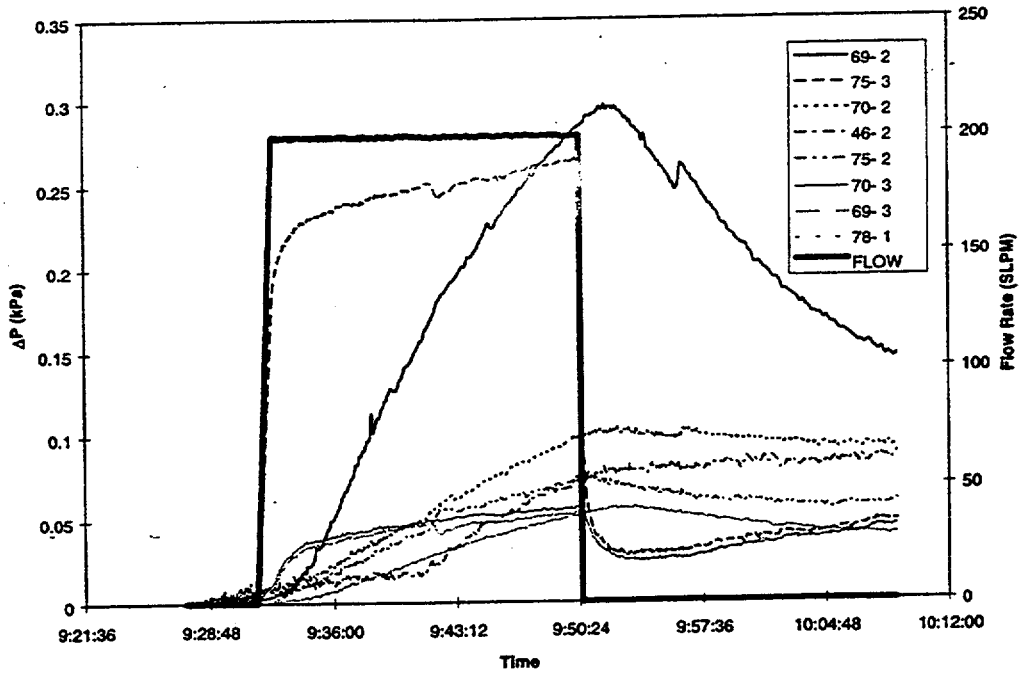

(b) ΔP < 5%: February 28, 1997

Figure 9-11. Interference Pressure Data From Injection in 75-1

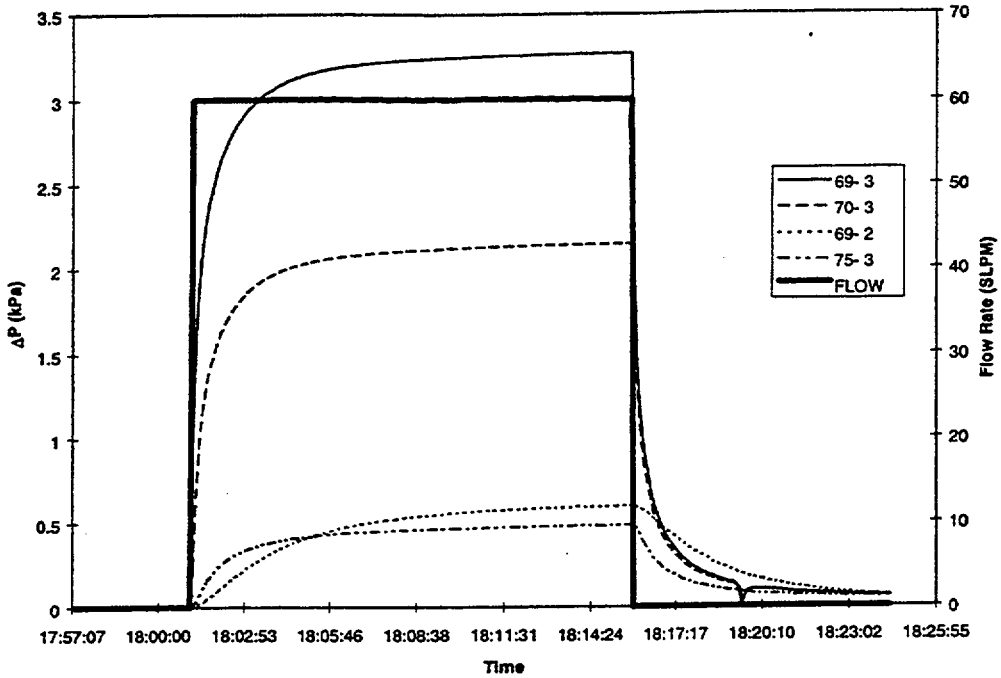

(a) ΔP > 5%: February 27, 1997

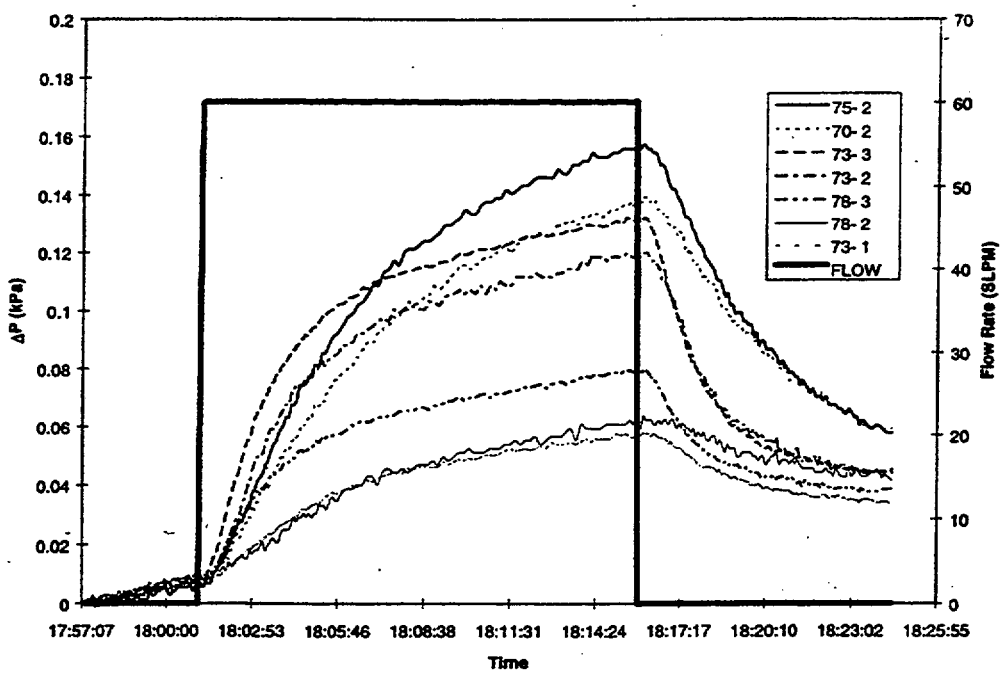

(b) ΔP ≤ 5%: February 27, 1997

Figure 9-12. Interference Pressure Data From Injection in 69-3

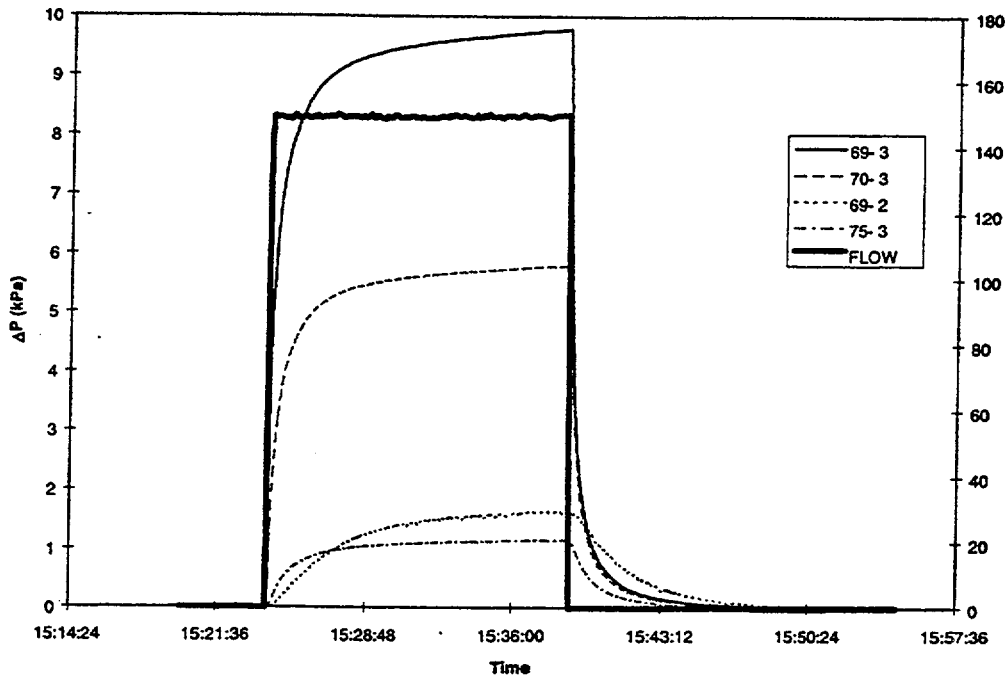

(c) ΔP > 3%: March 5, 1997

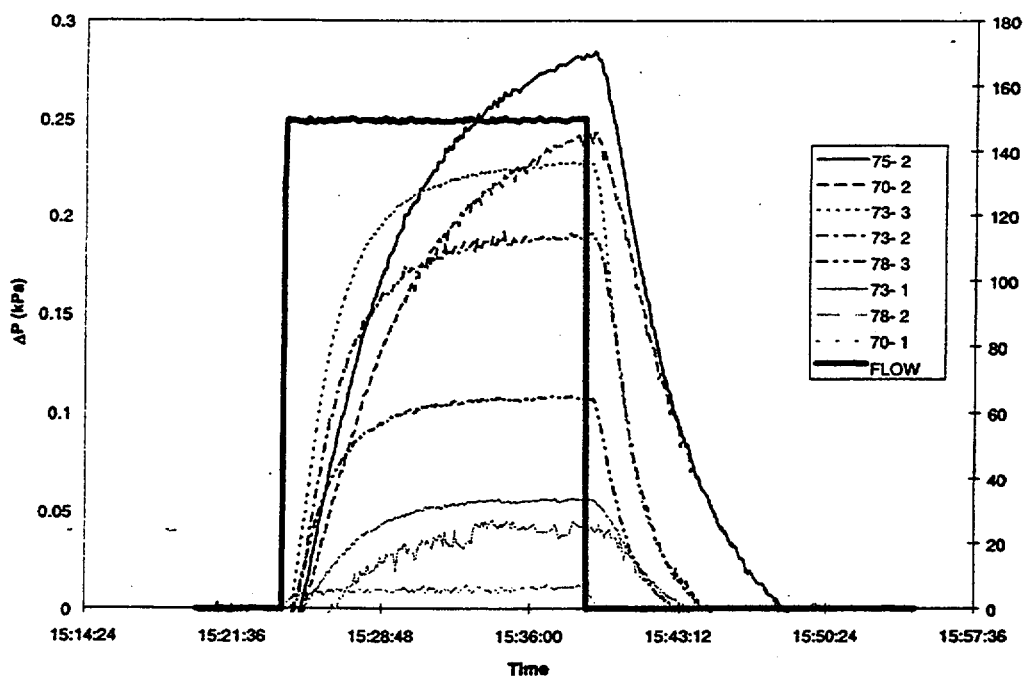

(d) ΔP ≤ 3%: March 5, 1997

Figure 9-12. Interference Pressure Data From Injection in 69-3 (continued)

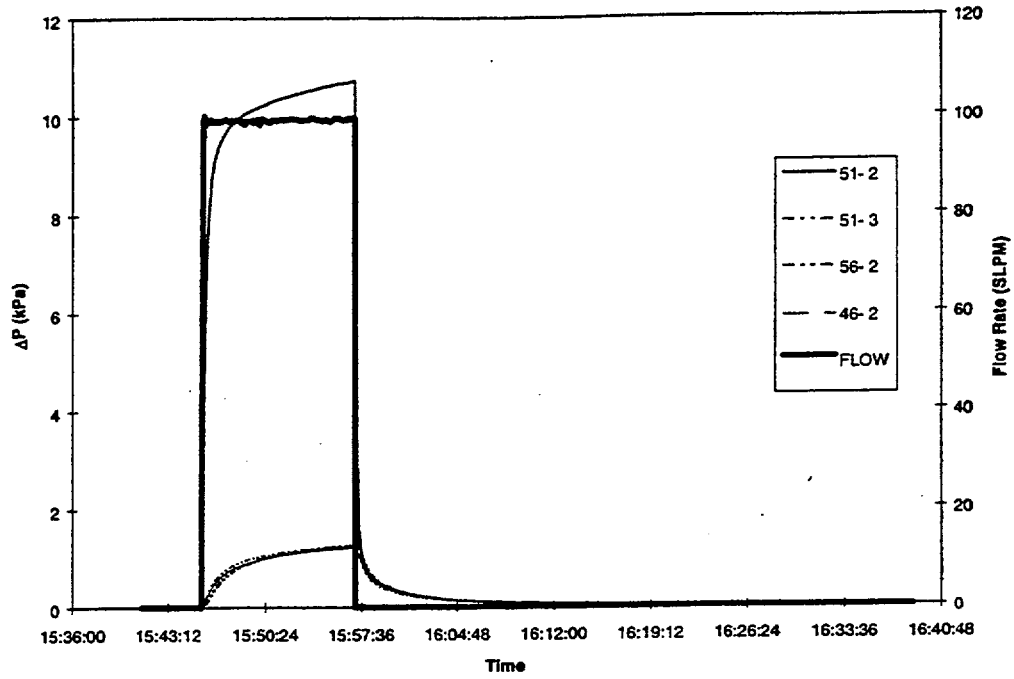

(a) ΔP > 10%: February 27, 1997

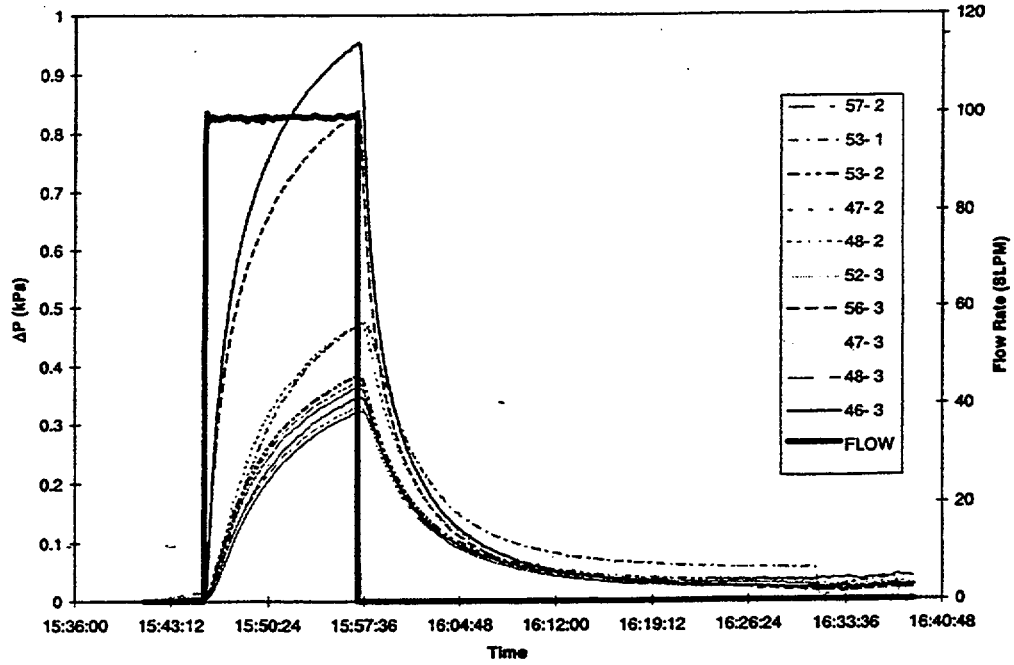

(b) ΔP ≥ 3%: February 27, 1997

Figure 9-13. Interference Pressure Data From Injection in 51-2

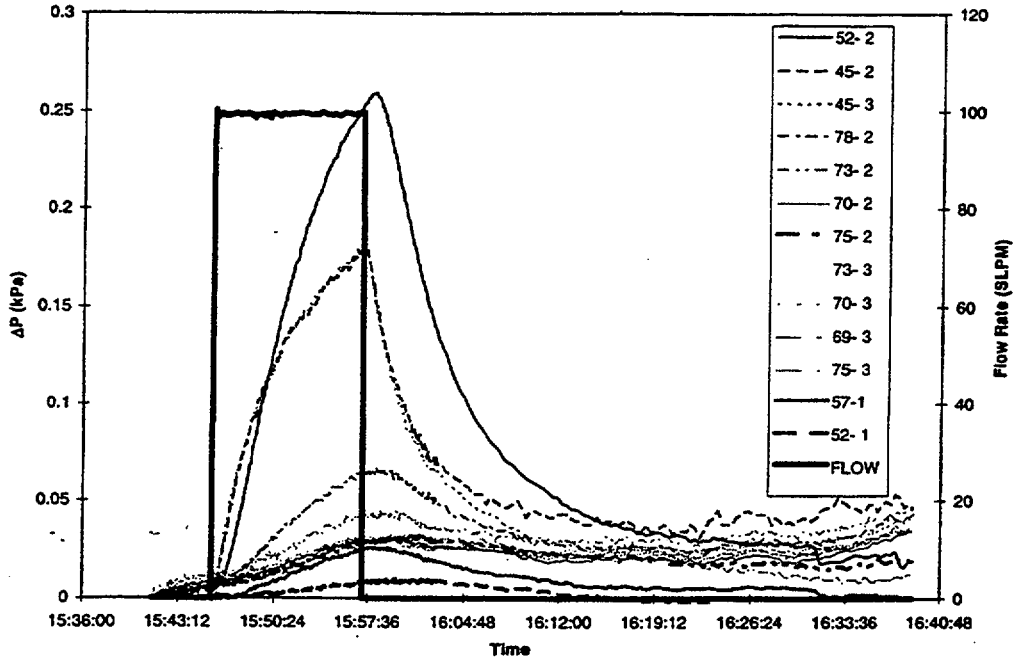

(c) ΔP < 3%: February 27, 1997

Figure 9-13. Interference Pressure Data From Injection in 51-2 (continued)

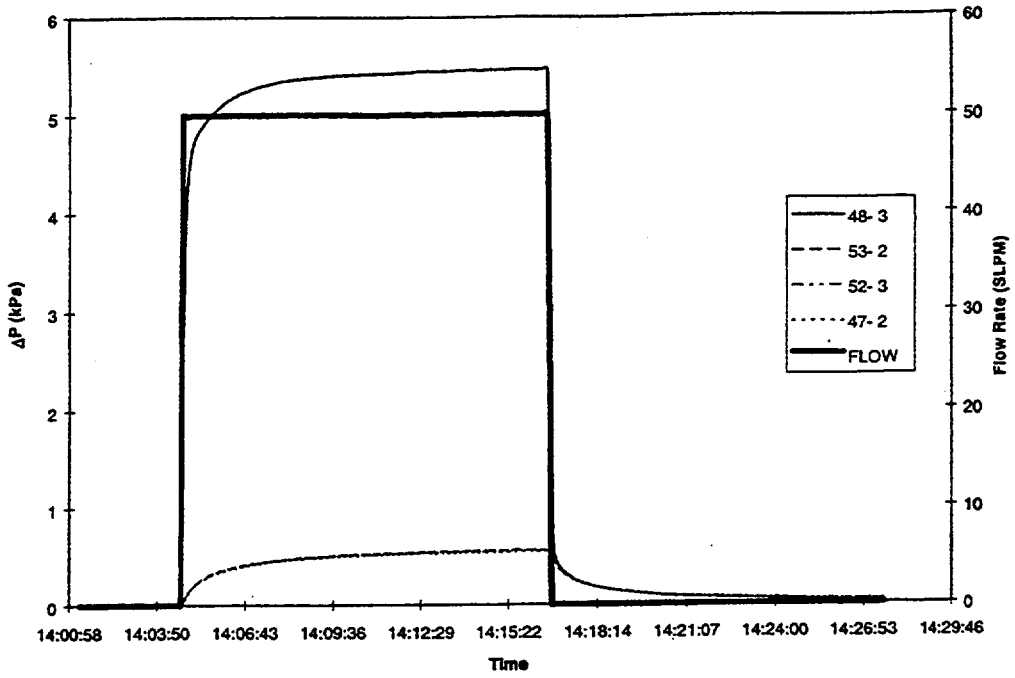

(a) ΔP > 8%: February 28, 1997

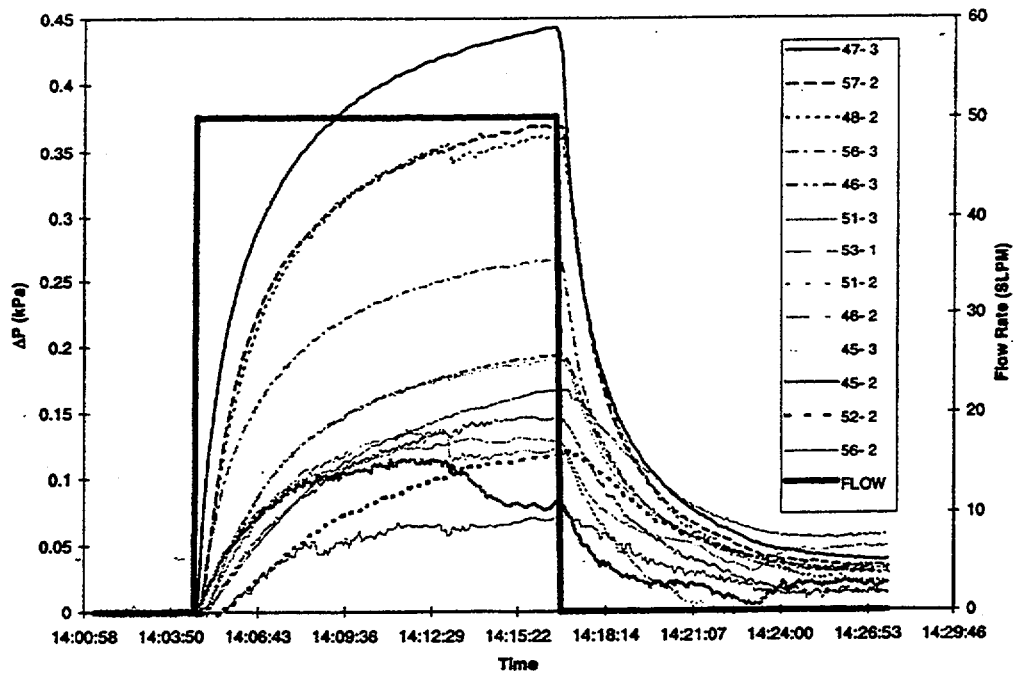

(b) ΔP ≤ 8%: February 28, 1997

Figure 9-14. Interference Pressure Data From Injection in 48-3

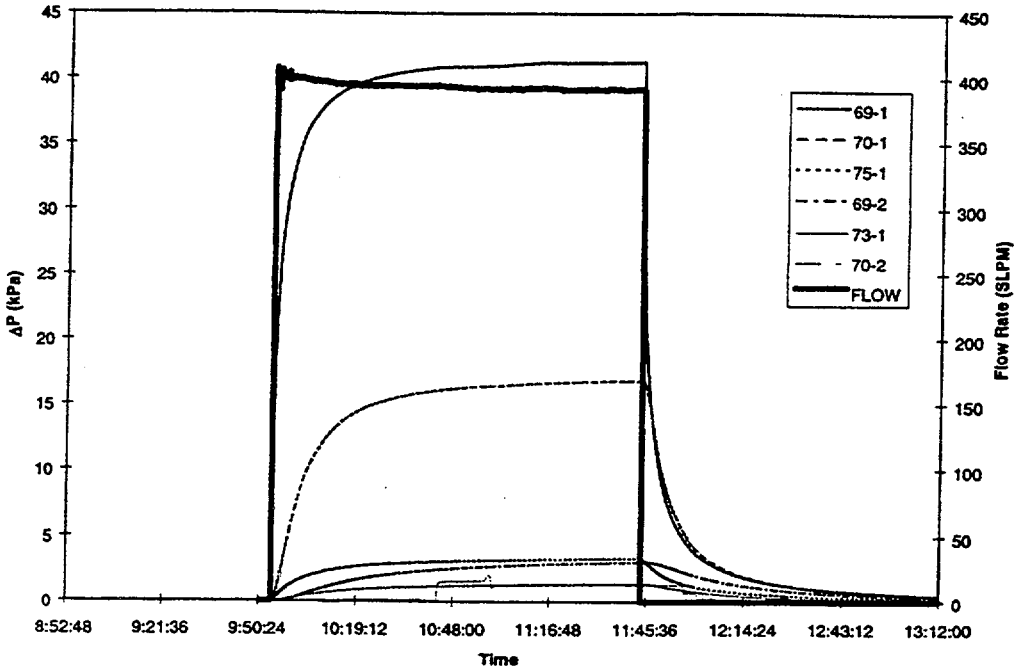

(a) ΔP > 1%: November 20, 1996

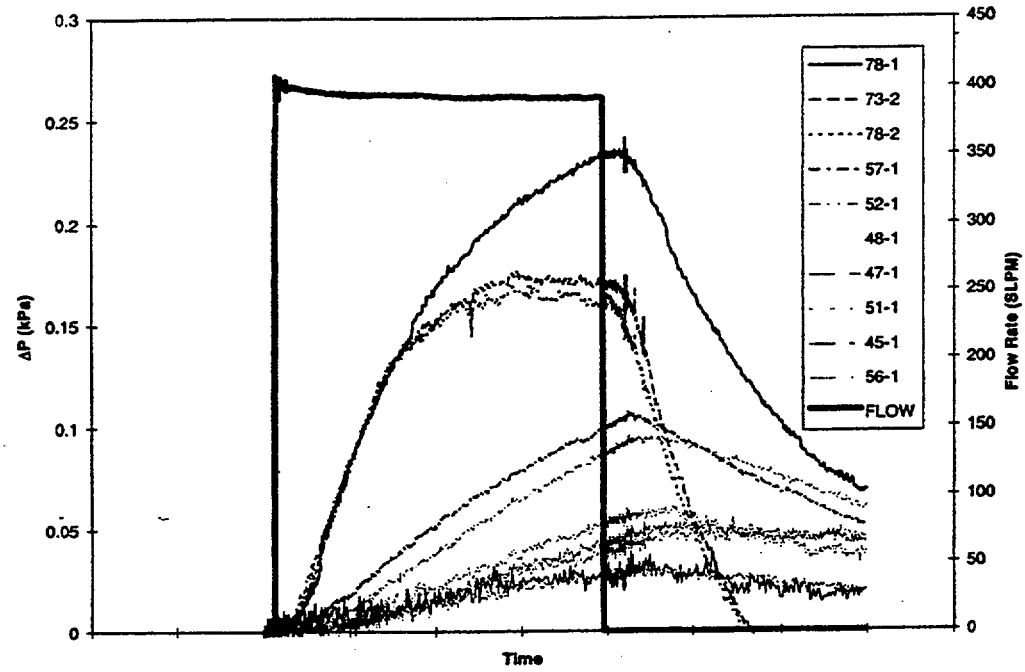

(b) ΔP < 1%: November 20, 1996

Figure 9-15. Interference Pressure Data From Injection in 69-1

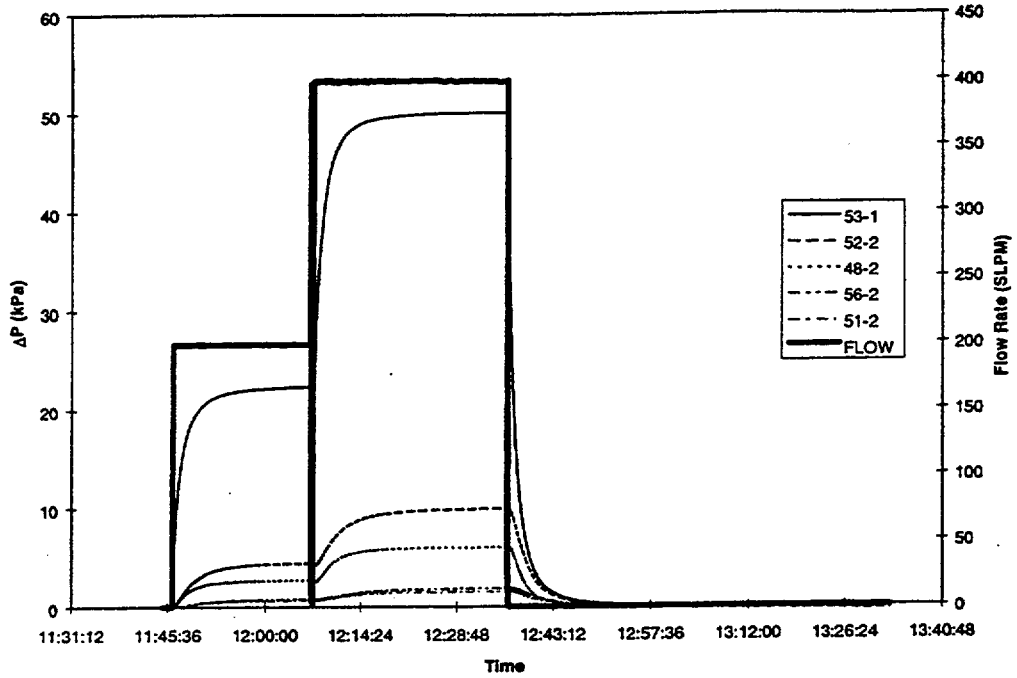

(a) ΔP ≥ 3%: November 22, 1996

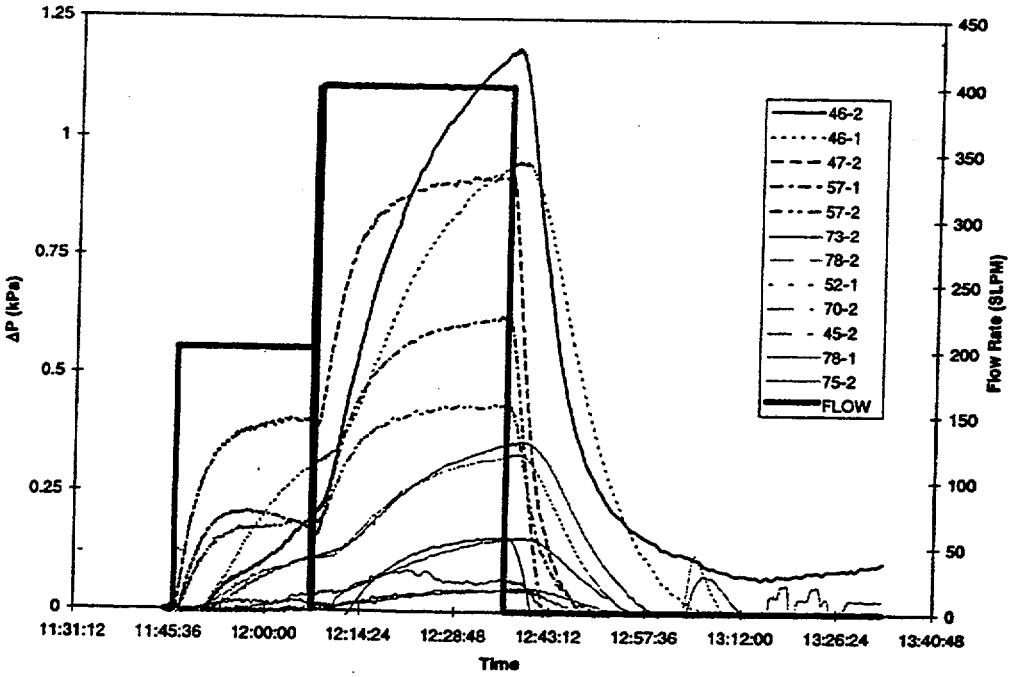

(b) ΔP < 3%: November 22, 1996

Figure 9-16. Interference Pressure Data From Injection in 53-1

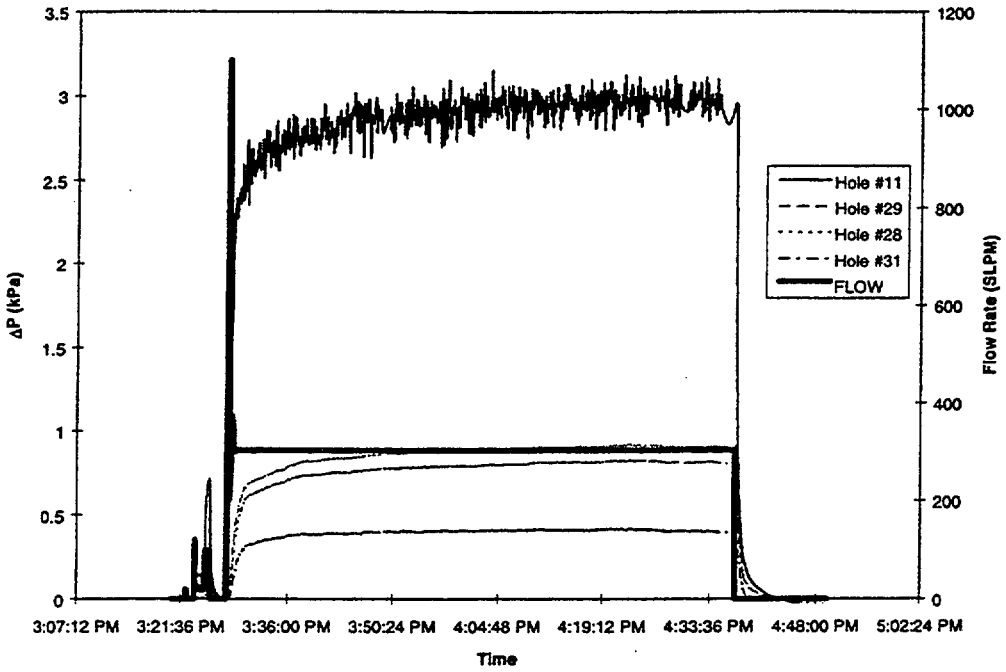

Figure 9-17. Pressure Response From Nearby Boreholes From Injection in Borehole 11 in SHT Block: May 28, 1996

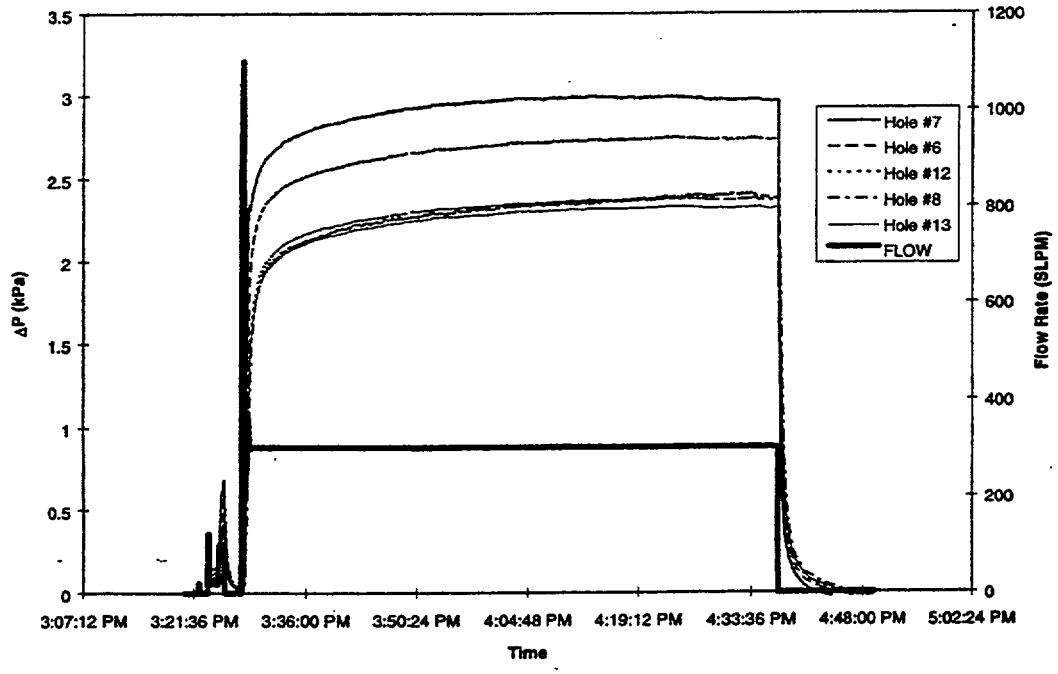

Figure 9-18. Pressure Response From Distant Boreholes From Injection in Borehole 11 in SHT Block: May 28, 1996

10. FIELD MEASUREMENTS: ADDITIONAL

10.1 INFRARED IMAGING

10.1.1 Objective and Description

The objective of the infrared imaging of rock surfaces was to establish the initial conditions on the drift walls prior to the onset of heating. For the duration of the DST, the rock surfaces on the "cold" side of the bulkhead near the heated drift and along the observation drift will be periodically examined using an infrared camera to determine what effect the heater has on rock surface temperatures. Monitoring surveys are performed to assess whether the thermal distribution from the heater can be observed on the rock surface, to determine if this can be related to any physical features known to exist in the rock, and perhaps to discover new features apparent only from thermal data. Such features could include surface outlets for pathways of fluids or gases induced by thermal changes.

This data has been entered into Automated Technical Data Tracking and were submitted to the Records Center under DTN LB970500123142.002 and TDIF #306134. The scientific notebook number is YMP-LBNL-JSW-1.2. All images obtained in this study were performed by qualified personnel and the equipment used was calibrated under the LBNL QA Program. All data presented are qualified data. Infrared imaging was performed in satisfaction of Level 4 Milestone SP5125M4 (Cook and Wang 1997).

10.1.2 Methodology

The observation drift was chosen for infrared study because it has a long, accessible surface, nearly parallel to the heated drift, as illustrated in Figure 2-2, and also because it has been characterized using air permeability techniques. Because the observation drift is predicted to be slow in its thermal response to the heaters due to its distance (~ 30 m) from the heated drift, the potentially fastest responding area, that of the bulkhead, was also chosen for the infrared study. The observation of changes in a thermal feature above the heater in the SHT face inspired the baseline study in the DST bulkhead area. Any thermal features to be observed near the bulkhead would likely be more easily detected to quantify heat transfer processes induced by the nearby heat source, as opposed to the more likely subtle and long range thermally induced changes along intrinsic features that might be observed in the observation drift.

This report concerns the baseline set of thermal pictures taken in May 1997. The baseline data will be compared with data taken later after the heater is turned on. Similar surveys are in progress in the SHT block. The DST covers a much larger area than the SHT block. Furthermore, the drift walls in the observation drift in the DST are not scheduled to be covered with protective sheaths, therefore infrared images can be taken on all exposed surfaces.

To establish an efficient approach for the DST surveys, a newly assembled infrared/moisture monitoring mobile cart was deployed for this DST baseline study. With the camera and sensors mounted on the cart and with computer control to automate data collection, the efficiency for

infrared/moisture survey has improved over earlier SHT surveys with hand-held infrared camera operations.

The procedure for acquiring infrared images involves using the cart-mounted infrared camera to take pictures of the region along the walls and ceilings of the observation drift and near the bulkhead area of the heated drift. Frames in a given data set were taken from approximately the same distance and perpendicular to the surface of interest. As before [Level 4 Milestone SP9230M4 *Infrared Imaging of the Single Heater Area*, January 1997 (LBNL 1997a); Level 4 Milestone SP9237M4 *Second Quarter Results of Infrared Imaging in the Single Heater Test Block*, April, 1997 (LBNL 1997b)], the temperature of a 100 percent infrared emissive object placed in the observation drift was checked through the camera against a calibrated thermometer. The temperature readings from the infrared camera are calibrated against a known temperature standard. Rock surfaces near the 100 percent emissive object have nearly the same temperature readings by the infrared camera, indicating that the rock surfaces had a nearly 100 percent emissivity value. The ambient temperature in the observation drift at the time of acquisition was 26°C. The area was ventilated during the survey with a relative humidity of 30-33 percent in the observation drift. Spatial references for images are taken from the rock bolts and borehole collars. Later in the study, a dedicated metallic frame with special heat reflective tape may be mounted along the observation drift and in other interesting locations near the heated drift bulkhead to provide extra spatial references in the infrared images.

The thermal images each cover approximately 1 m^2 at the distance from which they were taken, and each contains 256 x 256 pixels stored in 12-bit digital format. The camera was focused manually. The infrared intensity from each pixel is converted into real temperature readings using the emissive object and the known range of the camera. The temperature resolution per pixel is 0.1°C. Individual frames can be manipulated to correct for emissivity and background radiation so as to match independently known temperatures of objects in the images. As currently used, these adjustments are now altered from the default and are held fixed for all images so that meaningful comparisons of temperature over time can be made. Spot measurements of the temperature can be taken for given features. For better visual cues of the temperature distribution, the images, which in their native form are grayscale, can be arbitrarily color-keyed to match a desired colored temperature legend.

The rock bolts provide a radiant conduit for heat from beneath the rock surface to the camera and therefore give a truer indication of the rock temperature than does the surface of the rock which is subject to the influence of tunnel air convection. However, open borehole collars, should they remain, would provide the best below-surface black-body features.

10.1.3 Results

Over 200 infrared images were taken in this survey with four traverses to cover the observation drift walls, mainly covering strips along the wall-ceiling junction and around the bulkhead. A representative image is shown in Figure 10-1 and will be used to compare data acquired after heater activation which is scheduled for December 1997. This image, shown in both gray scale and color, illustrates the coolness of the boreholes in the observation drift. The possibility of taking infrared images with a robotic cart traversing the drift in the dark will be evaluated to address light interference problems.

NOTE: Blue corresponds to cooler image.

(a) Color Image

(b) Grayscale Image

Figure 10-1. Representative Infrared Image From the DST Block

After the boreholes in the observation drift are instrumented for the DST heater test, infrared images will be taken of the borehole collars to assess the remaining infrared contrast between the borehole and the surrounding rock wall surfaces. The borehole collars are black-body features that could be used for spatial references in the infrared surveys, provided these boreholes do not become heat transfer pathways from the heated drift to the observation drift and other outside walls.

10.2 RAPID EVALUATION OF K (THERMAL CONDUCTIVITY) AND ALPHA (THERMAL DIFFUSIVITY)

10.2.1 Objective and Description

The objective of the REKA thermal probe measurements was to evaluate thermal conductivity and thermal diffusivity at five different locations in the DST bed at Yucca Mountain. The REKA method provides in situ values which are useful to validate empirical models for rock mass effect, to identify initial convective effects, to monitor rock dryout due to ventilation, and to support hydrothermal site characterization.

The scientific notebook number is 00230 for the REKA data. The data in this section are qualified.

10.2.2 Methodology

The REKA method can be applied to determine two thermophysical properties—thermal conductivity and thermal diffusivity. The system employed to measure the thermal properties of the rock is comprised of a REKA thermal probe, an HP3421A data acquisition unit, and an HP71B controller. The REKA probe consists of a linear array of six thermocouples, centered one inch apart, and an integral heater which is powered at 8.0 volts and 0.89 amps by an HP3611A DC power supply. The thermocouples were mounted on a flexible, expandable Kapton foil. Thin, flexible copper rings were placed under each thermocouple sensor and provided an average temperature reading along the circumference of the borehole at each thermocouple location. The probe heater was positioned nearer the rock wall surface and was centered four inches from the closest thermocouple of the array. The heater is mechanically expandable to provide sufficient thermal contact between the heating element and the rock surface.

Using an input temperature field, a two-dimensional optimization procedure (Danko and Mousset-Jones 1989) was used as a core evaluation to obtain the best prediction for six thermal conductivity and thermal diffusivity values, respectively, along the probe axis. This optimization is based on the least-squares-fit of a simulated temperature field, T, to the measure temperature field, T^m. Assuming M readings of the temperatures, the following minimum condition is used for each of the six measurement stations:

$$\sum_{i=1}^{M} (T_i - T_i^m)^2 = minimum \qquad (10\text{-}1)$$

The temperature simulation in the optimization procedure is based on the numerical solution of the heat transfer equation in spherical coordinates of r and θ. Assuming symmetry over θ, only one spatial variable, r, remains in the differential equation:

$$\frac{\partial^2 T}{\partial r^2} + \frac{2}{r}\frac{\partial T}{\partial r} - \frac{1}{\alpha}\frac{\partial T}{\partial t} - \frac{T}{K}B(r) = \frac{1}{k}A(r,t) \tag{10-2}$$

In Equation (10-2), function $A(r,t)$ represents a time- and space-variable source or sink term in W/m^3, while function $B(r)$ is the coefficient of convection in W/(m^3-K).

The domain of space and time, assuming a borehole radius of a, is as follows:

$$\begin{array}{c} a \le r < \infty \\ t > 0 \end{array} \tag{10-3}$$

The initial and boundary conditions are:

$$\begin{array}{c} t \le 0\text{: } T=0 \\ t > 0 \quad \text{and} \quad -\frac{L}{2} \le \sqrt{r^2 - a^2} \le \frac{L}{2} \end{array} \tag{10-4}$$

and normal to the borehole surface:

$$-\frac{\partial T}{\partial r}\Big|_{r=a} = \frac{1}{k}\,[1 - C(t)]\,q(t) \tag{10-5}$$

$$t > 0 \quad \text{and} \quad \left|\sqrt{r^2 - a^2}\right| > \frac{L}{2} : q(t)=0$$

$$r \to \infty: \quad T(r) = 0,$$

where q(t) is the heat flux density on the surface of the heater of length L, and diameter a, and C(t) is a function, $0 \leq C(t) \leq 1$, representing a direct convective loss from the heater of the probe. A numerical procedure was developed for the solution of Equation (10-2) with the initial and boundary conditions. Although the procedure allows for the solution of a more general case, only constant k, α, A, B, and C were applied during the exercises. While k and α were calculated using a two-dimensional optimizing procedure, A, B, and C were determined manually, using a number of trial-and-error calculations, minimizing spatial variances of k and α, and the error of fit between the input and the simulated temperature fields.

Five locations were selected for testing in the DST block based on the competency of the wall rock at this site including minimal fracturing, sufficient separation from rock bolts, and similarity of density (as determined by drilling rate). All five locations that were chosen for analysis appear to have similar characteristics based on these criteria. The boreholes were drilled in random directions to average the effects of unseen physical phenomena (faulting, stress relief, etc.).

The measurements were taken at various times over a period of five days. The boreholes were drilled to a depth of 28 inches (the length of the longest drill bit available) with a hammer drill. This depth was considered acceptable with regard to the cooling effects of the rockmass and the short sampling time (between 9 and 14 hours). A minimum of one hour was allowed for each borehole, for cooling the probe heater and for acclimation of the probe to the borehole temperature before each measurement was begun. A thin paper tube was inserted prior to the insertion of the REKA probe to minimize abrasion during probe insertion and removal.

Measurement locations are shown in Figure 10-2. Measurement locations 1 and 5 were from the observation drift and measurement locations 2, 3, and 4 were close to the heated drift. At each location, 36 cycles of temperature data were collected at the following incremental time intervals: Site 1, 1400 sec.; Sites 2, 3, and 5, 1200 sec.; and Site 4, 900 sec. Upon completion of each measurement, the acquired data file was transferred from the HP71B to an HP9114 floppy disk drive for hard storage.

10.2.3 Results

Results of thermal conductivity and thermal diffusivity measurements using the REKA probe are presented in Table 10-1 and Table 10-2. Table 10-1 shows the REKA evaluation results assuming that the rock mass temperature is only affected by the REKA probe's heater during the 12-hour measurement period; therefore, no rock mass background temperature correction was performed.

Table 10-2 shows the REKA results assuming that the rock mass temperature changes with time during the 12-hour measurement period because of the REKA probe's heater, and some other heating or cooling effect, such as a change in the ambient temperature. A rock mass temperature correction was applied based on the assumption that the rock mass temperature changed uniformly along the length of the REKA probe. Also, it was based on the assumption that the change in the background temperature, as a function of time, equaled the difference between the simulated and measured temperatures with time taken at the thermocouple of the probe farthest away from the heater's center.

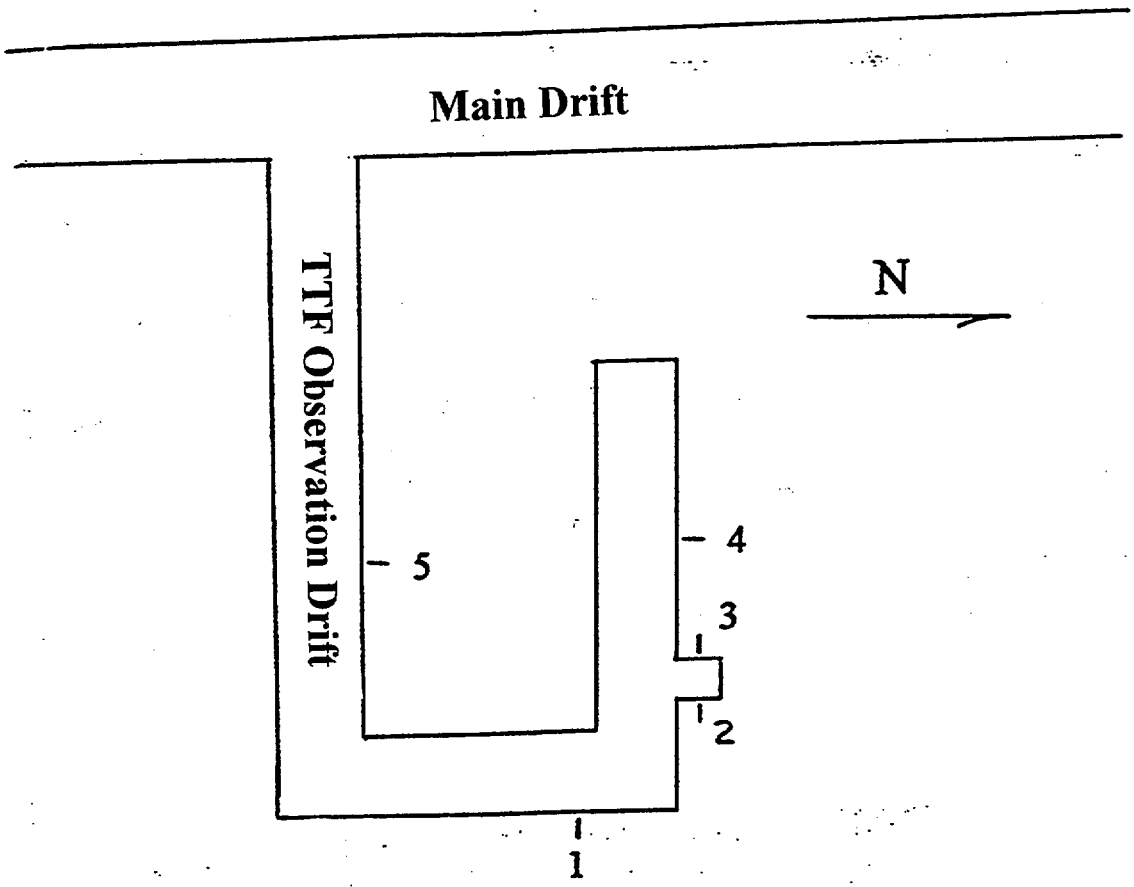

Figure 10-2. Site Locations for REKA Measurements

Table 10-1. REKA Results with No Background Temperature Correction

REKA Location	Error of Fit[1] (°C)	Thermal Conductivity, K (W/m-°C)	Thermal Diffusivity, Alpha (m^2/s)
1	0.033	1.69	0.76×10^{-6}
2	0.037	1.95	0.77×10^{-6}
3	0.024	1.86	0.91×10^{-6}
4	0.039	1.88	0.82×10^{-6}
5	0.025	1.70	0.85×10^{-6}

[1] Error of Fit is the Root Mean Square between the simulated and measured temperature fields, all having 35 readings with time and 6 readings along the length of the Sierra Science REKA probe.

Table 10-2. REKA Results with Background Temperature Correction

REKA Location	Error of Fit[1] (°C)	Thermal Conductivity, K (W/m-°C)	Thermal Diffusivity, Alpha (m^2/s)
1	0.015	1.72	0.93×10^{-6}
2	0.010	1.92	0.90×10^{-6}
3	0.018	1.89	1.04×10^{-6}
4	0.015	1.93	1.09×10^{-6}
5	0.025	1.76	0.97×10^{-6}

[1] Error of Fit is the Root Mean Square between the simulated and measured temperature fields, all having 35 readings with time and 6 readings along the length of the Sierra Science REKA probe.

The simulated temperature is obtained using the best estimate for thermal conductivity and thermal diffusivity.

The evaluation results in Table 10-2 have a significantly better fit between the measured and simulated temperature fields than those without temperature correction (see Table 10-1). However, the influence of the temperature correction, which cannot be verified by direct measurement, may result in a distortion of the thermophysical properties, especially thermal diffusivity. Consequently, the results in Table 10-2 need to be used with caution until more analytical and experimental results are obtained regarding the effects of the rock mass background temperature correction.

10.3 BOREHOLE VIDEO LOGS

10.3.1 Objective and Description

The objective of borehole video logs was to provide descriptive visual information from boreholes in the DST block, and to supplement other available characterization data. Borehole video logs were also used to help select appropriate depths for packer settings for the air permeability testing described in Section 9. They are considered qualified data. Borehole videos were run following

Los Alamos National Laboratories procedure LANL-EES-13-DP-613, R0. They were submitted under DTN LAR0831422AQ97.001 (SHT) and LAR0831422AQ97.002 (DST).

10.3.2 Methodology

The borehole television camera consists of the downhole video camera system, monitor, and VCR. The TV/VCR was first configured to record, and then the camera was inserted into the borehole. The camera was paused as needed. The video tape was viewed to ensure visibility and adequacy. The process was repeated if the video information was inadequate. Any unusable entries or videos were identified as inadequate. The following information was recorded in the scientific notebook: borehole identifier, date, measuring & test equipment serial numbers if applicable, the location of the zero datum point, traceability between the notebook and the video, depth correction measurements if applicable, and the total depth reached. It is estimated that 137 of the 147 boreholes in the DST block will be videoed prior to heater activation.

10.3.3 Results

A listing of video logs from DST boreholes is presented in Table 10-3.

10.4 IN SITU STRESS MEASUREMENTS

10.4.1 Objective and Description

The objective of this field investigation was to determine the magnitude and orientation of the two principal, horizontal stresses. These in situ stresses were determined from hydraulic fracturing measurements. The principal, vertical stress was not determined since hydraulic fractures in the horizontal direction were not created. In situ stress measurements provide initial and boundary conditions for numerical simulations of the DST block and for the design and performance assessment of the repository.

The information presented in this section is the summation of a Level 4 Milestone (SP327JM4) report (SNL 1997b). The TDIF number is 305878 and the DTN is SNF 37100195002.001. The data is considered qualified and it was collected in accordance with Sandia National Laboratories Technical Procedure TP-253, *Hydraulic Fracturing Stress Measurements*, based on ASTM D 4645-87.

10.4.2 Methodology

Hydraulic fracturing in situ stress measurements were conducted in October 1996 in borehole ESF-AOD-HDFR#1. The borehole is located approximately at station 0+134 of the observation drift. Surveyed locations for ESF-AOD-HDFR#1 borehole can be found in the Kiewit/PB field survey department. The collar of the borehole is at an elevation of 1052.5 m. The borehole is vertical, about 30-m deep, and has a diameter of approximately 76 mm (N-size).

Table 10-3. Video Logs from DST Boreholes

Borehole #	Well Name	Depth (ft)	Date
42	ESF-SDM-MPBX-1	86.1	10/16/96
43	ESF-SDM-MPBX-2	75.0	11/25/96
44	ESF-SDM-MPBX-3	85.0	11/25/96
45	ESF-HD-ERT-1	129.3	11/07/96
46	ESF-HD-ERT-2	122.0	11/05/96
47	ESF-HD-NEU-1	81.5	11/05/96
48	ESF-HD-NEU-2	91.0	11/05/96
49	ESF-HD-NEU-3	131.5	06/23/97
50	ESF-HD-NEU-4	131.4	06/23/97
51	ESF-HD-NEU-5	130.0	11/07/96
52	ESF-HD-CHE-1	130.6	10/31/96
53	ESF-HD-CHE-2	50.0	06/23/97
54	ESF-HD-CHE-3	130.3	06/23/97
55	ESF-HD-CHE-4	62.5	06/23/97
56	ESF-HD-CHE-5	130.9	10/31/96
57	ESF-HD-HYD-1	130.3	06/20/97
58	ESF-HD-HYD-2	113.5	06/20/97
59	ESF-HD-HYD-3	129.8	06/20/97
60	ESF-HD-HYD-4	129.8	06/20/97
61	ESF-HD-HYD-5	131.3	06/20/97
64	ESF-HD-NEU-6	131.2	05/02/97
65	ESF-HD-NEU-7	131.1	05/02/97
66	ESF-HD-NEU-8	131.6	05/02/97
67	ESF-HD-NEU-9	129.5	05/16/97
68	ESF-HD-NEU-10	130.3	05/16/97
69	ESF-HD-CHE-6	130.4	11/08/96
70	ESF-HD-CHE-7	130.8	11/08/96
71	ESF-HD-CHE-8	131.4	05/29/97
72	ESF-HD-CHE-9	131.5	05/29/97
73	ESF-HD-CHE-10	129.5	11/08/96
74	ESF-HD-HYD-6	131.0	04/22/97
75	ESF-HD-HYD-7	124.1	11/04/96
76	ESF-HD-HYD-8	131.5	04/22/97
77	ESF-HD-HYD-9	101.8	04/22/97
78	ESF-HD-HYD-10	130.3	11/04/96
79	ESF-HD-TEMP-1	194.9	12/17/96
80	ESF-HD-TEMP-2	195.4	07/01/97
81	ESF-HD-MPBX-1	150.9	01/07/97
82	ESF-HD-MPBX-2	151.3	07/01/97
83	ESF-HD-WH-1	38.0	05/06/97
84	ESF-HD-WH-2	38.1	05/15/97
85	ESF-HD-WH-3	38.0	04/24/97
86	ESF-HD-WH-4	37.6	04/24/97
87	ESF-HD-WH-5	37.5	04/24/97
88	ESF-HD-WH-6	37.8	05/30/97
89	ESF-HD-WH-7	37.2	05/30/97

Table 10-3. Video Logs from DST Boreholes (continued)

Borehole #	Well Name	Depth (ft)	Date
90	ESF-HD-WH-8	38.0	05/15/97
91	ESF-HD-WH-9	38.3	05/15/97
92	ESF-HD-WH-10	37.9	05/30/97
93	ESF-HD-WH-11	37.7	06/17/97
94	ESF-HD-WH-12	37.5	06/17/97
95	ESF-HD-WH-13	37.7	06/17/97
96	ESF-HD-WH-14	37.7	06/17/97
97	ESF-HD-WH-15	37.8	06/17/97
98	ESF-HD-WH-16	38.1	06/17/97
99	ESF-HD-WH-17	37.6	06/17/97
100	ESF-HD-WH-18	37.8	06/18/97
101	ESF-HD-WH-19	37.3	06/18/97
102	ESF-HD-WH-20	37.5	06/18/97
103	ESF-HD-WH-21	38.0	06/18/97
104	ESF-HD-WH-22	38.0	06/18/97
105	ESF-HD-WH-23	37.8	06/18/97
106	ESF-HD-WH-24	38.0	06/18/97
107	ESF-HD-WH-25	38.0	06/18/97
108	ESF-HD-WH-26	37.8	06/18/97
109	ESF-HD-WH-27	37.8	06/18/97
110	ESF-HD-WH-28	32.5	06/18/97
111	ESF-HD-WH-29	37.8	06/18/97
112	ESF-HD-WH-30	38.1	06/18/97
113	ESF-HD-WH-31	37.9	06/18/97
114	ESF-HD-WH-32	37.7	06/18/97
115	ESF-HD-WH-33	37.8	06/18/97
116	ESF-HD-WH-34	36.9	06/17/97
117	ESF-HD-WH-35	37.0	06/17/97
118	ESF-HD-WH-36	37.8	06/17/97
119	ESF-HD-WH-37	38.0	06/17/97
120	ESF-HD-WH-38	37.3	06/17/97
121	ESF-HD-WH-39	37.9	06/17/97
122	ESF-HD-WH-40	38.0	06/17/97
123	ESF-HD-WH-41	20.0	05/30/97
124	ESF-HD-WH-42	38.4	05/15/97
125	ESF-HD-WH-43	38.0	05/15/97
126	ESF-HD-WH-44	38.2	05/30/97
127	ESF-HD-WH-45	38.2	05/30/97
128	ESF-HD-WH-46	37.8	05/15/97
129	ESF-HD-WH-47	18.0	04/24/97
130	ESF-HD-WH-48	37.8	04/24/97
131	ESF-HD-WH-49	37.9	05/15/97
132	ESF-HD-WH-50	37.7	05/06/97
133	ESF-HD-TEMP-3	65.8	05/06/97
134	ESF-HD-TEMP-4	50.2	05/06/97
135	ESF-HD-ERT-5	65.5	05/06/97

Table 10-3. Video Logs from DST Boreholes (continued)

Borehole #	Well Name	Depth (ft)	Date
136	ESF-HD-ERT-6	50.0	05/06/97
137	ESF-HD-TEMP-5	65.0	06/09/97
138	ESF-HD-TEMP-6	64.8	06/09/97
139	ESF-HD-TEMP-7	64.8	06/09/97
140	ESF-HD-TEMP-8	62.0	06/04/97
141	ESF-HD-TEMP-9	68.4	06/09/97
142	ESF-HD-TEMP-10	65.0	06/09/97
143	ESF-HD-TEMP-11	65.5	06/09/97
144	ESF-HD-TEMP-12	66.9	06/09/97
145	ESF-HD-ERT-7	65.8	06/09/97
146	ESF-HD-ERT-8	38.0	06/04/97
147	ESF-HD-MPBX-3	49.3	05/30/97
148	ESF-HD-MPBX-4	48.5	05/30/97
149	ESF-HD-MPBX-5	49.5	05/30/97
150	ESF-HD-MPBX-6	51.0	06/04/97
154	ESF-HD-MPBX-7	49.3	06/30/97
155	ESF-HD-MPBX-8	49.5	06/30/97
156	ESF-HD-MPBX-9	49.2	06/30/97
157	ESF-HD-MPBX-10	50.8	06/30/97
158	ESF-HD-TEMP-13	66.0	07/15/97
159	ESF-HD-TEMP-14	64.1	07/15/97
160	ESF-HD-TEMP-15	65.7	07/15/97
161	ESF-HD-TEMP-16	62.5	07/15/97
162	ESF-HD-TEMP-17	64.5	07/15/97
163	ESF-HD-TEMP-18	66.2	07/15/97
164	ESF-HD-TEMP-19	64.2	07/15/97
165	ESF-HD-TEMP-20	65.5	07/15/97
166	ESF-HD-ERT-9	65.0	07/15/97
167	ESF-HD-ERT-10	50.8	07/15/97
168	ESF-HD-TEMP-21	66.2	07/16/97
169	ESF-HD-TEMP-22	69.8	07/16/97
170	ESF-HD-TEMP-23	66.2	07/16/97
171	ESF-HD-TEMP-24	65.6	07/16/97
172	ESF-HD-TEMP-25	67.0	07/16/97
173	ESF-HD-TEMP-26	69.7	07/16/97
174	ESF-HD-TEMP-27	64.2	07/16/97
175	ESF-HD-TEMP-28	65.8	07/16/97
176	ESF-HD-ERT-11	66.0	07/16/97
177	ESF-HD-ERT-12	49.2	07/16/97
178	ESF-HD-MPBX-11	49.4	06/30/97
179	ESF-HD-MPBX-12	49.7	06/30/97
180	ESF-HD-MPBX-13	49.5	06/30/97
181	ESF-HD-MPBX-14	51.3	06/30/97
182	ESF-HD-PERM-1	65.0	01/28/97
183	ESF-HD-PERM-2	60.0	01/28/97
184	ESF-HD-PERM-3	64.8	01/28/97

Table 10-3. Video Logs from DST Boreholes (continued)

Borehole #	Well Name	Depth (ft)	Date
185	ESF-HD-HYD-11	131.4	04/23/97
186	ESF-HD-HYD-12	130.8	04/23/97
187	ESF-PL-MPBX-1	11.4	02/07/97
188	ESF-PL-MPBX-2	11.1	02/07/97

Test intervals were selected after visually inspecting the extracted core at the Sample Management Facility. These intervals were picked so as to span segments free of visible natural fractures, joints, or other partings. The following segments were selected for hydraulic fracturing test intervals.

Test Number	Interval
1	11.0 to 11.6 m
2	11.6 to 12.4 m
3	17.7 to 18.6 m
4	18.9 to 19.5 m
5	19.7 to 20.3 m
6	21.8 to 22.8 m

The test in the deepest interval (21.8 m through 22.8 m) was attempted but had to be abandoned after failing to pressurize, probably as a result of some pre-existing open fractures not visible on the inspected core.

The downhole testing equipment consisted of a hydraulic fracturing straddle packer system. It contained two 0.9-m long inflatable rubber packer elements rigidly connected so as to straddle a 0.5-m interval. An internal hollow steel shaft separated two hydraulic lines, one for the inflation of the packers and the other for the pressurization of the interval.

The tool was lowered into the borehole on the drill rig wireline. A high pressure hose was connected hydraulically to the two inflatable packers and was lowered simultaneously by strapping it to the wireline. An additional high-pressure hose provided the conduit for test-interval hydraulic pressurization and was similarly strapped to the wireline. The surface equipment consisted of two 70 MPa air-activated hydraulic pumps that supplied the hydraulic pressure, one pump to the test interval and the other to the packers. A personal computer data acquisition system provided real time digital recording and analog viewing of the interval pressure and the flowrate (monitored by a pressure transducer and an in-line turbine flow meter respectively).

A listing of the key steps in the hydraulic fracturing testing follows:

- The hydraulic fracturing tool was assembled and tested on the surface.

- The tool was lowered into the borehole to the predetermined depth. The inflatable packers were set by hydraulic pressurization. The straddled test interval was then pressurized.

- Interval pressurization for hydraulic fracturing was conducted at a nearly constant flow rate until peak pressure P_c (also called breakdown pressure) was reached. Pumping was continued for a short time to extend the fracture beyond the zone of influence of the borehole, and was subsequently shut off allowing the pressure to decay. The shut-in pressure P_s, representing the point at which the fracture closed back, was later picked out from this portion of the pressure record. Several minutes into the shut-off phase the pressure was vented and allowed to return to atmospheric conditions, while recording the water flow-back from the borehole. The pressurization cycle was then repeated two more times, recording the fracture reopening pressure P_r, and additional readings of P_s.

- At the completion of all the pressurization cycles, the packers were deflated and the straddle packer was moved to the next test zone. The procedure outlined above was repeated for each test.

- Test-interval pressure and flow rate were monitored in real time on a laptop computer and digitally saved on disk for later data processing.

Knowledge of hydraulic fracture orientation is crucial to establishing the directions of the principal stresses. An impression packer orienting tool was used to obtain an oriented trace of the induced hydraulic fracture on the borehole wall. The impression packer consisted of a 90-cm long inflatable packer element covered with a thin layer of semi-cured rubber (impression sleeve) which could be easily dented permanently by a sharp protrusion or gap in the borehole wall. The following steps were taken in fracture impression tests:

- The impression packer was prepared on the surface by marking a reference ('scribe') line on the outside of the impression sleeve and ensuring that it was aligned with a permanent line scribed on the outside of the magnetic orienting tool. This line was itself aligned with the direction of the radial line on the face of the magnetic compass inside the orienting-tool housing.

- The impression packer was lowered into the borehole to the precise depth of a previously hydraulic-fractured interval, using the drill rig wireline. A high pressure hose connecting the packer to a pump on the surface was strapped to the wireline. A magnetic orienting tool, consisting of a camera, angle unit, and magnetic compass, was rigidly attached to the top of the impression packer.

- The impression packer was pressurized to a level approximately equal to the estimated shut-in pressure of the interval. The packer pressure was maintained for about 15 to 20 minutes to allow the impression sleeve to protrude into induced hydraulic fracture(s) and take a permanent imprint.

- At the preset time the camera shutter inside the orienting tool opened and a photograph of the angle unit and magnetic compass face was taken, indicating the direction of a reference line marked on the compass face, and previously aligned with the scribe line on the outside of the packer. This was later used to determine the orientation of the imprinted hydraulic fractures.

- At the completion of the test the impression packer was deflated and retrieved together with the orienting tool. The camera was removed and the photograph was developed. The impression packer was examined for fracture traces. These were marked with an indelible marker, and traced with respect to the scribe line on a transparent plastic sheet wrapped around the packer for later detailed analysis.

10.4.3 Results

A series of five successful hydraulic fracturing tests were conducted. Test number 4, centered at 19.2 m from the collar of the borehole, yielded the typical pressure-time signature obtained during hydraulic fracturing of intact test intervals. The other test results showed signs of possible pre-existing fracturing, probably induced during drilling. In addition, two tests conducted at approximately 10 m from the alcove may also have been within the zone of influence of that excavation.

Thus, the most reliable hydraulic fracturing results were obtained in test number 4. Based on these results, and on the average vertical hydraulic fracture strikes in all tests, the estimate of the state of in situ stress around borehole ESF-AOD-HDFR#1 is:

$\sigma_h = 1.7\ (\pm 0.1)$ MPa acting in the N 75° W ($\pm$14°)
$\sigma_H = 2.9\ (\pm 0.4)$ MPa acting in the N 15° E ($\pm$14°)

The measured stress state is small which is consistent with the dominant local normal faults. The north-northeastern maximum horizontal stress direction is subparallel to the average strike of these faults, and is supported by previous measurements in the Yucca Mountain area.

INTENTIONALLY LEFT BLANK

11. SUMMARY

Data have been compiled that characterize the DST block of the ESF Thermal Test Facility. Laboratory tests characterizing thermal, mechanical, hydrological, and chemical properties and field measurements characterizing local geology, in situ hydrology, and local rock mass quality are discussed in terms of their description and measured values. These data characterize the ambient conditions of the local rock mass prior to heating to assist in the analysis and interpretation of the coupled thermal, mechanical, hydrological, and chemical processes anticipated in the DST block. Results of this characterization of the DST block were compared to similar measurements in the SHT block (CRWMS M&O 1996). In general, the measurements are consistent with the results reported for the SHT block and the results of previous studies in the same thermal/mechanical and lithostratigraphic unit (Brechtel et al. 1995; Kicker et al. 1996).

This report largely completes the planned, pre-test characterization of the DST block. Additional laboratory work is ongoing, however, for thermomechanical properties, mineralogy and petrology, and hydrologic properties. Other pending characterization activities include electrical resistivity tomography, ground penetrating radar (also laboratory calibration), neutron logging, infrared and video imaging of the heated drift (rock, floor heaters, etc.), gas sampling (from chemistry boreholes and possibly hydrology boreholes) and analysis, REKA probing, and acoustic emission/high frequency seismic imaging. The results of these measurements will be documented in the DST as-built report scheduled to be prepared in February, 1998. At least one week of pre-heating data will be collected on all instrumentation wired to the DCS which will complete the pre-test characterization of the DST block. Also, additional characterization data from the SHT block were reported.

INTENTIONALLY LEFT BLANK

12. QUALITY ASSURANCE

This report is a presentation of data for the ambient characterization of the DST block of the ESF TTF. This report is a compilation of data from site characterization activities performed by Scientific Programs personnel and was prepared entirely by Scientific Programs personnel. There are no other interfaces associated with the development of this report. Thus, it was determined that a Technical Document Preparation Plan was not required.

There is no QAP-2-3, *Classification of Permanent Item Evaluations*, application to the compilation of this report. NLP-2-0, *Determination of Importance Evaluations*, is not applicable to the compilation of this report. The NLP-2-0 requirements associated with field activities that generated the data contained in this report were addressed by the organization collecting the data.

The data presented in this report are relevant to the characterization of the natural barrier, which is on the Q-List by direct inclusion of the U.S. Department of Energy (DOE). The preparation of this report is subject to *Quality Assurance Requirements and Description* controls, because the document contains information that will provide input for the ESF Thermal Test, and the results of these tests may be used to support performance confirmation/assessment. The report was prepared under QAP-SIII-1, *Scientific Investigation Control*. It will be reviewed under QAP-SIII-2, *Review of Scientific Documents and Data*. This document will be controlled in accordance with QAP-6-1, *Submittal and Use of Controlled Documents,* and QA records generated will be handled in accordance with AP-17.1Q, *Record Source Responsibilities for Inclusionary Records*. Scientific, engineering, or computational computer software was not used to develop this report, so it is not subject to QAP-SI Series procedural requirements.

This report does not make, nor rely upon, any new assumptions. Any assumptions discussed originated within the individual source documents. Results of laboratory testing and field measurements presented in this report were generated under QA procedures governing the various technical organizations involved in the activities. Further discussion is presented in the methodology section for each data type. Section 13.2 presents a summary of the procedures or standards that were used for each data-generating activity. Generally, one of three types of procedures were followed:

- National consensus standards or professional standards such as those utilized by ASTM or ISRM.
- Participant technical organizations DOE OCRWM-approved procedures.
- A Scientific Notebook Procedure, in cases where flexibility was required to accommodate unexpected situations encountered in field activities.

All data presented in this report are to be considered qualified data except for the following: Schmidt Hammer Rebound Index testing (Section 8) which was performed as a non-qualified activity. Therefore, these data are considered to be preliminary. If utilized by other organizations, these data must be clearly identified as unqualified, and tracked by the affected organization's appropriate procedure.

INTENTIONALLY LEFT BLANK

13. REFERENCES

NOTE: Data references are presented in Table 13-1.

13.1 REFERENCED DOCUMENTS

Barton, N.; Lien, R.; and Lunde, J. 1974. "Engineering Classification of Rock Masses for the Design of Tunnel Support." *Rock Mechanics.* Vol. 6, pp. 189-236. New York, New York: Springer-Verlag.

Benson, L.V. and McKinley, P.W. 1985. "Chemical Composition of Ground Water in the Yucca Mountain Area, Nevada, 1971-84." *USGS Open-File Report 85-484.* Denver, Colorado: U.S. Geological Survey. (NNA.19870610.0027) (NNA.19890522.0210) (NNA.19900207.0281) (GS920408312321.003)

Bieniawski, Z.T. 1974. "Geomechanics Classification of Rock Masses and its Application in Tunneling." *Proceedings of the Third Congress of the International Society for Rock Mechanics.* Denver, Colorado, September 1-7, 1974. Washington, D.C.: National Academy of Sciences. (HQ5.880517.2256)

Birkholzer, J.H. and Tsang, Y.W. 1996. *Forecast of Thermal-Hydrological Conditions and Air Injection Test Results of the Single Heater Test.* Yucca Mountain Site Characterization Project Milestone SP918M4. Berkeley, California: Lawrence Berkeley National Laboratory. (MOY-970521-04) (WBS 1.2.3.14.2)

Brechtel, C.E.; Lin, M.; Martin, E.; and Kessel, D.S. 1995. "Geotechnical Characterization of the North Ramp of the Exploratory Studies Facility." *SAND95-0488.* Albuquerque, New Mexico: Sandia National Laboratories. (MOL 19950502.0004)

Brown, E.T., ed. 1981. *Rock Characterization Testing and Monitoring, ISRM Suggested Methods.* Published for the Commission on Testing Methods, International Society for Rock Mechanics. Elmsford, New York: Pergamon Press. (NAA.890713.0194)

Buesch, D.C.; Spengler, R.W.; Moyer, T.C.; and Geslin, J.K. 1996. "Proposed Stratigraphic Nomenclature and Macroscopic Identification of Lithostratigraphic Units of the Paintbrush Group Exposed at Yucca Mountain, Nevada." *U.S. Geological Survey Open File Report 94-469.* p. 47. Denver, Colorado: U.S. Geological Survey. (GS931208314211.049)

Chung, F.H. 1974. "Quantitative Interpretation of X-ray Diffraction Patterns of Mixtures. I. Matrix-Flushing Method for Quantitative Multicomponent Analysis." *Journal of Applied Crystallography.* Vol. 7, pp. 519-525. Copenhagen, Denmark: Munksgaard International Booksellers and Publishers.

Cook, P. and Wang, J. 1997. "Pre-Heat Baseline Infrared Imaging in the Drift Scale Test Area." *Yucca Mountain Site Characterization Project, Level 4 Milestone SP5125M4.* Berkeley, California: Lawrence Berkeley National Laboratory.

CRWMS M&O (Civilian Radioactive Waste Management System Management and Operating Contractor) 1996. *Characterization of the ESF Thermal Test Area.* B00000000-01717-5705-00047, REV 01. Las Vegas, Nevada: Civilian Radioactive Waste Management System Management and Operating Contractor.

Danko, G. and Mousset-Jones, P.F. 1989. "In Situ Mine Measurement of Rock Thermophysical Property Measurement and Site Characterization," *Proceedings, 31st Heat Transfer and Fluid Mechanics Institute.* Sacramento, California: California State University, Sacramento.

Deere, D.U. 1963. "Technical Description of Rock Cores for Engineering Purposes," *Felsmechanik und Ingeniergeologie* (Rock Mechanics and Engineering Geology). Vol. 1, No. 1, pp. 16-22. New York, New York: Springer-Verlag (International Society for Rock Mechanics). (NAA.900827.0239)

Deere, D.U. and Deere, D.W. 1988. "The Rock Quality Designation (RQD) Index in Practice." *Rock Classification Systems for Engineering Purposes.* STP-984. Philadelphia, Pennsylvania: American Society for Testing and Materials.

DOE (U.S. Department of Energy) 1997. *Quality Assurance Requirements and Description.* DOE/RW-0333P. Washington, D.C.: U.S. Department of Energy.

Feynman, R.P.; Leighton, R.B.; and Sands, M. 1964. *The Feynman Lectures on Physics.* Vol. II, p. 12-2. Reading, Massachusetts: Addison-Wesley Publishing Company.

Flint, L.E. 1996. "Matrix Properties of Hydrogeologic Units at Yucca Mountain, Nevada," *U. S. Geological Survey Water Resources Investigation Report.* Denver, Colorado: U.S. Geological Survey. (MOL.19970324.0046) (GS950308312231.02)

Geslin, J.J.; Moyer, T.C.; and Buesch, D.C. 1995. "Summary of Lithologic Logging of New and Existing Boreholes at Yucca Mountain, Nevada, August 1993 to February 1994. *U.S. Geological Survey, Open File Report 94-342.* Denver, Colorado: U.S. Geological Survey.

Guzman, A.G.; Geddis, A.M.; Henrich, M.J.; Lohrstorfer, C.F.; and Neuman, S.P. 1996. "Summary of Air Permeability Data from Single-Hole Injection Tests in Unsaturated Fractured Tuffs at the Apache Leap Research Site; Results of Steady-State Interpretation." *U.S. Nuclear Regulatory Commission Report NUREG/CR-6360.* Washington D.C.: U.S. Nuclear Regulatory Commission.

Holcomb, D.J. and McNamee, M.J. 1984. "Displacement Gage for the Rock Mechanics Laboratory." *SAND84-0651.* Albuquerque, New Mexico: Sandia National Laboratories.

Hvorslev, M.J. 1951. "Time Lag and Soil Permeability in Groundwater Observations." *Bulletin 36, U.S. Army Corps of Engineers, Water Ways Experimental Station.* Vicksburg, Michigan: U.S. Army Corps of Engineers.

Johnson, T.M. and DePaolo, D.J. 1997. "Rapid Exchange Effects on Isotope Ratios in Groundwater Systems. I. Development of a Transport-Dissolution-Exchange Model." *Water Resources Research.* Vol. 33, pp. 187-195. Washington, D.C.: American Geophysical Union.

Kicker, D.C.; Martin, E.R.; Brechtel, C.E.; Stone, C.A.; and Kessel, D.S. 1996. "Geotechnical Characterization of the Main Drift of the Exploratory Studies Facility." *SAND95-2183*. Albuquerque, New Mexico: Sandia National Laboratories.

LeCain, G.D. 1995. "Pneumatic Testing in 45-Degree-Inclined Boreholes in Ash-Flow Tuff Near Superior, Arizona." *USGS Water Resources Investigations Report 95-4073*. Denver, Colorado: U.S. Geological Survey.

LBNL (Lawrence Berkeley National Laboratory) 1997a. *Infrared Imaging of the Single Heater Area*. Level 4 Milestone SP9230M4. January 1997. Berkeley, California: Lawrence Berkeley National Laboratory.

Lin, W. 1997. "Characterize Drift Scale Test Area and Prepare Report." *Yucca Mountain Site Characterization Project, Level 4 Milestone SP5110M4*. Livermore, California: Lawrence Livermore National Labs.

Lum, C.C. 1997. "Rock Mass Quality Assessment of the Drift Scale Heater Test Area." *Yucca Mountain Site Characterization Project, Level 4 Milestone SP140M4*. Albuguerque, New Mexico: Sandia National Laboratories.

LBNL 1997b. *Second Quarter Results of Infrared Imaging in the Single Heater Test Block*. Level 4 Milestone SP9237M4. April 1997. Berkeley, California: Lawrence Berkeley National Laboratory.

Ortiz, T.S.; Williams, R.L.; Nimick, F.B.; Whittet, B.C.; and South, D.L. 1985. "A Three-Dimensional Model of Reference Thermal/Mechanical and Hydrological Stratigraphy at Yucca Mountain, Southern Nevada." *SAND84-1076*. p. 76. Albuquerque, New Mexico: Sandia National Laboratories.

Paterson, M.S. 1978. *Experimental Rock Deformation--The Brittle Field*. Berlin, Germany and New York, New York: Springer Verlag.

Roberts, S.K. and Viani, B.E. 1997a. "Mineral Abundances for Samples from Instrumentation Boreholes in the Access Drift Scale Test Area (DST) of the ESF." *Yucca Mountain Site Characterization Project, Level 4 Milestone*. SP9511M4. Livermore, California: Lawrence Livermore National Laboratory.

Roberts, S.K. and Viani, B.E. 1997b. "Mineral Abundances for Samples from Six Chemistry (Seamist) Boreholes in the Drift Scale Test Area (DST) of the ESF." *Yucca Mountain Site Charactrization Project Level 4 Milestone*. SP9510M4. Livermore, California: Lawrence Livermore National Laboratory.

Rousseau, J.P.; Kwickles, E.W.; and Gillies, D.C., eds. 1996. "Hydrogeology of the Unsaturated Zone, North Ramp Area of Exploratory Studies Facility, Yucca Mountain, Nevada." *U.S. Geological Survey Water-Resources Investigations Report*. Denver, Colorado: U.S. Geological Survey. [MOL:19960702.0147]

Sandia National Laboratories 1997a. "Thermal Expansion and Thermal Conductivity of Test Specimens from the Drift Scale Test Area of the Exploratory Studies Facility at Yucca Mountain, Nevada." TDIF 306127. *Yucca Mountain Site Characterization Project, Level 4 Milestone.* SP5145M. Albuquerque, New Mexico: Sandia National Laboratories.

Sandia National Laboratories 1997b. "Hydraulic Fracturing Stress Measurements in Test Hole ESF-AOD-HDFR#1, Thermal Test Facility, Exploratory Studies Facility at Yucca Mountain." *Yucca Mountain Site Characterization Project, Level 4 Milestone.* SP3275M4. Albuquerque, New Mexico: Sandia National Laboratories.

Sandia National Laboratories 1997c. "Unconfined Compression Tests on Specimens from the Drift Scale Test Area of the Exploratory Studies Facility at Yucca Mountain, Nevada." TDIF 306126. *Yucca Mountain Site Characterization Project, Level 4 Milestone.* SP5145M. Albuquerque, New Mexico: Sandia National Laboratories.

Snyder, R.L. and Bish, D.L. 1989. "Quantitative Anlaysis." Bish, D.L. and Post, J.E., eds. *Modern Powder Diffraction: Reviews in Mineralogy.* pp. 101-144. Washington, D.C.: Mineralogical Society of America.

Sonnenthal, E. and Ahlers, C.F. 1997. "Fracture and Fault Properties for the LBNL Unsaturated Zone Flow Model." *Yucca Mountain Site Characterization Project Level 4 Milestone.* SP24UFM4. Berkeley, California: Lawrence Berkeley National Laboratory. (DTN: LB960601233129.001)

Steighner, J. and Singleton, B. 1997. "Geotechnical Report, Mass Quality Ratings, Alcove #5 Cross Drift & Heated Drift of the Exploratory Studies Facility." *Yucca Mountain Site Characterization Project, Level 4 Milestone.* SPG42FM4. Denver, Colorado: U.S. Geologic Survey.

Tsang, Y.W.; Wang, J.; Freifeld, B.; Cook, P.; Suárez-Rivera, R.; and Tokunaga, T. 1996. *Letter Report on Hydrological Characterization of the Single Heater Test Area in the ESF.* Yucca Mountain Site Characterization Project Milestone OS327322DI. Berkeley, California: Lawrence Berkeley National Laboratory. (MOY-970512-07-B) (DTN:LB960500834244.001)

Tsang, Y.W. and Cook, P. 1997. "Ambient Characterization of the ESF Drift Scale Test Area by Field Air Permeability Measurements." *Yucca Mountain Site Characterization Project, Level 4 Milestone.* SP9512M4. Berkeley, California: Lawrence Berkeley National Laboratory.

Viani, B.E. and Roberts, S.K. 1996. "Determination of Mineral Abudances in Core Samples From the Exploratory Studies Facility Using X-ray Diffraction." Analysis Report Supporting Yucca Mountain Project TDIF#30-5632 (305632); *Mineral Abundances for Temperature Samples from the Thermal Area of the ESF.* Livermore, California: Lawrence Livermore National Laboratory.

Wang, J. and Suarez-Rivera, R. 1997. "Laboratory Test Results of Hydrologic Properties from Dry Drilled and Wet Drilled Cores in the Drift Scale Test Area and in the Single Heater Test Area of the Thermal Test Facility." *Yucca Mountain Site Characterization Project, Level 4 Milestone.* SP5130M4. Berkeley, California: Lawrence Berkeley National Laboratory.

Weast, R.C., ed. 1974. *CRC Handbook of Chemistry and Physics*. 55th ed. Cleveland, Ohio: CRC Press. p. F109, F-112.

Yang, I.C.; Rattray, G.W.; and Yu, P. 1996. "Interpretation of Chemical and Isotopic Data From Boreholes in the Unsaturated Zone at Yucca Mountain, Nevada." *U.S. Geologic Survey Water Resources Investigations Report 96-0458*. Denver, Colorado: U.S. Geologic Survey.

Yang, A.; Futa, K; Marshall, B.; Neymark, L.; Paces, J.; Whelan, J. 1997. "Submission of Milestone SPH37DM4." *Yucca Mountain Site Characterization Project, Level 4 Milestone*. SPH37DM4. Memorandum to Robert Craig, Chief, Yucca Mountain Project Branch. Denver, Colorado: U.S. Geological Survey.

Young, R.A. 1993. "Introduction to the Rietveld Method." *The Rietveld Method*. International Union of Crystallography Monographs on Crystallography. Vol. 5, pp. 1-38. New York, New York: Oxford University Press.

13.2 STANDARDS AND PROCEDURES

American Society for Testing Materials

F433-77, *Evaluating Thermal Conductivity of Gasket Materials*
E1225-87, *Method for Thermal Conductivity of Solids by Means of Guarded Comparative-Longitudinal Heat Flow Technique*
E228-85, *Method for Linear Thermal Expansion of Solid Materials With a Vitreous Silica Dilatometer*
D4535-85, *Methods for Measurement of Thermal Expansion of Rock Using a Dilatometer*
D4645-87, *Determination of the In-Situ Stress in Rock Using the Hydraulic Fracturing Method*

CRWMS M&O Procedures

AP-17.1Q, *Record Source Responsibilities for Inclusionary Records*
NLP-2-0, *Determination of Importance Evaluations*
QAP-2-3, *Classification of Permanent Item Evaluations*
QAP-6-1, *Submittal and Use of Controlled Documents*
QAP-SIII-1, *Scientific Investigation Control*
QAP-SIII-2, *Review of Scientific Documents and Data*

LANL Procedures

EES-13-DP-613, R0, *Conducting Video Logs of Boreholes*

SNL Procedures

SNL QAIP 20-3, *Sample Control*
SNL TP-051, *Preparing Cylindrical Samples, Including Inspection of Dimension and Shape Tolerances*
SNL TP-064, *Procedures for Vacuum Saturation of Geologic Core Samples*
SNL TP-065, *Drying Geologic Samples to Constant Weight*
SNL TP-200, *Inspection of Samples Used in Thermal Properties Measurements*

SNL TP-202, *Measurement of Thermal Conductivity of Geologic Samples Using the Guarded-Heat-Flow-Meter Method*
SNL TP-203, *Measurement of Thermal Expansion of Geologic Materials Using a Push Rod Dilatometer*
SNL TP-215, *Calibration of Lawson Board Systems*
SNL TP-219, *Unconfined Compression Experiments at Ambient Conditions and Constant Strain Rate*
SNL TP-234, *Conducting Rock Mass Quality Assessment*
SNL TP-253, *Hydraulic Fracturing Stress Measurements*
SNL TP-257, *LVDT Calibration at Sandia National Laboratories*

USGS Procedures
GCP-03, Rev. 3, *Uranium-Thorium Disequilibrium Studies*
GCP-12, Rev. 4, *Rubidium - Strontium Isotope Geochemistry*
GCP-17, *Determinatin of the Isotopic Ratio of H/D in H_2O*
HP-126, *Extraction of Residual Water From Tuff Samples by Vacuum Distillation*
HP-204, *Liquid Scintillation Spectronometry Method for Tritium Measurement of Water Samples*
TP-GP-32, *Underground Geologic Mapping*

Table 13-1. Tabulation of Report Location, TDIFs/DTNs, Procedures, Milestone Numbers, References, and Q-Status of Characterization Data

Data	Report Section	TDIF/DTN	Procedure(s)	Level 4 Milestone	Q/non-Q
Laboratory thermal properties	3	TDIF: 306127 DTN: SNL22100196001.001	Thermal conductivity: SNL TP-051, SNL TP-200, SNL QAIP-20-3, SNL TP-064, SNL TP-215, SNL TP-202, ASTM F433-77, ASTM E1225-87	SP5145M4 (SNL, 1997a)	Q
			Thermal expansion: SNL TP-051, SNL TP-200, SNL QAIP-20-3, ASTM D-4535-85, ASTM E 228-85, SNL TP-203		
Laboratory mechanical properties	4	TDIF: 306126 DTN: SNL02100196001.001	SNL TP-051, SNL TP-065, SNL TP-257, SNL TP-219	SP5145M4 (SNL, 1997b)	Q
					Schmidt Hammer Tests: non-Q
Laboratory hydrological properties	5	Saturation, porosity, bulk density, and gravimetric water content: TDIF: 306135 DTN: LB9705001234142.003	Scientific Notebooks YMP-LBNL-JSW-4-1.0 and YMP-LBNL-JSW-4-1.1	SP5130M4 (Wang and Suarez-Rivera, 1997)	Q
		Moisture imbibition potential: TDIF: 306238 DTN: LL97070904244.035	Scientific Notebooks	SP5110M4 (Lin, 1997)	Q
Laboratory chemical properties: Mineralogy and petrology	6.1	TDIF: 306139 DTN: LL970600304244.032	LLNL Scientific Notebook 269	SP9511M4 (Roberts and Viani, 1997a)	Q

Table 13-1. Tabulation of Report Location, TDIFs/DTNs, Procedures, Milestone Numbers, References, and Q-Status of Characterization Data (continued)

Data	Report Section	TDIF/DTN	Procedure(s)	Level 4 Milestone	Q/non-Q
Laboratory chemical properties: Pore-water analyses	6.2	Strontium isotopes TDIF: 306137 DTN GS970508312272.002	Strontium isotopes: USGS TP GCP-12, Rev 4	SPH37DM4 (Yang et al., 1997)	Q
		Uranium isotopes TDIF: 306136 DTN: GS970508312272.001	Uranium isotopes: USGS TP GCP-03, Rev 3		
		Stable isotopes TDIF: 306141 DTN: GS970608312272.004	Stable isotopes: USGS TP HP-126, Rev. 1, USGS TP GCP-17, Rev.3, and Scientific Notebook SN-0058		
		Tritium analyses TDIF: 306145 DTN: GS970608312272.005	Tritium analyses: USGS TP HP-126, Rev 1, and USGS TP HP-204, Rev 0		
		Sodium and potassium ratios TDIF: 306138 DTN: GS970508312272.003	Sodium and potassium ratios: USGS TP HP-126, Rev 1		
Field facture mapping	7	TDIF: GS970608314224.007 and GS970608314224.006 DTN: 306177 & 306176	USGS TP GP-32	SPG42FM4 (Steighner and Singleton, 1997)	Q
Field rock mass classification	8	Drift Scale Test: TDIF: 306063 DTN: SNF21020196001.015	SNL TP-234, REV 1	SP5140M4 (Lum, 1997)	Q
		Single Heater Test: (also previously reported in CRWMS M&O 1996) TDIF: 305579 DTN: SNF32020196001.010			
Field air permeability testing	9	TDIF: 306164 DTN: LB970600123142.001	Scientific Notebook YMP-LBNL-YWT-1.3	SP9512M4 (Tsang and Cook, 1997)	Q
Field infrared imaging	10.1	TDIF: 306134 DTN: LB970500123142.002	Scientific Notebook YMP-LBNL-JSW-1.2	SP5125M4 (Cook and Wang, 1997)	Q
Field REKA measurements	10.2		LLNL Scientific Notebook 00230		Q

Table 13-1. Tabulation of Report Location, TDIFs/DTNs, Procedures, Milestone Numbers, References, and Q-Status of Characterization Data (continued)

Data	Report Section	TDIF/DTN	Procedure(s)	Level 4 Milestone	Q/non-Q
Borehole video logs	10.3	Single Heater Test: DTN: LAR0831422AQ97.001 Drift Scale Test: DTN: LAR0831422AQ97.002	LANL-EES-13-DP-613, RO Scientific Notebook LA-EES-13-LV-NBK-96-001 (SHT) LA-EES-13-LV-NBK-97-002 (DST)		Q
In situ stress measurements	10.4	TDIF: 305878 DTN: SNF3710195002.001	SNL TP-253, ASTM D4645-87	SP327JM4 (SNL 1997B)	Q

INTENTIONALLY LEFT BLANK

APPENDIX A

THERMAL EXPANSION DATA: SUMMARY SHEET FOR EACH TEST CYCLE

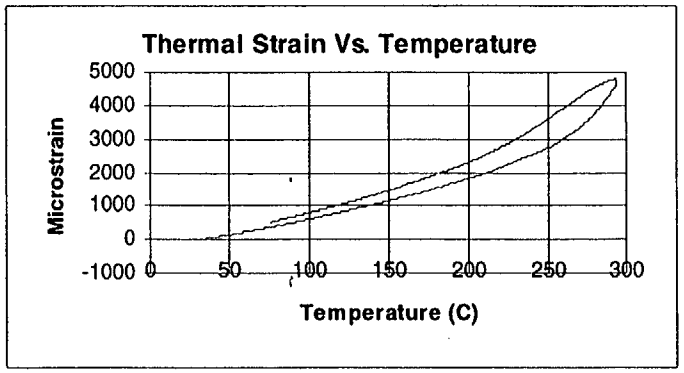

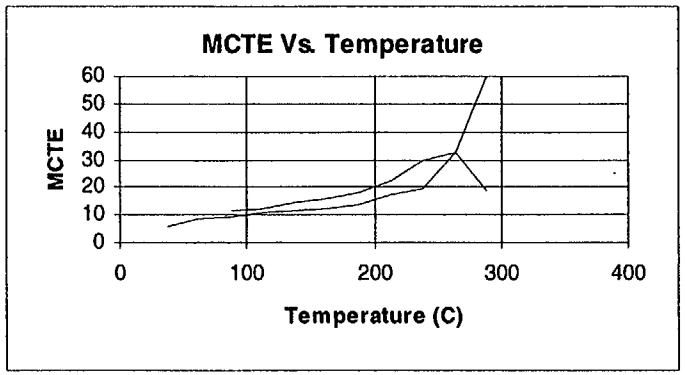

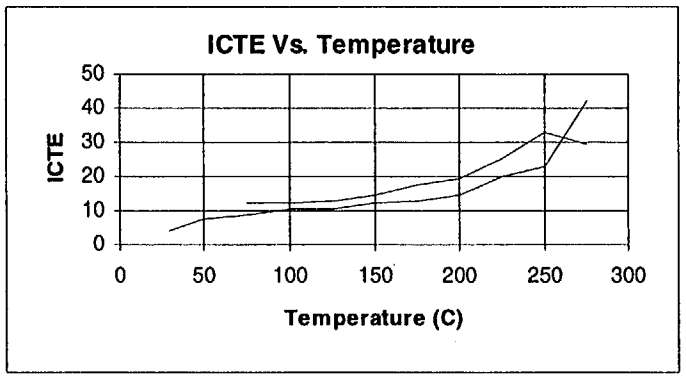

Specimen ID:	ESF-SDM-MPBX1-1.0-B
Date of Test Completion:	3/28/97
Thermal/Mechanical Unit:	TSw2
Lithostratigraphic Unit:	Tptpmn
Original Location:	ESF; Alcove 5;Thermal Drift Scale Test Area
Initial Moisture Content	Air-dried (As-is)
Nominal Dimensions:	50.8 mm (L) 25.4 mm (D)

Specimen Data:	Length (mm)	Mass (g)
Pre-test:	50.8	58.872
Post-test:	50.8	58.566
Change:	0	0.306

Temp Range (C)		(C)	Mean Temp (C)	Mean CTE (10^{-6}/C)
25	-	50	37.5	5.99
50	-	75	62.5	8.71
75	-	100	87.5	9.73
100	-	125	112.5	10.68
125	-	150	137.5	11.52
150	-	175	162.5	12.53
175	-	200	187.5	13.88
200	-	225	212.5	17.17
225	-	250	237.5	19.67
250	-	275	262.5	32.67
275	-	300	287.5	59.99
300	-	325	312.5	-
325	-	300	312.5	-
300	-	275	287.5	19.12
275	-	250	262.5	32.86
250	-	225	237.5	29.46
225	-	200	212.5	22.32
200	-	175	187.5	17.74
175	-	150	162.5	16.15
150	-	125	137.5	14.11
125	-	100	112.5	12.64
100	-	75	87.5	11.77
75	-	50	62.5	-
50	-	30	40	-

Temp Range (C)		(C)	Mean Temp (C)	Instant. CTE (10^{-6}/C)
27.5	-	32.5	30	3.96
47.5	-	52.5	50	7.51
72.5	-	77.5	75	8.67
97.5	-	102.5	100	10.57
122.5	-	127.5	125	10.39
147.5	-	152.5	150	12.34
172.5	-	177.5	175	12.67
197.5	-	202.5	200	14.78
222.5	-	227.5	225	19.78
247.5	-	252.5	250	22.72
272.5	-	277.5	275	42.26
297.5	-	302.5	300	-
302.5	-	297.5	300	-
277.5	-	272.5	275	29.65
252.5	-	247.5	250	32.68
227.5	-	222.5	225	25.08
202.5	-	197.5	200	19.21
177.5	-	172.5	175	17.91
152.5	-	147.5	150	14.66
127.5	-	122.5	125	13.06
102.5	-	97.5	100	12.24
77.5	-	72.5	75	12.10
52.5	-	47.5	50	-

Figure A-1. Thermal Expansion Data for Specimen ESF-SDM-MPBX1-1.0-B for First Thermal Cycle

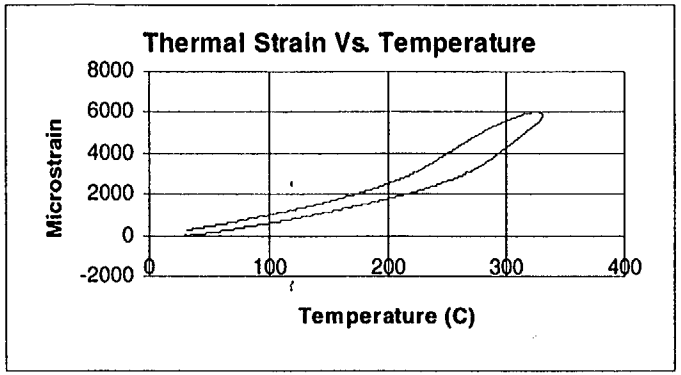

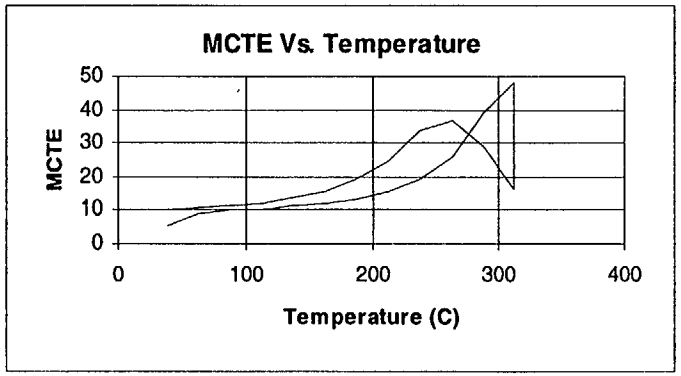

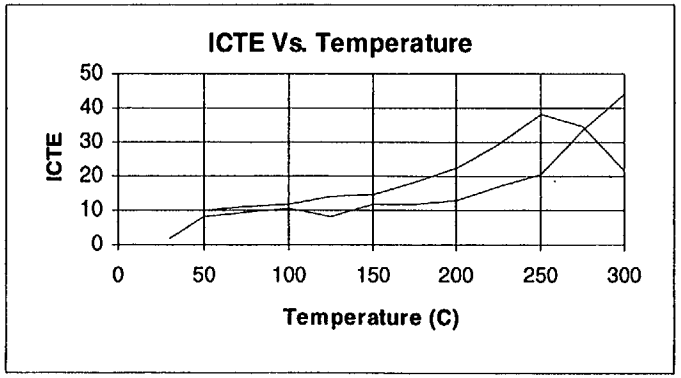

Specimen ID:	ESF-SDM-MPBX1-1.0-B
Date of Test Completion:	4/21/97
Thermal/Mechanical Unit:	TSw2
Lithostratigraphic Unit:	Tptpmn
Original Location:	ESF; Alcove 5;Thermal Drift Scale Test Area
Initial Moisture Content	Air-dried (As-is)
Nominal Dimensions:	50.8 mm (L) 25.4 mm (D)

Specimen Data:	Length (mm)	Mass (g)
Pre-test:	50.77	58.66
Post-test:	50.80	58.572
Change:	-0.03	0.088

Temp Range (C)		(C)	Mean Temp (C)	Mean CTE (10^{-6}/C)
25	-	50	37.5	5.32
50	-	75	62.5	8.97
75	-	100	87.5	10.04
100	-	125	112.5	10.54
125	-	150	137.5	11.44
150	-	175	162.5	12.02
175	-	200	187.5	13.19
200	-	225	212.5	15.81
225	-	250	237.5	19.18
250	-	275	262.5	25.85
275	-	300	287.5	39.39
300	-	325	312.5	47.97
325	-	300	312.5	16.31
300	-	275	287.5	28.67
275	-	250	262.5	36.82
250	-	225	237.5	33.75
225	-	200	212.5	24.43
200	-	175	187.5	19.07
175	-	150	162.5	15.58
150	-	125	137.5	13.74
125	-	100	112.5	12.30
100	-	75	87.5	11.21
75	-	50	62.5	10.63
50	-	30	40	10.31

Temp Range (C)		(C)	Mean Temp (C)	Instant. CTE (10^{-6}/C)
27.5	-	32.5	30	1.49
47.5	-	52.5	50	7.99
72.5	-	77.5	75	9.50
97.5	-	102.5	100	10.62
122.5	-	127.5	125	8.16
147.5	-	152.5	150	11.48
172.5	-	177.5	175	11.89
197.5	-	202.5	200	13.23
222.5	-	227.5	225	16.86
247.5	-	252.5	250	20.57
272.5	-	277.5	275	33.52
297.5	-	302.5	300	44.30
302.5	-	297.5	300	21.89
277.5	-	272.5	275	34.82
252.5	-	247.5	250	38.25
227.5	-	222.5	225	29.28
202.5	-	197.5	200	22.52
177.5	-	172.5	175	18.17
152.5	-	147.5	150	14.87
127.5	-	122.5	125	14.06
102.5	-	97.5	100	11.99
77.5	-	72.5	75	11.30
52.5	-	47.5	50	9.87

Figure A-2. Thermal Expansion Data for Specimen ESF-SDM-MPBX1-1.0-B for Second Thermal Cycle

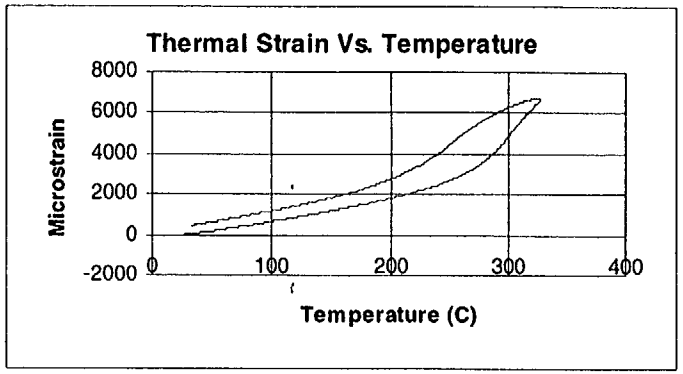

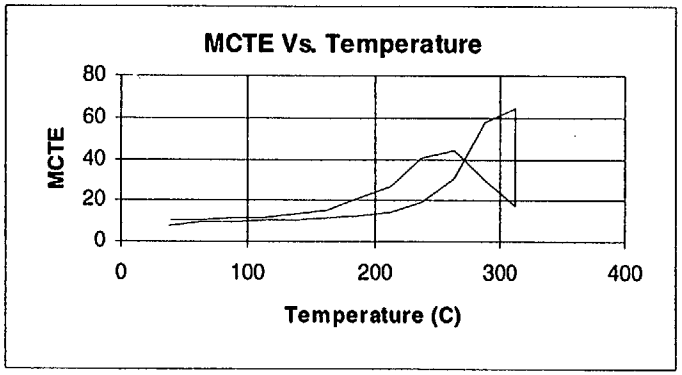

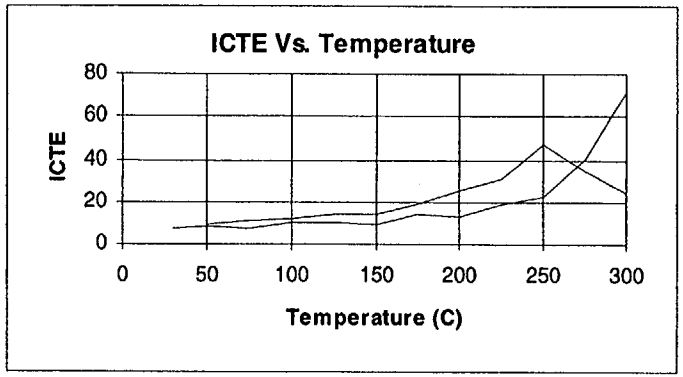

Specimen ID:	ESF-SDM-MPBX1-21.0-B
Date of Test Completion:	4/4/97
Thermal/Mechanical Unit:	TSw2
Lithostratigraphic Unit:	Tptpmn
Original Location:	ESF; Alcove 5;Thermal Drift Scale Test Area
Initial Moisture Content	Air-dried (As-is)
Nominal Dimensions:	50.8 mm (L) 25.4 mm (D)

Specimen Data:	Length (mm)	Mass (g)
Pre-test:	50.8	58.235
Post-test:	50.8	57.788
Change:	0	0.447

Temp Range (C)		(C)	Mean Temp (C)	Mean CTE (10^{-6}/C)
25	-	50	37.5	7.43
50	-	75	62.5	9.25
75	-	100	87.5	9.92
100	-	125	112.5	10.44
125	-	150	137.5	11.07
150	-	175	162.5	11.99
175	-	200	187.5	12.64
200	-	225	212.5	14.82
225	-	250	237.5	19.63
250	-	275	262.5	30.52
275	-	300	287.5	57.84
300	-	325	312.5	64.42
325	-	300	312.5	17.80
300	-	275	287.5	30.35
275	-	250	262.5	43.99
250	-	225	237.5	40.13
225	-	200	212.5	27.24
200	-	175	187.5	20.99
175	-	150	162.5	15.43
150	-	125	137.5	13.50
125	-	100	112.5	12.03
100	-	75	87.5	11.46
75	-	50	62.5	10.36
50	-	30	40	10.20

Temp Range (C)		(C)	Mean Temp (C)	Instant. CTE (10^{-6}/C)
27.5	-	32.5	30	7.35
47.5	-	52.5	50	8.34
72.5	-	77.5	75	7.46
97.5	-	102.5	100	10.45
122.5	-	127.5	125	10.02
147.5	-	152.5	150	9.65
172.5	-	177.5	175	13.97
197.5	-	202.5	200	13.45
222.5	-	227.5	225	18.42
247.5	-	252.5	250	22.14
272.5	-	277.5	275	40.66
297.5	-	302.5	300	71.18
302.5	-	297.5	300	24.69
277.5	-	272.5	275	34.77
252.5	-	247.5	250	47.21
227.5	-	222.5	225	31.18
202.5	-	197.5	200	25.70
177.5	-	172.5	175	19.22
152.5	-	147.5	150	13.94
127.5	-	122.5	125	13.95
102.5	-	97.5	100	12.17
77.5	-	72.5	75	11.72
52.5	-	47.5	50	9.14

Figure A-3. Thermal Expansion Data for Specimen ESF-SDM-MPBX1-21.0-B for First Thermal Cycle

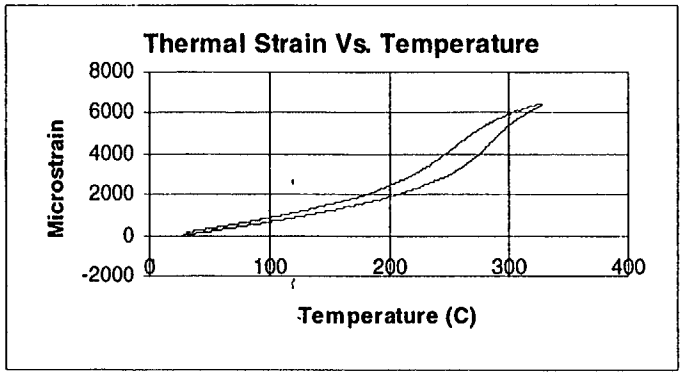

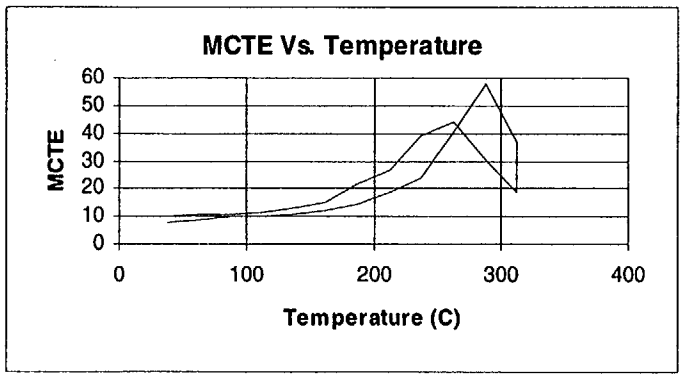

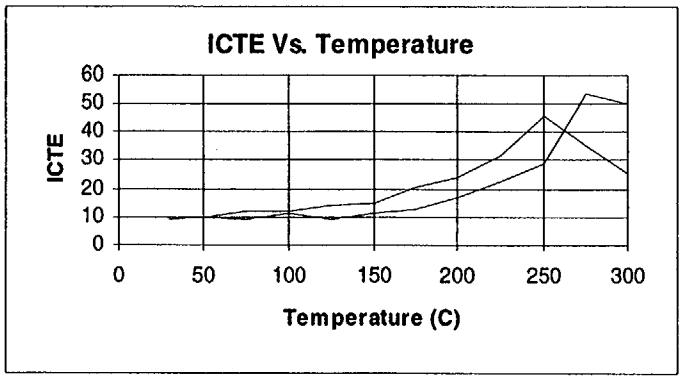

Specimen ID:	ESF-SDM-MPBX1-21.0-B
Date of Test Completion:	4/27/97
Thermal/Mechanical Unit:	TSw2
Lithostratigraphic Unit:	Tptpmn
Original Location:	ESF; Alcove 5;Thermal Drift Scale Test Area
Initial Moisture Content	Air-dried (As-is)
Nominal Dimensions:	50.8 mm (L) 25.4 mm (D)

Specimen Data:	Length (mm)	Mass (g)
Pre-test:	50.80	57.869
Post-test:	50.80	57.799
Change:	0	0.07

Temp Range (C)		(C)	Mean Temp (C)	Mean CTE (10^{-6}/C)
25	-	50	37.5	7.67
50	-	75	62.5	9.01
75	-	100	87.5	9.88
100	-	125	112.5	10.46
125	-	150	137.5	11.19
150	-	175	162.5	12.28
175	-	200	187.5	14.32
200	-	225	212.5	19.02
225	-	250	237.5	23.99
250	-	275	262.5	40.69
275	-	300	287.5	58.17
300	-	325	312.5	36.66
325	-	300	312.5	18.86
300	-	275	287.5	30.47
275	-	250	262.5	44.14
250	-	225	237.5	39.09
225	-	200	212.5	27.06
200	-	175	187.5	21.42
175	-	150	162.5	15.36
150	-	125	137.5	13.36
125	-	100	112.5	11.88
100	-	75	87.5	11.10
75	-	50	62.5	10.53
50	-	30	40	9.78

Temp Range (C)		(C)	Mean Temp (C)	Instant. CTE (10^{-6}/C)
27.5	-	32.5	30	8.98
47.5	-	52.5	50	9.55
72.5	-	77.5	75	9.37
97.5	-	102.5	100	11.31
122.5	-	127.5	125	9.40
147.5	-	152.5	150	11.35
172.5	-	177.5	175	12.74
197.5	-	202.5	200	17.28
222.5	-	227.5	225	22.53
247.5	-	252.5	250	29.26
272.5	-	277.5	275	53.87
297.5	-	302.5	300	50.45
302.5	-	297.5	300	25.40
277.5	-	272.5	275	35.43
252.5	-	247.5	250	46.09
227.5	-	222.5	225	31.63
202.5	-	197.5	200	24.07
177.5	-	172.5	175	20.59
152.5	-	147.5	150	14.50
127.5	-	122.5	125	14.05
102.5	-	97.5	100	12.28
77.5	-	72.5	75	12.15
52.5	-	47.5	50	9.72

Figure A-4. Thermal Expansion Data for Specimen ESF-SDM-MPBX1-21.0-B for Second Thermal Cycle

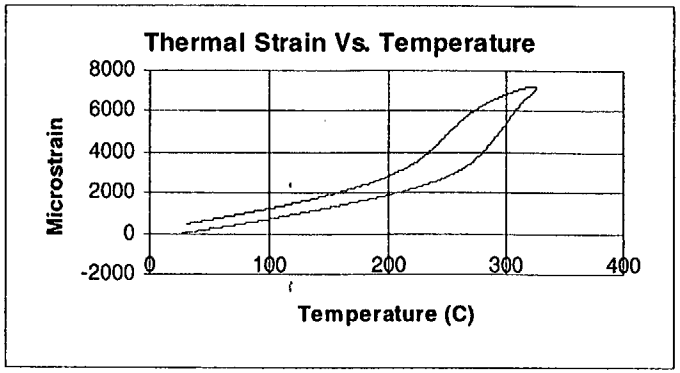

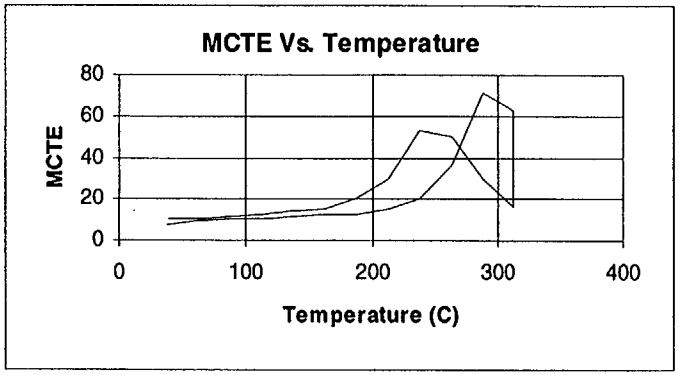

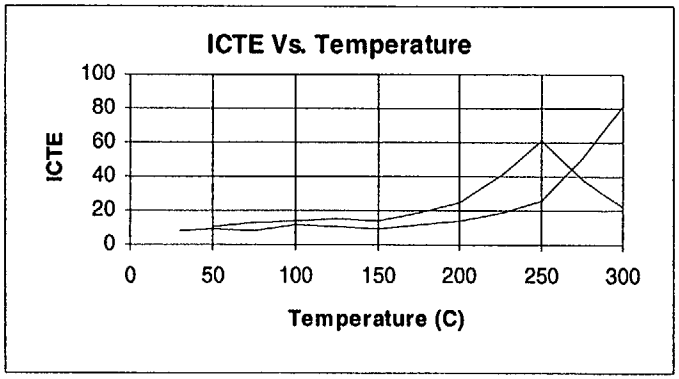

Specimen ID:	ESF-SDM-MPBX1-32.0-B
Date of Test Completion:	4/5/97
Thermal/Mechanical Unit:	TSw2
Lithostratigraphic Unit:	Tptpmn
Original Location:	ESF; Alcove 5;Thermal Drift Scale Test Area
Initial Moisture Content	Air-dried (As-is)
Nominal Dimensions:	50.8 mm (L) 25.4 mm (D)

Specimen Data:	Length (mm)	Mass (g)
Pre-test:	50.8	57.811
Post-test:	50.8	57.459
Change:	0	0.352

Temp Range (C)		(C)	Mean Temp (C)	Mean CTE (10^{-6}/C)
25	-	50	37.5	7.88
50	-	75	62.5	9.49
75	-	100	87.5	10.42
100	-	125	112.5	10.93
125	-	150	137.5	11.54
150	-	175	162.5	12.47
175	-	200	187.5	12.91
200	-	225	212.5	15.25
225	-	250	237.5	20.44
250	-	275	262.5	36.22
275	-	300	287.5	71.46
300	-	325	312.5	63.09
325	-	300	312.5	15.95
300	-	275	287.5	29.45
275	-	250	262.5	49.79
250	-	225	237.5	52.55
225	-	200	212.5	29.79
200	-	175	187.5	20.24
175	-	150	162.5	15.89
150	-	125	137.5	14.03
125	-	100	112.5	12.67
100	-	75	87.5	11.68
75	-	50	62.5	10.77
50	-	30	40	10.31

Temp Range (C)		(C)	Mean Temp (C)	Instant. CTE (10^{-6}/C)
27.5	-	32.5	30	7.93
47.5	-	52.5	50	9.30
72.5	-	77.5	75	8.65
97.5	-	102.5	100	11.34
122.5	-	127.5	125	10.84
147.5	-	152.5	150	9.73
172.5	-	177.5	175	11.62
197.5	-	202.5	200	14.35
222.5	-	227.5	225	18.61
247.5	-	252.5	250	26.39
272.5	-	277.5	275	51.53
297.5	-	302.5	300	80.90
302.5	-	297.5	300	22.87
277.5	-	272.5	275	37.44
252.5	-	247.5	250	60.60
227.5	-	222.5	225	41.05
202.5	-	197.5	200	24.75
177.5	-	172.5	175	19.36
152.5	-	147.5	150	14.28
127.5	-	122.5	125	14.87
102.5	-	97.5	100	13.80
77.5	-	72.5	75	12.78
52.5	-	47.5	50	10.15

Figure A-5. Thermal Expansion Data for Specimen ESF-SDM-MPBX1-32.0-B for First Thermal Cycle

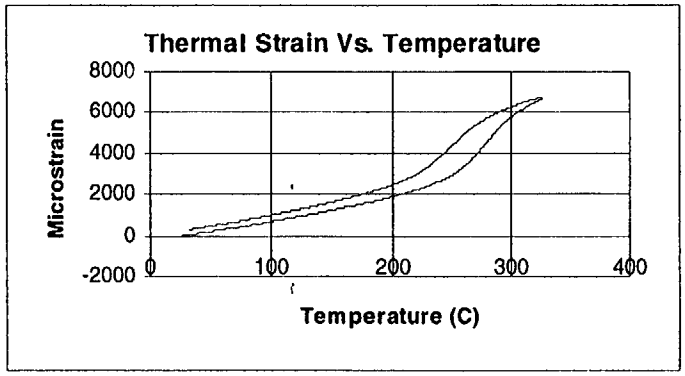

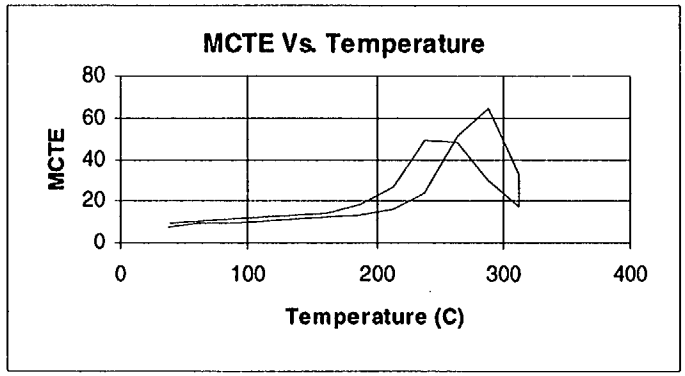

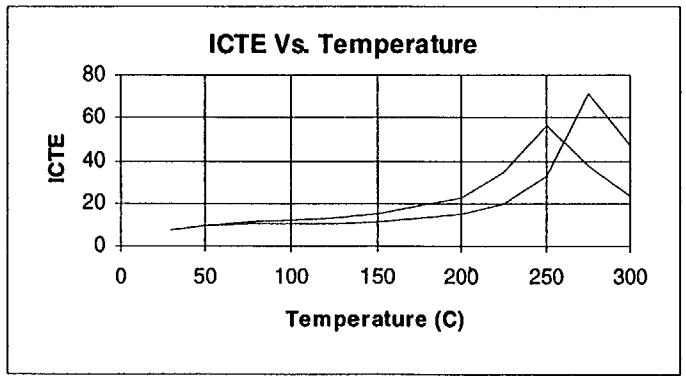

Specimen ID:	ESF-SDM-MPBX1-32.0-B
Date of Test Completion:	4/29/97
Thermal/Mechanical Unit:	TSw2
Lithostratigraphic Unit:	Tptpmn
Original Location:	ESF; Alcove 5;Thermal Drift Scale Test Area
Initial Moisture Content	Air-dried (As-is)
Nominal Dimensions:	50.8 mm (L) 25.4 mm (D)

Specimen Data:	Length (mm)	Mass (g)
Pre-test:	50.80	57.542
Post-test:	50.80	57.459
Change:	0	0.083

Temp Range (C)		(C)	Mean Temp (C)	Mean CTE (10^{-6}/C)
25	-	50	37.5	7.30
50	-	75	62.5	9.36
75	-	100	87.5	10.10
100	-	125	112.5	10.60
125	-	150	137.5	11.29
150	-	175	162.5	12.73
175	-	200	187.5	13.60
200	-	225	212.5	16.84
225	-	250	237.5	24.43
250	-	275	262.5	50.93
275	-	300	287.5	64.29
300	-	325	312.5	32.73
325	-	300	312.5	17.65
300	-	275	287.5	29.92
275	-	250	262.5	48.39
250	-	225	237.5	48.98
225	-	200	212.5	27.09
200	-	175	187.5	18.16
175	-	150	162.5	14.64
150	-	125	137.5	13.28
125	-	100	112.5	12.06
100	-	75	87.5	11.14
75	-	50	62.5	10.39
50	-	30	40	9.71

Temp Range (C)		(C)	Mean Temp (C)	Instant. CTE (10^{-6}/C)
27.5	-	32.5	30	7.49
47.5	-	52.5	50	9.60
72.5	-	77.5	75	10.21
97.5	-	102.5	100	10.65
122.5	-	127.5	125	10.06
147.5	-	152.5	150	11.20
172.5	-	177.5	175	13.64
197.5	-	202.5	200	15.06
222.5	-	227.5	225	20.11
247.5	-	252.5	250	32.92
272.5	-	277.5	275	71.57
297.5	-	302.5	300	47.46
302.5	-	297.5	300	23.19
277.5	-	272.5	275	37.89
252.5	-	247.5	250	56.37
227.5	-	222.5	225	35.27
202.5	-	197.5	200	22.49
177.5	-	172.5	175	18.63
152.5	-	147.5	150	14.95
127.5	-	122.5	125	13.62
102.5	-	97.5	100	12.38
77.5	-	72.5	75	11.54
52.5	-	47.5	50	9.62

Figure A-6. Thermal Expansion Data for Specimen ESF-SDM-MPBX1-32.0-B for Second Thermal Cycle

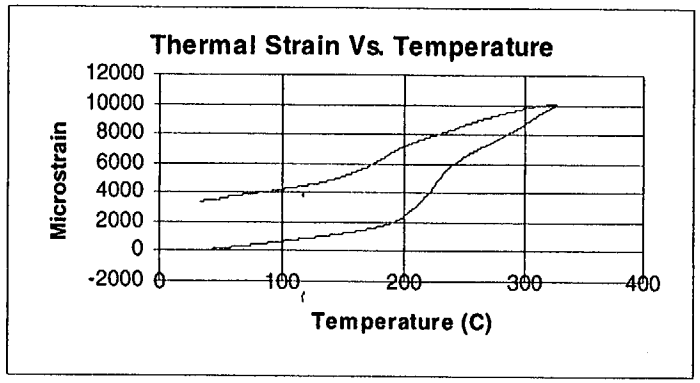

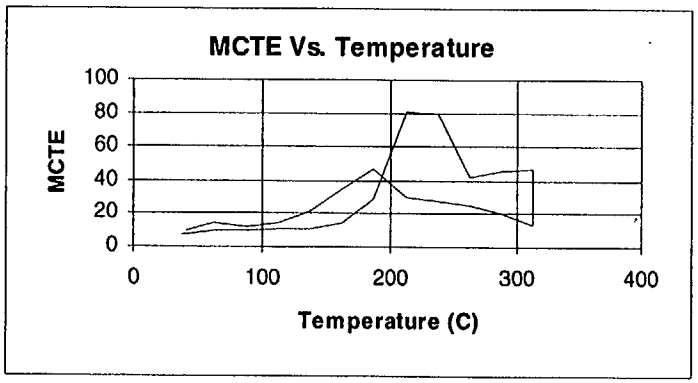

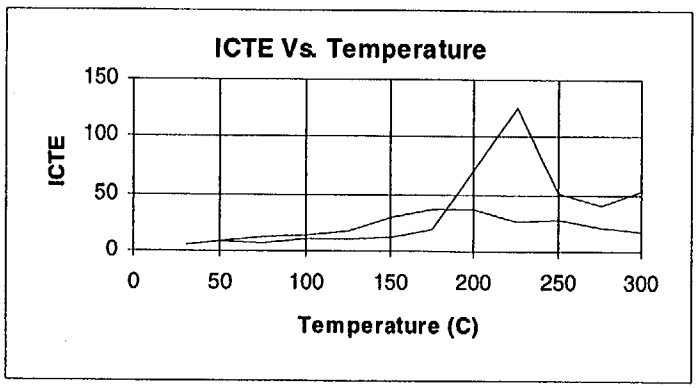

Specimen ID:	ESF-SDM-MPBX1-40.4-B
Date of Test Completion:	3/31/97
Thermal/Mechanical Unit:	TSw2
Lithostratigraphic Unit:	Tptpmn
Original Location:	ESF; Alcove 5;Thermal Drift Scale Test Area
Initial Moisture Content	Air-dried (As-is)
Nominal Dimensions:	50.8 mm (L) 25.4 mm (D)

Specimen Data:	Length (mm)	Mass (g)
Pre-test:	50.8	56.289
Post-test:	50.88	55.953
Change:	-0.08	0.336

Temp Range (C)		(C)	Mean Temp (C)	Mean CTE (10^{-6}/C)
25	-	50	37.5	7.40
50	-	75	62.5	9.13
75	-	100	87.5	10.06
100	-	125	112.5	10.74
125	-	150	137.5	11.42
150	-	175	162.5	14.15
175	-	200	187.5	29.02
200	-	225	212.5	80.75
225	-	250	237.5	78.92
250	-	275	262.5	42.15
275	-	300	287.5	46.29
300	-	325	312.5	47.45
325	-	300	312.5	13.17
300	-	275	287.5	20.20
275	-	250	262.5	25.53
250	-	225	237.5	27.93
225	-	200	212.5	29.79
200	-	175	187.5	47.17
175	-	150	162.5	34.79
150	-	125	137.5	21.80
125	-	100	112.5	14.40
100	-	75	87.5	11.95
75	-	50	62.5	14.21
50	-	30	40	10.10

Temp Range (C)		(C)	Mean Temp (C)	Instant. CTE (10^{-6}/C)
27.5	-	32.5	30	5.11
47.5	-	52.5	50	8.99
72.5	-	77.5	75	6.70
97.5	-	102.5	100	11.01
122.5	-	127.5	125	11.20
147.5	-	152.5	150	12.44
172.5	-	177.5	175	19.30
197.5	-	202.5	200	70.67
222.5	-	227.5	225	125.01
247.5	-	252.5	250	51.84
272.5	-	277.5	275	40.49
297.5	-	302.5	300	52.68
302.5	-	297.5	300	16.87
277.5	-	272.5	275	21.38
252.5	-	247.5	250	29.07
227.5	-	222.5	225	27.35
202.5	-	197.5	200	36.53
177.5	-	172.5	175	36.71
152.5	-	147.5	150	30.50
127.5	-	122.5	125	17.12
102.5	-	97.5	100	13.67
77.5	-	72.5	75	12.44
52.5	-	47.5	50	9.48

Figure A-7. Thermal Expansion Data for Specimen ESF-SDM-MPBX1-40.4-B for First Thermal Cycle

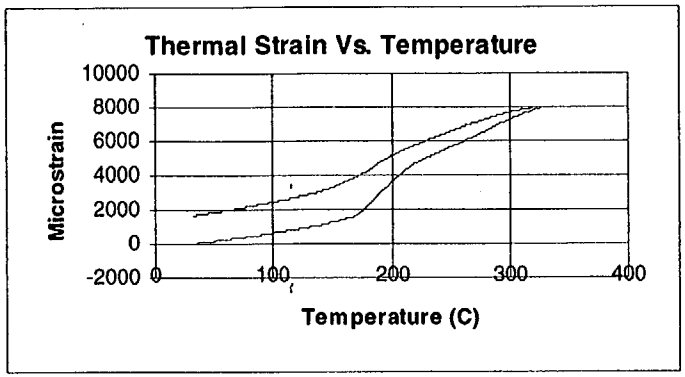

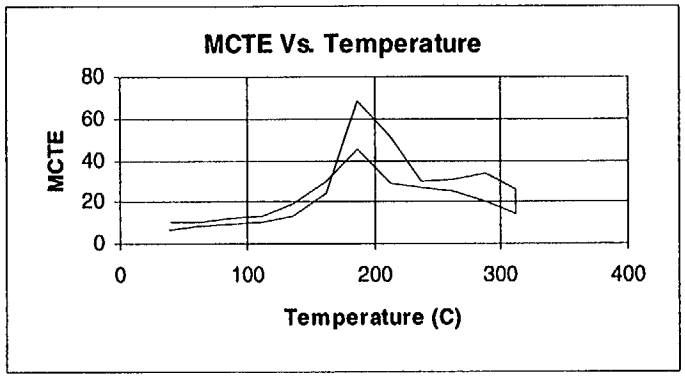

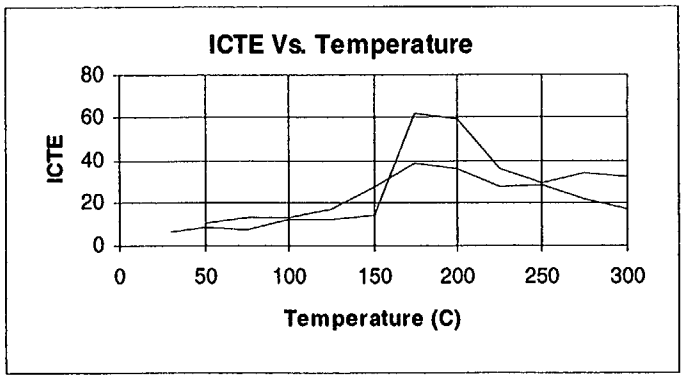

Specimen ID:	ESF-SDM-MPBX1-40.4-B
Date of Test Completion:	4/22/97
Thermal/Mechanical Unit:	TSw2
Lithostratigraphic Unit:	Tptpmn
Original Location:	ESF; Alcove 5;Thermal Drift Scale Test Area
Initial Moisture Content	Air-dried (As-is)
Nominal Dimensions:	50.8 mm (L) 25.4 mm (D)

Specimen Data:	Length (mm)	Mass (g)
Pre-test:	50.90	56.037
Post-test:	50.90	55.981
Change:	0	0.056

Temp Range (C)		(C)	Mean Temp (C)	Mean CTE (10^{-6}/C)
25	-	50	37.5	7.00
50	-	75	62.5	9.04
75	-	100	87.5	9.77
100	-	125	112.5	10.83
125	-	150	137.5	13.59
150	-	175	162.5	23.69
175	-	200	187.5	68.42
200	-	225	212.5	50.62
225	-	250	237.5	30.28
250	-	275	262.5	31.03
275	-	300	287.5	34.14
300	-	325	312.5	26.00
325	-	300	312.5	14.13
300	-	275	287.5	20.40
275	-	250	262.5	24.67
250	-	225	237.5	26.99
225	-	200	212.5	28.71
200	-	175	187.5	45.77
175	-	150	162.5	29.89
150	-	125	137.5	18.99
125	-	100	112.5	13.87
100	-	75	87.5	12.18
75	-	50	62.5	10.41
50	-	30	40	10.94

Temp Range (C)		(C)	Mean Temp (C)	Instant. CTE (10^{-6}/C)
27.5	-	32.5	30	6.15
47.5	-	52.5	50	8.47
72.5	-	77.5	75	7.43
97.5	-	102.5	100	11.89
122.5	-	127.5	125	11.79
147.5	-	152.5	150	14.04
172.5	-	177.5	175	62.47
197.5	-	202.5	200	58.88
222.5	-	227.5	225	35.49
247.5	-	252.5	250	29.13
272.5	-	277.5	275	34.20
297.5	-	302.5	300	32.20
302.5	-	297.5	300	16.68
277.5	-	272.5	275	21.58
252.5	-	247.5	250	27.89
227.5	-	222.5	225	27.19
202.5	-	197.5	200	35.35
177.5	-	172.5	175	38.58
152.5	-	147.5	150	27.00
127.5	-	122.5	125	16.61
102.5	-	97.5	100	13.35
77.5	-	72.5	75	13.29
52.5	-	47.5	50	10.46

Figure A-7. Thermal Expansion Data for Specimen ESF-SDM-MPBX1-40.4-B for Second Thermal Cycle

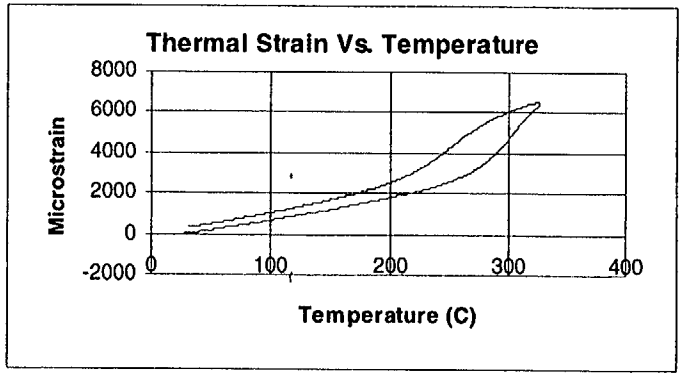

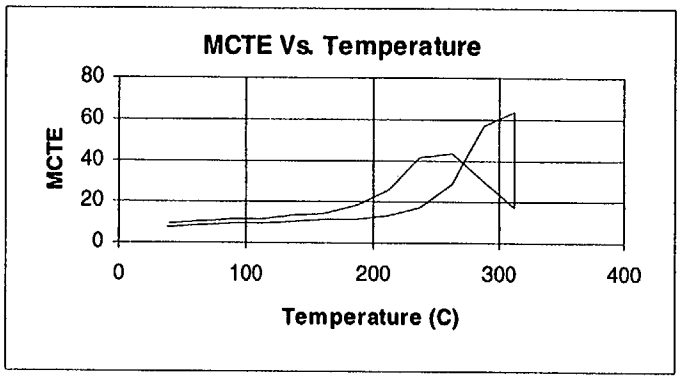

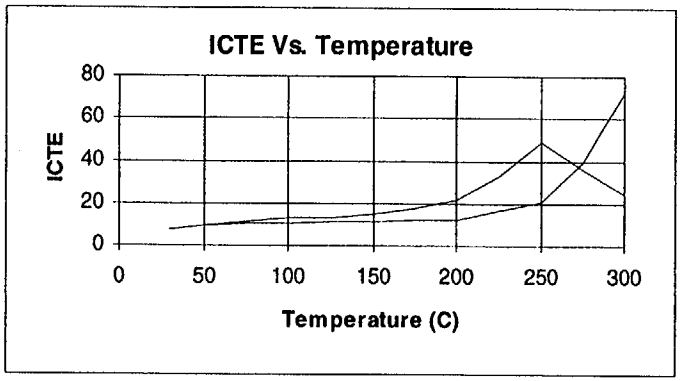

Specimen ID:	ESF-SDM-MPBX1-62.0-B
Date of Test Completion:	4/10/97
Thermal/Mechanical Unit:	TSw2
Lithostratigraphic Unit:	Tptpmn
Original Location:	ESF; Alcove 5;Thermal Drift Scale Test Area
Initial Moisture Content	Air-dried (As-is)
Nominal Dimensions:	50.8 mm (L) 25.4 mm (D)

Specimen Data:	Length (mm)	Mass (g)
Pre-test:	50.8	58.470
Post-test:	50.8	57.975
Change:	0	0.495

Temp Range (C)		(C)	Mean Temp (C)	Mean CTE (10^{-6}/C)
25	-	50	37.5	7.68
50	-	75	62.5	9.15
75	-	100	87.5	9.73
100	-	125	112.5	10.06
125	-	150	137.5	10.62
150	-	175	162.5	11.60
175	-	200	187.5	11.94
200	-	225	212.5	13.52
225	-	250	237.5	17.70
250	-	275	262.5	29.01
275	-	300	287.5	57.27
300	-	325	312.5	63.98
325	-	300	312.5	17.73
300	-	275	287.5	30.23
275	-	250	262.5	43.48
250	-	225	237.5	41.91
225	-	200	212.5	26.49
200	-	175	187.5	18.74
175	-	150	162.5	14.75
150	-	125	137.5	13.21
125	-	100	112.5	11.91
100	-	75	87.5	11.11
75	-	50	62.5	10.50
50	-	30	40	10.03

Temp Range (C)		(C)	Mean Temp (C)	Instant. CTE (10^{-6}/C)
27.5	-	32.5	30	7.15
47.5	-	52.5	50	9.83
72.5	-	77.5	75	10.51
97.5	-	102.5	100	10.51
122.5	-	127.5	125	11.03
147.5	-	152.5	150	11.08
172.5	-	177.5	175	12.35
197.5	-	202.5	200	12.20
222.5	-	227.5	225	16.83
247.5	-	252.5	250	20.94
272.5	-	277.5	275	39.77
297.5	-	302.5	300	72.67
302.5	-	297.5	300	24.12
277.5	-	272.5	275	35.61
252.5	-	247.5	250	49.31
227.5	-	222.5	225	33.30
202.5	-	197.5	200	21.79
177.5	-	172.5	175	17.90
152.5	-	147.5	150	15.09
127.5	-	122.5	125	13.28
102.5	-	97.5	100	13.29
77.5	-	72.5	75	11.76
52.5	-	47.5	50	9.55

Figure A-9. Thermal Expansion Data for Specimen ESF-SDM-MPBX1-62.0-B for First Thermal Cycle

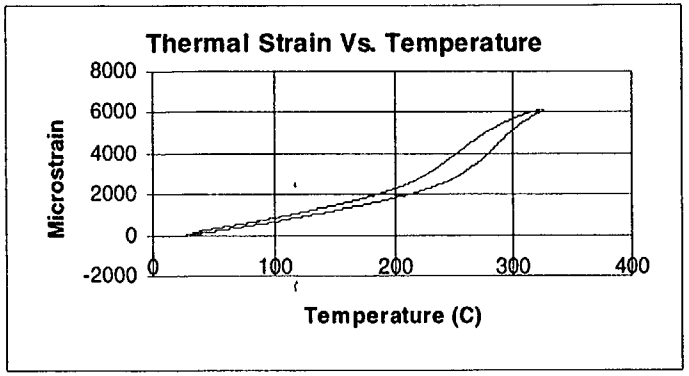

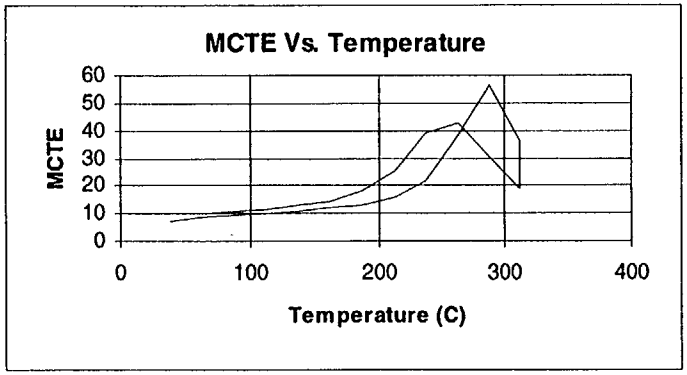

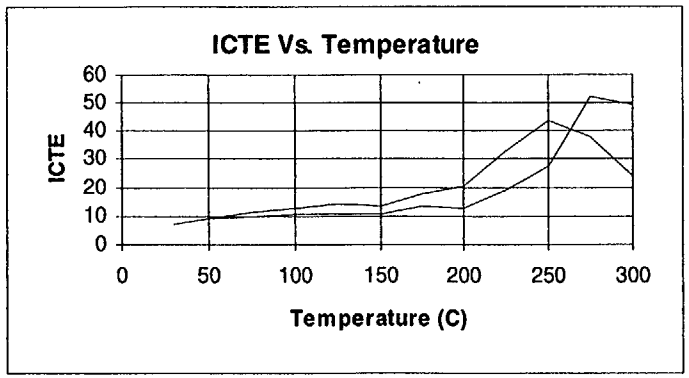

Specimen ID:	ESF-SDM-MPBX1-62.0-B
Date of Test Completion:	5/3/97
Thermal/Mechanical Unit:	TSw2
Lithostratigraphic Unit:	Tptpmn
Original Location:	ESF; Alcove 5;Thermal Drift Scale Test Area
Initial Moisture Content	Air-dried (As-is)
Nominal Dimensions:	50.8 mm (L) 25.4 mm (D)

Specimen Data:	Length (mm)	Mass (g)
Pre-test:	50.80	58.074
Post-test:	50.80	58.002
Change:	0	0.072

Temp Range (C)		(C)	Mean Temp (C)	Mean CTE (10^{-6}/C)
25	-	50	37.5	7.42
50	-	75	62.5	8.89
75	-	100	87.5	9.66
100	-	125	112.5	10.42
125	-	150	137.5	10.90
150	-	175	162.5	12.22
175	-	200	187.5	13.30
200	-	225	212.5	16.13
225	-	250	237.5	22.02
250	-	275	262.5	38.55
275	-	300	287.5	56.74
300	-	325	312.5	35.84
325	-	300	312.5	18.83
300	-	275	287.5	30.08
275	-	250	262.5	42.50
250	-	225	237.5	38.88
225	-	200	212.5	25.10
200	-	175	187.5	18.28
175	-	150	162.5	14.49
150	-	125	137.5	13.00
125	-	100	112.5	11.65
100	-	75	87.5	11.00
75	-	50	62.5	10.20
50	-	30	.40	9.88

Temp Range (C)		(C)	Mean Temp (C)	Instant. CTE (10^{-6}/C)
27.5	-	32.5	30	6.98
47.5	-	52.5	50	9.22
72.5	-	77.5	75	10.03
97.5	-	102.5	100	10.66
122.5	-	127.5	125	10.62
147.5	-	152.5	150	10.35
172.5	-	177.5	175	13.51
197.5	-	202.5	200	12.57
222.5	-	227.5	225	19.28
247.5	-	252.5	250	27.55
272.5	-	277.5	275	52.00
297.5	-	302.5	300	49.64
302.5	-	297.5	300	24.31
277.5	-	272.5	275	37.85
252.5	-	247.5	250	43.68
227.5	-	222.5	225	33.10
202.5	-	197.5	200	20.79
177.5	-	172.5	175	17.77
152.5	-	147.5	150	13.70
127.5	-	122.5	125	14.05
102.5	-	97.5	100	12.52
77.5	-	72.5	75	11.05
52.5	-	47.5	50	9.48

Figure A-10. Thermal Expansion Data for Specimen ESF-SDM-MPBX1-62.0-B for Second Thermal Cycle

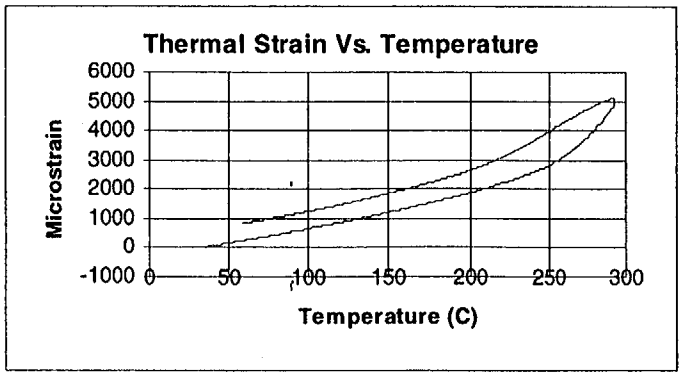

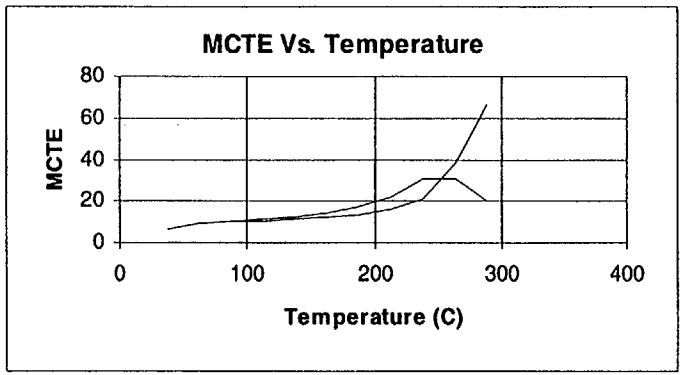

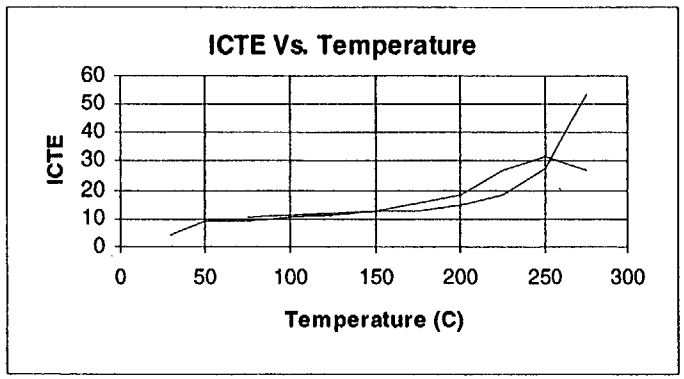

Specimen ID:	ESF-SDM-MPBX1-80.7-B
Date of Test Completion:	3/21/97
Thermal/Mechanical Unit:	TSw2
Lithostratigraphic Unit:	Tptpmn
Original Location:	ESF; Alcove 5;Thermal Drift Scale Test Area
Initial Moisture Content	Air-dried (As-Is)
Nominal Dimensions:	50.8 mm (L) 25.4 mm (D)

Specimen Data:	Length (mm)	Mass (g)
Pre-test:	50.8	59.393
Post-test:	50.8	58.909
Change:	0	0.484

Temp Range (C)		(C)	Mean Temp (C)	Mean CTE (10^{-6}/C)
25	-	50	37.5	6.87
50	-	75	62.5	9.39
75	-	100	87.5	10.15
100	-	125	112.5	10.93
125	-	150	137.5	11.65
150	-	175	162.5	12.37
175	-	200	187.5	13.64
200	-	225	212.5	16.20
225	-	250	237.5	21.65
250	-	275	262.5	38.26
275	-	300	287.5	66.58
300	-	325	312.5	-
325	-	300	312.5	-
300	-	275	287.5	20.56
275	-	250	262.5	30.61
250	-	225	237.5	31.10
225	-	200	212.5	21.94
200	-	175	187.5	17.13
175	-	150	162.5	14.27
150	-	125	137.5	12.63
125	-	100	112.5	11.48
100	-	75	87.5	10.57
75	-	50	62.5	9.84
50	-	30	40	0.00

Temp Range (C)		(C)	Mean Temp (C)	Instant. CTE (10^{-6}/C)
27.5	-	32.5	30	4.35
47.5	-	52.5	50	8.85
72.5	-	77.5	75	9.32
97.5	-	102.5	100	10.73
122.5	-	127.5	125	10.94
147.5	-	152.5	150	12.76
172.5	-	177.5	175	12.80
197.5	-	202.5	200	14.97
222.5	-	227.5	225	18.65
247.5	-	252.5	250	27.61
272.5	-	277.5	275	53.41
297.5	-	302.5	300	-
302.5	-	297.5	300	-
277.5	-	272.5	275	27.02
252.5	-	247.5	250	31.84
227.5	-	222.5	225	27.00
202.5	-	197.5	200	18.14
177.5	-	172.5	175	15.35
152.5	-	147.5	150	12.63
127.5	-	122.5	125	11.77
102.5	-	97.5	100	11.61
77.5	-	72.5	75	10.55
52.5	-	47.5	50	-

Figure A-11. Thermal Expansion Data for Specimen ESF-SDM-MPBX1-80.7-B for First Thermal Cycle

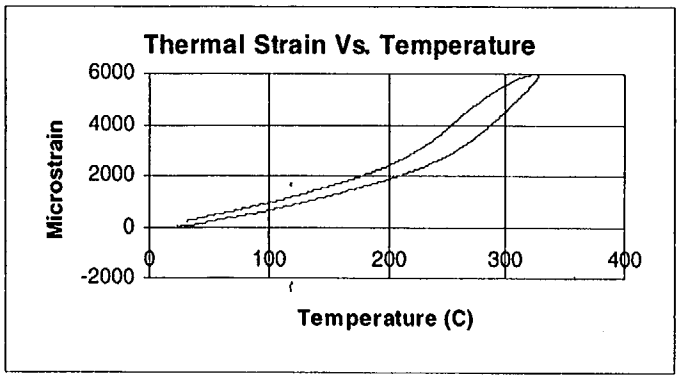

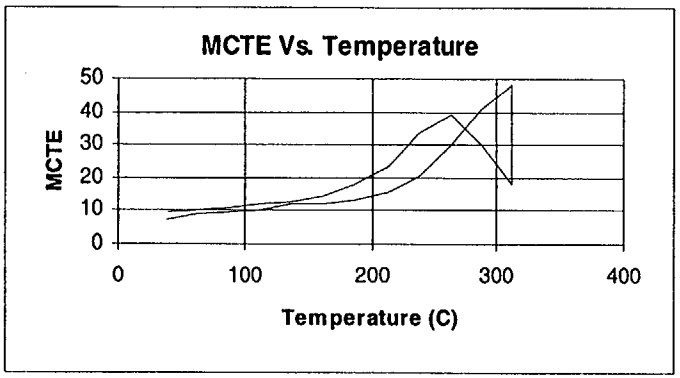

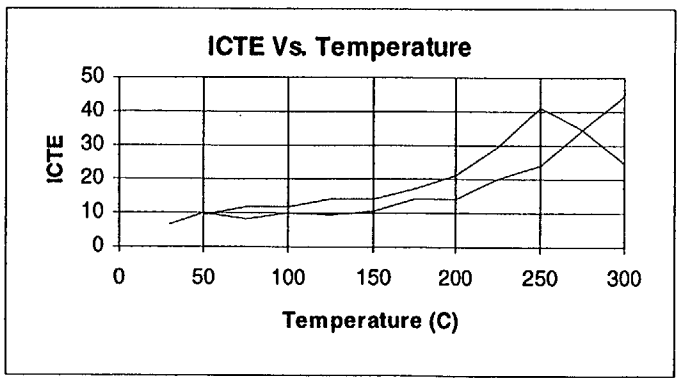

Specimen ID:	ESF-SDM-MPBX1-80.7-B
Date of Test Completion:	4/20/97
Thermal/Mechanical Unit:	TSw2
Lithostratigraphic Unit:	Tptpmn
Original Location:	ESF; Alcove 5;Thermal Drift Scale Test Area
Initial Moisture Content	Air-dried (As-is)
Nominal Dimensions:	50.8 mm (L) 25.4 mm (D)

Specimen Data:	Length (mm)	Mass (g)
Pre-test:	50.8	59.014
Post-test:	50.8	58.911
Change:	0	0.103

Temp Range (C)		(C)	Mean Temp (C)	Mean CTE (10^{-6}/C)
25	-	50	37.5	7.44
50	-	75	62.5	8.90
75	-	100	87.5	9.73
100	-	125	112.5	10.43
125	-	150	137.5	11.86
150	-	175	162.5	12.18
175	-	200	187.5	13.41
200	-	225	212.5	15.86
225	-	250	237.5	20.29
250	-	275	262.5	29.84
275	-	300	287.5	40.94
300	-	325	312.5	48.06
325	-	300	312.5	18.32
300	-	275	287.5	30.36
275	-	250	262.5	38.95
250	-	225	237.5	33.64
225	-	200	212.5	23.50
200	-	175	187.5	18.05
175	-	150	162.5	14.67
150	-	125	137.5	12.87
125	-	100	112.5	11.78
100	-	75	87.5	11.09
75	-	50	62.5	10.38
50	-	30	40	9.66

Temp Range (C)		(C)	Mean Temp (C)	Instant. CTE (10^{-6}/C)
27.5	-	32.5	30	6.56
47.5	-	52.5	50	10.00
72.5	-	77.5	75	8.49
97.5	-	102.5	100	9.77
122.5	-	127.5	125	9.17
147.5	-	152.5	150	10.57
172.5	-	177.5	175	14.08
197.5	-	202.5	200	14.36
222.5	-	227.5	225	19.94
247.5	-	252.5	250	24.39
272.5	-	277.5	275	34.58
297.5	-	302.5	300	44.70
302.5	-	297.5	300	24.87
277.5	-	272.5	275	34.83
252.5	-	247.5	250	41.18
227.5	-	222.5	225	29.25
202.5	-	197.5	200	20.95
177.5	-	172.5	175	17.23
152.5	-	147.5	150	14.10
127.5	-	122.5	125	13.91
102.5	-	97.5	100	11.49
77.5	-	72.5	75	11.49
52.5	-	47.5	50	9.17

Figure A-12. Thermal Expansion Data for Specimen ESF-SDM-MPBX1-80.7-B for Second Thermal Cycle

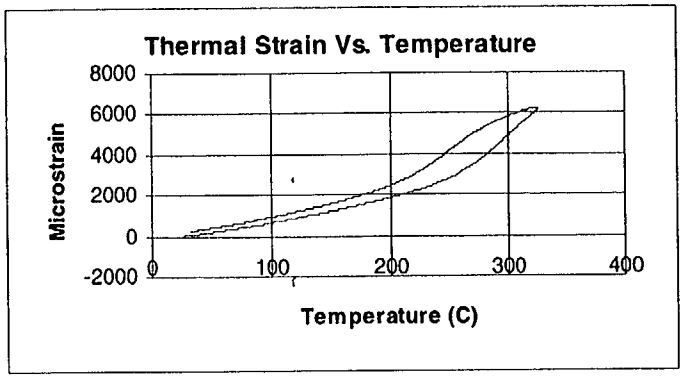

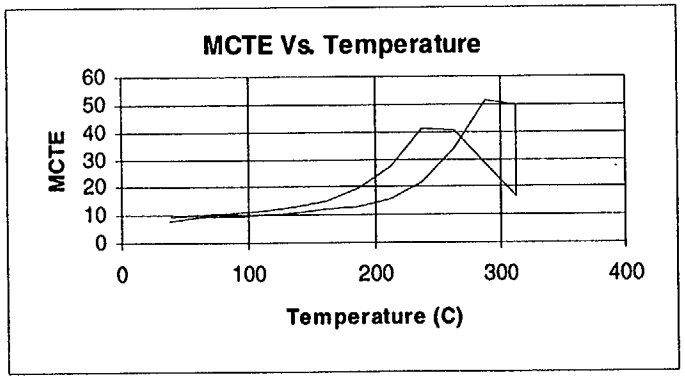

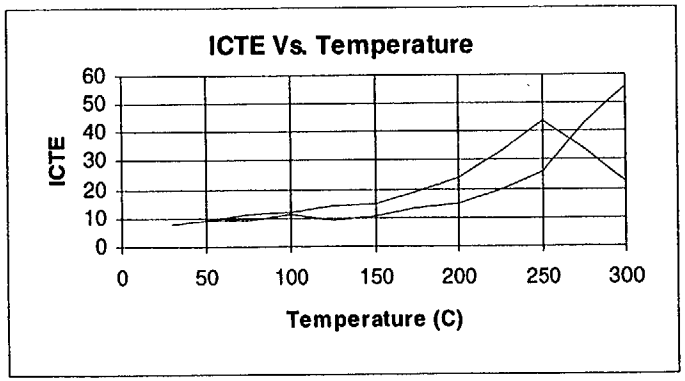

Specimen ID:	ESF-SDM-MPBX2-29.0-B
Date of Test Completion:	4/11/97
Thermal/Mechanical Unit:	TSw2
Lithostratigraphic Unit:	Tptpmn
Original Location:	ESF; Alcove 5;Thermal Drift Scale Test Area
Initial Moisture Content	Air-dried (As-is)
Nominal Dimensions:	50.8 mm (L) 25.4 mm (D)

Specimen Data:	Length (mm)	Mass (g)
Pre-test:	50.8	59.019
Post-test:	50.8	58.73
Change:	0	0.289

Temp Range (C)		(C)	Mean Temp (C)	Mean CTE (10^{-6}/C)
25	-	50	37.5	7.84
50	-	75	62.5	9.06
75	-	100	87.5	9.69
100	-	125	112.5	10.11
125	-	150	137.5	11.05
150	-	175	162.5	12.50
175	-	200	187.5	13.30
200	-	225	212.5	16.04
225	-	250	237.5	21.77
250	-	275	262.5	33.93
275	-	300	287.5	50.98
300	-	325	312.5	49.55
325	-	300	312.5	16.55
300	-	275	287.5	28.27
275	-	250	262.5	40.63
250	-	225	237.5	41.13
225	-	200	212.5	27.11
200	-	175	187.5	19.26
175	-	150	162.5	15.31
150	-	125	137.5	13.33
125	-	100	112.5	11.88
100	-	75	87.5	10.79
75	-	50	62.5	10.04
50	-	30	40	9.47

Temp Range (C)		(C)	Mean Temp (C)	Instant. CTE (10^{-6}/C)
27.5	-	32.5	30	7.90
47.5	-	52.5	50	9.29
72.5	-	77.5	75	9.21
97.5	-	102.5	100	11.30
122.5	-	127.5	125	9.17
147.5	-	152.5	150	10.54
172.5	-	177.5	175	13.33
197.5	-	202.5	200	14.75
222.5	-	227.5	225	19.62
247.5	-	252.5	250	26.32
272.5	-	277.5	275	42.79
297.5	-	302.5	300	55.44
302.5	-	297.5	300	22.51
277.5	-	272.5	275	34.15
252.5	-	247.5	250	43.69
227.5	-	222.5	225	32.88
202.5	-	197.5	200	24.11
177.5	-	172.5	175	19.33
152.5	-	147.5	150	14.90
127.5	-	122.5	125	13.87
102.5	-	97.5	100	12.23
77.5	-	72.5	75	11.34
52.5	-	47.5	50	9.05

Figure A-13. Thermal Expansion Data for Specimen ESF-SDM-MPBX2-29.0-B for First Thermal Cycle

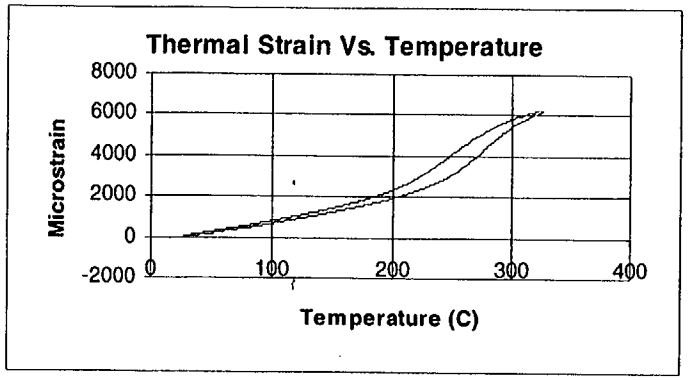

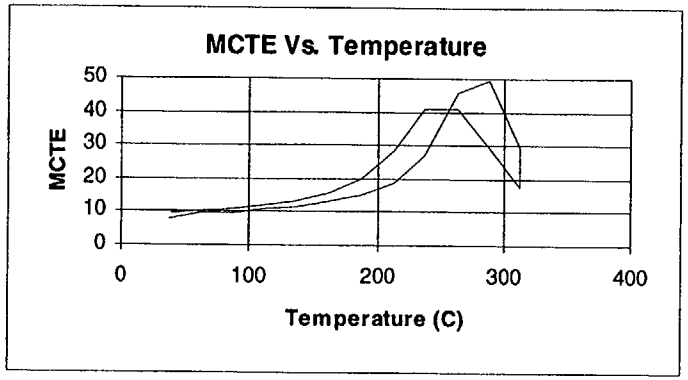

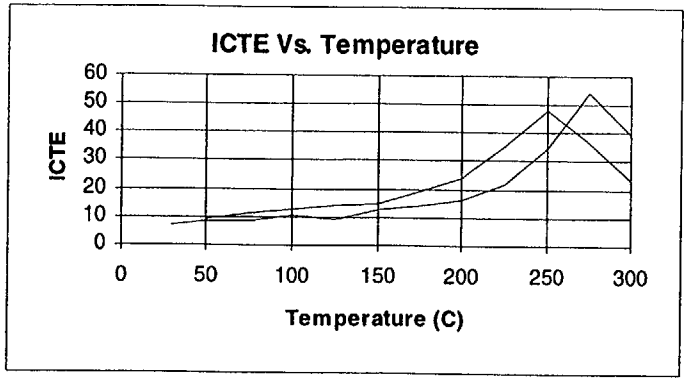

Specimen ID:	ESF-SDM-MPBX2-29.0-B
Date of Test Completion:	4/18/97
Thermal/Mechanical Unit:	TSw2
Lithostratigraphic Unit:	Tptpmn
Original Location:	ESF; Alcove 5;Thermal Drift Scale Test Area
Initial Moisture Content	Air-dried (As-is)
Nominal Dimensions:	50.8 mm (L) 25.4 mm (D)

Specimen Data:	Length (mm)	Mass (g)
Pre-test:	50.8	58.763
Post-test:	50.8	58.733
Change:	0	0.030

Temp Range (C)		(C)	Mean Temp (C)	Mean CTE (10^{-6}/C)
25	-	50	37.5	7.70
50	-	75	62.5	9.35
75	-	100	87.5	9.87
100	-	125	112.5	10.69
125	-	150	137.5	11.69
150	-	175	162.5	13.38
175	-	200	187.5	14.87
200	-	225	212.5	18.80
225	-	250	237.5	26.97
250	-	275	262.5	45.52
275	-	300	287.5	49.43
300	-	325	312.5	29.37
325	-	300	312.5	17.50
300	-	275	287.5	29.50
275	-	250	262.5	40.91
250	-	225	237.5	40.88
225	-	200	212.5	28.23
200	-	175	187.5	20.16
175	-	150	162.5	15.70
150	-	125	137.5	13.49
125	-	100	112.5	12.03
100	-	75	87.5	10.89
75	-	50	62.5	10.24
50	-	30	40	9.82

Temp Range (C)		(C)	Mean Temp (C)	Instant. CTE (10^{-6}/C)
27.5	-	32.5	30	7.27
47.5	-	52.5	50	8.22
72.5	-	77.5	75	8.37
97.5	-	102.5	100	10.38
122.5	-	127.5	125	9.30
147.5	-	152.5	150	12.57
172.5	-	177.5	175	14.25
197.5	-	202.5	200	16.12
222.5	-	227.5	225	22.05
247.5	-	252.5	250	34.87
272.5	-	277.5	275	54.54
297.5	-	302.5	300	39.42
302.5	-	297.5	300	23.24
277.5	-	272.5	275	36.69
252.5	-	247.5	250	47.91
227.5	-	222.5	225	35.15
202.5	-	197.5	200	23.80
177.5	-	172.5	175	19.40
152.5	-	147.5	150	14.93
127.5	-	122.5	125	14.47
102.5	-	97.5	100	12.69
77.5	-	72.5	75	11.01
52.5	-	47.5	50	9.05

Figure A-14. Thermal Expansion Data for Specimen ESF-SDM-MPBX2-29.0-B for Second Thermal Cycle

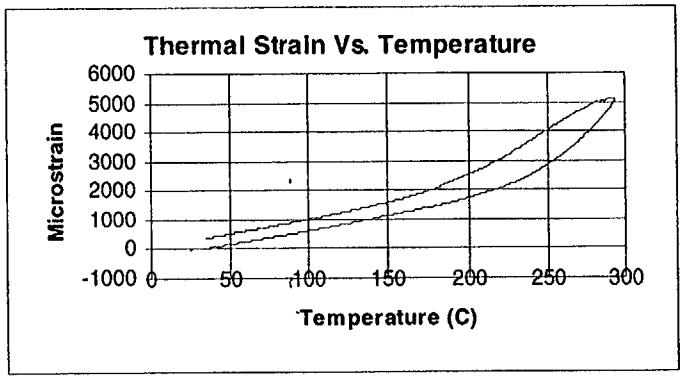

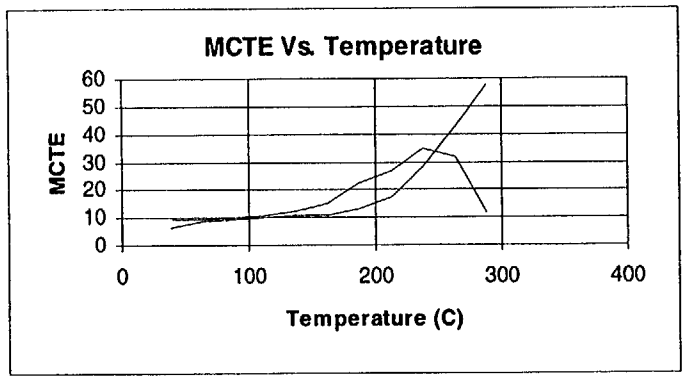

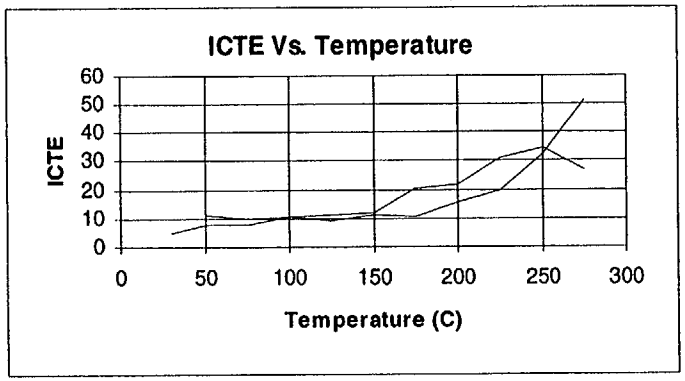

Specimen ID:	ESF-SDM-MPBX2-48.6-B
Date of Test Completion:	3/20/97
Thermal/Mechanical Unit:	TSw2
Lithostratigraphic Unit:	Tptpmn
Original Location:	ESF; Alcove 5;Thermal Drift Scale Test Area
Initial Moisture Content	Air-dried (As-is)
Nominal Dimensions:	50.8 mm (L) 25.4 mm (D)

Specimen Data:	Length (mm)	Mass (g)
Pre-test:	50.8	57.152
Post-test:	50.8	56.76
Change:	0	0.392

Temp Range (C)		(C)	Mean Temp (C)	Mean CTE (10⁻⁶/C)
25	-	50	37.5	6.76
50	-	75	62.5	8.80
75	-	100	87.5	9.42
100	-	125	112.5	10.07
125	-	150	137.5	10.51
150	-	175	162.5	11.11
175	-	200	187.5	12.66
200	-	225	212.5	17.30
225	-	250	237.5	28.12
250	-	275	262.5	42.64
275	-	300	287.5	57.77
300	-	325	312.5	-
325	-	300	312.5	-
300	-	275	287.5	11.81
275	-	250	262.5	31.81
250	-	225	237.5	34.40
225	-	200	212.5	26.83
200	-	175	187.5	22.06
175	-	150	162.5	15.36
150	-	125	137.5	12.20
125	-	100	112.5	11.01
100	-	75	87.5	10.14
75	-	50	62.5	9.47
50	-	30	40	9.32

Temp Range (C)		(C)	Mean Temp (C)	Instant. CTE (10⁻⁶/C)
27.5	-	32.5	30	5.04
47.5	-	52.5	50	7.99
72.5	-	77.5	75	8.10
97.5	-	102.5	100	10.34
122.5	-	127.5	125	9.31
147.5	-	152.5	150	11.29
172.5	-	177.5	175	10.52
197.5	-	202.5	200	15.49
222.5	-	227.5	225	19.68
247.5	-	252.5	250	32.75
272.5	-	277.5	275	51.34
297.5	-	302.5	300	-
302.5	-	297.5	300	-
277.5	-	272.5	275	27.05
252.5	-	247.5	250	34.53
227.5	-	222.5	225	30.96
202.5	-	197.5	200	21.69
177.5	-	172.5	175	20.40
152.5	-	147.5	150	12.10
127.5	-	122.5	125	11.44
102.5	-	97.5	100	10.45
77.5	-	72.5	75	10.01
52.5	-	47.5	50	11.56

Figure A-15. Thermal Expansion Data for Specimen ESF-SDM-MPBX2-48.6-B for First Thermal Cycle

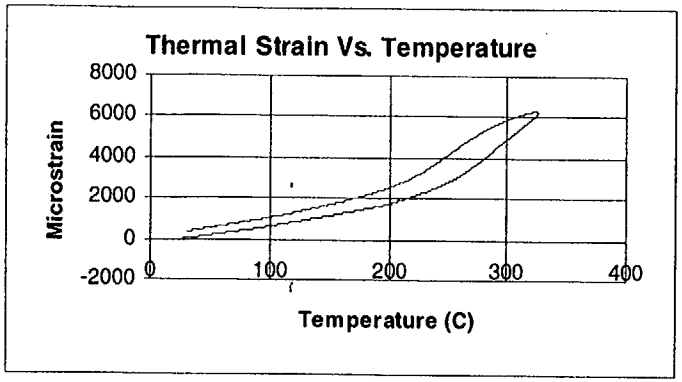

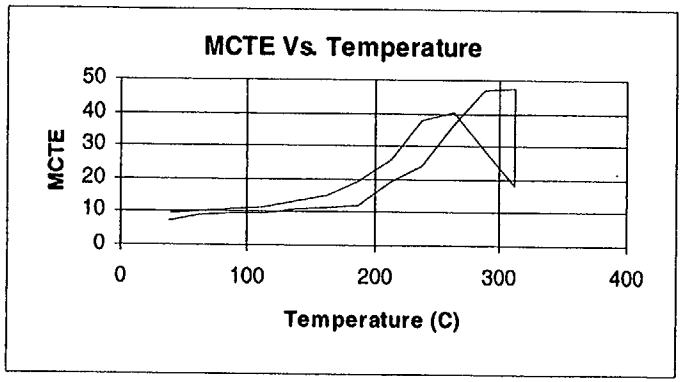

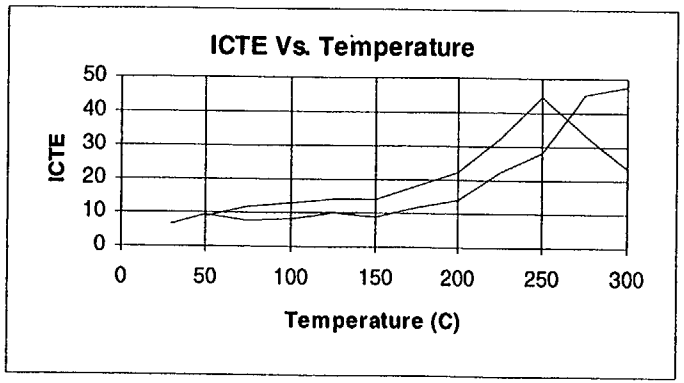

Specimen ID:	ESF-SDM-MPBX2-48.6-B
Date of Test Completion:	4/19/97
Thermal/Mechanical Unit:	TSw2
Lithostratigraphic Unit:	Tptpmn
Original Location:	ESF; Alcove 5;Thermal Drift Scale Test Area
Initial Moisture Content	Air-dried (As-is)
Nominal Dimensions:	50.8 mm (L) 25.4 mm (D)

Specimen Data:	Length (mm)	Mass (g)
Pre-test:	50.8	56.887
Post-test:	50.8	56.774
Change:	0	0.113

Temp Range (C)		(C)	Mean Temp (C)	Mean CTE (10^{-6}/C)
25	-	50	37.5	7.12
50	-	75	62.5	8.78
75	-	100	87.5	9.37
100	-	125	112.5	9.91
125	-	150	137.5	10.55
150	-	175	162.5	11.54
175	-	200	187.5	12.23
200	-	225	212.5	19.05
225	-	250	237.5	23.84
250	-	275	262.5	36.88
275	-	300	287.5	47.25
300	-	325	312.5	47.85
325	-	300	312.5	17.88
300	-	275	287.5	28.81
275	-	250	262.5	40.39
250	-	225	237.5	37.67
225	-	200	212.5	26.16
200	-	175	187.5	19.22
175	-	150	162.5	15.03
150	-	125	137.5	12.96
125	-	100	112.5	11.69
100	-	75	87.5	10.92
75	-	50	62.5	10.16
50	-	30	40	9.74

Temp Range (C)		(C)	Mean Temp (C)	Instant. CTE (10^{-6}/C)
27.5	-	32.5	30	6.34
47.5	-	52.5	50	9.49
72.5	-	77.5	75	7.65
97.5	-	102.5	100	8.06
122.5	-	127.5	125	10.24
147.5	-	152.5	150	8.99
172.5	-	177.5	175	12.00
197.5	-	202.5	200	14.18
222.5	-	227.5	225	22.16
247.5	-	252.5	250	28.01
272.5	-	277.5	275	45.41
297.5	-	302.5	300	47.39
302.5	-	297.5	300	23.43
277.5	-	272.5	275	33.74
252.5	-	247.5	250	44.47
227.5	-	222.5	225	32.11
202.5	-	197.5	200	22.38
177.5	-	172.5	175	18.04
152.5	-	147.5	150	14.07
127.5	-	122.5	125	13.86
102.5	-	97.5	100	12.79
77.5	-	72.5	75	11.93
52.5	-	47.5	50	8.80

Figure A-16. Thermal Expansion Data for Specimen ESF-SDM-MPBX2-48.6-B for Second Thermal Cycle

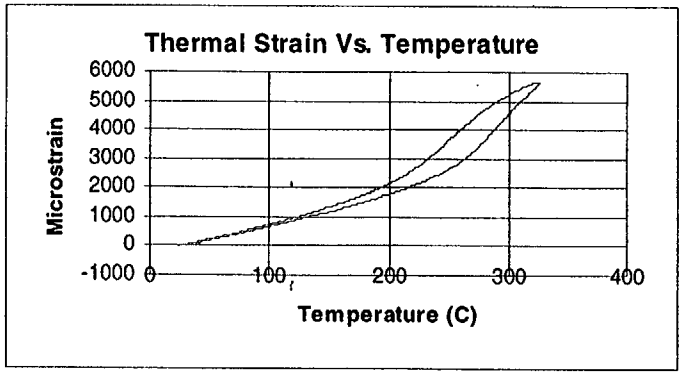

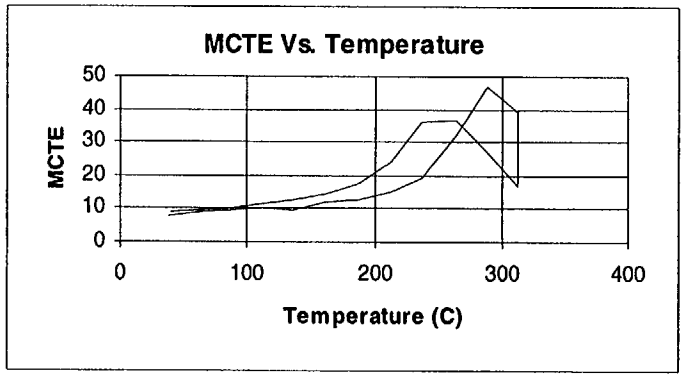

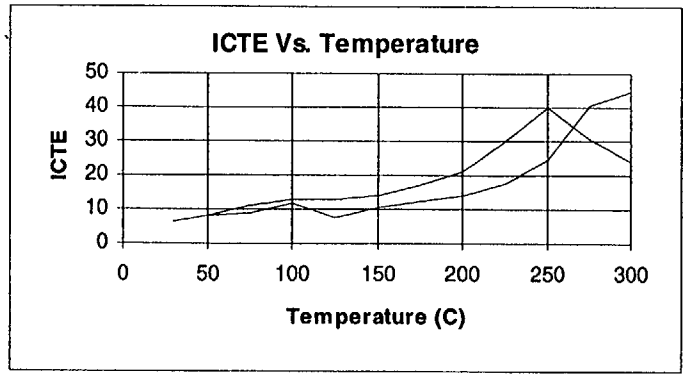

Specimen ID:	ESF-SDM-MPBX2-72.0-B
Date of Test Completion:	4/12/97
Thermal/Mechanical Unit:	TSw2
Lithostratigraphic Unit:	Tptpmn
Original Location:	ESF; Alcove 5;Thermal Drift Scale Test Area
Initial Moisture Content	Air-dried (As-is)
Nominal Dimensions:	50.8 mm (L) 25.4 mm (D)

Specimen Data:	Length (mm)	Mass (g)
Pre-test:	50.8	59.321
Post-test:	50.8	59.037
Change:	0	0.284

Temp Range (C)		(C)	Mean Temp (C)	Mean CTE (10^{-6}/C)
25	-	50	37.5	7.68
50	-	75	62.5	9.18
75	-	100	87.5	9.58
100	-	125	112.5	10.20
125	-	150	137.5	9.75
150	-	175	162.5	11.93
175	-	200	187.5	12.68
200	-	225	212.5	14.85
225	-	250	237.5	19.52
250	-	275	262.5	32.22
275	-	300	287.5	46.93
300	-	325	312.5	39.28
325	-	300	312.5	17.03
300	-	275	287.5	27.17
275	-	250	262.5	36.81
250	-	225	237.5	36.39
225	-	200	212.5	24.12
200	-	175	187.5	17.58
175	-	150	162.5	14.39
150	-	125	137.5	12.68
125	-	100	112.5	11.24
100	-	75	87.5	10.40
75	-	50	62.5	9.75
50	-	30	40	9.25

Temp Range (C)		(C)	Mean Temp (C)	Instant. CTE (10^{-6}/C)
27.5	-	32.5	30	6.38
47.5	-	52.5	50	8.46
72.5	-	77.5	75	9.02
97.5	-	102.5	100	11.74
122.5	-	127.5	125	7.61
147.5	-	152.5	150	10.47
172.5	-	177.5	175	12.23
197.5	-	202.5	200	14.40
222.5	-	227.5	225	17.86
247.5	-	252.5	250	24.69
272.5	-	277.5	275	40.87
297.5	-	302.5	300	44.67
302.5	-	297.5	300	24.31
277.5	-	272.5	275	30.71
252.5	-	247.5	250	39.78
227.5	-	222.5	225	29.96
202.5	-	197.5	200	21.07
177.5	-	172.5	175	17.35
152.5	-	147.5	150	14.32
127.5	-	122.5	125	12.99
102.5	-	97.5	100	12.75
77.5	-	72.5	75	11.27
52.5	-	47.5	50	8.47

Figure A-17. Thermal Expansion Data for Specimen ESF-SDM-MPBX2-72.0-B for First Thermal Cycle

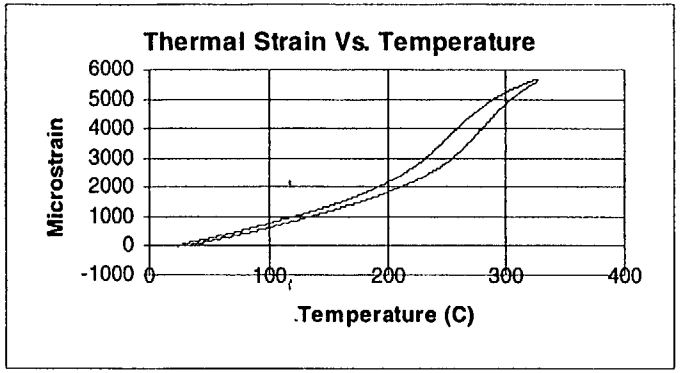

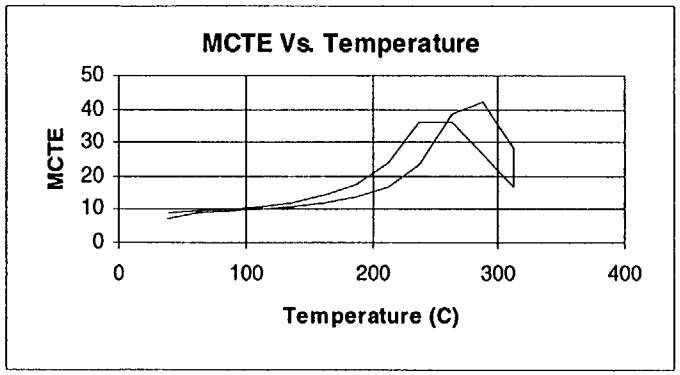

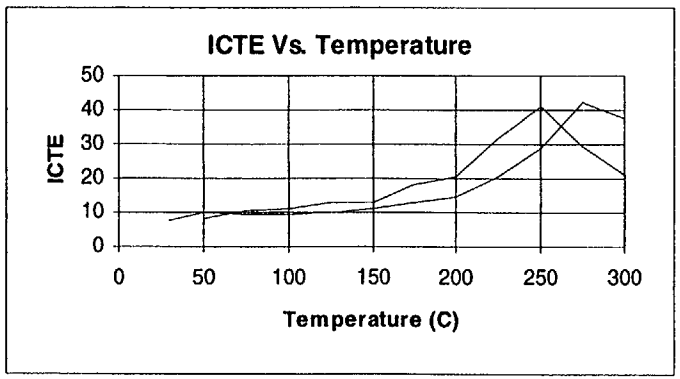

Specimen ID:	ESF-SDM-MPBX2-72.0-B
Date of Test Completion:	5/7/97
Thermal/Mechanical Unit:	TSw2
Lithostratigraphic Unit:	Tptpmn
Original Location:	ESF; Alcove 5;Thermal Drift Scale Test Area
Initial Moisture Content	Air-dried (As-is)
Nominal Dimensions:	50.8 mm (L) 25.4 mm (D)

Specimen Data:	Length (mm)	Mass (g)
Pre-test:	50.80	59.083
Post-test:	50.80	59.020
Change:	0	0.063

Temp Range (C)		(C)	Mean Temp (C)	Mean CTE (10^{-6}/C)
25	-	50	37.5	7.00
50	-	75	62.5	8.76
75	-	100	87.5	9.48
100	-	125	112.5	10.11
125	-	150	137.5	11.09
150	-	175	162.5	12.30
175	-	200	187.5	13.69
200	-	225	212.5	16.74
225	-	250	237.5	23.22
250	-	275	262.5	38.64
275	-	300	287.5	42.24
300	-	325	312.5	28.17
325	-	300	312.5	16.82
300	-	275	287.5	26.36
275	-	250	262.5	36.00
250	-	225	237.5	36.06
225	-	200	212.5	24.13
200	-	175	187.5	17.74
175	-	150	162.5	14.35
150	-	125	137.5	12.15
125	-	100	112.5	10.81
100	-	75	87.5	10.44
75	-	50	62.5	9.72
50	-	30	40	8.86

Temp Range (C)		(C)	Mean Temp (C)	Instant. CTE (10^{-6}/C)
27.5	-	32.5	30	7.54
47.5	-	52.5	50	9.98
72.5	-	77.5	75	9.64
97.5	-	102.5	100	9.36
122.5	-	127.5	125	10.03
147.5	-	152.5	150	11.00
172.5	-	177.5	175	13.24
197.5	-	202.5	200	14.61
222.5	-	227.5	225	20.71
247.5	-	252.5	250	28.99
272.5	-	277.5	275	42.47
297.5	-	302.5	300	37.69
302.5	-	297.5	300	21.33
277.5	-	272.5	275	29.47
252.5	-	247.5	250	41.43
227.5	-	222.5	225	31.89
202.5	-	197.5	200	20.50
177.5	-	172.5	175	18.31
152.5	-	147.5	150	13.00
127.5	-	122.5	125	13.12
102.5	-	97.5	100	11.27
77.5	-	72.5	75	10.56
52.5	-	47.5	50	8.35

Figure A-18. Thermal Expansion Data for Specimen ESF-SDM-MPBX2-72.0-B for Second Thermal Cycle

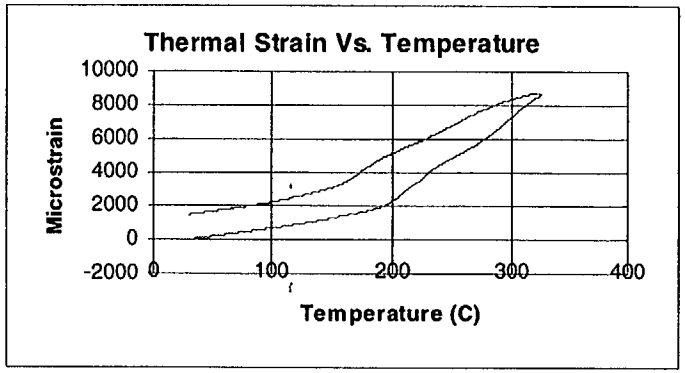

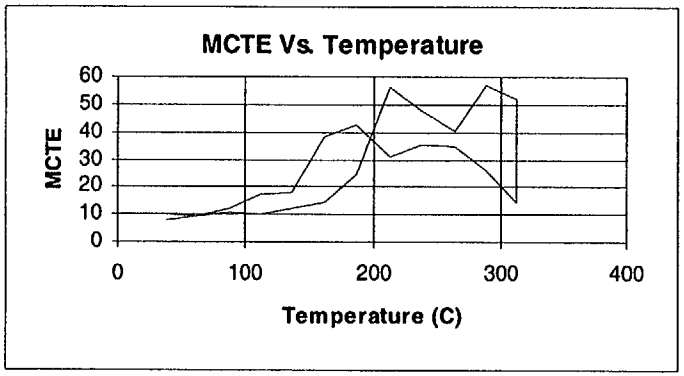

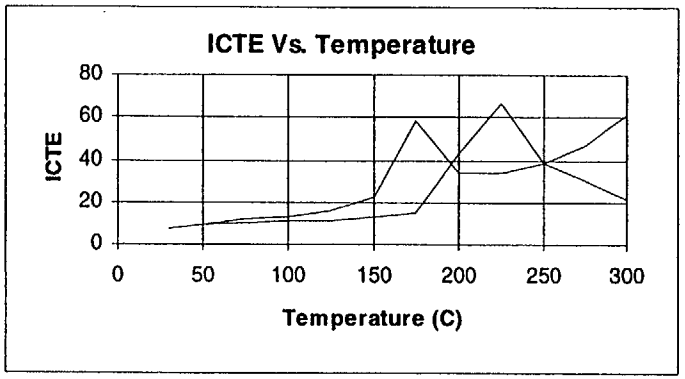

Specimen ID:	ESF-SDM-MPBX2-85.0-B
Date of Test Completion:	4/15/97
Thermal/Mechanical Unit:	TSw2
Lithostratigraphic Unit:	Tptpmn
Original Location:	ESF; Alcove 5;Thermal Drift Scale Test Area
Initial Moisture Content	Air-dried (As-is)
Nominal Dimensions:	50.8 mm (L) 25.4 mm (D)

Specimen Data:	Length (mm)	Mass (g)
Pre-test:	50.77	58.538
Post-test:	50.85	58.156
Change:	-0.08	0.382

Temp Range (C)		(C)	Mean Temp (C)	Mean CTE (10^{-6}/C)
25	-	50	37.5	8.11
50	-	75	62.5	9.57
75	-	100	87.5	10.57
100	-	125	112.5	10.12
125	-	150	137.5	12.30
150	-	175	162.5	14.17
175	-	200	187.5	24.58
200	-	225	212.5	56.34
225	-	250	237.5	47.64
250	-	275	262.5	40.73
275	-	300	287.5	56.99
300	-	325	312.5	52.31
325	-	300	312.5	14.12
300	-	275	287.5	26.39
275	-	250	262.5	34.80
250	-	225	237.5	35.52
225	-	200	212.5	30.76
200	-	175	187.5	42.84
175	-	150	162.5	38.38
150	-	125	137.5	17.78
125	-	100	112.5	17.59
100	-	75	87.5	11.93
75	-	50	62.5	9.17
50	-	30	40	10.34

Temp Range (C)		(C)	Mean Temp (C)	Instant. CTE (10^{-6}/C)
27.5	-	32.5	30	7.77
47.5	-	52.5	50	9.05
72.5	-	77.5	75	10.43
97.5	-	102.5	100	11.71
122.5	-	127.5	125	11.64
147.5	-	152.5	150	13.36
172.5	-	177.5	175	15.26
197.5	-	202.5	200	42.98
222.5	-	227.5	225	66.40
247.5	-	252.5	250	38.83
272.5	-	277.5	275	46.88
297.5	-	302.5	300	61.56
302.5	-	297.5	300	22.11
277.5	-	272.5	275	29.84
252.5	-	247.5	250	38.53
227.5	-	222.5	225	34.01
202.5	-	197.5	200	33.99
177.5	-	172.5	175	58.29
152.5	-	147.5	150	22.28
127.5	-	122.5	125	16.27
102.5	-	97.5	100	13.55
77.5	-	72.5	75	12.51
52.5	-	47.5	50	9.81

Figure A-19. Thermal Expansion Data for Specimen ESF-SDM-MPBX2-85.0-B for First Thermal Cycle

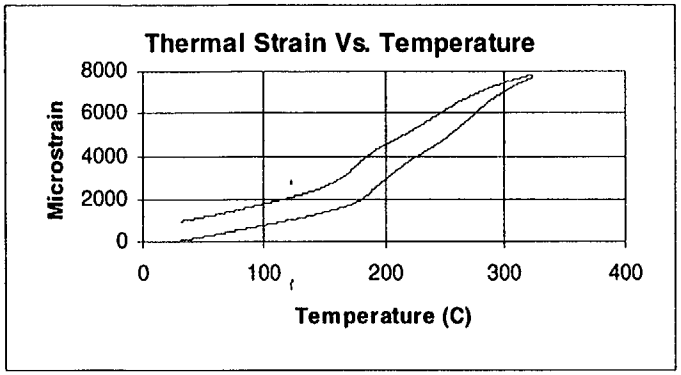

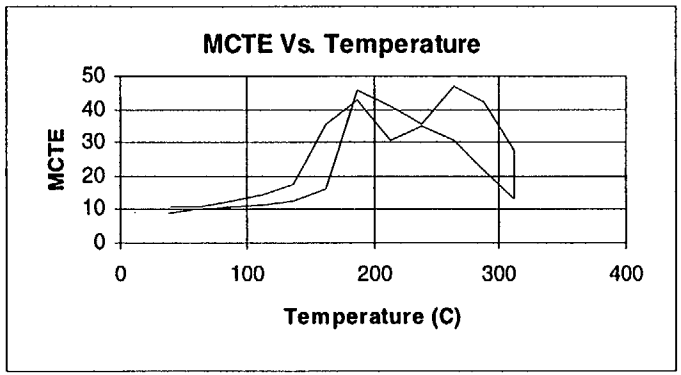

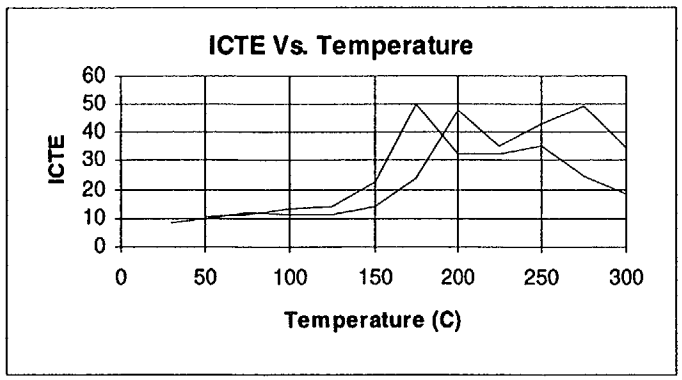

Specimen ID:	ESF-SDM-MPBX2-85.0-B
Date of Test Completion:	5/7/97
Thermal/Mechanical Unit:	TSw2
Lithostratigraphic Unit:	Tptpmn
Original Location:	ESF; Alcove 5;Thermal Drift Scale Test Area
Initial Moisture Content	Air-dried (As-is)
Nominal Dimensions:	50.8 mm (L) 25.4 mm (D)

Specimen Data:	Length (mm)	Mass (g)
Pre-test:	50.85	58.242
Post-test:	50.85	58.155
Change:	0	0.087

Temp Range (C)		(C)	Mean Temp (C)	Mean CTE (10^{-6}/C)
25	-	50	37.5	9.21
50	-	75	62.5	10.53
75	-	100	87.5	10.78
100	-	125	112.5	11.36
125	-	150	137.5	12.89
150	-	175	162.5	16.00
175	-	200	187.5	45.87
200	-	225	212.5	41.14
225	-	250	237.5	35.77
250	-	275	262.5	46.78
275	-	300	287.5	42.41
300	-	325	312.5	27.52
325	-	300	312.5	13.21
300	-	275	287.5	21.45
275	-	250	262.5	30.44
250	-	225	237.5	35.20
225	-	200	212.5	30.86
200	-	175	187.5	42.65
175	-	150	162.5	35.27
150	-	125	137.5	17.52
125	-	100	112.5	14.27
100	-	75	87.5	12.53
75	-	50	62.5	11.13
50	-	30	40	10.83

Temp Range (C)		(C)	Mean Temp (C)	Instant. CTE (10^{-6}/C)
27.5	-	32.5	30	8.14
47.5	-	52.5	50	9.81
72.5	-	77.5	75	11.84
97.5	-	102.5	100	11.39
122.5	-	127.5	125	11.17
147.5	-	152.5	150	14.07
172.5	-	177.5	175	24.35
197.5	-	202.5	200	48.27
222.5	-	227.5	225	35.17
247.5	-	252.5	250	43.00
272.5	-	277.5	275	49.25
297.5	-	302.5	300	34.28
302.5	-	297.5	300	18.20
277.5	-	272.5	275	24.46
252.5	-	247.5	250	35.16
227.5	-	222.5	225	32.37
202.5	-	197.5	200	32.45
177.5	-	172.5	175	50.13
152.5	-	147.5	150	22.75
127.5	-	122.5	125	14.41
102.5	-	97.5	100	13.56
77.5	-	72.5	75	11.21
52.5	-	47.5	50	10.72

Figure A-20. Thermal Expansion Data for Specimen ESF-SDM-MPBX2-85.0-B for Second Thermal Cycle

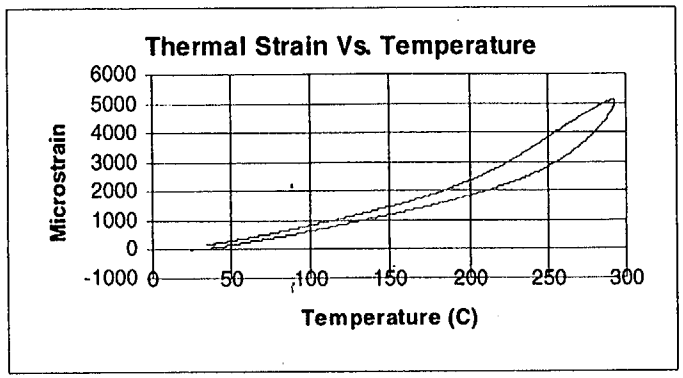

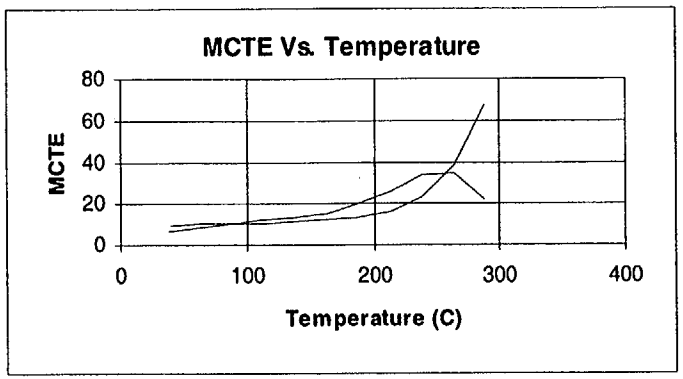

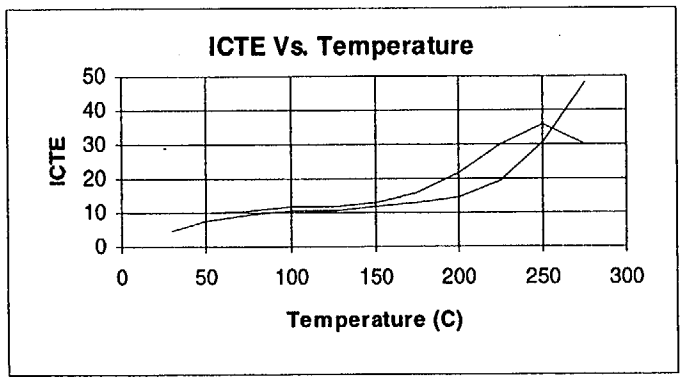

Specimen ID:	ESF-SDM-MPBX-3-17.5B
Date of Test Completion:	3/19/97
Thermal/Mechanical Unit:	TSw2
Lithostratigraphic Unit:	Tptpmn
Original Location:	ESF; Alcove 5;Thermal Drift Scale Test Area
Initial Moisture Content	Air-dried (As-is)
Nominal Dimensions:	50.8 mm (L) 25.4 mm (D)

Specimen Data:	Length (mm)	Mass (g)
Pre-test:	50.83	58.723
Post-test:	50.8	58.203
Change:	0.03	0.52

Temp Range (C)		(C)	Mean Temp (C)	Mean CTE (10⁻⁶/C)
25	-	50	37.5	6.70
50	-	75	62.5	9.11
75	-	100	87.5	10.16
100	-	125	112.5	10.60
125	-	150	137.5	11.27
150	-	175	162.5	12.10
175	-	200	187.5	13.78
200	-	225	212.5	16.20
225	-	250	237.5	22.95
250	-	275	262.5	38.27
275	-	300	287.5	67.89
300	-	325	312.5	-
325	-	300	312.5	-
300	-	275	287.5	21.82
275	-	250	262.5	34.34
250	-	225	237.5	34.20
225	-	200	212.5	25.87
200	-	175	187.5	19.99
175	-	150	162.5	15.13
150	-	125	137.5	13.38
125	-	100	112.5	12.11
100	-	75	87.5	11.07
75	-	50	62.5	10.27
50	-	30	40	9.41

Temp Range (C)		(C)	Mean Temp (C)	Instant. CTE (10⁻⁶/C)
27.5	-	32.5	30	4.93
47.5	-	52.5	50	7.83
72.5	-	77.5	75	9.64
97.5	-	102.5	100	10.84
122.5	-	127.5	125	10.75
147.5	-	152.5	150	11.58
172.5	-	177.5	175	12.72
197.5	-	202.5	200	14.83
222.5	-	227.5	225	19.39
247.5	-	252.5	250	30.57
272.5	-	277.5	275	48.48
297.5	-	302.5	300	-
302.5	-	297.5	300	-
277.5	-	272.5	275	30.06
252.5	-	247.5	250	36.09
227.5	-	222.5	225	30.19
202.5	-	197.5	200	22.01
177.5	-	172.5	175	16.10
152.5	-	147.5	150	12.94
127.5	-	122.5	125	11.79
102.5	-	97.5	100	11.67
77.5	-	72.5	75	10.80
52.5	-	47.5	50	9.85

Figure A-21. Thermal Expansion Data for Specimen ESF-SDM-MPBX3-17.5-B for First Thermal Cycle

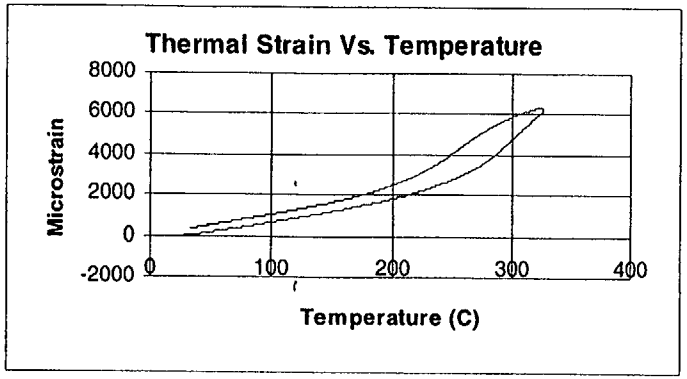

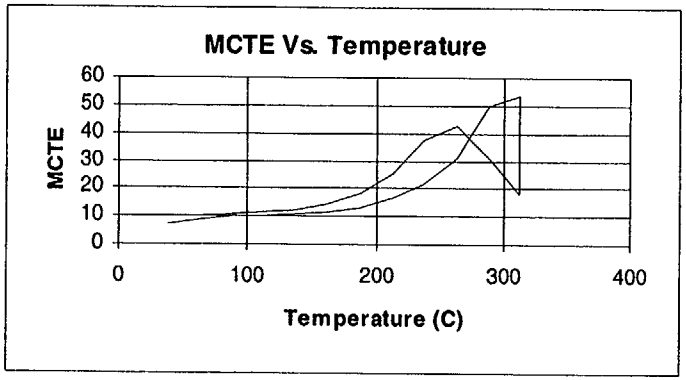

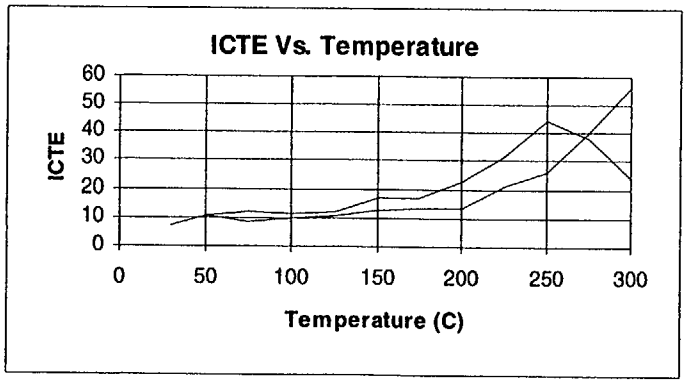

Specimen ID:	ESF-SDM-MPBX3-17.5-B
Date of Test Completion:	5/6/97
Thermal/Mechanical Unit:	TSw2
Lithostratigraphic Unit:	Tptpmn
Original Location:	ESF; Alcove 5;Thermal Drift Scale Test Area
Initial Moisture Content	Air-dried (As-is)
Nominal Dimensions:	50.8 mm (L) 25.4 mm (D)

Specimen Data:	Length (mm)	Mass (g)
Pre-test:	50.80	58.399
Post-test:	50.80	58.211
Change:	0	0.188

Temp Range (C)		(C)	Mean Temp (C)	Mean CTE (10^{-6}/C)
25	-	50	37.5	6.93
50	-	75	62.5	8.63
75	-	100	87.5	9.89
100	-	125	112.5	10.26
125	-	150	137.5	10.73
150	-	175	162.5	11.90
175	-	200	187.5	13.06
200	-	225	212.5	16.54
225	-	250	237.5	21.42
250	-	275	262.5	31.27
275	-	300	287.5	50.12
300	-	325	312.5	53.72
325	-	300	312.5	17.93
300	-	275	287.5	30.83
275	-	250	262.5	42.98
250	-	225	237.5	37.87
225	-	200	212.5	25.63
200	-	175	187.5	18.03
175	-	150	162.5	14.51
150	-	125	137.5	12.43
125	-	100	112.5	11.26
100	-	75	87.5	10.65
75	-	50	62.5	10.20
50	-	30	40	10.20

Temp Range (C)		(C)	Mean Temp (C)	Instant. CTE (10^{-6}/C)
27.5	-	32.5	30	7.03
47.5	-	52.5	50	10.60
72.5	-	77.5	75	8.47
97.5	-	102.5	100	9.99
122.5	-	127.5	125	10.42
147.5	-	152.5	150	12.58
172.5	-	177.5	175	13.27
197.5	-	202.5	200	13.17
222.5	-	227.5	225	21.11
247.5	-	252.5	250	25.92
272.5	-	277.5	275	40.12
297.5	-	302.5	300	56.36
302.5	-	297.5	300	24.31
277.5	-	272.5	275	37.93
252.5	-	247.5	250	44.58
227.5	-	222.5	225	31.97
202.5	-	197.5	200	22.69
177.5	-	172.5	175	17.11
152.5	-	147.5	150	16.91
127.5	-	122.5	125	11.96
102.5	-	97.5	100	11.17
77.5	-	72.5	75	12.32
52.5	-	47.5	50	10.27

Figure A-22. Thermal Expansion Data for Specimen ESF-SDM-MPBX3-17.5-B for Second Thermal Cycle

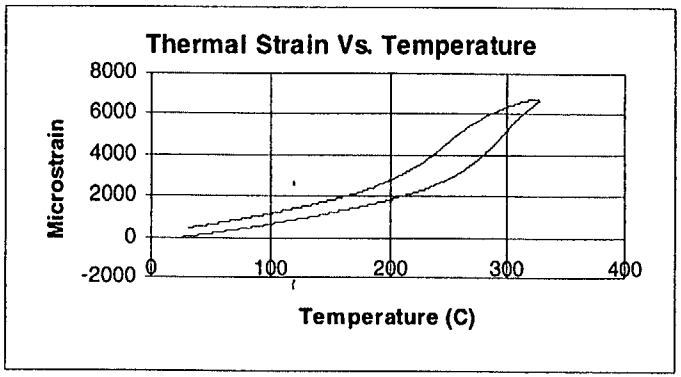

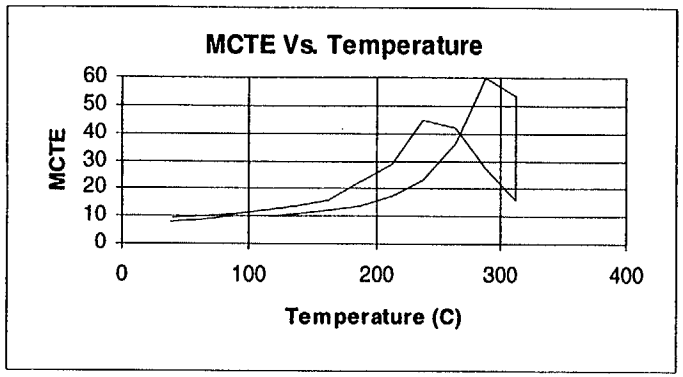

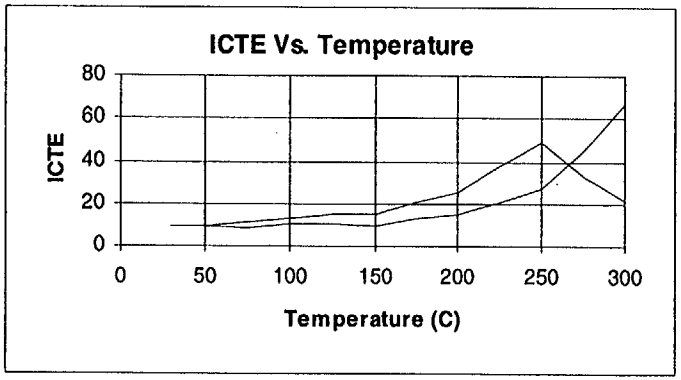

Specimen ID:	ESF-SDM-MPBX3-38.5-B
Date of Test Completion:	4/3/97
Thermal/Mechanical Unit:	TSw2
Lithostratigraphic Unit:	Tptpmn
Original Location:	ESF; Alcove 5;Thermal Drift Scale Test Area
Initial Moisture Content	Air-dried (As-is)
Nominal Dimensions:	50.8 mm (L) 25.4 mm (D)

Specimen Data:	Length (mm)	Mass (g)
Pre-test:	50.8	58.329
Post-test:	50.8	58.049
Change:	0	0.28

Temp Range (C)		(C)	Mean Temp (C)	Mean CTE (10^{-6}/C)
25	-	50	37.5	7.60
50	-	75	62.5	8.94
75	-	100	87.5	9.77
100	-	125	112.5	10.20
125	-	150	137.5	11.00
150	-	175	162.5	12.16
175	-	200	187.5	13.66
200	-	225	212.5	17.33
225	-	250	237.5	23.14
250	-	275	262.5	36.40
275	-	300	287.5	59.65
300	-	325	312.5	53.30
325	-	300	312.5	16.08
300	-	275	287.5	27.42
275	-	250	262.5	42.00
250	-	225	237.5	44.91
225	-	200	212.5	28.98
200	-	175	187.5	22.20
175	-	150	162.5	16.25
150	-	125	137.5	13.57
125	-	100	112.5	12.07
100	-	75	87.5	11.13
75	-	50	62.5	10.23
50	-	30	40	9.58

Temp Range (C)		(C)	Mean Temp (C)	Instant. CTE (10^{-6}/C)
27.5	-	32.5	30	9.03
47.5	-	52.5	50	9.54
72.5	-	77.5	75	8.71
97.5	-	102.5	100	10.66
122.5	-	127.5	125	10.48
147.5	-	152.5	150	9.53
172.5	-	177.5	175	12.86
197.5	-	202.5	200	14.70
222.5	-	227.5	225	20.44
247.5	-	252.5	250	26.86
272.5	-	277.5	275	44.81
297.5	-	302.5	300	66.45
302.5	-	297.5	300	21.71
277.5	-	272.5	275	32.56
252.5	-	247.5	250	49.11
227.5	-	222.5	225	37.95
202.5	-	197.5	200	25.86
177.5	-	172.5	175	20.45
152.5	-	147.5	150	14.63
127.5	-	122.5	125	15.05
102.5	-	97.5	100	12.72
77.5	-	72.5	75	11.49
52.5	-	47.5	50	9.19

Figure A-23. Thermal Expansion Data for Specimen ESF-SDM-MPBX3-38.5-B for First Thermal Cycle

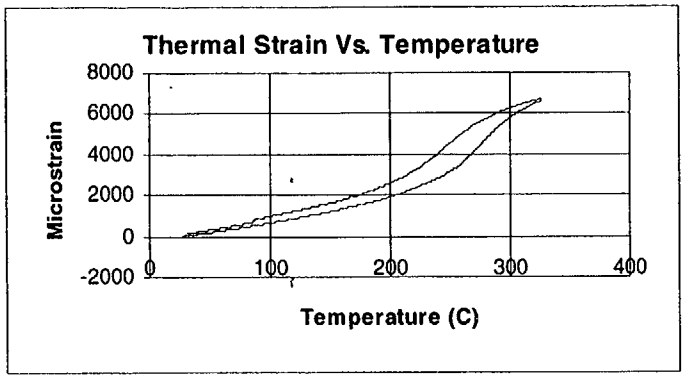

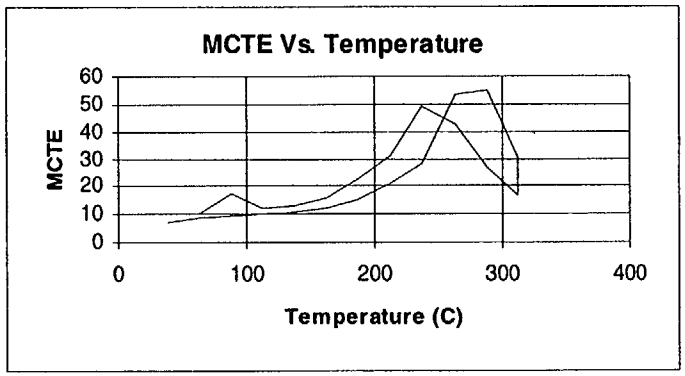

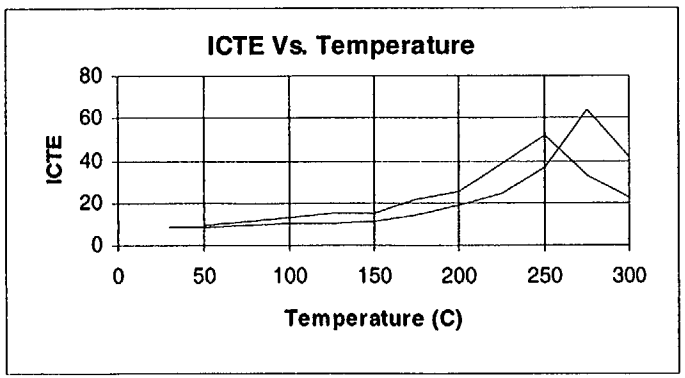

Specimen ID:	ESF-SDM-MPBX3-38.5-B
Date of Test Completion:	4/26/97
Thermal/Mechanical Unit:	TSw2
Lithostratigraphic Unit:	Tptpmn
Original Location:	ESF; Alcove 5;Thermal Drift Scale Test Area
Initial Moisture Content	Air-dried (As-is)
Nominal Dimensions:	50.8 mm (L) 25.4 mm (D)

Specimen Data:	Length (mm)	Mass (g)
Pre-test:	50.80	58.116
Post-test:	50.80	58.038
Change:	0	0.078

Temp Range (C)	Mean Temp (C)	Mean CTE (10^{-6}/C)
25 - 50	37.5	7.47
50 - 75	62.5	8.67
75 - 100	87.5	9.58
100 - 125	112.5	10.19
125 - 150	137.5	11.19
150 - 175	162.5	12.59
175 - 200	187.5	15.21
200 - 225	212.5	21.02
225 - 250	237.5	28.15
250 - 275	262.5	53.43
275 - 300	287.5	54.98
300 - 325	312.5	30.09
325 - 300	312.5	16.49
300 - 275	287.5	26.55
275 - 250	262.5	42.70
250 - 225	237.5	49.10
225 - 200	212.5	30.83
200 - 175	187.5	22.20
175 - 150	162.5	15.93
150 - 125	137.5	13.13
125 - 100	112.5	12.07
100 - 75	87.5	17.67
75 - 50	62.5	10.36
50 - 30	40	9.93

Temp Range (C)	Mean Temp (C)	Instant. CTE (10^{-6}/C)
27.5 - 32.5	30	8.19
47.5 - 52.5	50	8.72
72.5 - 77.5	75	9.37
97.5 - 102.5	100	10.15
122.5 - 127.5	125	10.60
147.5 - 152.5	150	11.46
172.5 - 177.5	175	14.43
197.5 - 202.5	200	19.25
222.5 - 227.5	225	24.12
247.5 - 252.5	250	36.77
272.5 - 277.5	275	64.32
297.5 - 302.5	300	41.48
302.5 - 297.5	300	22.33
277.5 - 272.5	275	33.14
252.5 - 247.5	250	51.85
227.5 - 222.5	225	38.54
202.5 - 197.5	200	25.25
177.5 - 172.5	175	21.79
152.5 - 147.5	150	14.81
127.5 - 122.5	125	14.67
102.5 - 97.5	100	13.50
77.5 - 72.5	75	11.41
52.5 - 47.5	50	9.19

Figure A-24. Thermal Expansion Data for Specimen ESF-SDM-MPBX3-38.5-B for Second Thermal Cycle

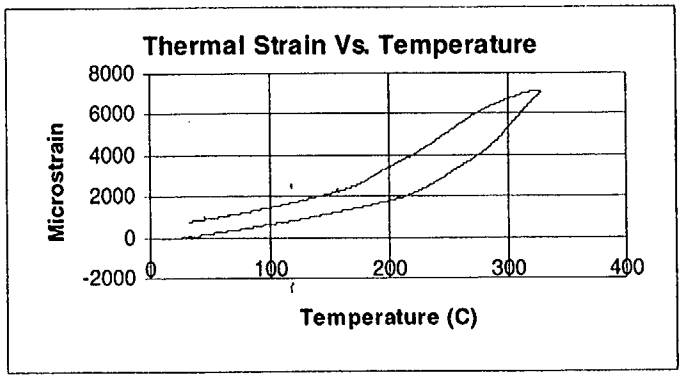

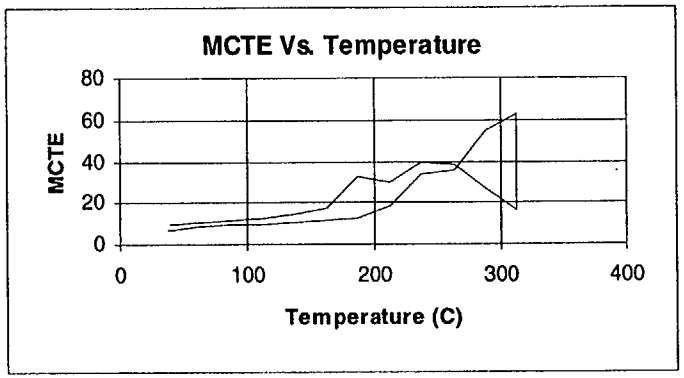

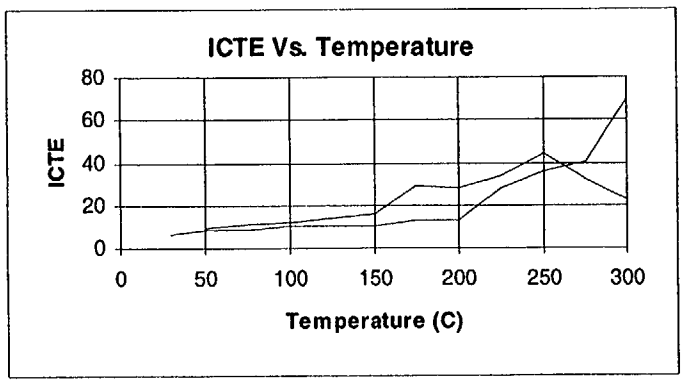

Specimen ID:	ESF-SDM-MPBX3-85.6-B
Date of Test Completion:	4/2/97
Thermal/Mechanical Unit:	TSw2
Lithostratigraphic Unit:	Tptpmn
Original Location:	ESF; Alcove 5;Thermal Drift Scale Test Area
Initial Moisture Content	Air-dried (As-is)
Nominal Dimensions:	50.8 mm (L) 25.4 mm (D)

Specimen Data:	Length (mm)	Mass (g)
Pre-test:	50.8	57.406
Post-test:	50.83	57.018
Change:	-0.03	0.388

Temp Range (C)		(C)	Mean Temp (C)	Mean CTE (10^{-6}/C)
25	-	50	37.5	7.22
50	-	75	62.5	8.88
75	-	100	87.5	9.50
100	-	125	112.5	9.92
125	-	150	137.5	10.55
150	-	175	162.5	11.57
175	-	200	187.5	12.96
200	-	225	212.5	18.73
225	-	250	237.5	33.91
250	-	275	262.5	35.34
275	-	300	287.5	54.92
300	-	325	312.5	62.93
325	-	300	312.5	16.05
300	-	275	287.5	26.73
275	-	250	262.5	38.50
250	-	225	237.5	39.07
225	-	200	212.5	29.40
200	-	175	187.5	32.74
175	-	150	162.5	17.81
150	-	125	137.5	14.05
125	-	100	112.5	12.32
100	-	75	87.5	11.35
75	-	50	62.5	10.29
50	-	30	40	10.09

Temp Range (C)		(C)	Mean Temp (C)	Instant. CTE (10^{-6}/C)
27.5	-	32.5	30	6.91
47.5	-	52.5	50	8.27
72.5	-	77.5	75	8.73
97.5	-	102.5	100	10.26
122.5	-	127.5	125	10.09
147.5	-	152.5	150	10.18
172.5	-	177.5	175	12.91
197.5	-	202.5	200	13.05
222.5	-	227.5	225	27.80
247.5	-	252.5	250	35.91
272.5	-	277.5	275	40.66
297.5	-	302.5	300	69.94
302.5	-	297.5	300	23.02
277.5	-	272.5	275	32.20
252.5	-	247.5	250	43.79
227.5	-	222.5	225	34.17
202.5	-	197.5	200	28.15
177.5	-	172.5	175	29.01
152.5	-	147.5	150	15.92
127.5	-	122.5	125	14.57
102.5	-	97.5	100	12.27
77.5	-	72.5	75	11.68
52.5	-	47.5	50	9.21

Figure A-25. Thermal Expansion Data for Specimen ESF-SDM-MPBX3-85.6-B for First Thermal Cycle

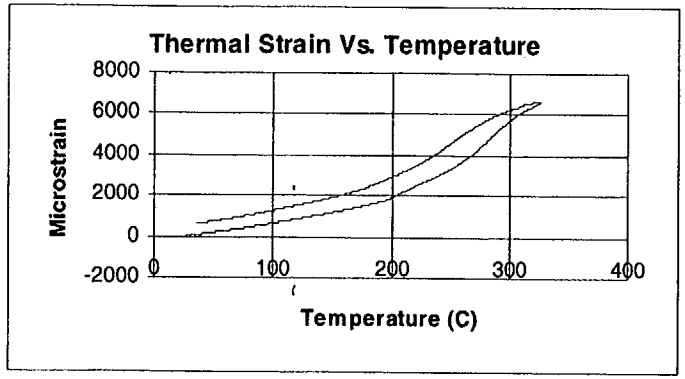

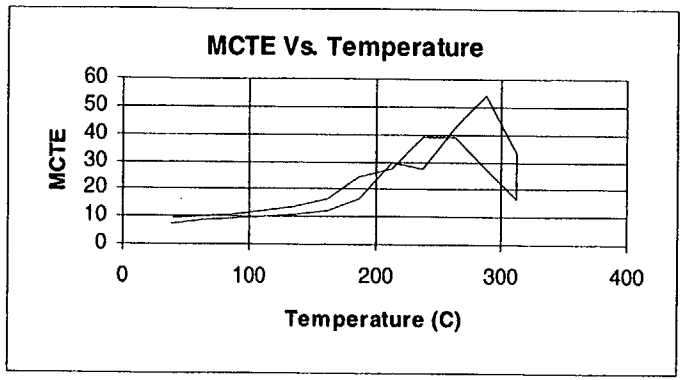

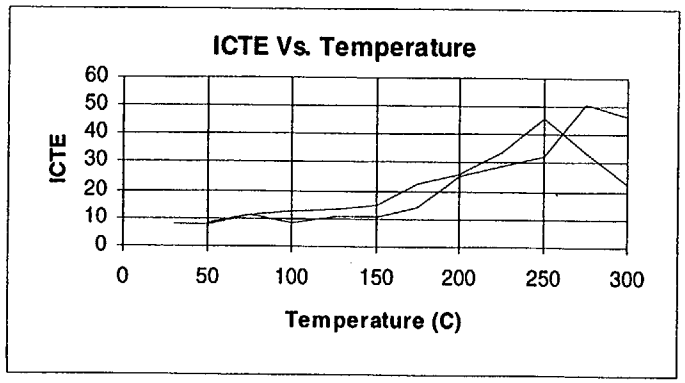

Specimen ID:	ESF-SDM-MPBX3-85.6-B
Date of Test Completion:	4/23/97
Thermal/Mechanical Unit:	TSw2
Lithostratigraphic Unit:	Tptpmn
Original Location:	ESF; Alcove 5;Thermal Drift Scale Test Area
Initial Moisture Content	Air-dried (As-is)
Nominal Dimensions:	50.8 mm (L) 25.4 mm (D)

Specimen Data:	Length (mm)	Mass (g)
Pre-test:	50.83	57.126
Post-test:	50.83	57.049
Change:	0	0.077

Temp Range (C)		(C)	Mean Temp (C)	Mean CTE (10^{-6}/C)
25	-	50	37.5	7.37
50	-	75	62.5	8.37
75	-	100	87.5	9.36
100	-	125	112.5	10.11
125	-	150	137.5	10.88
150	-	175	162.5	12.47
175	-	200	187.5	16.30
200	-	225	212.5	29.43
225	-	250	237.5	27.75
250	-	275	262.5	42.54
275	-	300	287.5	54.57
300	-	325	312.5	33.00
325	-	300	312.5	16.96
300	-	275	287.5	27.38
275	-	250	262.5	39.36
250	-	225	237.5	39.21
225	-	200	212.5	27.30
200	-	175	187.5	24.61
175	-	150	162.5	16.34
150	-	125	137.5	13.48
125	-	100	112.5	11.98
100	-	75	87.5	10.71
75	-	50	62.5	10.04
50	-	30	40	9.69

Temp Range (C)		(C)	Mean Temp (C)	Instant. CTE (10^{-6}/C)
27.5	-	32.5	30	7.62
47.5	-	52.5	50	7.74
72.5	-	77.5	75	11.09
97.5	-	102.5	100	8.54
122.5	-	127.5	125	10.91
147.5	-	152.5	150	10.91
172.5	-	177.5	175	14.28
197.5	-	202.5	200	25.26
222.5	-	227.5	225	28.89
247.5	-	252.5	250	32.46
272.5	-	277.5	275	51.08
297.5	-	302.5	300	46.40
302.5	-	297.5	300	22.56
277.5	-	272.5	275	33.95
252.5	-	247.5	250	45.58
227.5	-	222.5	225	34.14
202.5	-	197.5	200	26.22
177.5	-	172.5	175	22.44
152.5	-	147.5	150	14.88
127.5	-	122.5	125	13.70
102.5	-	97.5	100	12.41
77.5	-	72.5	75	11.64
52.5	-	47.5	50	8.55

Figure A-26. Thermal Expansion Data for Specimen ESF-SDM-MPBX3-85.6-B for Second Thermal Cycle

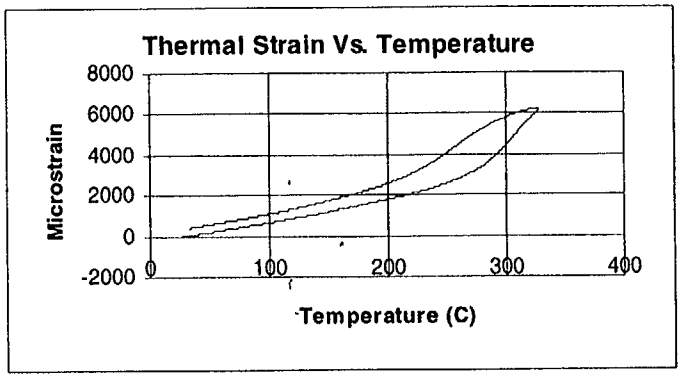

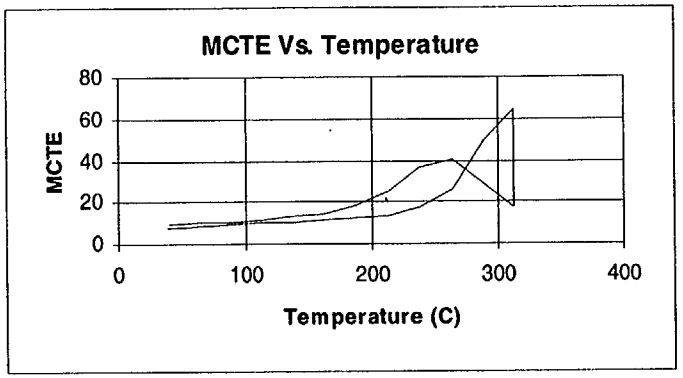

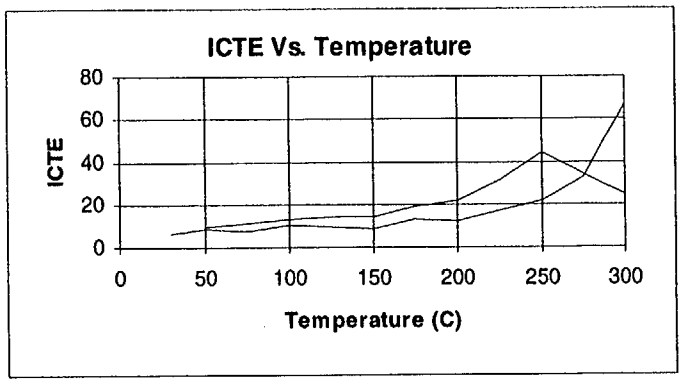

Specimen ID:	ESF-AOD-HDFR1-9.0-B
Date of Test Completion:	4/1/97
Thermal/Mechanical Unit:	TSw2
Lithostratigraphic Unit:	Tptpmn
Original Location:	ESF; Alcove 5;Thermal Drift Scale Test Area
Initial Moisture Content	Air-dried (As-is)
Nominal Dimensions:	50.8 mm (L) 25.4 mm (D)

Specimen Data:	Length (mm)	Mass (g)
Pre-test:	50.8	58.27
Post-test:	50.8	57.84
Change:	0	0.43

Temp Range (C)		(C)	Mean Temp (C)	Mean CTE (10^{-6}/C)
25	-	50	37.5	7.31
50	-	75	62.5	9.08
75	-	100	87.5	9.61
100	-	125	112.5	10.27
125	-	150	137.5	10.90
150	-	175	162.5	11.74
175	-	200	187.5	12.35
200	-	225	212.5	13.84
225	-	250	237.5	17.62
250	-	275	262.5	26.32
275	-	300	287.5	49.15
300	-	325	312.5	64.15
325	-	300	312.5	17.76
300	-	275	287.5	29.17
275	-	250	262.5	40.52
250	-	225	237.5	36.38
225	-	200	212.5	24.81
200	-	175	187.5	18.51
175	-	150	162.5	14.87
150	-	125	137.5	13.06
125	-	100	112.5	11.77
100	-	75	87.5	10.94
75	-	50	62.5	10.14
50	-	30	40	9.85

Temp Range (C)		(C)	Mean Temp (C)	Instant. CTE (10^{-6}/C)
27.5	-	32.5	30	6.83
47.5	-	52.5	50	8.37
72.5	-	77.5	75	7.82
97.5	-	102.5	100	10.45
122.5	-	127.5	125	9.87
147.5	-	152.5	150	8.42
172.5	-	177.5	175	13.40
197.5	-	202.5	200	11.94
222.5	-	227.5	225	16.93
247.5	-	252.5	250	22.02
272.5	-	277.5	275	33.00
297.5	-	302.5	300	66.96
302.5	-	297.5	300	24.23
277.5	-	272.5	275	34.25
252.5	-	247.5	250	43.98
227.5	-	222.5	225	31.44
202.5	-	197.5	200	22.05
177.5	-	172.5	175	18.73
152.5	-	147.5	150	14.11
127.5	-	122.5	125	14.10
102.5	-	97.5	100	13.41
77.5	-	72.5	75	11.71
52.5	-	47.5	50	9.15

Figure A-27. Thermal Expansion Data for Specimen ESF-AOD-HDFR1-9.0-B for First Thermal Cycle

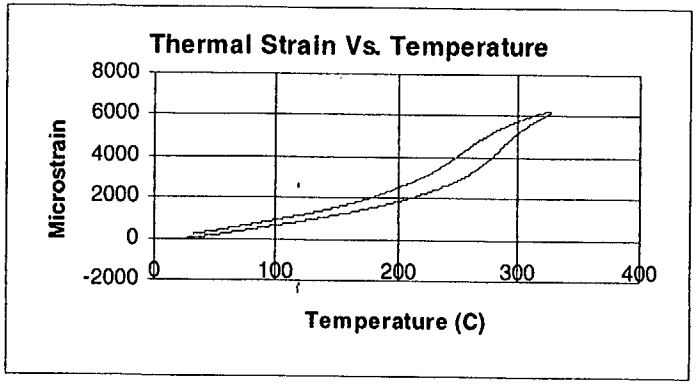

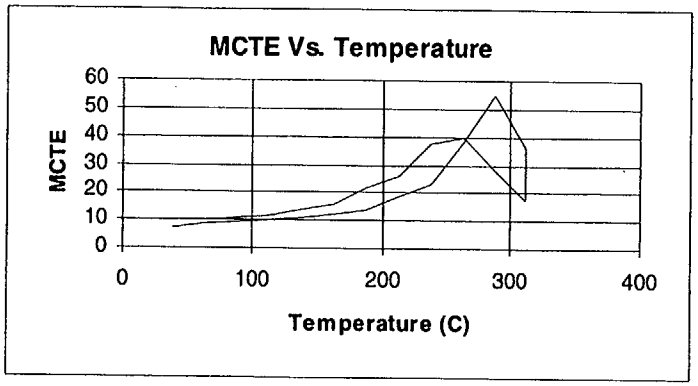

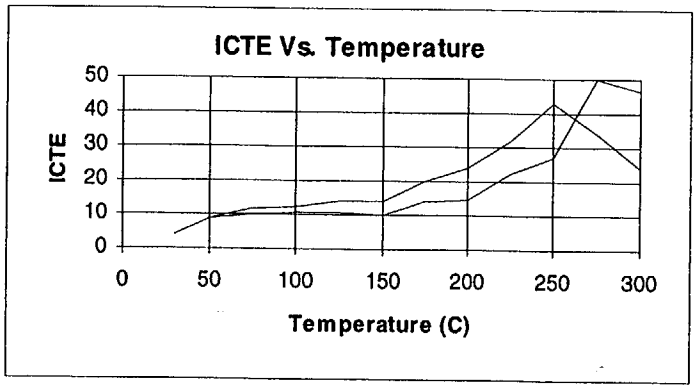

Specimen ID:	ESF-AOD-HDFR1-9.0-B
Date of Test Completion:	4/23/97
Thermal/Mechanical Unit:	TSw2
Lithostratigraphic Unit:	Tptpmn
Original Location:	ESF; Alcove 5;Thermal Drift Scale Test Area
Initial Moisture Content	Air-dried (As-is)
Nominal Dimensions:	50.8 mm (L) 25.4 mm (D)

Specimen Data:	Length (mm)	Mass (g)
Pre-test:	50.80	57.938
Post-test:	50.80	57.847
Change:	0	0.091

Temp Range (C)		(C)	Mean Temp (C)	Mean CTE (10^{-6}/C)
25	-	50	37.5	6.90
50	-	75	62.5	8.70
75	-	100	87.5	9.49
100	-	125	112.5	9.96
125	-	150	137.5	10.95
150	-	175	162.5	12.30
175	-	200	187.5	13.87
200	-	225	212.5	18.75
225	-	250	237.5	23.30
250	-	275	262.5	38.25
275	-	300	287.5	55.08
300	-	325	312.5	35.99
325	-	300	312.5	17.46
300	-	275	287.5	28.08
275	-	250	262.5	39.60
250	-	225	237.5	37.86
225	-	200	212.5	25.67
200	-	175	187.5	22.04
175	-	150	162.5	15.81
150	-	125	137.5	13.54
125	-	100	112.5	11.79
100	-	75	87.5	10.93
75	-	50	62.5	10.19
50	-	30	40	10.11

Temp Range (C)		(C)	Mean Temp (C)	Instant. CTE (10^{-6}/C)
27.5	-	32.5	30	4.20
47.5	-	52.5	50	9.05
72.5	-	77.5	75	10.11
97.5	-	102.5	100	10.86
122.5	-	127.5	125	10.87
147.5	-	152.5	150	10.15
172.5	-	177.5	175	14.39
197.5	-	202.5	200	14.80
222.5	-	227.5	225	22.63
247.5	-	252.5	250	26.78
272.5	-	277.5	275	49.73
297.5	-	302.5	300	46.39
302.5	-	297.5	300	24.04
277.5	-	272.5	275	33.93
252.5	-	247.5	250	43.10
227.5	-	222.5	225	31.90
202.5	-	197.5	200	24.40
177.5	-	172.5	175	20.17
152.5	-	147.5	150	14.07
127.5	-	122.5	125	14.14
102.5	-	97.5	100	12.19
77.5	-	72.5	75	12.06
52.5	-	47.5	50	9.00

Figure A-28. Thermal Expansion Data for Specimen ESF-AOD-HDFR1-9.0-B for Second Thermal Cycle

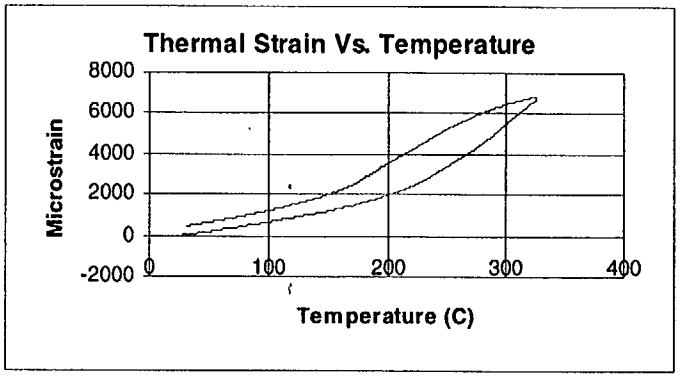

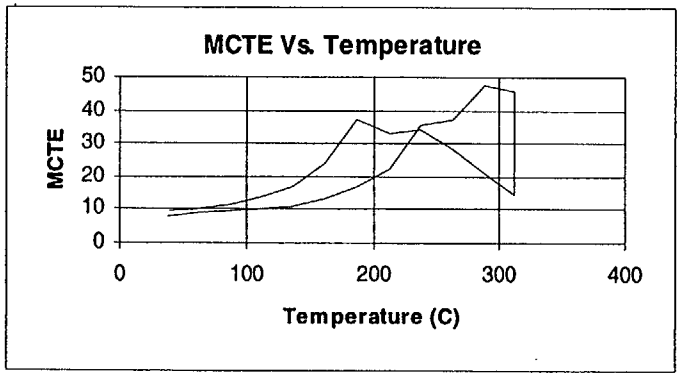

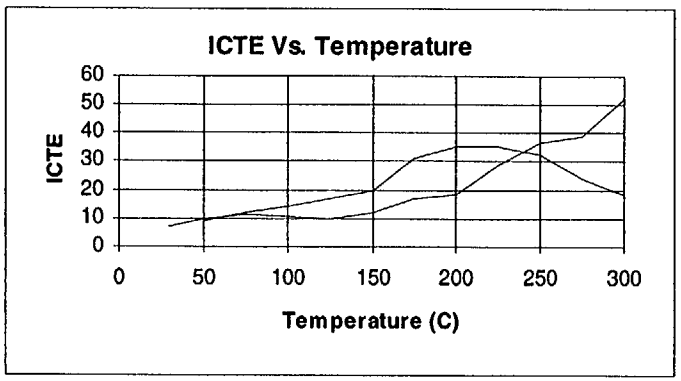

Specimen ID:	ESF-AOD-HDFR1-48.5
Date of Test Completion:	4/7/97
Thermal/Mechanical Unit:	TSw2
Lithostratigraphic Unit:	Tptpmn
Original Location:	ESF; Alcove 5;Thermal Drift Scale Test Area
Initial Moisture Content	Air-dried (As-is)
Nominal Dimensions:	50.8 mm (L) 25.4 mm (D)

Specimen Data:	Length (mm)	Mass (g)
Pre-test:	50.8	57.725
Post-test:	50.8	57.419
Change:	0	0.306

Temp Range (C)		(C)	Mean Temp (C)	Mean CTE (10^{-6}/C)
25	-	50	37.5	7.99
50	-	75	62.5	8.93
75	-	100	87.5	9.67
100	-	125	112.5	10.10
125	-	150	137.5	11.05
150	-	175	162.5	13.28
175	-	200	187.5	16.92
200	-	225	212.5	22.22
225	-	250	237.5	35.73
250	-	275	262.5	37.16
275	-	300	287.5	47.52
300	-	325	312.5	45.58
325	-	300	312.5	14.74
300	-	275	287.5	21.22
275	-	250	262.5	28.04
250	-	225	237.5	34.32
225	-	200	212.5	33.24
200	-	175	187.5	37.55
175	-	150	162.5	24.13
150	-	125	137.5	16.75
125	-	100	112.5	13.61
100	-	75	87.5	11.71
75	-	50	62.5	10.45
50	-	30	40	9.72

Temp Range (C)		(C)	Mean Temp (C)	Instant. CTE (10^{-6}/C)
27.5	-	32.5	30	7.07
47.5	-	52.5	50	9.67
72.5	-	77.5	75	11.17
97.5	-	102.5	100	10.67
122.5	-	127.5	125	9.65
147.5	-	152.5	150	11.88
172.5	-	177.5	175	16.90
197.5	-	202.5	200	18.17
222.5	-	227.5	225	28.85
247.5	-	252.5	250	36.86
272.5	-	277.5	275	39.07
297.5	-	302.5	300	52.58
302.5	-	297.5	300	18.65
277.5	-	272.5	275	23.90
252.5	-	247.5	250	32.19
227.5	-	222.5	225	35.05
202.5	-	197.5	200	35.13
177.5	-	172.5	175	31.21
152.5	-	147.5	150	20.11
127.5	-	122.5	125	17.28
102.5	-	97.5	100	14.34
77.5	-	72.5	75	12.31
52.5	-	47.5	50	9.39

Figure A-29. Thermal Expansion Data for Specimen ESF-AOD-HDFR1-48.5 for First Thermal Cycle

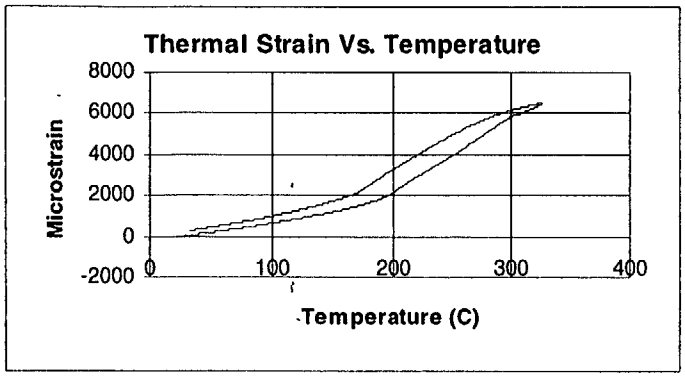

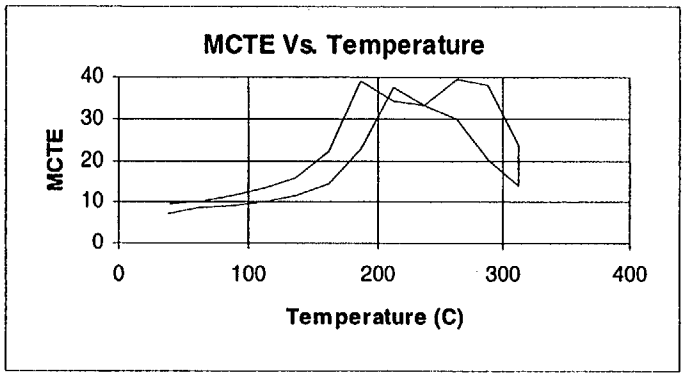

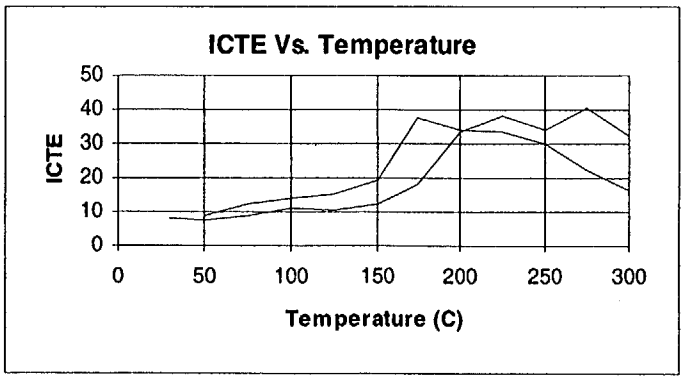

Specimen ID:	ESF-AOD-HDFR1-48.5-B
Date of Test Completion:	5/1/97
Thermal/Mechanical Unit:	TSw2
Lithostratigraphic Unit:	Tptpmn
Original Location:	ESF; Alcove 5;Thermal Drift Scale Test Area
Initial Moisture Content	Air-dried (As-is)
Nominal Dimensions:	50.8 mm (L) 25.4 mm (D)

Specimen Data:	Length (mm)	Mass (g)
Pre-test:	50.80	57.503
Post-test:	50.80	57.423
Change:	0	0.080

Temp Range (C)	(C)	Mean Temp (C)	Mean CTE (10^{-6}/C)
25 -	50	37.5	7.25
50 -	75	62.5	8.63
75 -	100	87.5	9.38
100 -	125	112.5	9.98
125 -	150	137.5	11.70
150 -	175	162.5	14.61
175 -	200	187.5	22.65
200 -	225	212.5	37.53
225 -	250	237.5	33.41
250 -	275	262.5	39.67
275 -	300	287.5	37.89
300 -	325	312.5	23.61
325 -	300	312.5	13.80
300 -	275	287.5	20.23
275 -	250	262.5	29.64
250 -	225	237.5	33.17
225 -	200	212.5	34.30
200 -	175	187.5	38.82
175 -	150	162.5	22.03
150 -	125	137.5	16.01
125 -	100	112.5	13.51
100 -	75	87.5	11.33
75 -	50	62.5	10.22
50 -	30	40	9.81

Temp Range (C)	(C)	Mean Temp (C)	Instant. CTE (10^{-6}/C)
27.5 -	32.5	30	8.47
47.5 -	52.5	50	7.65
72.5 -	77.5	75	8.61
97.5 -	102.5	100	11.24
122.5 -	127.5	125	10.88
147.5 -	152.5	150	12.11
172.5 -	177.5	175	18.52
197.5 -	202.5	200	33.44
222.5 -	227.5	225	38.07
247.5 -	252.5	250	34.24
272.5 -	277.5	275	40.61
297.5 -	302.5	300	32.61
302.5 -	297.5	300	16.61
277.5 -	272.5	275	22.07
252.5 -	247.5	250	29.79
227.5 -	222.5	225	33.71
202.5 -	197.5	200	34.30
177.5 -	172.5	175	37.71
152.5 -	147.5	150	19.25
127.5 -	122.5	125	15.02
102.5 -	97.5	100	13.90
77.5 -	72.5	75	12.17
52.5 -	47.5	50	8.81

Figure A-30. Thermal Expansion Data for Specimen ESF-AOD-HDFR1-48.5-B for Second Thermal Cycle

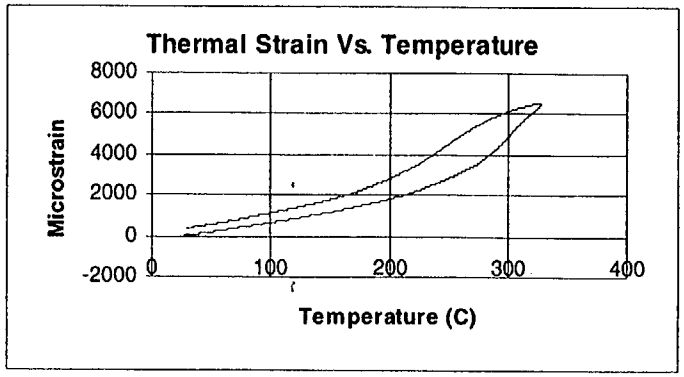

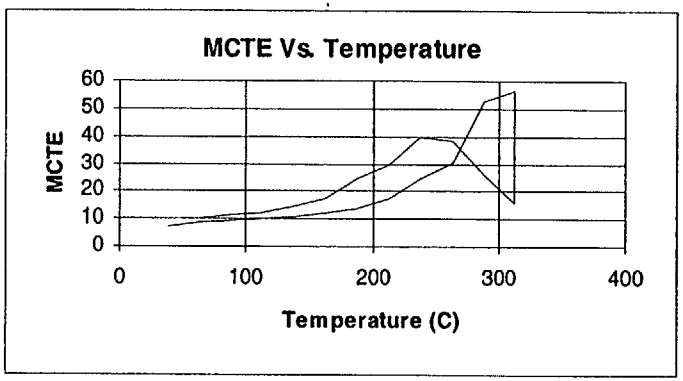

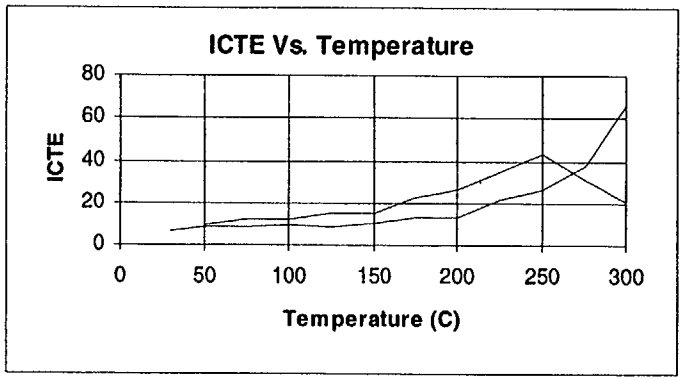

Specimen ID:	ESF-AOD-HDFR1-68.6-B
Date of Test Completion:	4/6/97
Thermal/Mechanical Unit:	TSw2
Lithostratigraphic Unit:	Tptpmn
Original Location:	ESF; Alcove 5;Thermal Drift Scale Test Area
Initial Moisture Content	Air-dried (As-Is)
Nominal Dimensions:	50.8 mm (L) 25.4 mm (D)

Specimen Data:	Length (mm)	Mass (g)
Pre-test:	50.8	57.201
Post-test:	50.8	56.769
Change:	0	0.432

Temp Range (C)		(C)	Mean Temp (C)	Mean CTE (10^{-6}/C)
25	-	50	37.5	7.57
50	-	75	62.5	8.81
75	-	100	87.5	9.43
100	-	125	112.5	9.98
125	-	150	137.5	10.54
150	-	175	162.5	11.95
175	-	200	187.5	13.52
200	-	225	212.5	17.46
225	-	250	237.5	24.28
250	-	275	262.5	30.43
275	-	300	287.5	52.55
300	-	325	312.5	56.59
325	-	300	312.5	16.06
300	-	275	287.5	26.06
275	-	250	262.5	38.22
250	-	225	237.5	39.46
225	-	200	212.5	29.38
200	-	175	187.5	24.23
175	-	150	162.5	17.23
150	-	125	137.5	14.50
125	-	100	112.5	12.51
100	-	75	87.5	11.28
75	-	50	62.5	10.31
50	-	30	40	9.80

Temp Range (C)		(C)	Mean Temp (C)	Instant. CTE (10^{-6}/C)
27.5	-	32.5	30	6.90
47.5	-	52.5	50	8.76
72.5	-	77.5	75	8.67
97.5	-	102.5	100	9.42
122.5	-	127.5	125	8.21
147.5	-	152.5	150	10.38
172.5	-	177.5	175	12.98
197.5	-	202.5	200	13.37
222.5	-	227.5	225	22.01
247.5	-	252.5	250	26.35
272.5	-	277.5	275	37.80
297.5	-	302.5	300	66.31
302.5	-	297.5	300	21.00
277.5	-	272.5	275	30.96
252.5	-	247.5	250	43.63
227.5	-	222.5	225	35.09
202.5	-	197.5	200	26.51
177.5	-	172.5	175	22.15
152.5	-	147.5	150	15.08
127.5	-	122.5	125	15.37
102.5	-	97.5	100	12.60
77.5	-	72.5	75	12.45
52.5	-	47.5	50	8.96

Figure A-31. Thermal Expansion Data for Specimen ESF-AOD-HDFR1-68.6-B for First Thermal Cycle

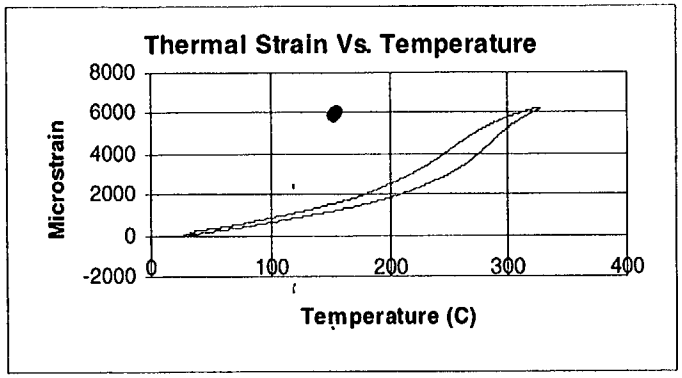

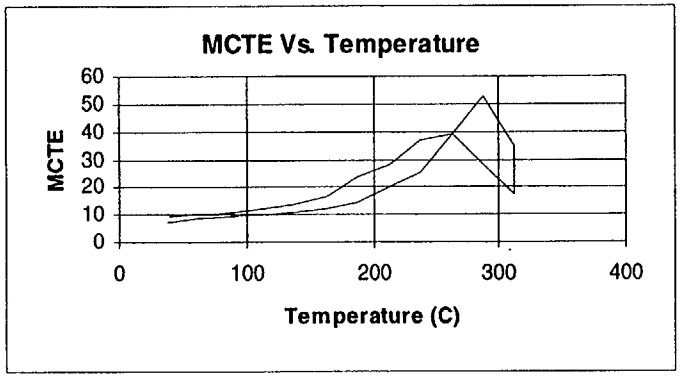

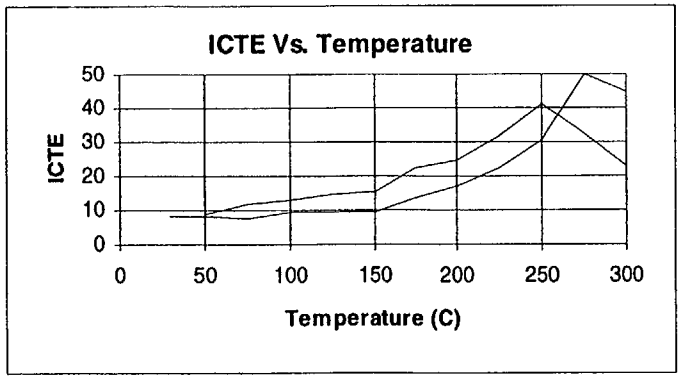

Specimen ID:	ESF-AOD-HDFR1-68.6-B
Date of Test Completion:	4/30/97
Thermal/Mechanical Unit:	TSw2
Lithostratigraphic Unit:	Tptpmn
Original Location:	ESF; Alcove 5;Thermal Drift Scale Test Area
Initial Moisture Content	Air-dried (As-Is)
Nominal Dimensions:	50.8 mm (L) 25.4 mm (D)

Specimen Data:	Length (mm)	Mass (g)
Pre-test:	50.80	56.872
Post-test:	50.80	56.774
Change:	0	0.098

Temp Range (C)		(C)	Mean Temp (C)	Mean CTE (10^{-6}/C)
25	-	50	37.5	7.31
50	-	75	62.5	8.60
75	-	100	87.5	9.23
100	-	125	112.5	9.78
125	-	150	137.5	10.73
150	-	175	162.5	12.51
175	-	200	187.5	14.67
200	-	225	212.5	20.19
225	-	250	237.5	25.35
250	-	275	262.5	39.21
275	-	300	287.5	52.66
300	-	325	312.5	34.73
325	-	300	312.5	17.60
300	-	275	287.5	28.09
275	-	250	262.5	39.17
250	-	225	237.5	36.88
225	-	200-	212.5	27.95
200	-	175	187.5	23.51
175	-	150	162.5	16.51
150	-	125	137.5	13.96
125	-	100	112.5	12.17
100	-	75	87.5	10.89
75	-	50	62.5	10.03
50	-	30	40	9.65

Temp Range (C)		(C)	Mean Temp (C)	Instant. CTE (10^{-6}/C)
27.5	-	32.5	30	8.05
47.5	-	52.5	50	8.16
72.5	-	77.5	75	7.59
97.5	-	102.5	100	9.67
122.5	-	127.5	125	9.49
147.5	-	152.5	150	9.44
172.5	-	177.5	175	13.51
197.5	-	202.5	200	17.26
222.5	-	227.5	225	22.14
247.5	-	252.5	250	30.42
272.5	-	277.5	275	49.81
297.5	-	302.5	300	44.77
302.5	-	297.5	300	22.91
277.5	-	272.5	275	32.42
252.5	-	247.5	250	41.05
227.5	-	222.5	225	31.66
202.5	-	197.5	200	24.70
177.5	-	172.5	175	22.63
152.5	-	147.5	150	15.28
127.5	-	122.5	125	14.97
102.5	-	97.5	100	13.14
77.5	-	72.5	75	11.66
52.5	-	47.5	50	8.94

Figure A-32. Thermal Expansion Data for Specimen ESF-AOD-HDFR1-68.6-B for Second Thermal Cycle

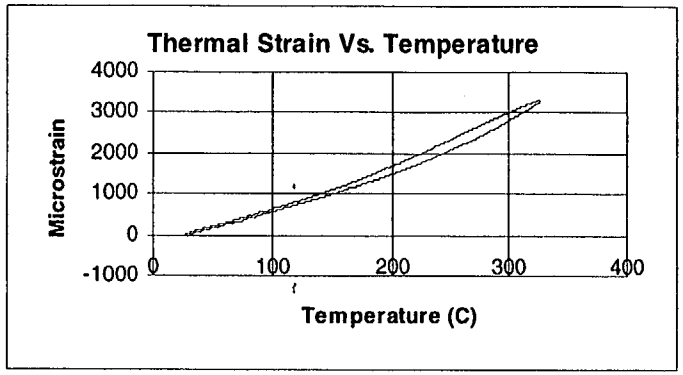

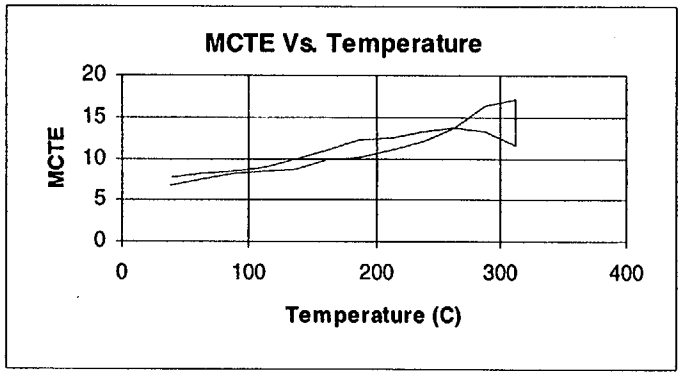

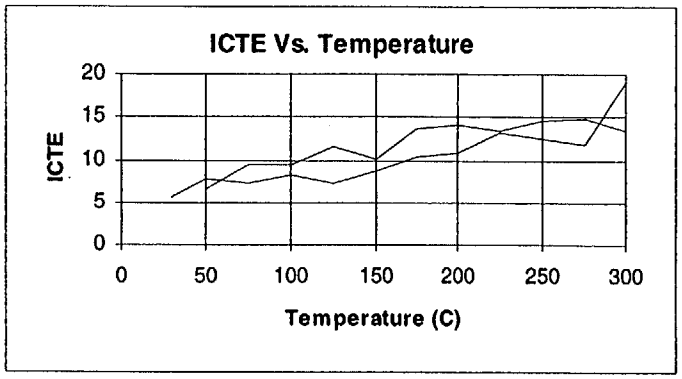

Specimen ID:	ESF-AOD-HDFR1-97.9
Date of Test Completion:	4/8/97
Thermal/Mechanical Unit:	TSw2
Lithostratigraphic Unit:	Tptpmn or Tptpll
Original Location:	ESF; Alcove 5;Thermal Drift Scale Test Area
Initial Moisture Content	Air-dried (As-is)
Nominal Dimensions:	50.8 mm (L) 25.4 mm (D)

Specimen Data:	Length (mm)	Mass (g)
Pre-test:	50.8	60.020
Post-test:	50.8	59.781
Change:	0	0.239

Temp Range (C)		(C)	Mean Temp (C)	Mean CTE (10^{-6}/C)
25	-	50	37.5	6.69
50	-	75	62.5	7.43
75	-	100	87.5	8.07
100	-	125	112.5	8.34
125	-	150	137.5	8.79
150	-	175	162.5	9.79
175	-	200	187.5	10.09
200	-	225	212.5	11.19
225	-	250	237.5	12.11
250	-	275	262.5	13.68
275	-	300	287.5	16.36
300	-	325	312.5	17.05
325	-	300	312.5	11.58
300	-	275	287.5	13.21
275	-	250	262.5	13.72
250	-	225	237.5	13.33
225	-	200	212.5	12.49
200	-	175	187.5	12.34
175	-	150	162.5	11.04
150	-	125	137.5	9.86
125	-	100	112.5	8.95
100	-	75	87.5	8.52
75	-	50	62.5	8.10
50	-	30	40	7.67

Temp Range (C)		(C)	Mean Temp (C)	Instant. CTE (10^{-6}/C)
27.5	-	32.5	30	5.59
47.5	-	52.5	50	7.84
72.5	-	77.5	75	7.29
97.5	-	102.5	100	8.14
122.5	-	127.5	125	7.31
147.5	-	152.5	150	8.80
172.5	-	177.5	175	10.24
197.5	-	202.5	200	10.84
222.5	-	227.5	225	13.13
247.5	-	252.5	250	12.42
272.5	-	277.5	275	11.83
297.5	-	302.5	300	19.13
302.5	-	297.5	300	13.52
277.5	-	272.5	275	14.72
252.5	-	247.5	250	14.61
227.5	-	222.5	225	13.49
202.5	-	197.5	200	14.15
177.5	-	172.5	175	13.66
152.5	-	147.5	150	10.15
127.5	-	122.5	125	11.60
102.5	-	97.5	100	9.35
77.5	-	72.5	75	9.41
52.5	-	47.5	50	6.53

Figure A-33. Thermal Expansion Data for Specimen ESF-AOD-HDFR1-97.9-B for First Thermal Cycle

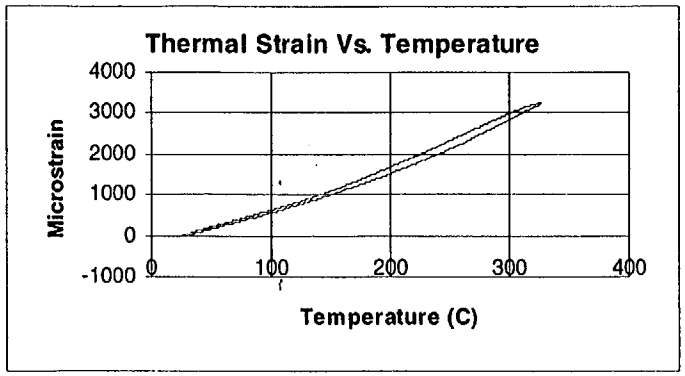

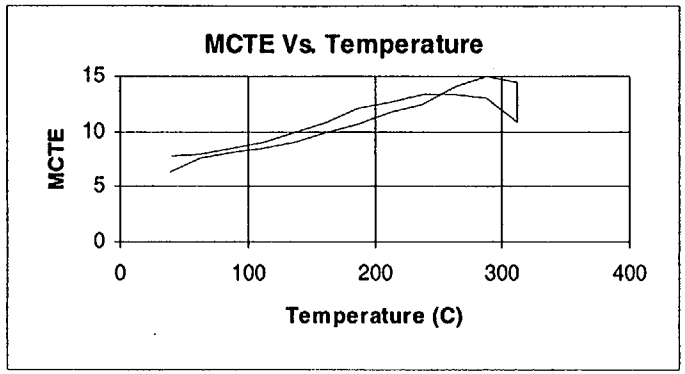

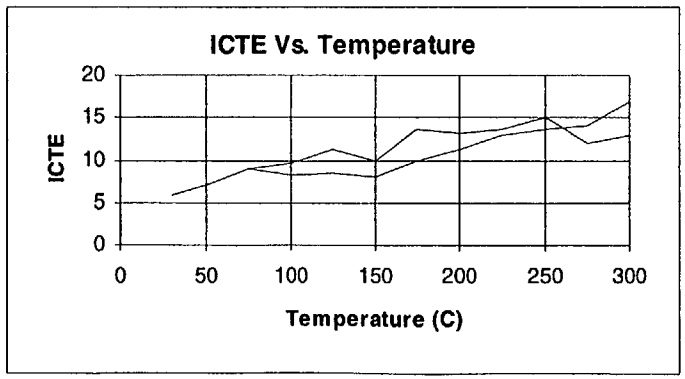

Specimen ID:	ESF-AOD-HDFR1-97.9-B
Date of Test Completion:	5/2/97
Thermal/Mechanical Unit:	TSw2
Lithostratigraphic Unit:	Tptpmn or Tptpll
Original Location:	ESF; Alcove 5;Thermal Drift Scale Test Area
Initial Moisture Content	Air-dried (As-is)
Nominal Dimensions:	50.8 mm (L) 25.4 mm (D)

Specimen Data:	Length (mm)	Mass (g)
Pre-test:	50.80	59.861
Post-test:	50.80	59.783
Change:	0	0.078

Temp Range (C)	(C)	Mean Temp (C)	Mean CTE (10^{-6}/C)
25 -	50	37.5	6.35
50 -	75	62.5	7.57
75 -	100	87.5	8.10
100 -	125	112.5	8.42
125 -	150	137.5	9.04
150 -	175	162.5	9.96
175 -	200	187.5	10.65
200 -	225	212.5	11.71
225 -	250	237.5	12.49
250 -	275	262.5	14.14
275 -	300	287.5	14.99
300 -	325	312.5	14.41
325 -	300	312.5	10.78
300 -	275	287.5	13.02
275 -	250	262.5	13.39
250 -	225	237.5	13.46
225 -	200	212.5	12.59
200 -	175	187.5	12.14
175 -	150	162.5	10.77
150 -	125	137.5	9.86
125 -	100	112.5	9.00
100 -	75	87.5	8.41
75 -	50	62.5	7.92
50 -	30	40	7.83

Temp Range (C)	(C)	Mean Temp (C)	Instant. CTE (10^{-6}/C)
27.5 -	32.5	30	5.79
47.5 -	52.5	50	6.99
72.5 -	77.5	75	8.83
97.5 -	102.5	100	8.19
122.5 -	127.5	125	8.48
147.5 -	152.5	150	7.93
172.5 -	177.5	175	9.98
197.5 -	202.5	200	11.26
222.5 -	227.5	225	12.95
247.5 -	252.5	250	13.53
272.5 -	277.5	275	14.15
297.5 -	302.5	300	16.96
302.5 -	297.5	300	12.82
277.5 -	272.5	275	11.89
252.5 -	247.5	250	15.17
227.5 -	222.5	225	13.55
202.5 -	197.5	200	13.11
177.5 -	172.5	175	13.53
152.5 -	147.5	150	9.93
127.5 -	122.5	125	11.24
102.5 -	97.5	100	9.59
77.5 -	72.5	75	9.00
52.5 -	47.5	50	6.97

Figure A-34. Thermal Expansion Data for Specimen ESF-AOD-HDFR1-97.9-B for Second Thermal Cycle

APPENDIX B

THERMAL EXPANSION DATA:
COMPARISON OF FIRST AND SECOND THERMAL CYCLES

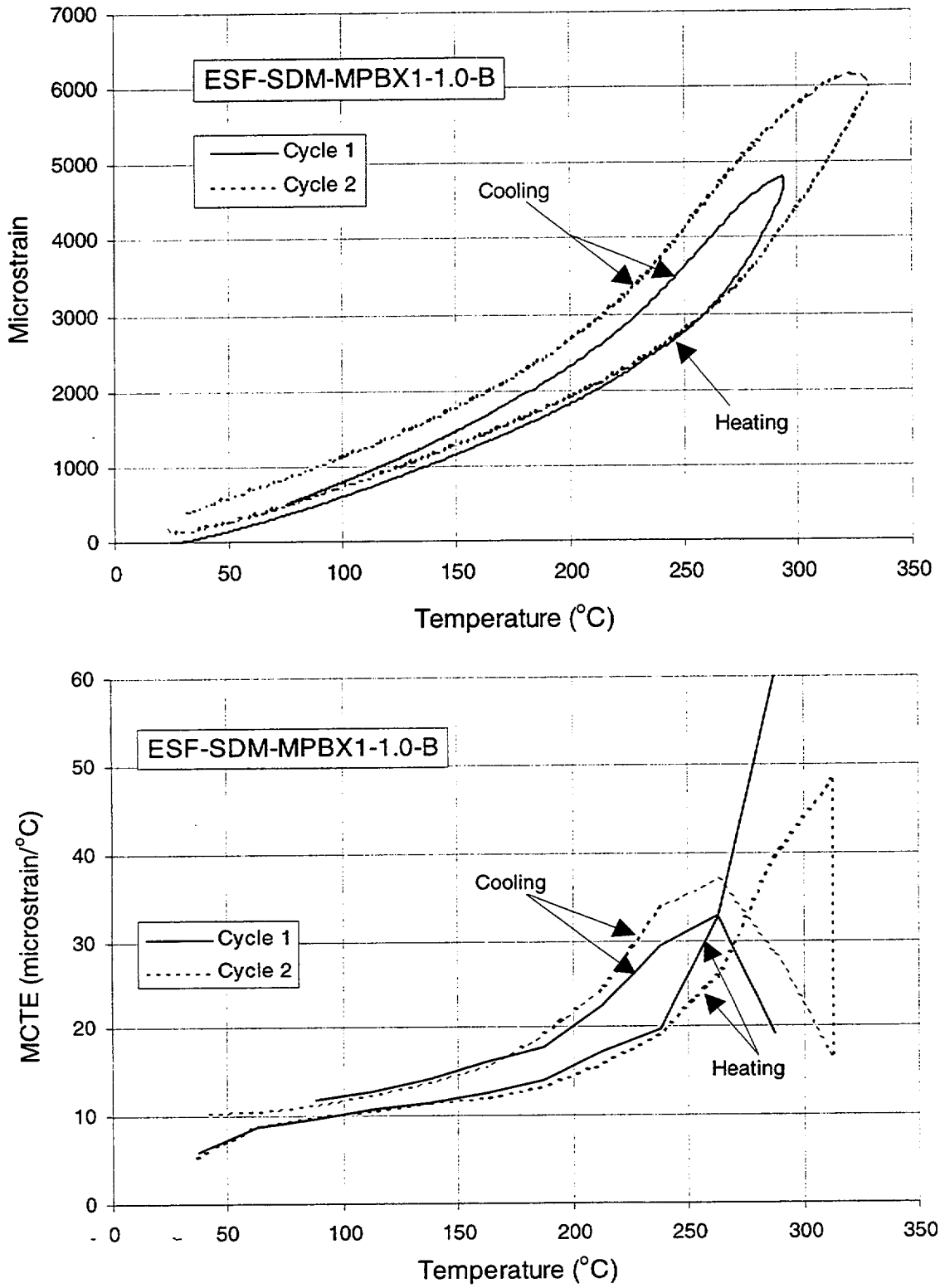

NOTE: These specimens are from the TSw2 thermal/mechanical unit and the Tptpmn lithostratigraphic unit.

Figure B-1. Plots of Strain Versus Temperature (Top) and MCTE Versus Temperature (Bottom) for Specimen ESF-SDM-MPBX1-1.0-B

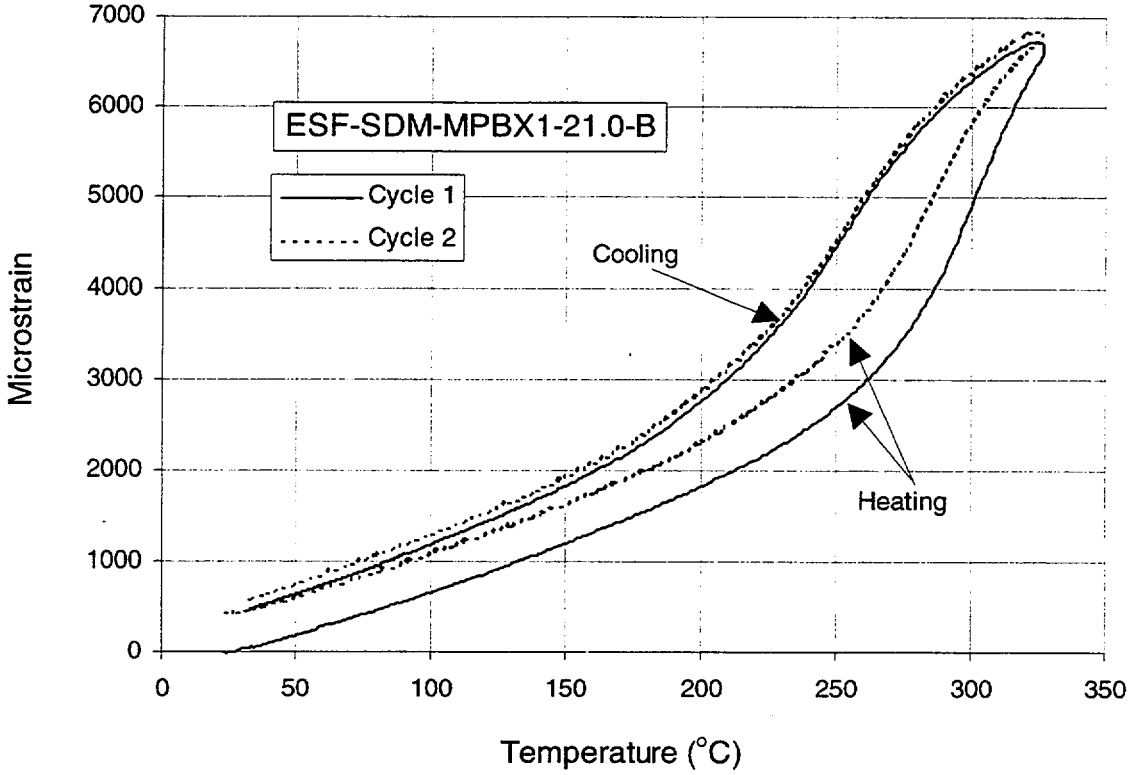

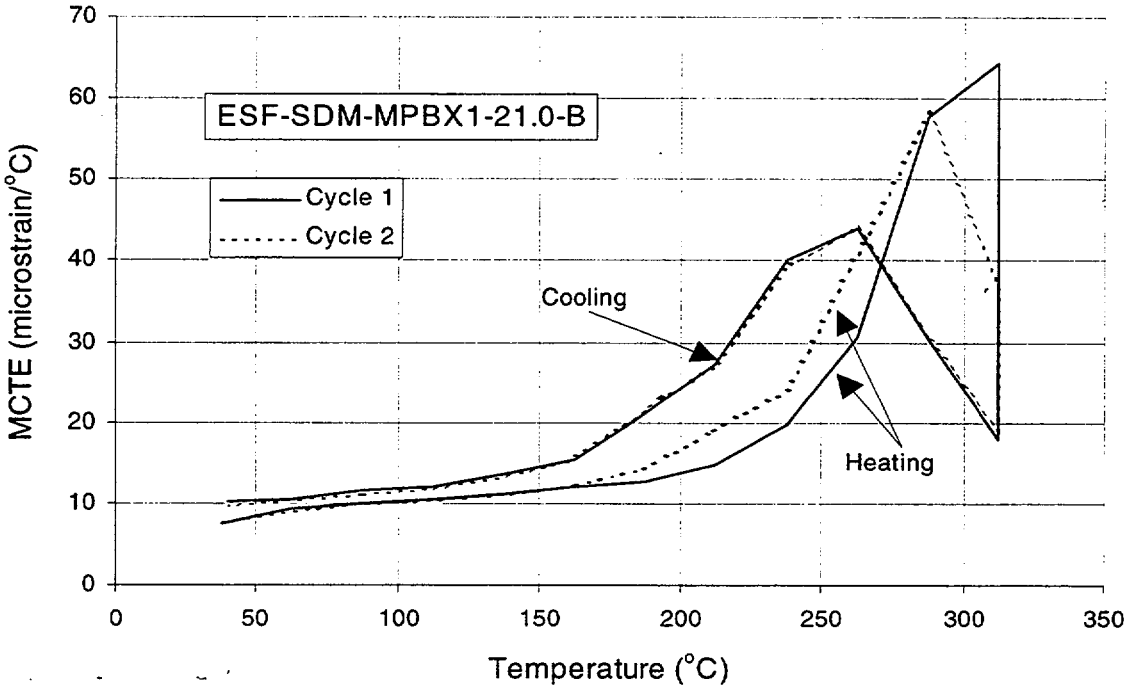

NOTE: These specimens are from the TSw2 thermal/mechanical unit and the Tptpmn lithostratigraphic unit.

Figure B-2. Plots of Strain Versus Temperature (Top) and MCTE Versus Temperature (Bottom) for Specimen ESF-SDM-MPBX1-21.0-B.

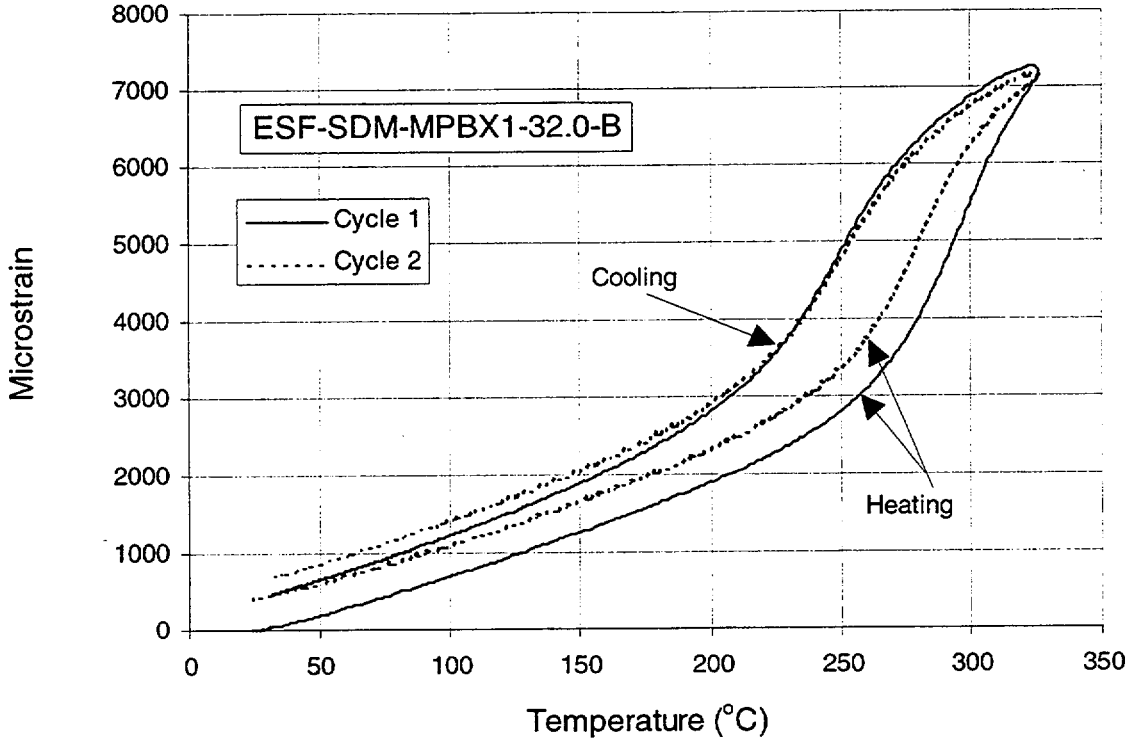

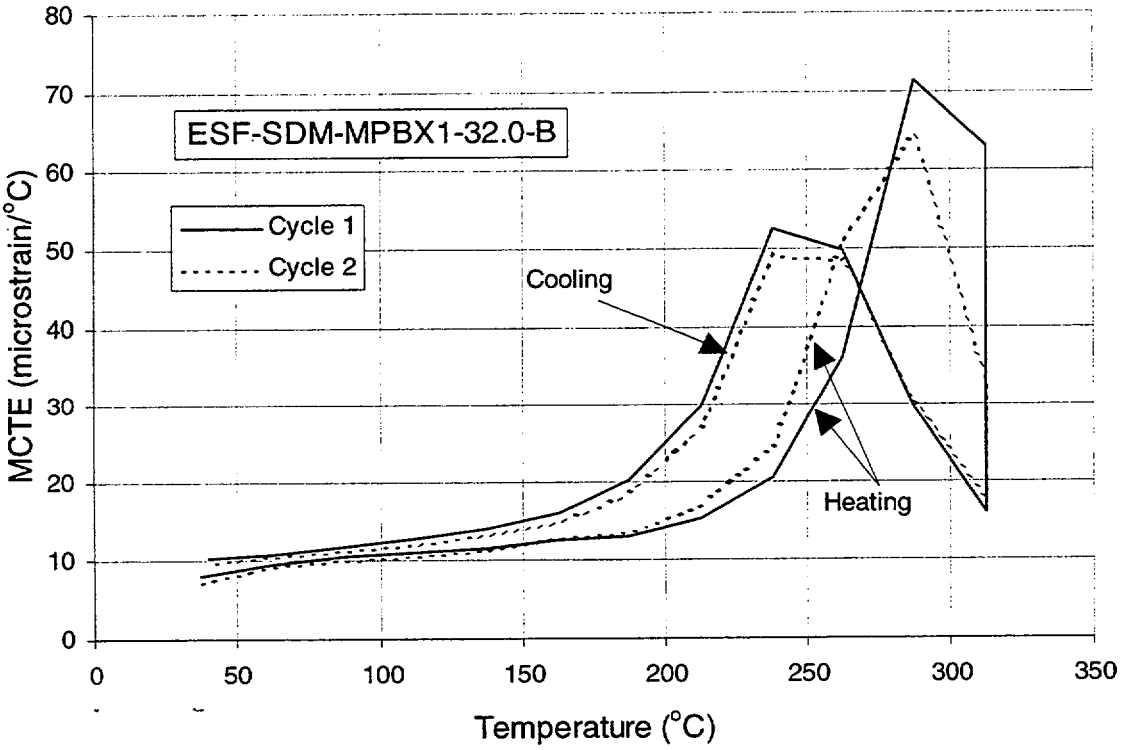

NOTE: These specimens are from the TSw2 thermal/mechanical unit and the Tptpmn lithostratigraphic unit.

Figure B-3. Plots of Strain Versus Temperature (Top) and MCTE Versus Temperature (Bottom) for Specimen ESF-SDM-MPBX1-32.0-B.

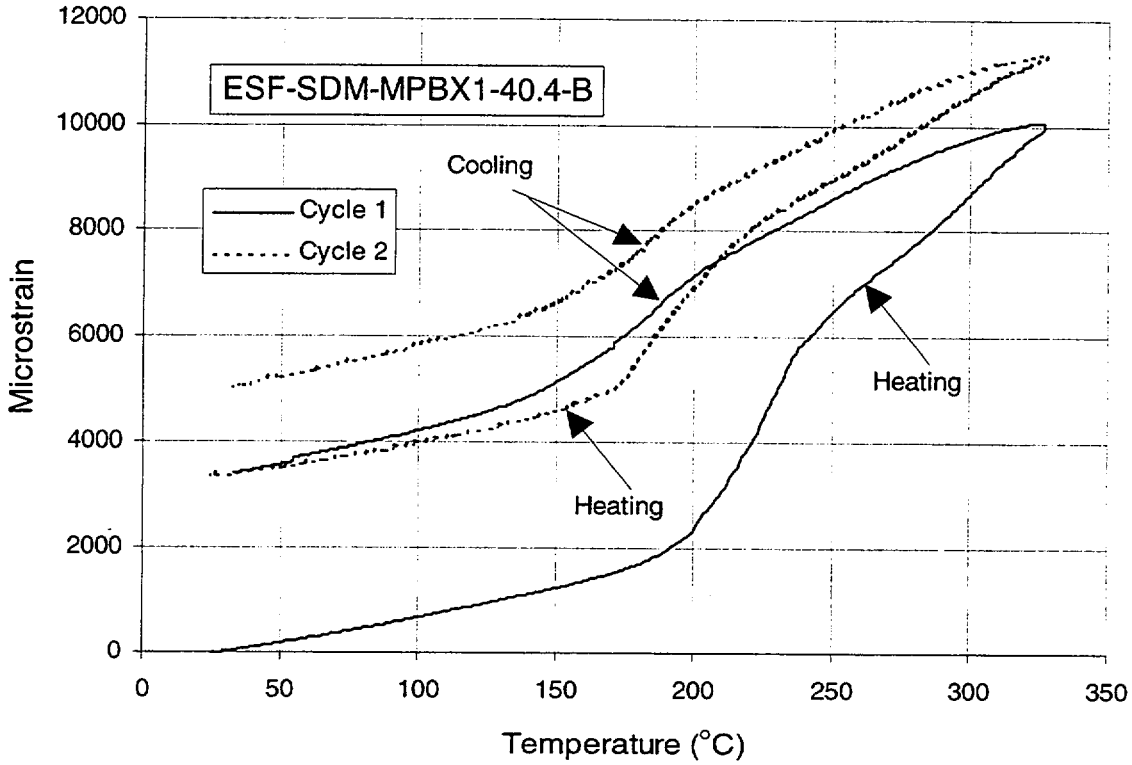

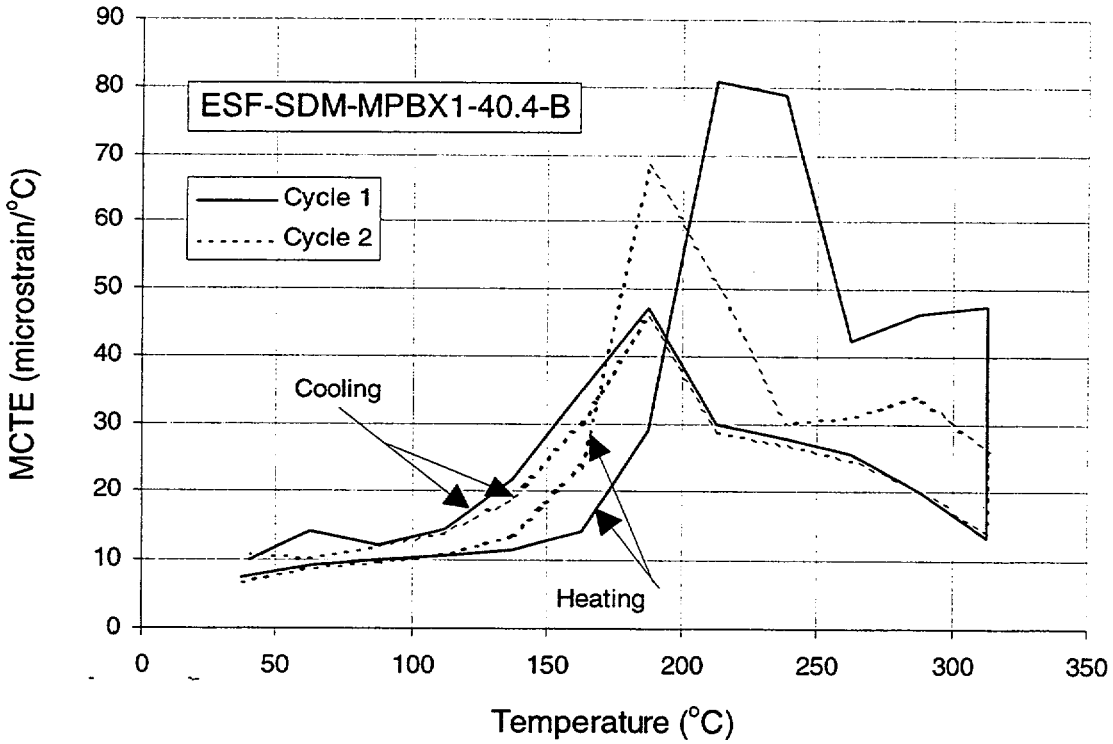

NOTE: These specimens are from the TSw2 thermal/mechanical unit and the Tptpmn lithostratigraphic unit.

Figure B-4. Plots of Strain Versus Temperature (Top) and MCTE Versus Temperature (Bottom) for Specimen ESF-SDM-MPBX1-40.4-B.

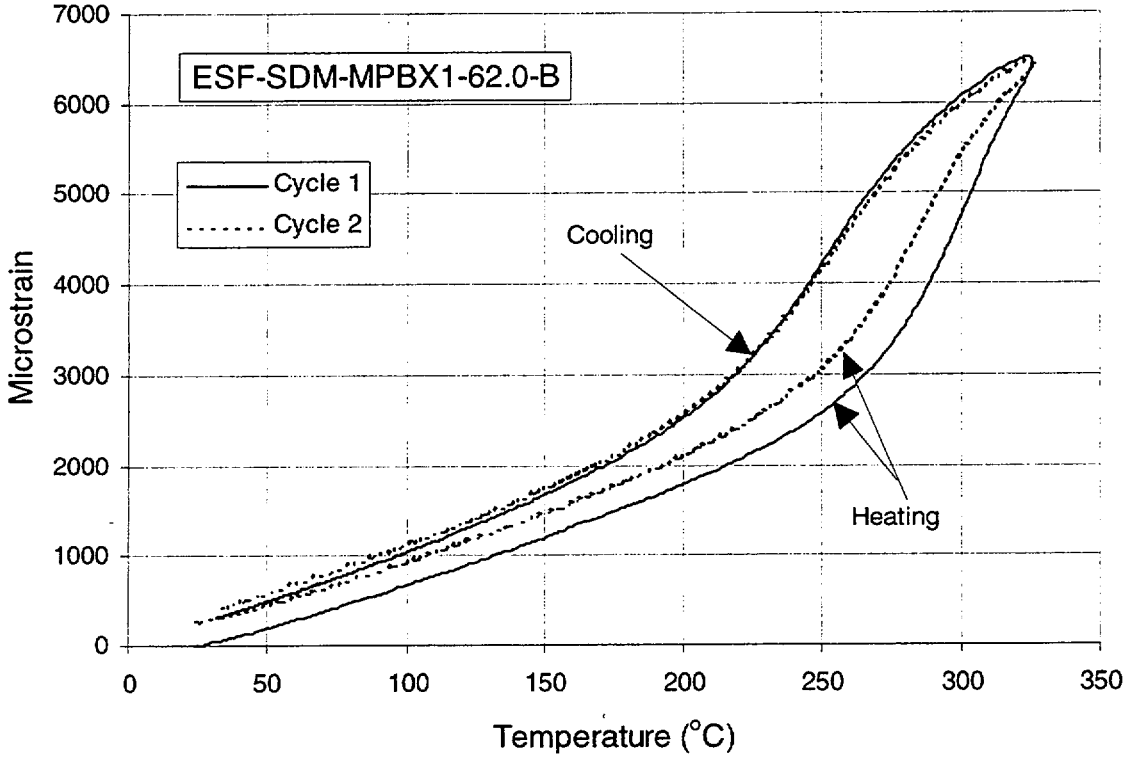

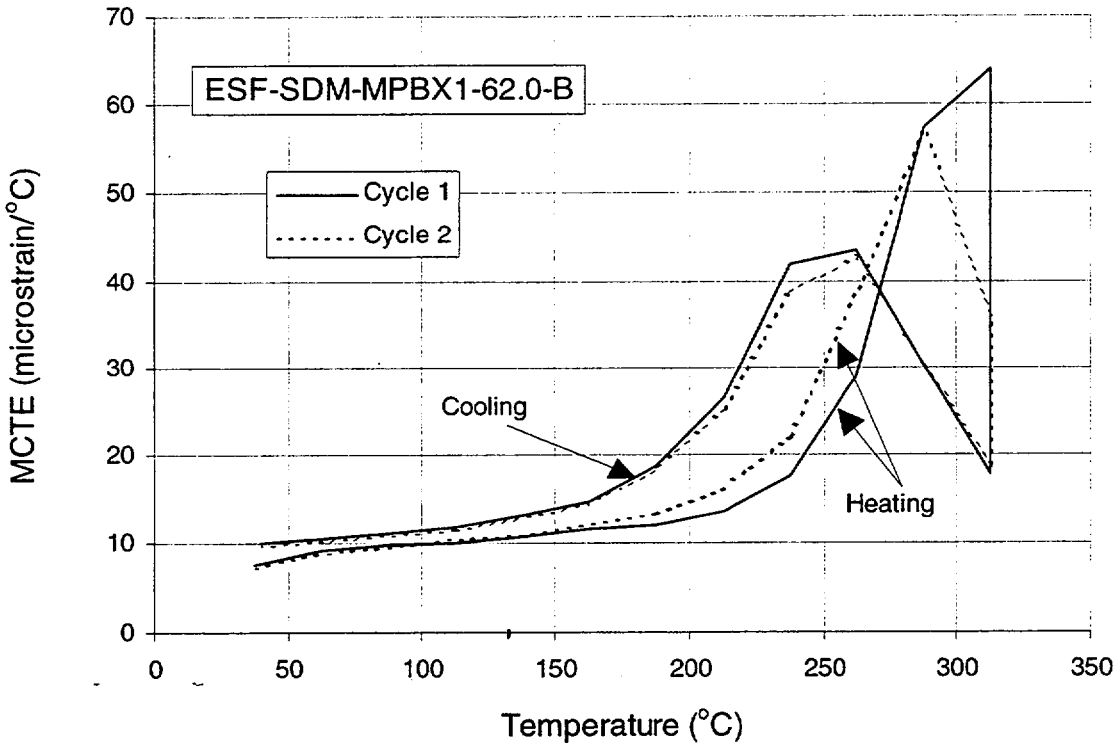

NOTE: These specimens are from the TSw2 thermal/mechanical unit and the Tptpmn lithostratigraphic unit.

Figure B-5. Plots of Strain Versus Temperature (Top) and MCTE Versus Temperature (Bottom) for Specimen ESF-SDM-MPBX1-62.0-B.

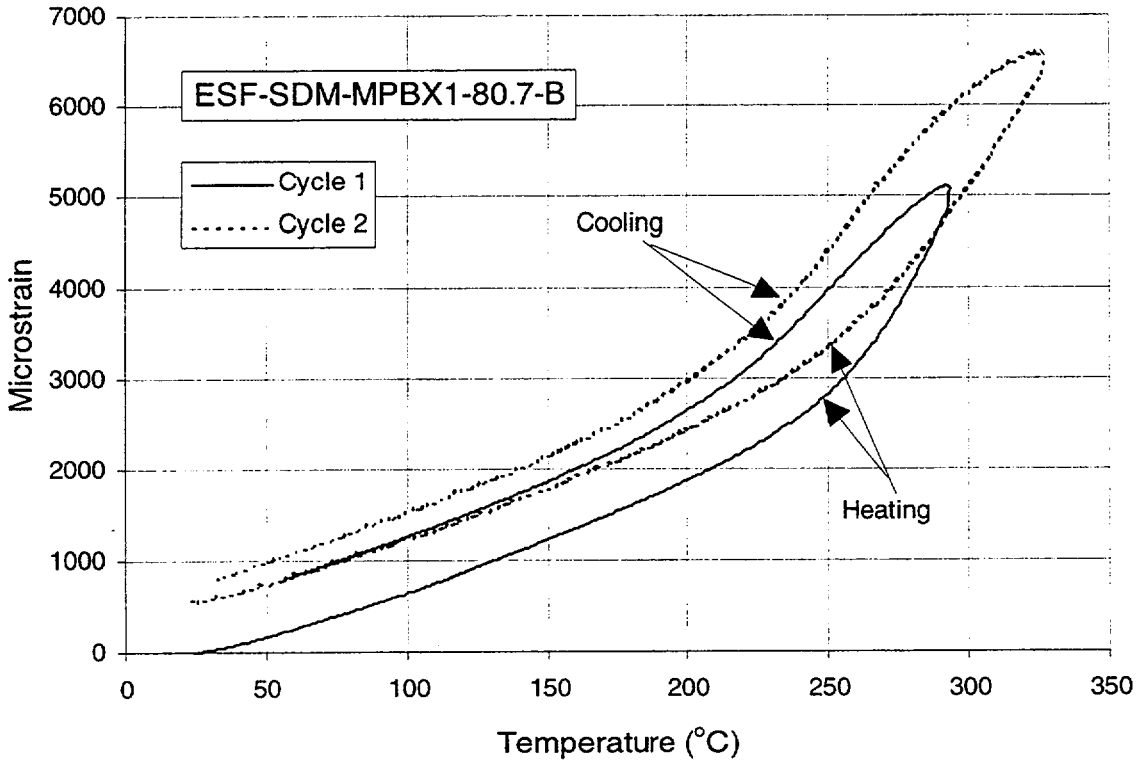

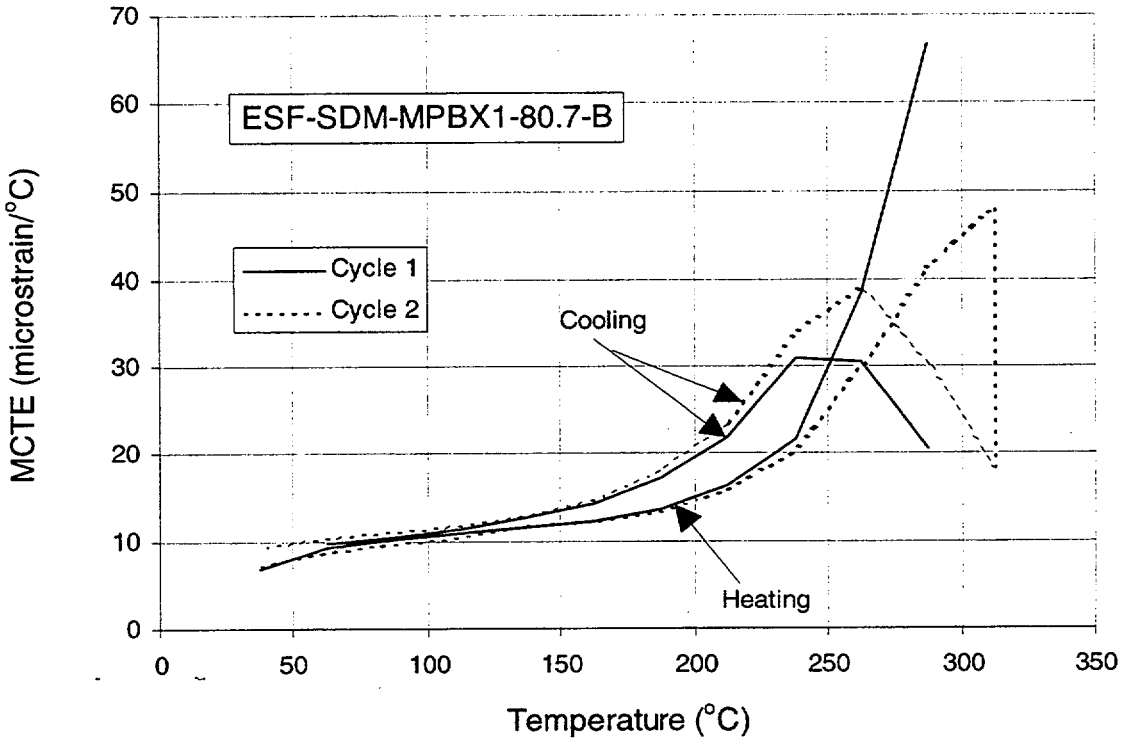

NOTE: These specimens are from the TSw2 thermal/mechanical unit and the Tptpmn lithostratigraphic unit.

Figure B-6. Plots of Strain Versus Temperature (Top) and MCTE Versus Temperature (Bottom) for Specimen ESF-SDM-MPBX1-80.7-B.

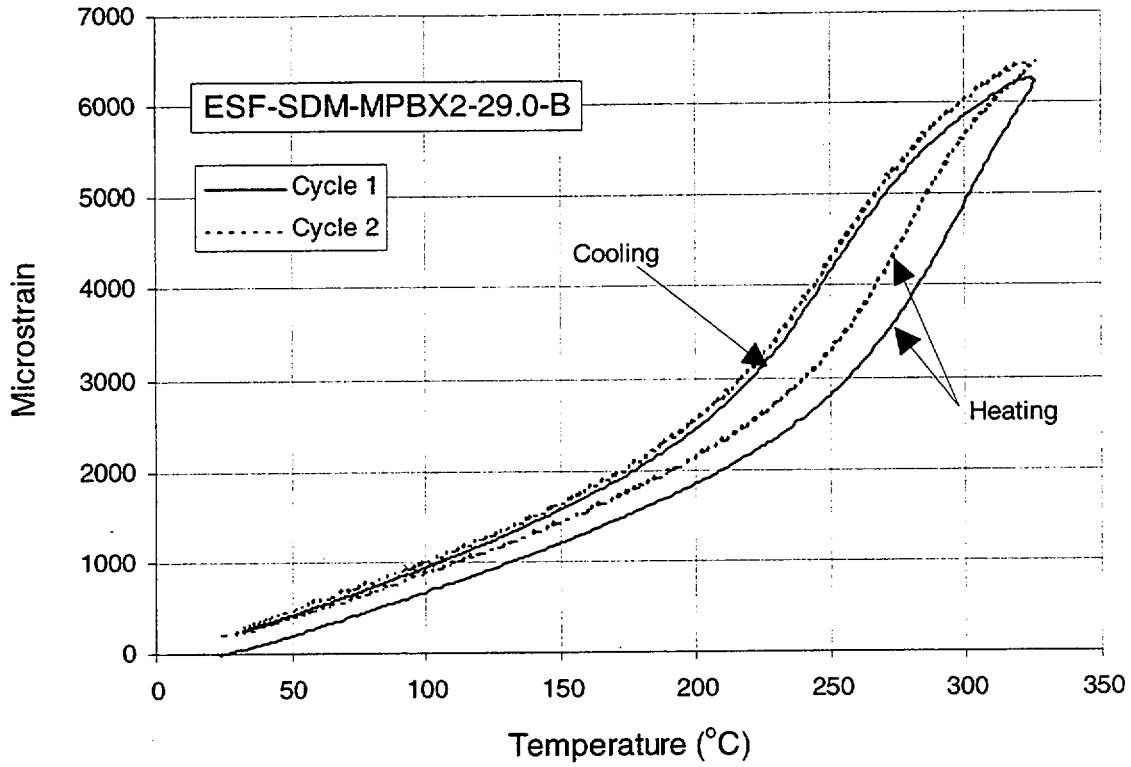

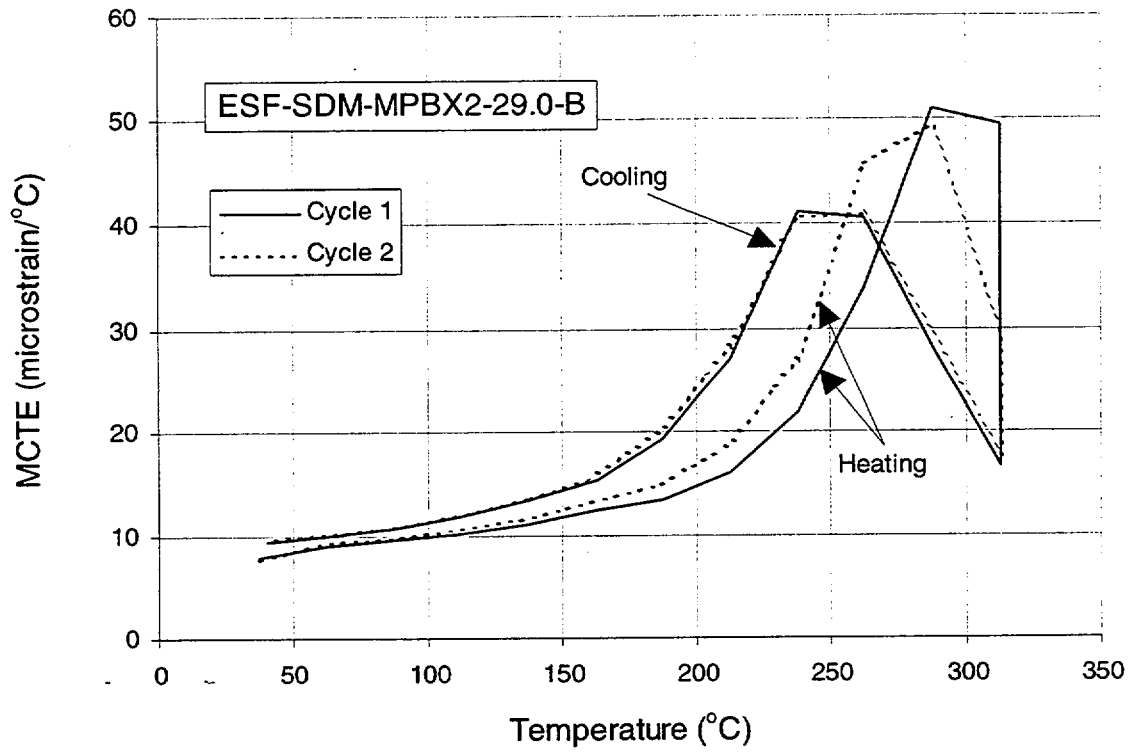

NOTE: These specimens are from the TSw2 thermal/mechanical unit and the Tptpmn lithostratigraphic unit.

Figure B-7. Plots of Strain Versus Temperature (Top) and MCTE Versus Temperature (Bottom) for Specimen ESF-SDM-MPBX2-29.0-B.

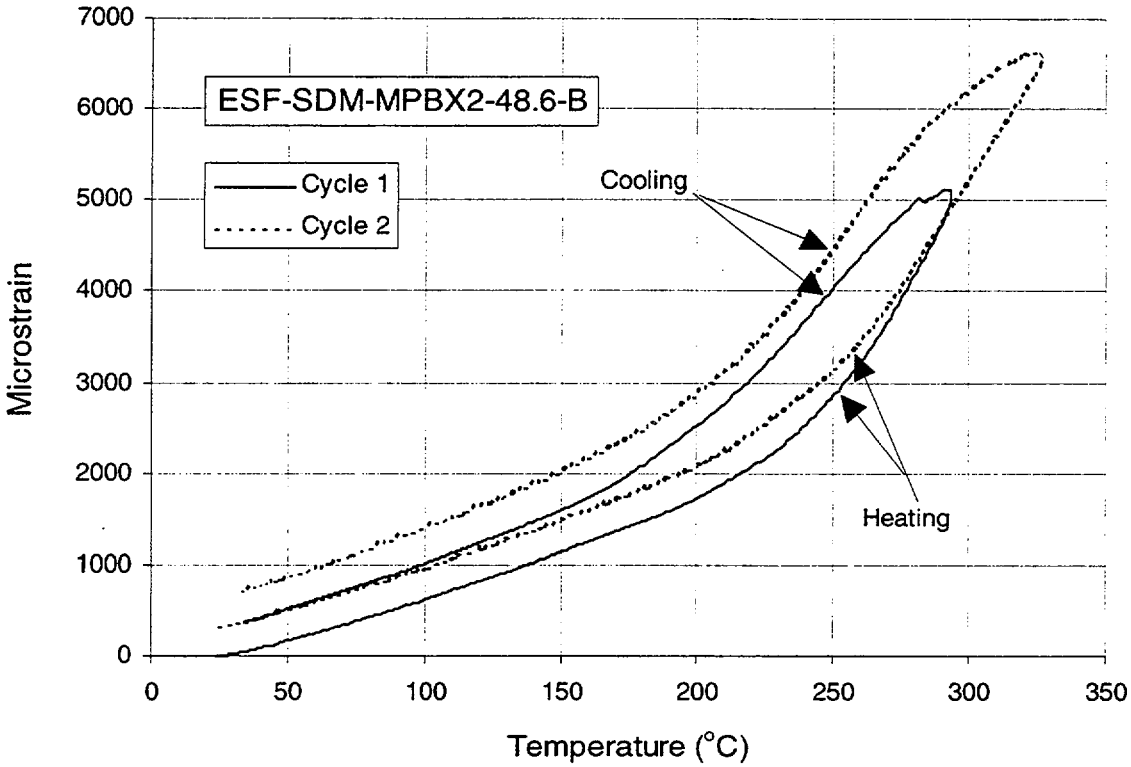

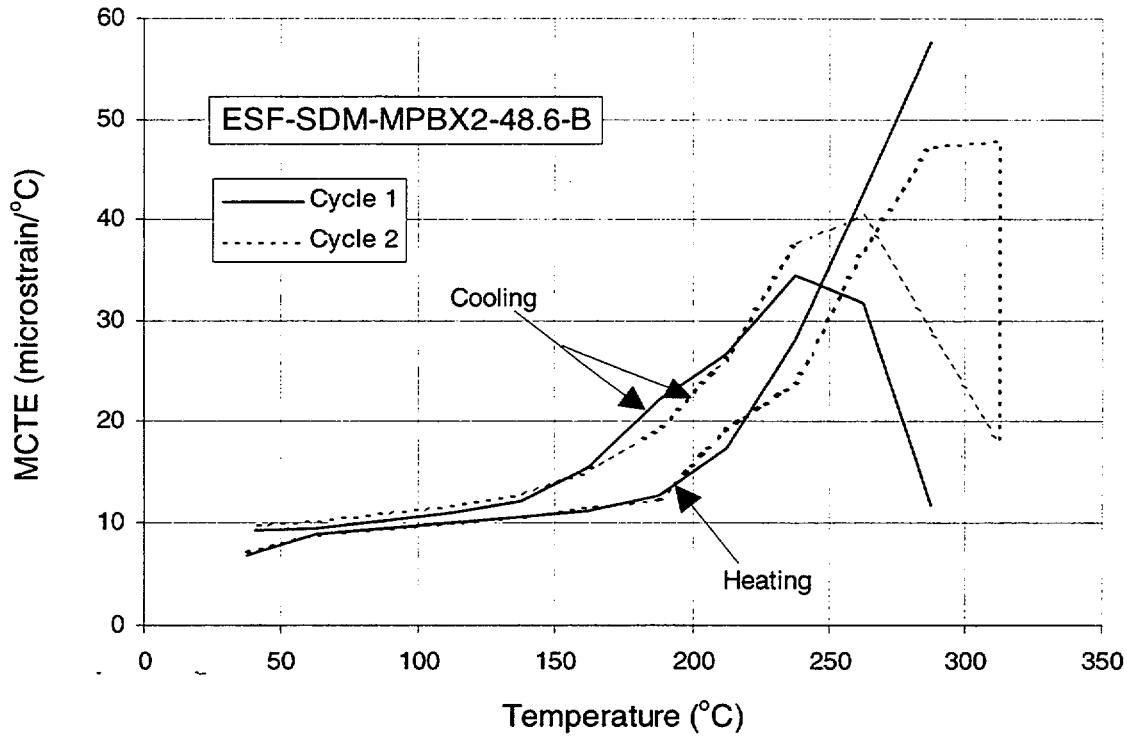

NOTE: These specimens are from the TSw2 thermal/mechanical unit and the Tptpmn lithostratigraphic unit.

Figure B-8. Plots of Strain Versus Temperature (Top) and MCTE Versus Temperature (Bottom) for Specimen ESF-SDM-MPBX2-48.6-B.

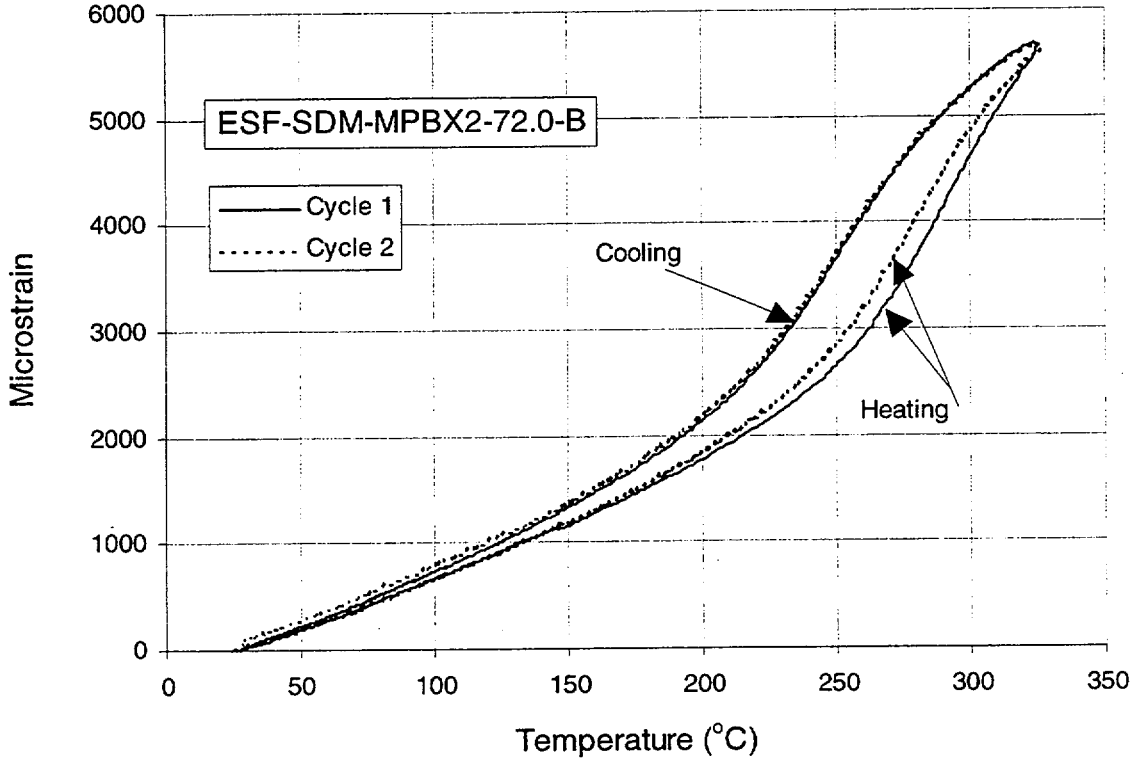

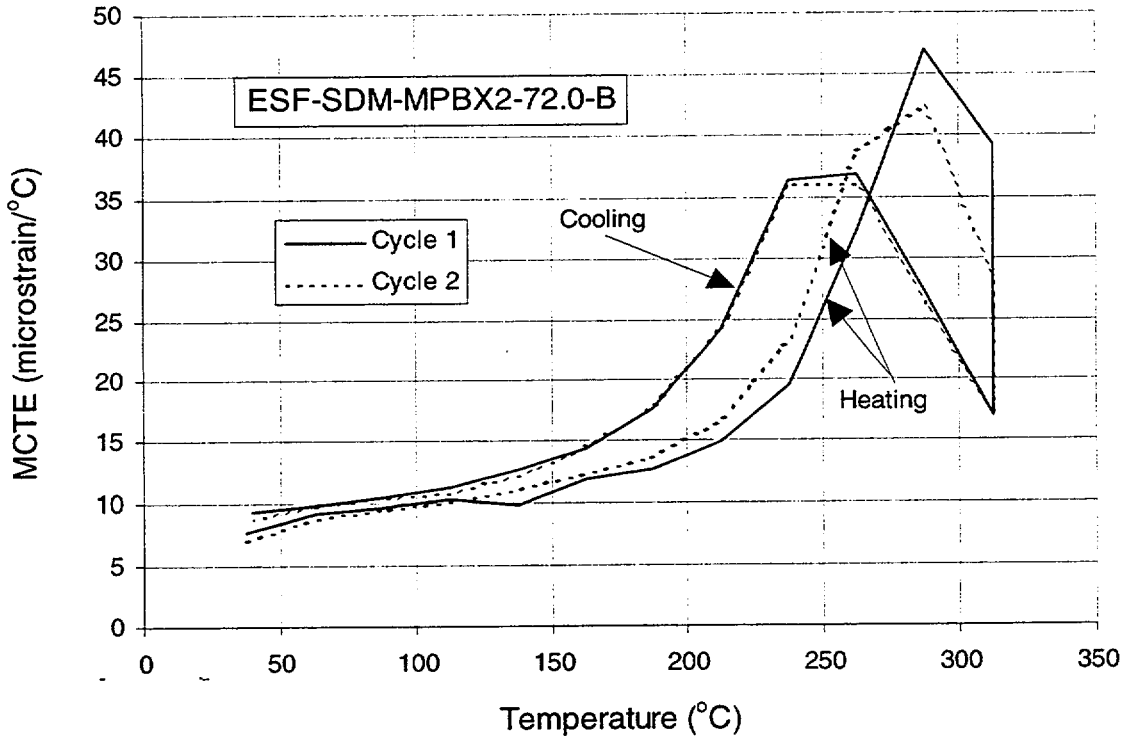

NOTE: These specimens are from the TSw2 thermal/mechanical unit and the Tptpmn lithostratigraphic unit.

Figure B-9. Plots of Strain Versus Temperature (Top) and MCTE Versus Temperature (Bottom) for Specimen ESF-SDM-MPBX2-72.0-B.

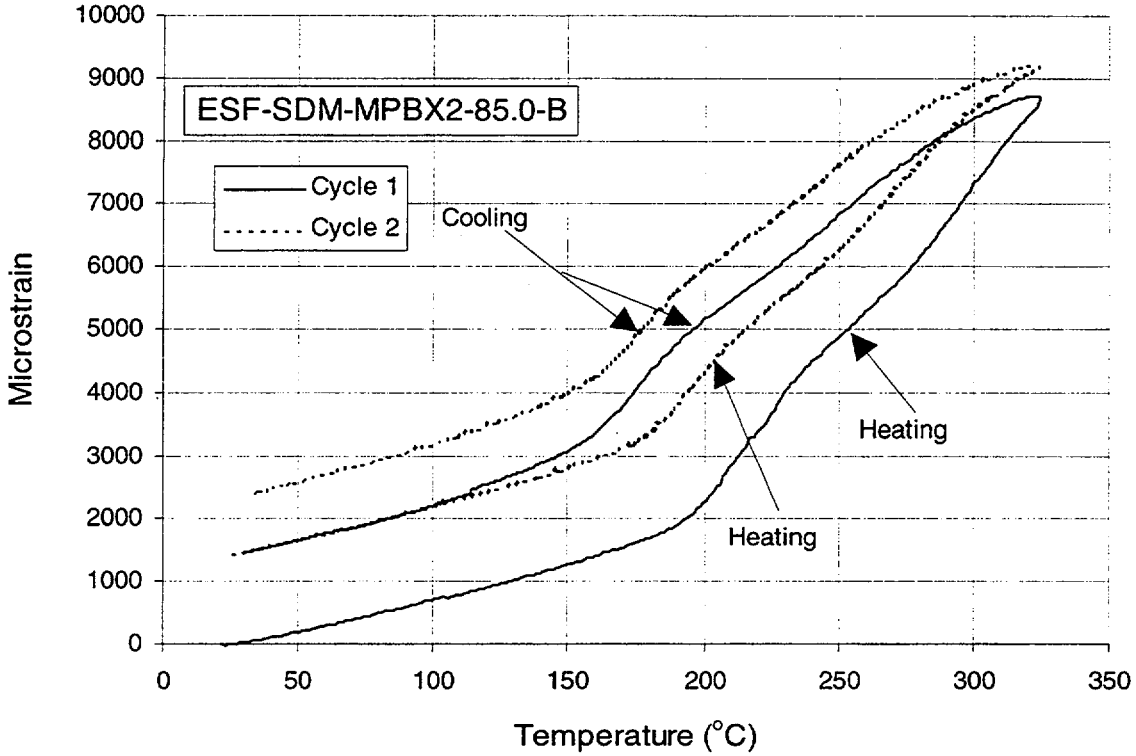

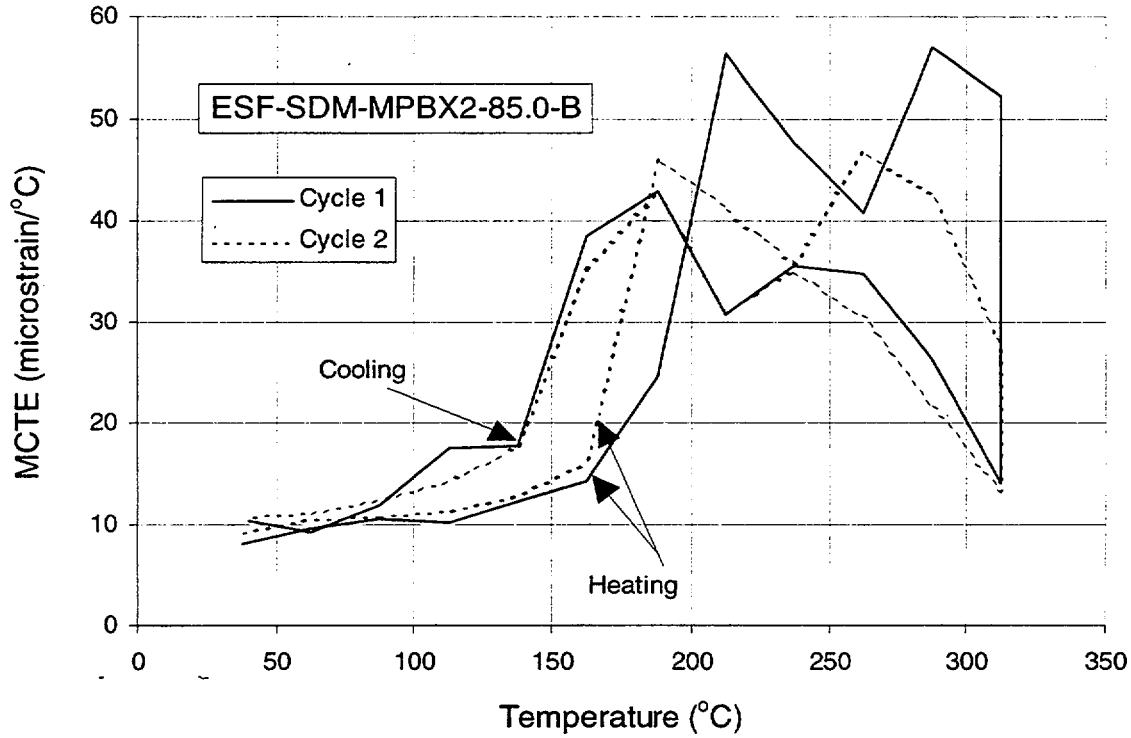

NOTE: These specimens are from the TSw2 thermal/mechanical unit and the Tptpmn lithostratigraphic unit.

Figure B-10. Plots of Strain Versus Temperature (Top) and MCTE Versus Temperature (Bottom) for Specimen ESF-SDM-MPBX2-85.0-B.

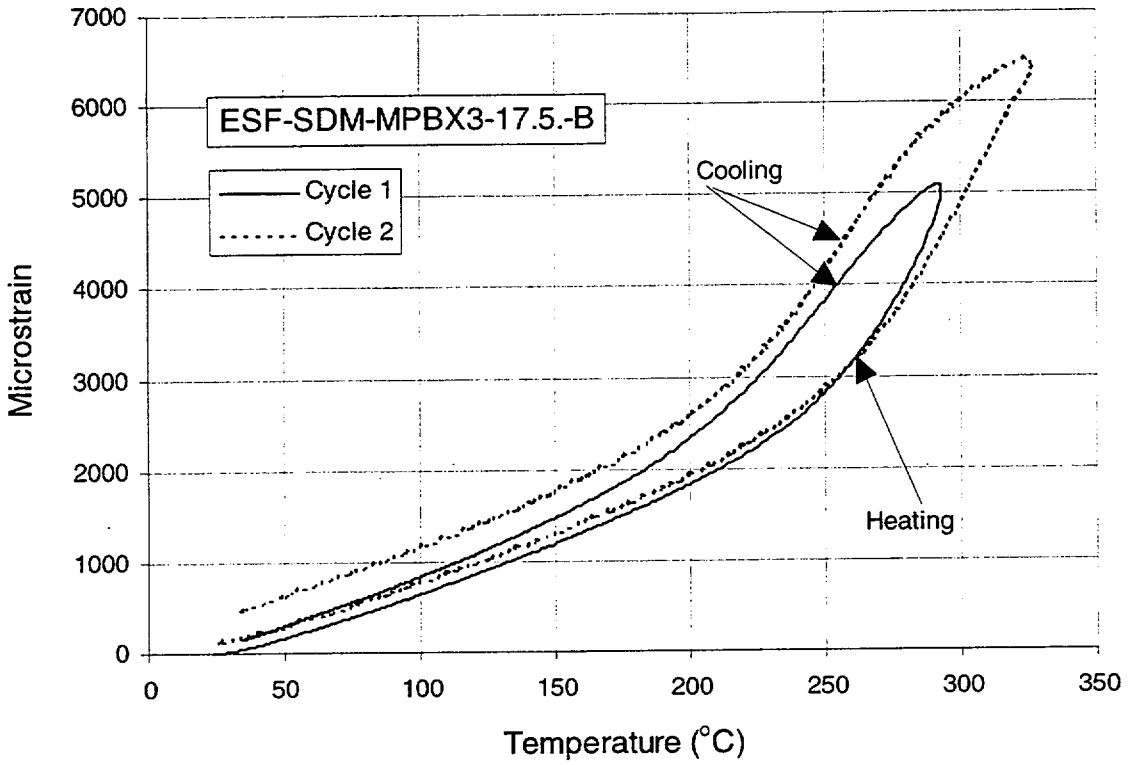

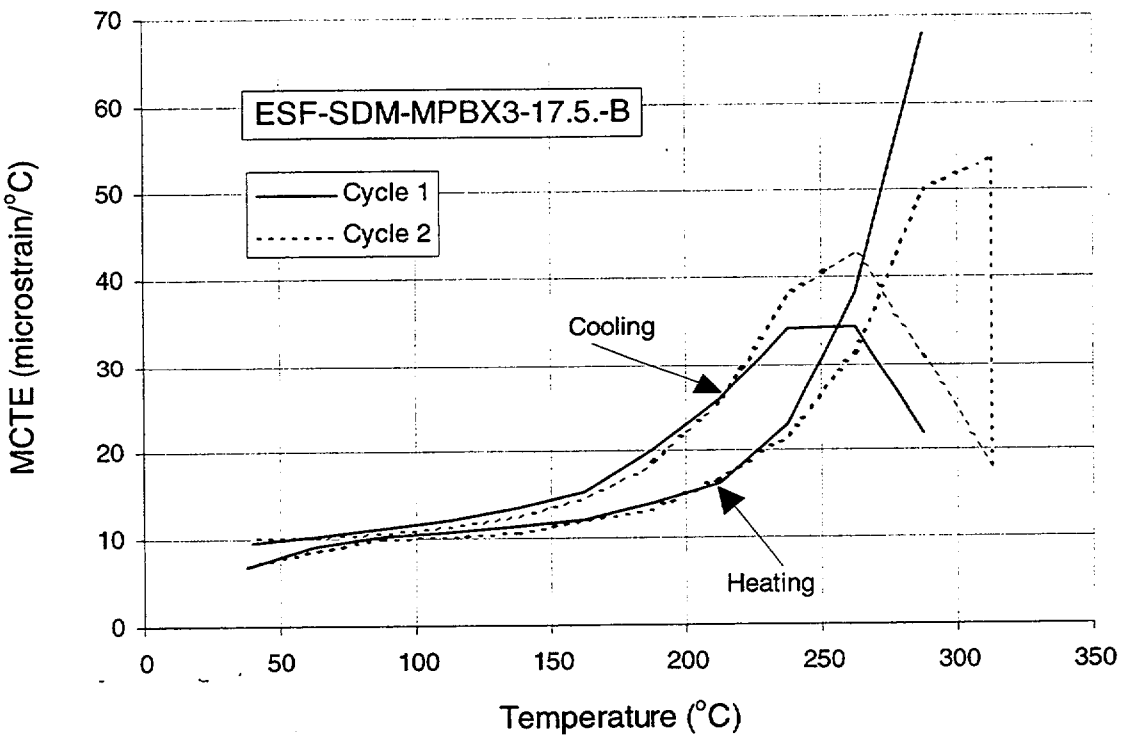

NOTE: These specimens are from the TSw2 thermal/mechanical unit and the Tptpmn lithostratigraphic unit.

Figure B-11. Plots of Strain Versus Temperature (Top) and MCTE Versus Temperature (Bottom) for Specimen ESF-SDM-MPBX3-17.5-B.

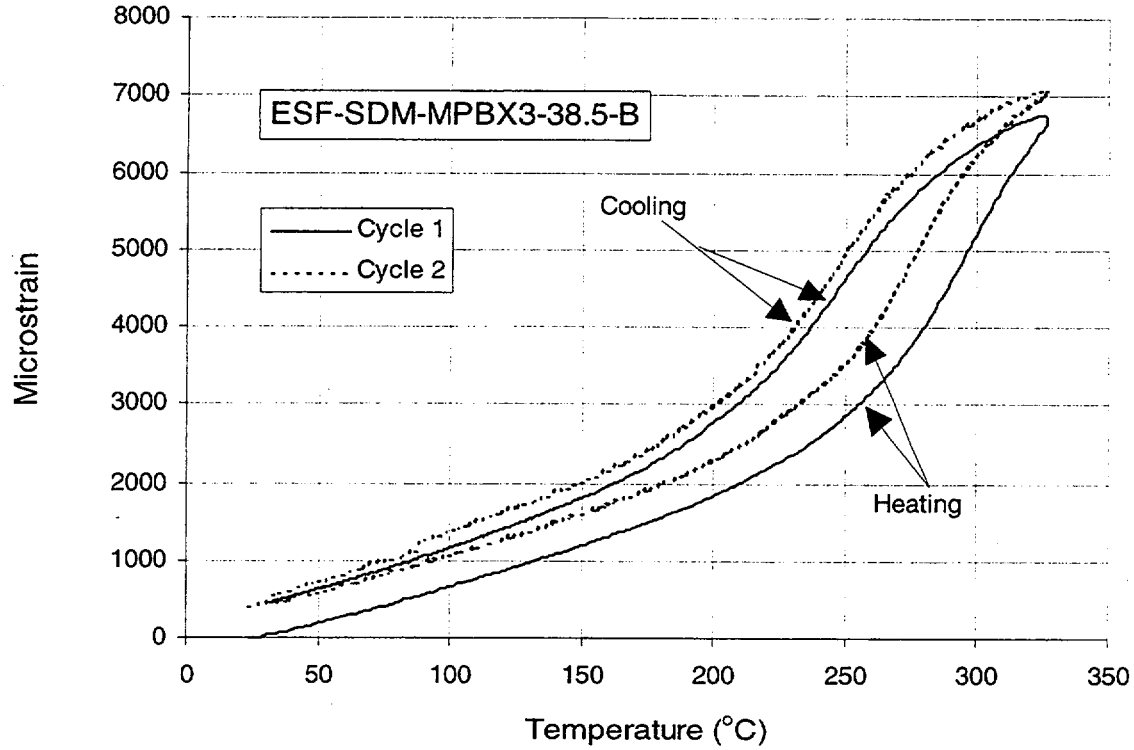

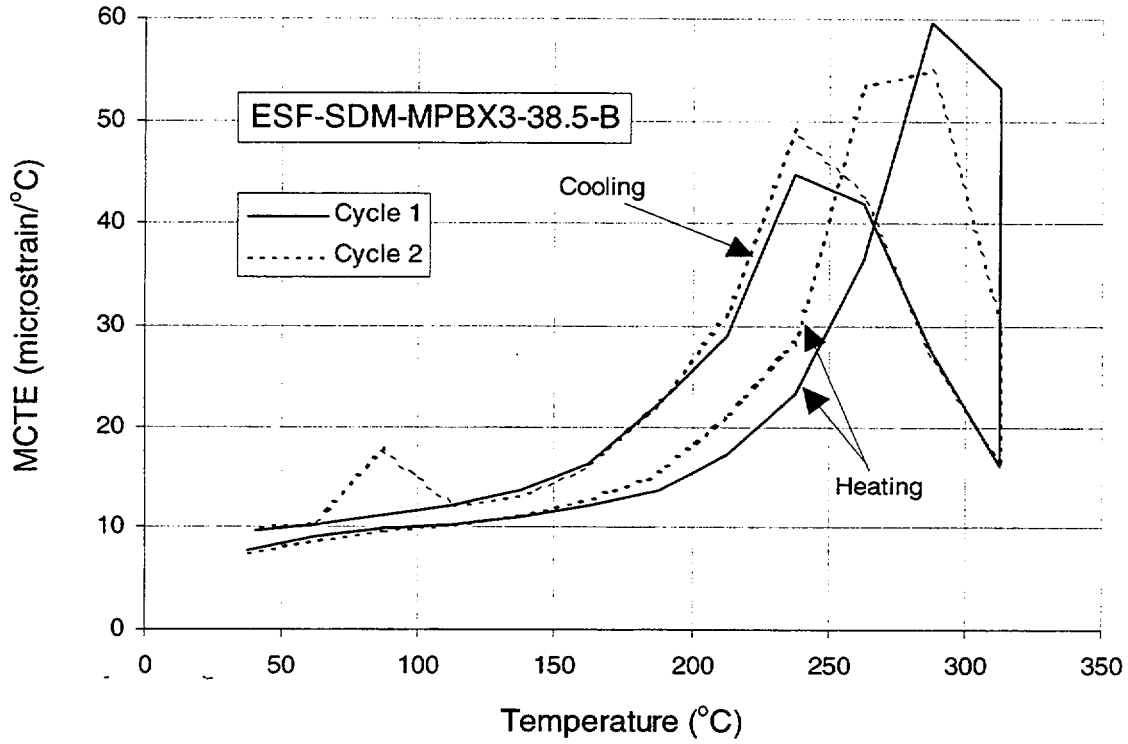

NOTE: These specimens are from the TSw2 thermal/mechanical unit and the Tptpmn lithostratigraphic unit.

Figure B-12. Plots of Strain Versus Temperature (Top) and MCTE Versus Temperature (Bottom) for Specimen ESF-SDM-MPBX3-38.5-B.

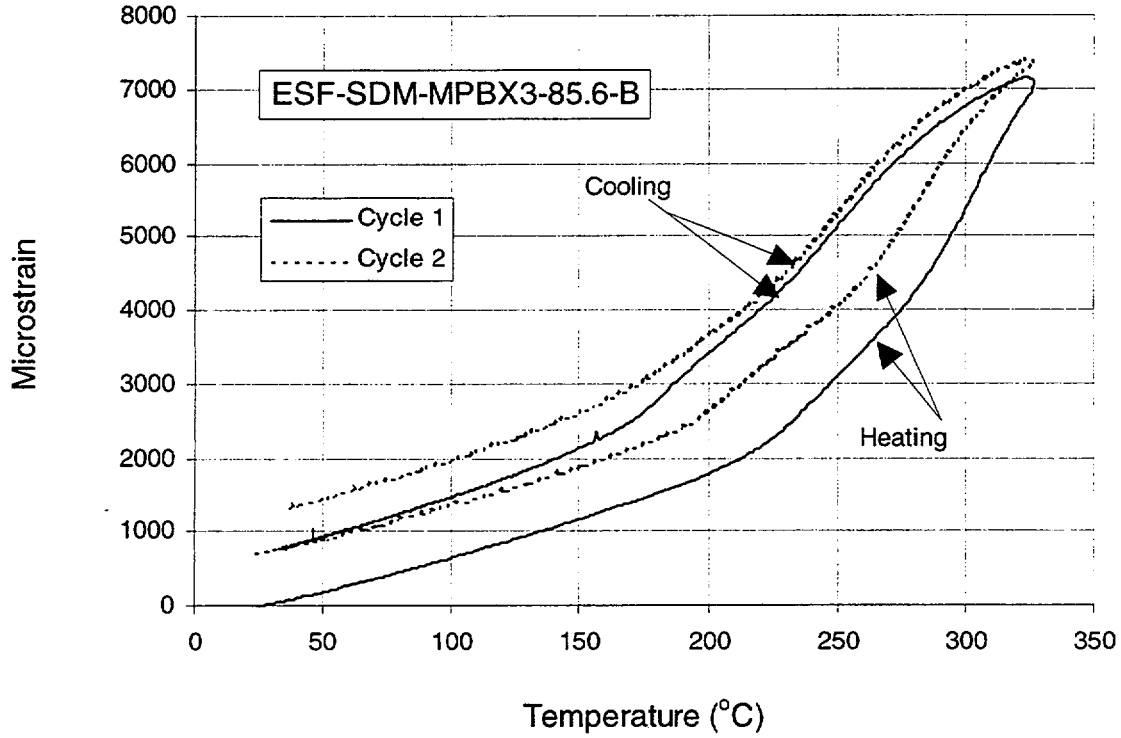

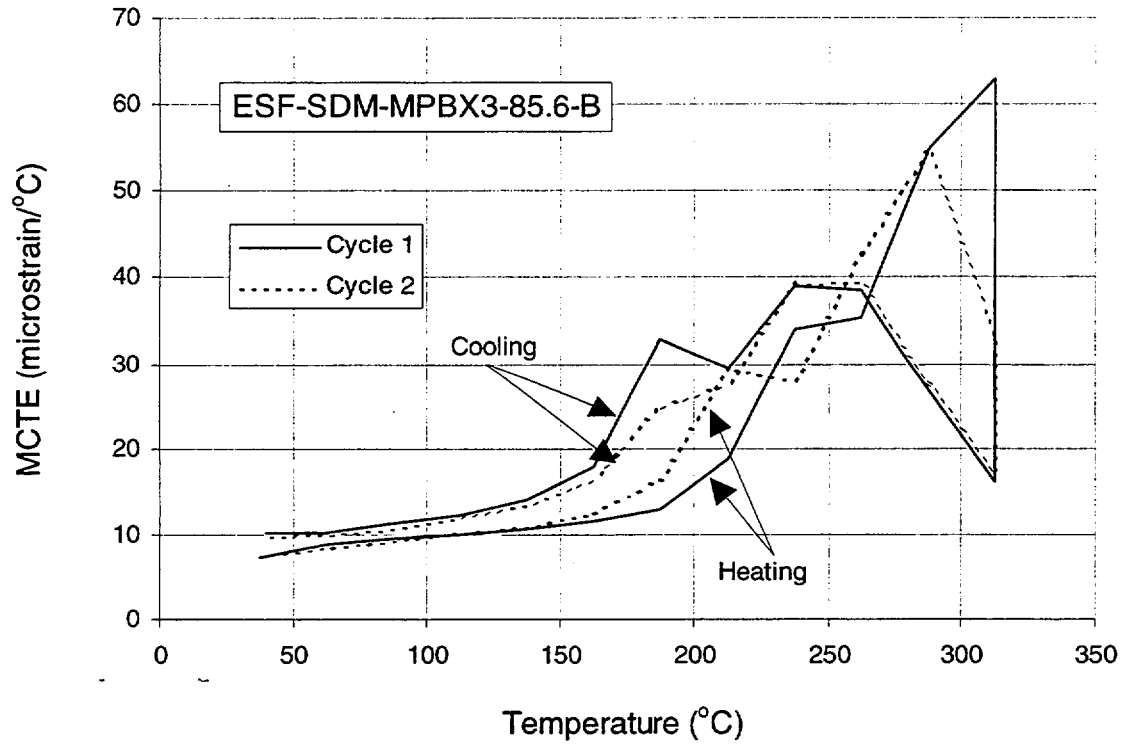

NOTE: These specimens are from the TSw2 thermal/mechanical unit and the Tptpmn lithostratigraphic unit.

Figure B-13. Plots of Strain Versus Temperature (Top) and MCTE Versus Temperature (Bottom) for Specimen ESF-SDM-MPBX3-85.6-B.

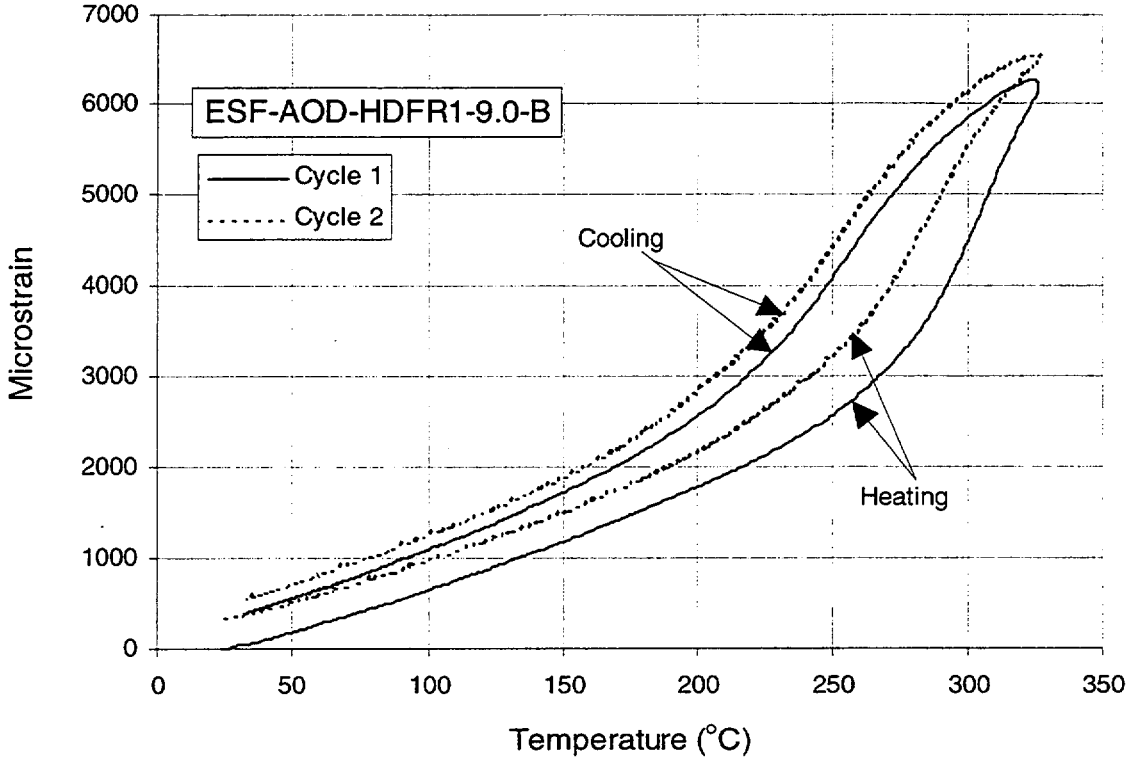

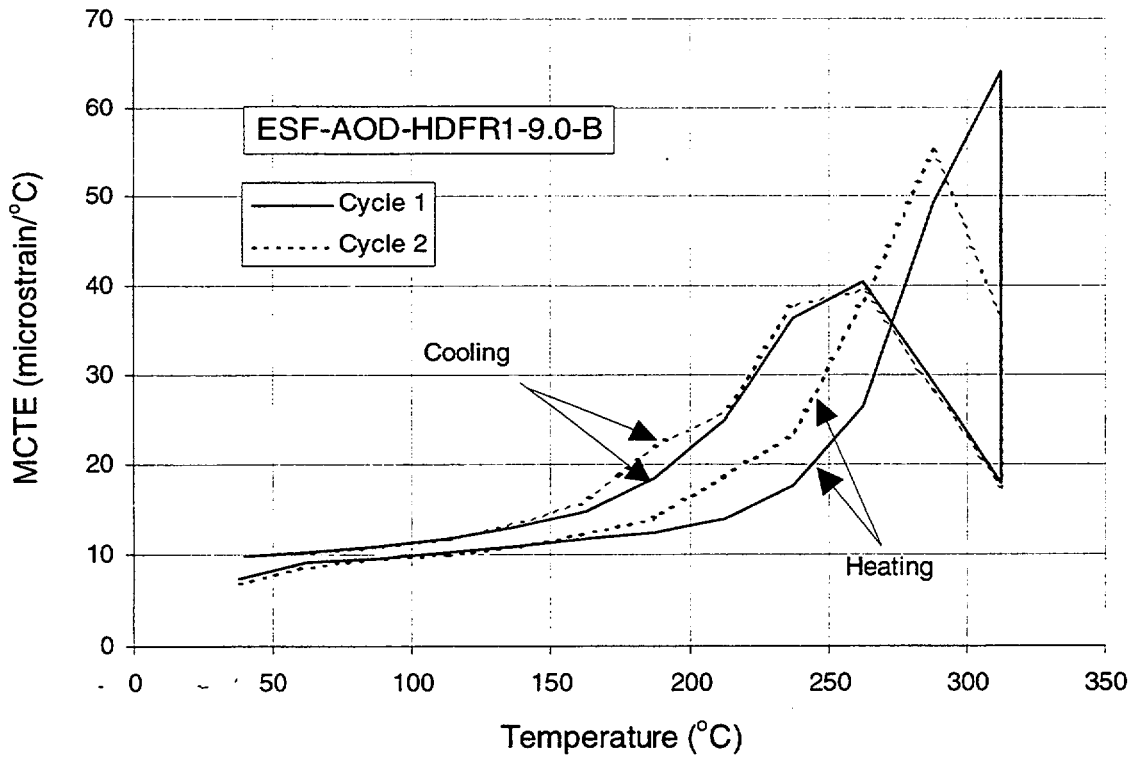

NOTE: These specimens are from the TSw2 thermal/mechanical unit and the Tptpmn lithostratigraphic unit.

Figure B-14. Plots of Strain Versus Temperature (Top) and MCTE Versus Temperature (Bottom) for Specimen ESF-AOD-HDFR1-9.0-B.

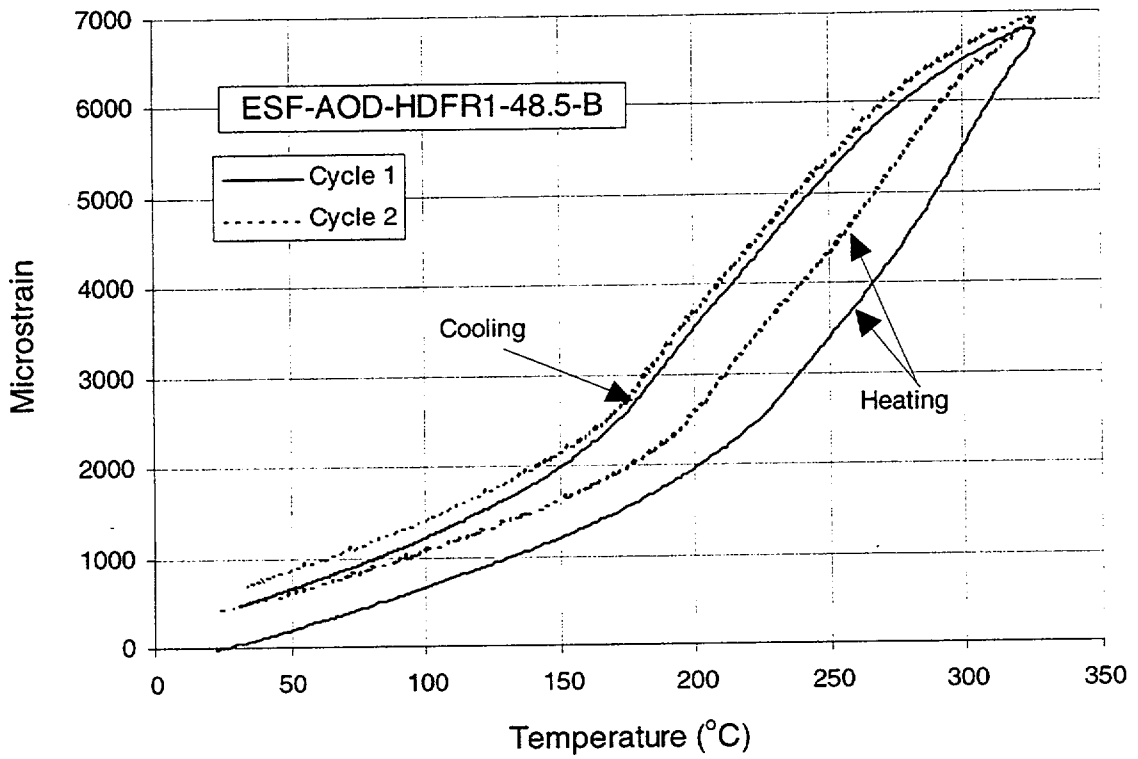

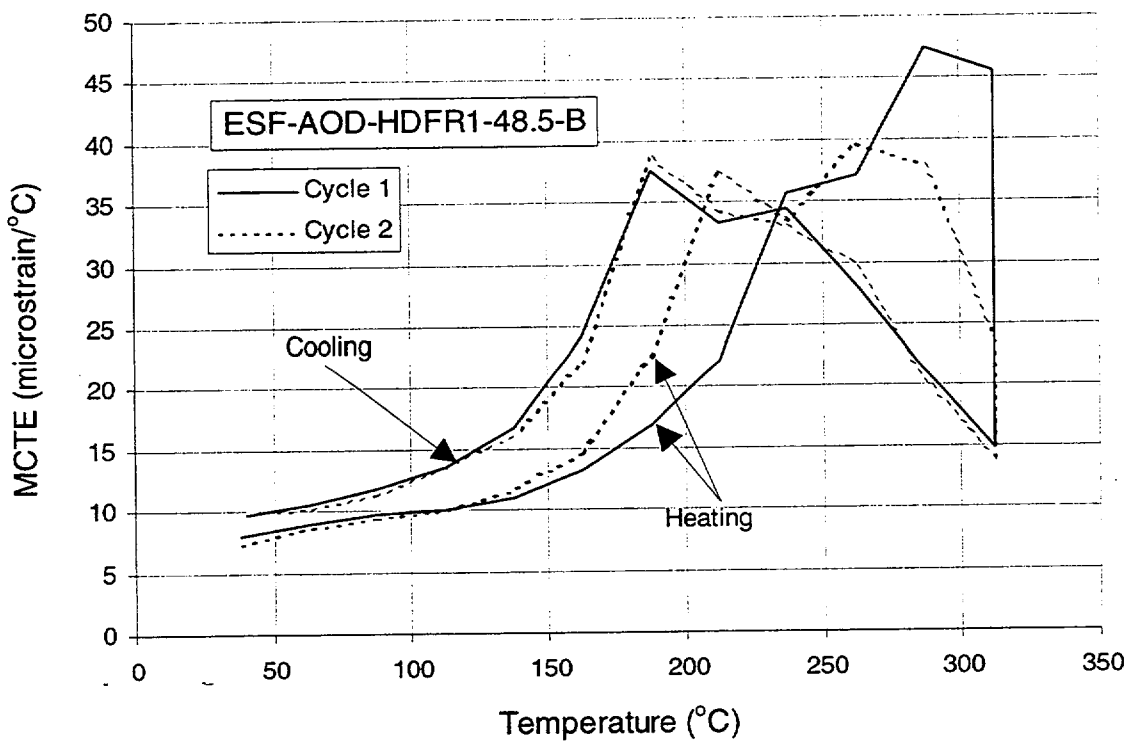

NOTE: These specimens are from the TSw2 thermal/mechanical unit and the Tptpmn lithostratigraphic unit.

Figure B-15. Plots of Strain Versus Temperature (Top) and MCTE Versus Temperature (Bottom) for Specimen ESF-AOD-HDFR1-48.5-B.

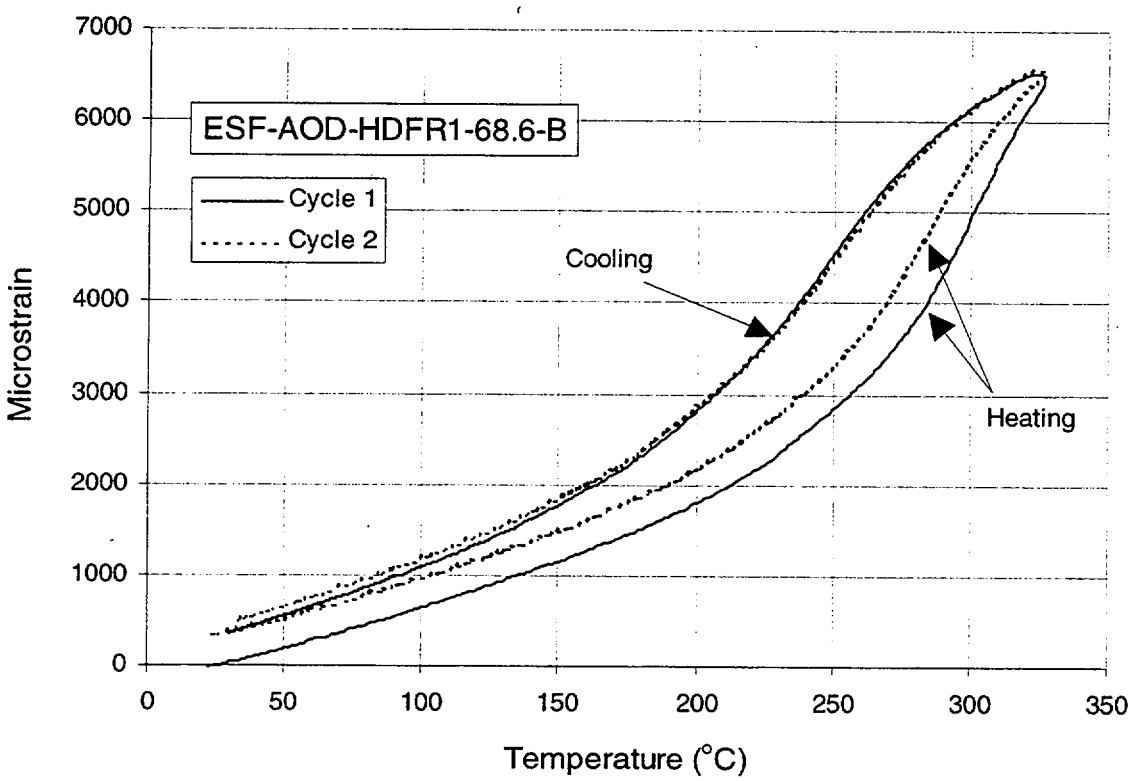

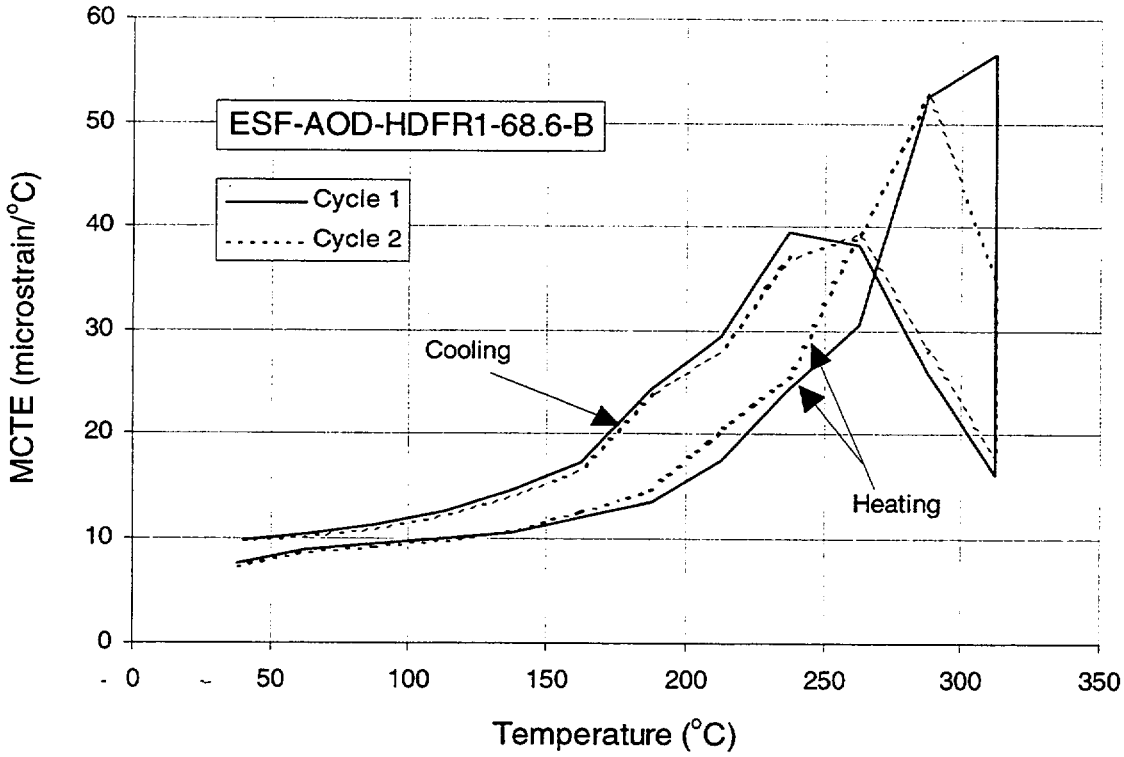

NOTE: These specimens are from the TSw2 thermal/mechanical unit and the Tptpmn lithostratigraphic unit.

Figure B-16. Plots of Strain Versus Temperature (Top) and MCTE Versus Temperature (Bottom) for Specimen ESF-AOD-HDFR1-68.6-B.

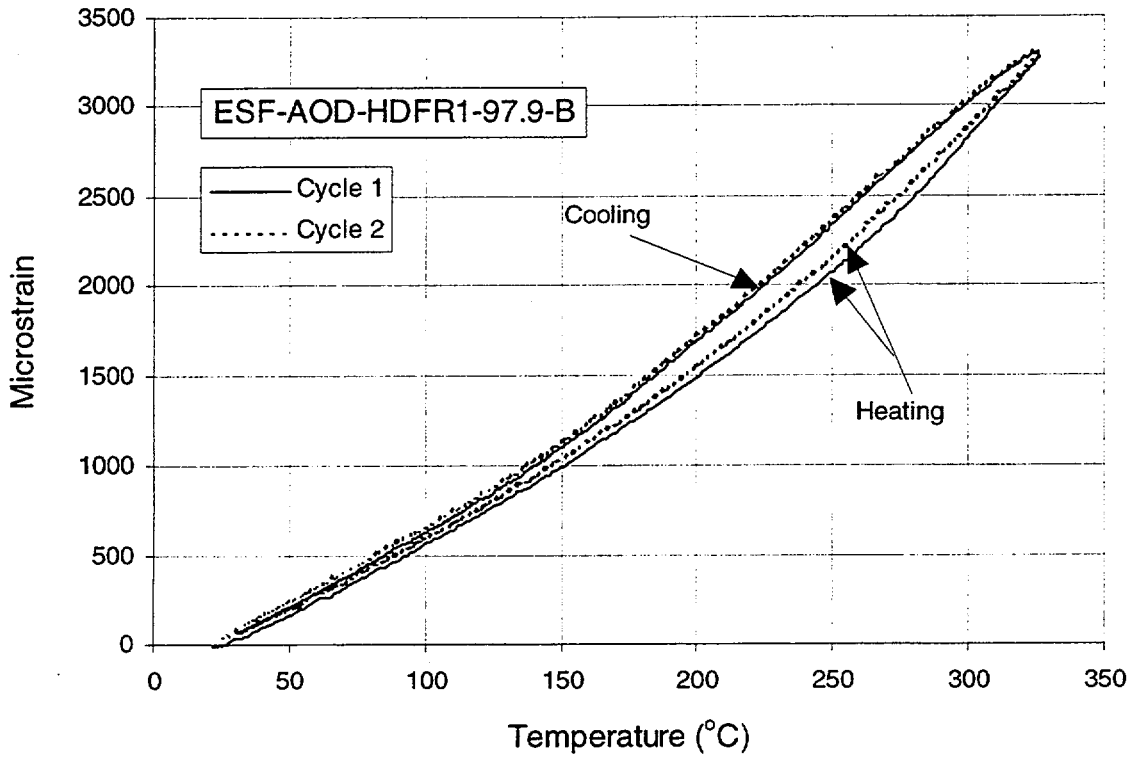

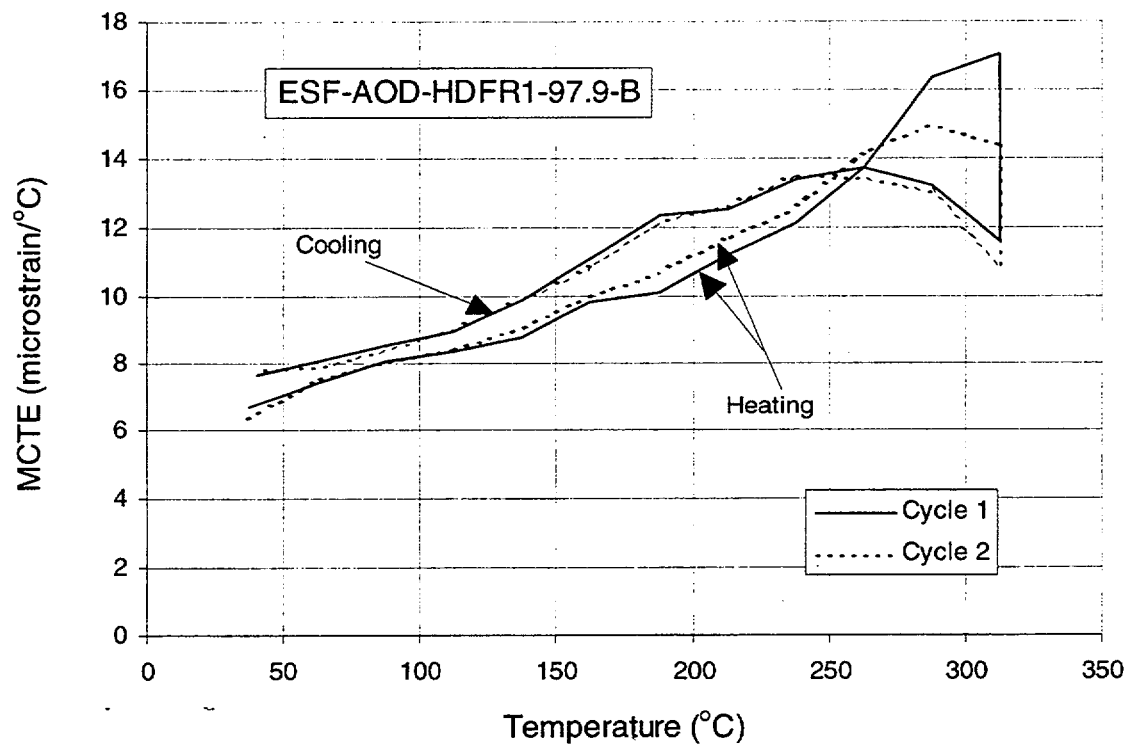

NOTE: These specimens are from the TSw2 thermal/mechanical unit and from either the Tptpmn or the Tptpmn lithostratigraphic unit.

Figure B-17. Plots of Strain Versus Temperature (Top) and MCTE Versus Temperature (Bottom) for Specimen ESF-AOD-HDFR1-97.9-B.

INTENTIONALLY LEFT BLANK

APPENDIX C

MECHANICAL PROPERTIES DATA: STRESS-STRAIN DIAGRAMS

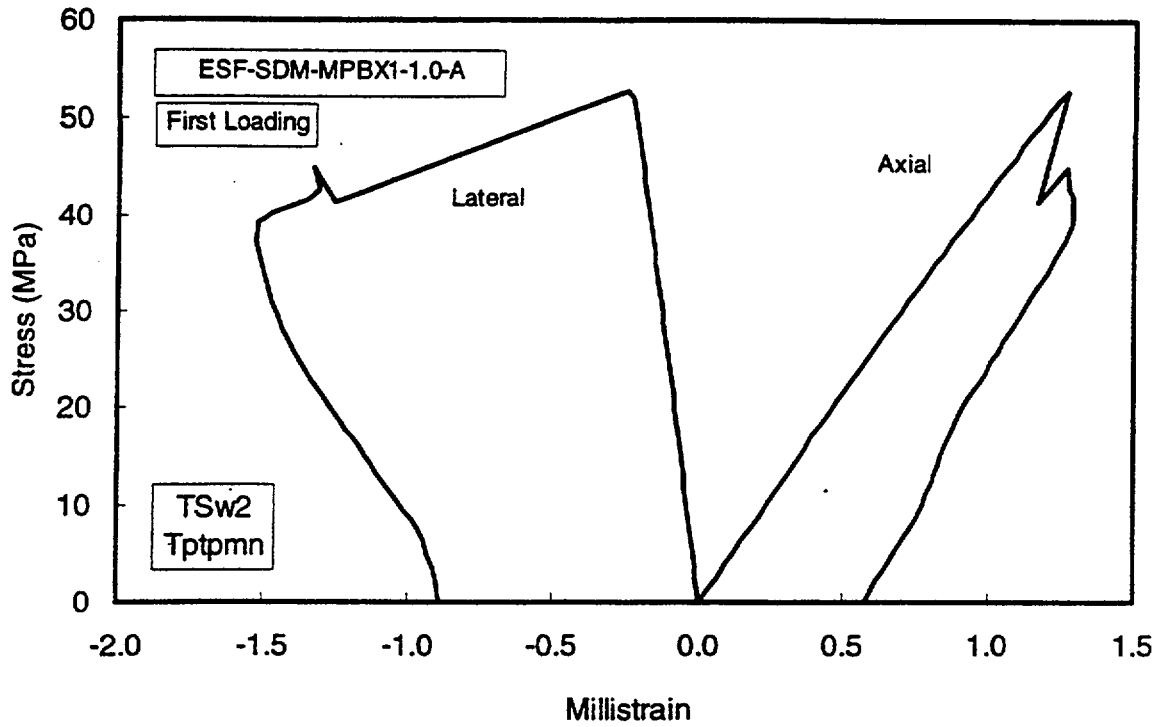

NOTE: Specimen is from TSw2 thermal/mechanical unit and Tptpmn lithostratigraphic unit.

Figure C-1. Stress-Strain Curves for Test UCDST001 on Specimen ESF-SDM-MPBX1-1.0-A

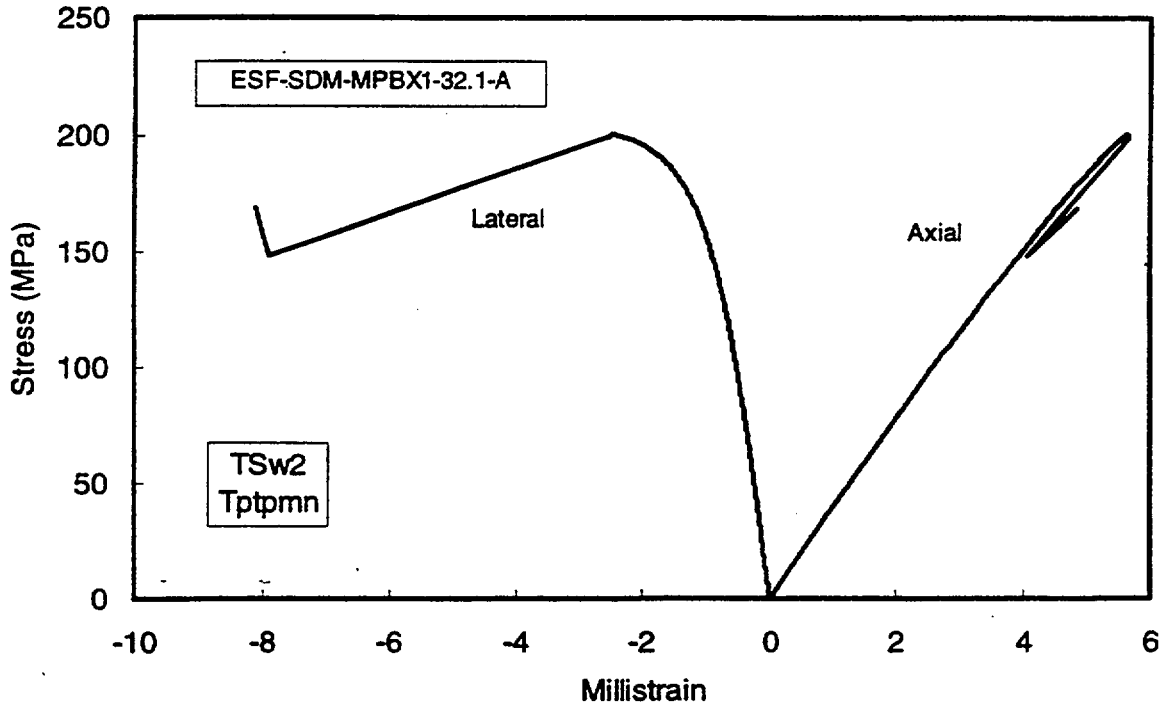

NOTE: Specimen is from TSw2 thermal/mechanical unit and Tptpmn lithostratigraphic unit.

Figure C-2. Stress-Strain Curves for Test UCDST002 on Specimen ESF-SDM-MPBX1-32.1-A

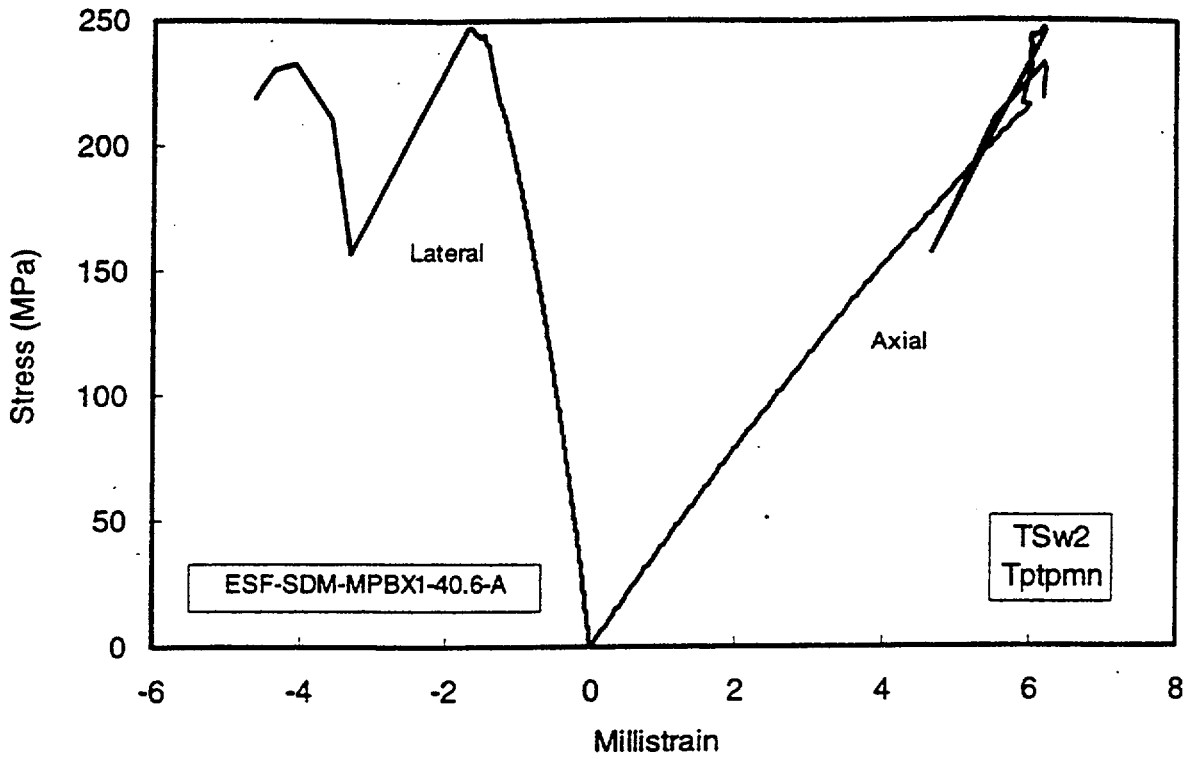

NOTE: Specimen is from TSw2 thermal/mechanical unit and Tptpmn lithostratigraphic unit.

Figure C-3. Stress-Strain Curves for Test UCDST003 on Specimen ESF-SDM-MPBX1-40.6-A

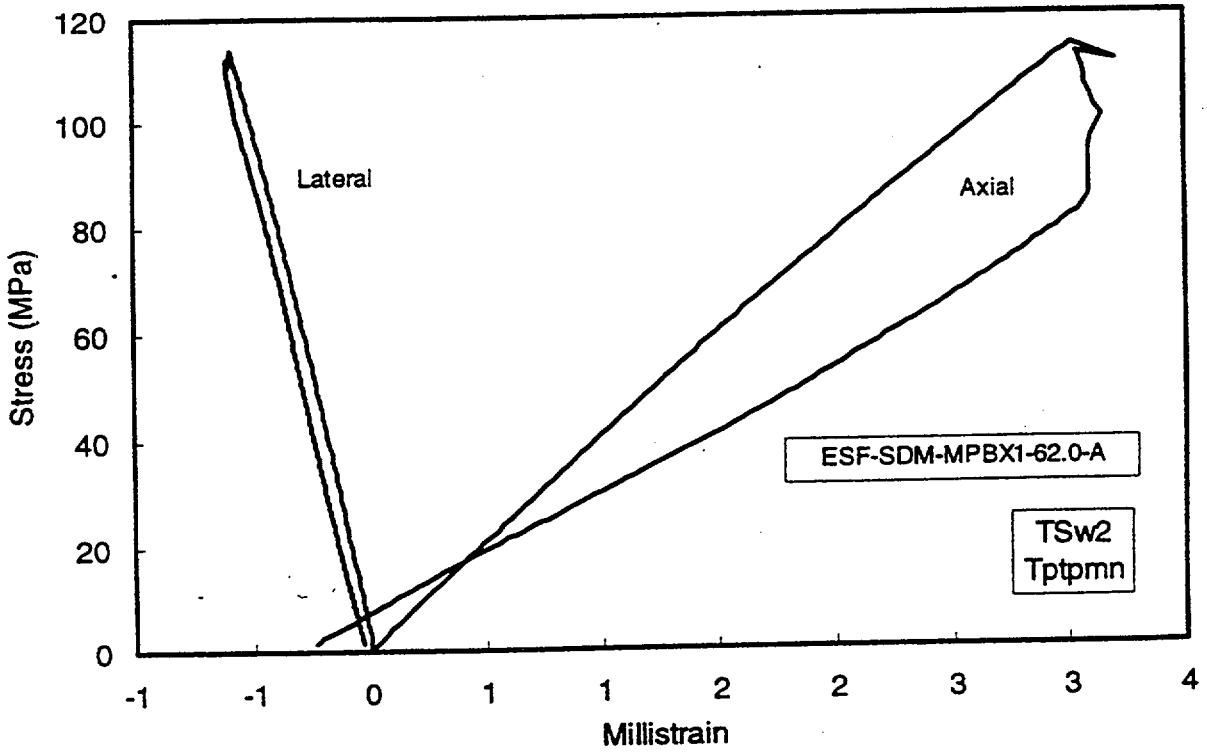

NOTE: Specimen is from TSw2 thermal/mechanical unit and Tptpmn lithostratigraphic unit.

Figure C-4. Stress-Strain Curves for Test UCDST004 on Specimen ESF-SDM-MPBX1-62.0-A

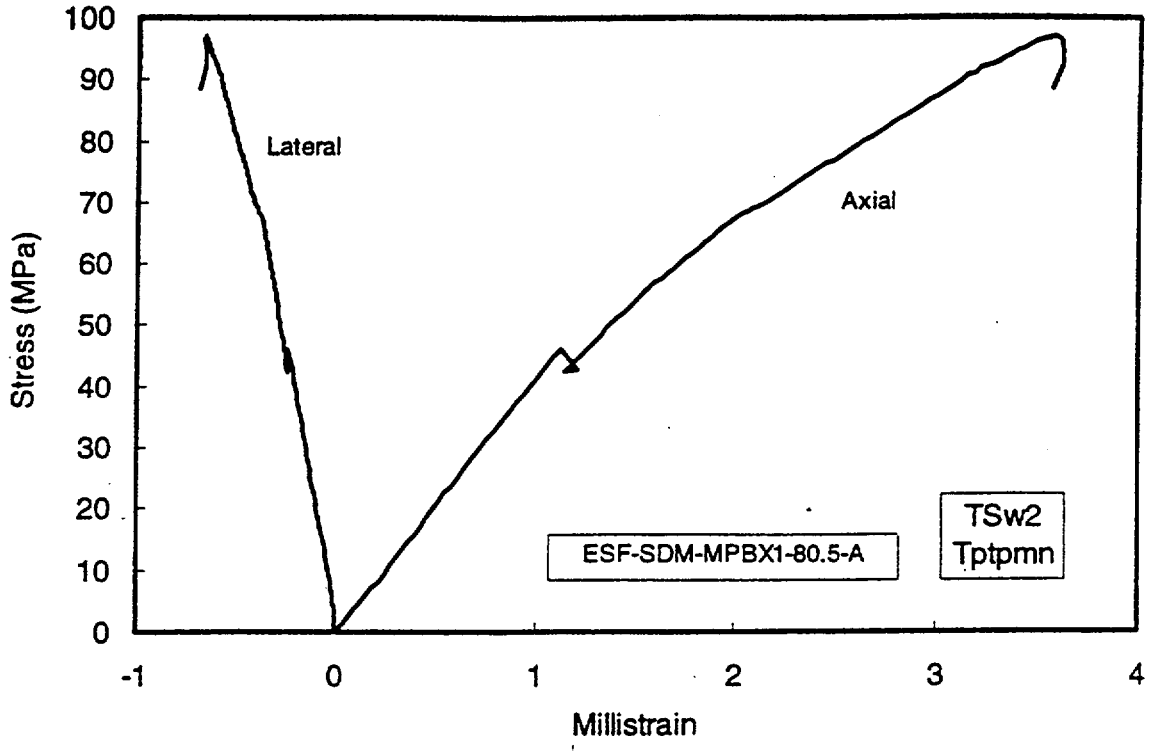

NOTE: Specimen is from TSw2 thermal/mechanical unit and Tptpmn lithostratigraphic unit.

Figure C-5. Stress-Strain Curves for Test UCDST005 on Specimen ESF-SDM-MPBX1-80.5-A

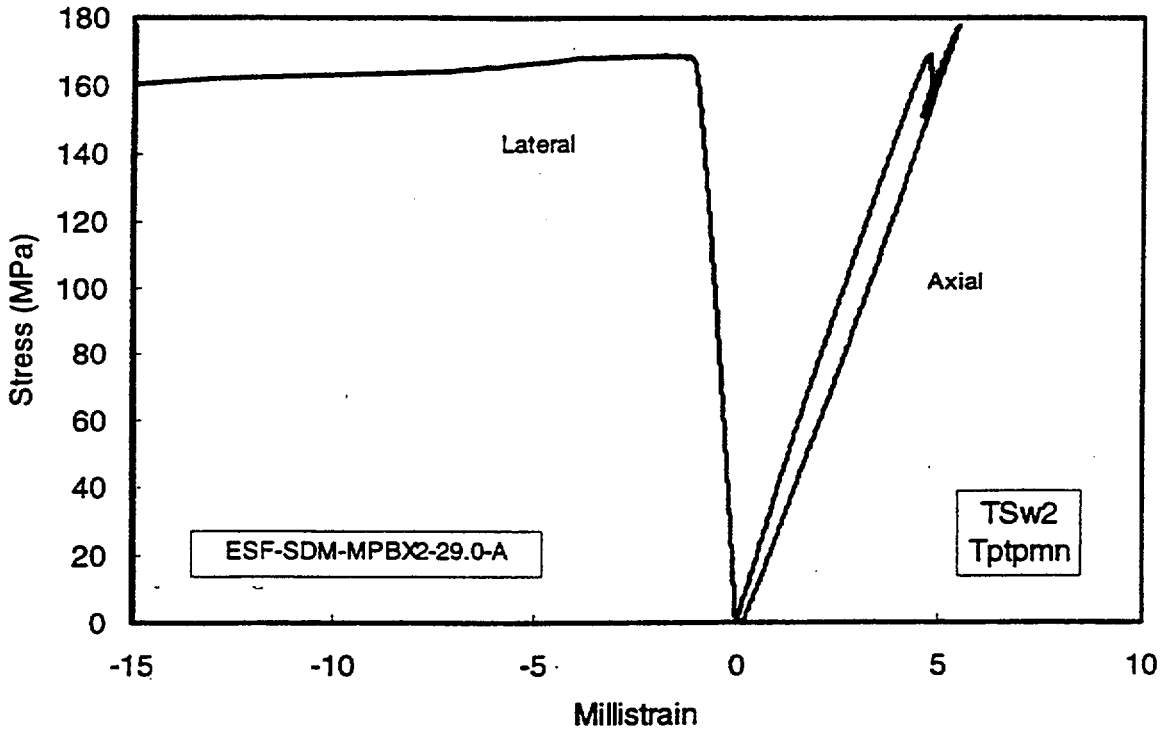

NOTE: Specimen is from TSw2 thermal/mechanical unit and Tptpmn lithostratigraphic unit.

Figure C-6. Stress-Strain Curves for Test UCDST006 on Specimen ESF-SDM-MPBX2-29.0-A

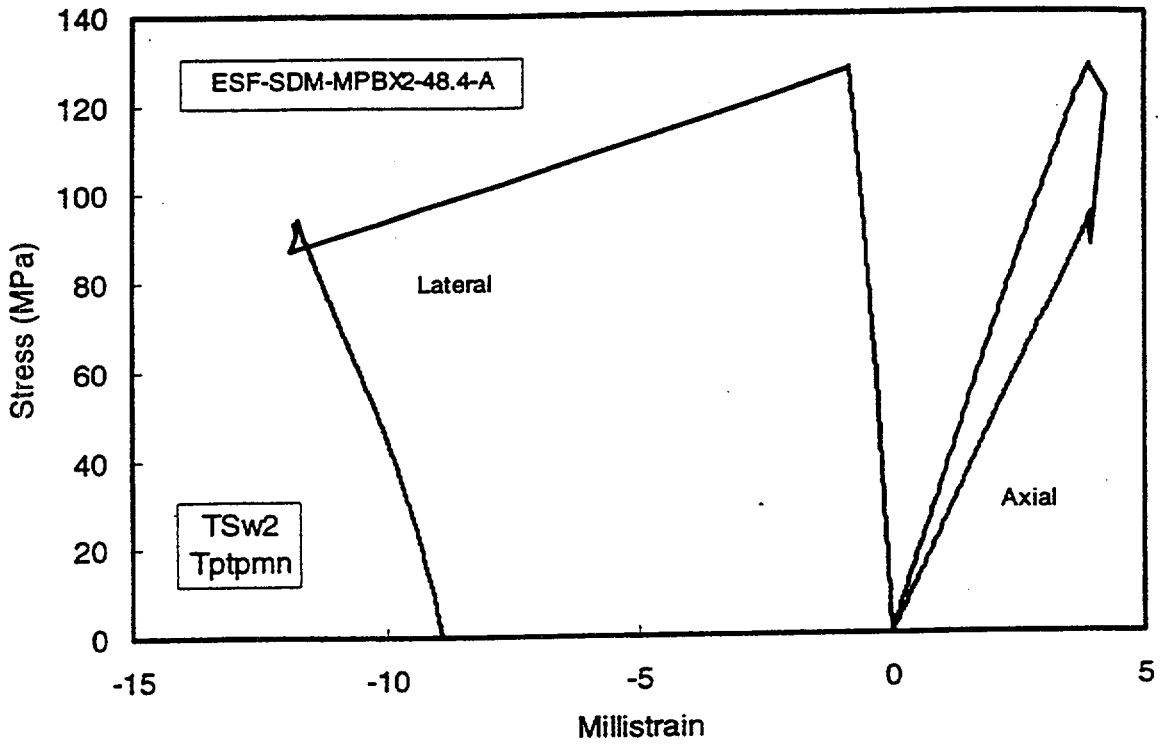

NOTE: Specimen is from TSw2 thermal/mechanical unit and Tptpmn lithostratigraphic unit.

Figure C-7. Stress-Strain Curves for Test UCDST007 on Specimen ESF-SDM-MPBX2-48.4-A

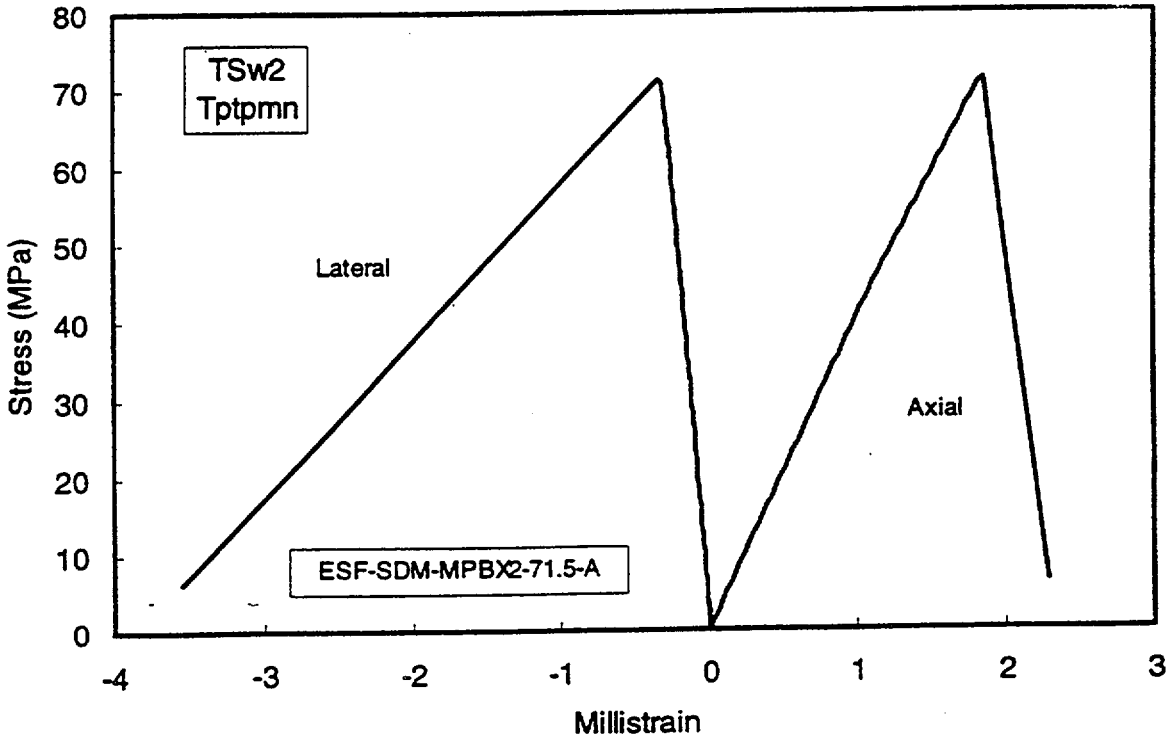

NOTE: Specimen is from TSw2 thermal/mechanical unit and Tptpmn lithostratigraphic unit.

Figure C-8. Stress-Strain Curves for Test UCDST008 on Specimen ESF-SDM-MPBX2-71.5-A

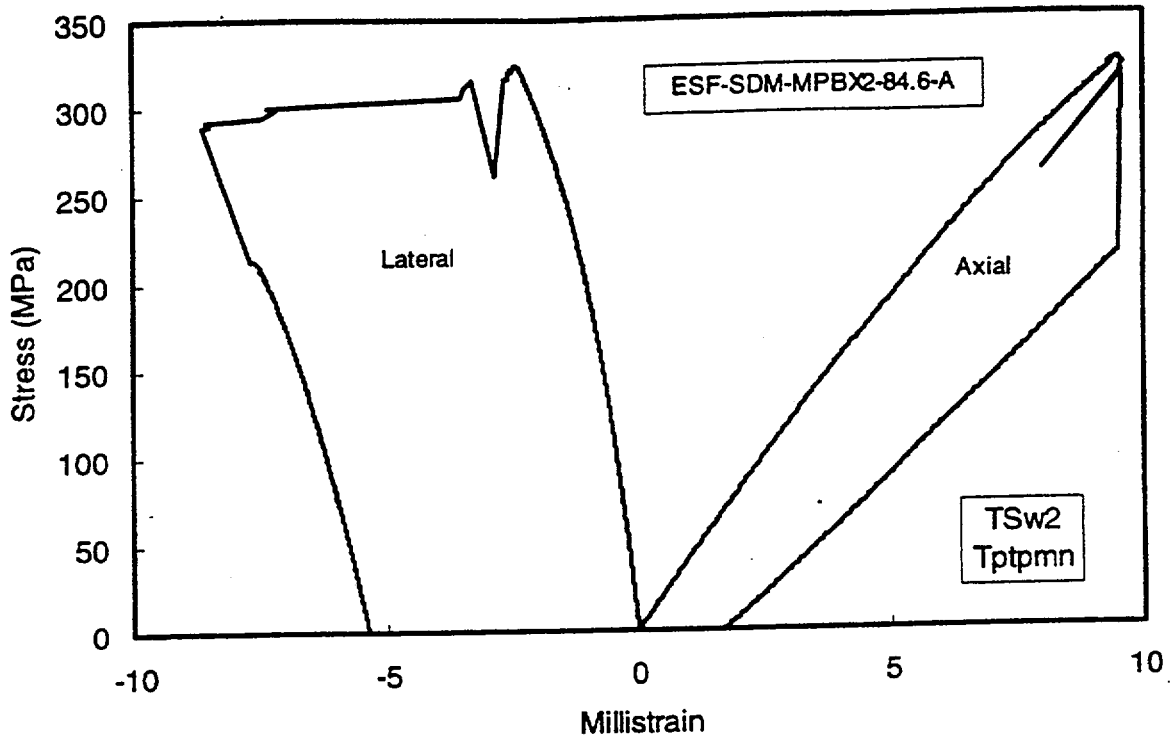

NOTE: Specimen is from TSw2 thermal/mechanical unit and Tptpmn lithostratigraphic unit.

Figure C-9. Stress-Strain Curves for Test UCDST009 on Specimen ESF-SDM-MPBX2-84.6-A

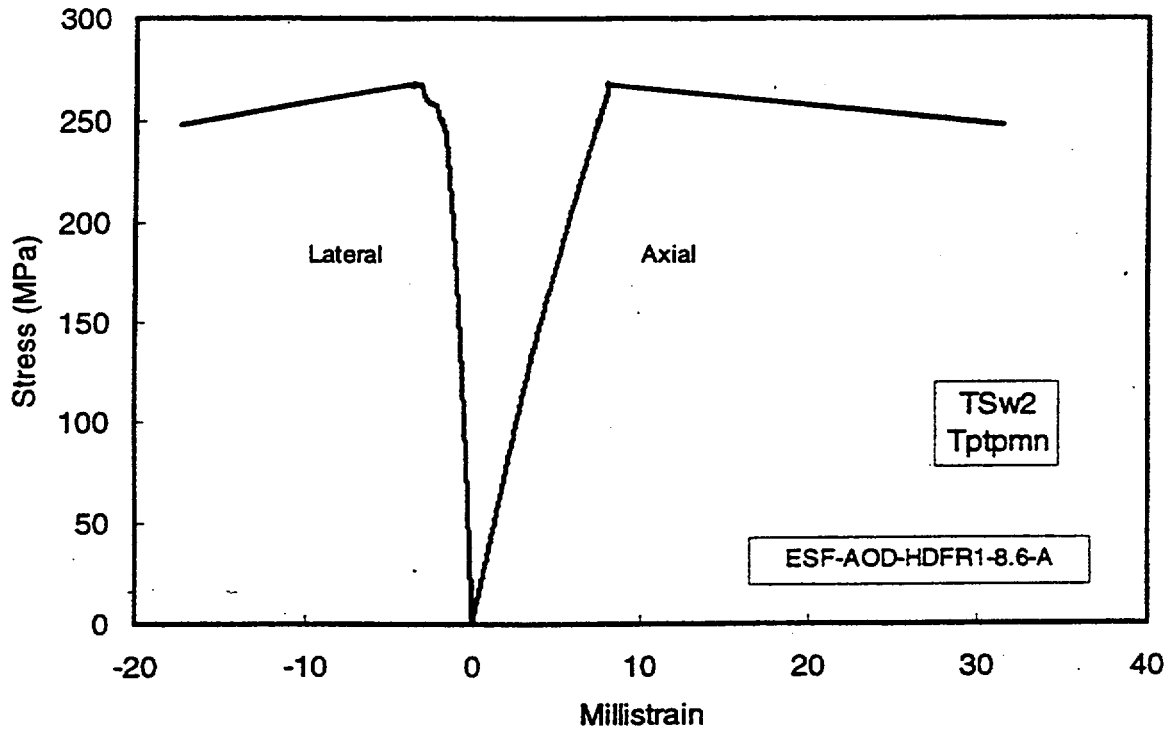

NOTE: Specimen is from TSw2 thermal/mechanical unit and Tptpmn lithostratigraphic unit.

Figure C-10. Stress-Strain Curves for Test UCDST010 on Specimen ESF-AOD-HDFR1-8.6-A

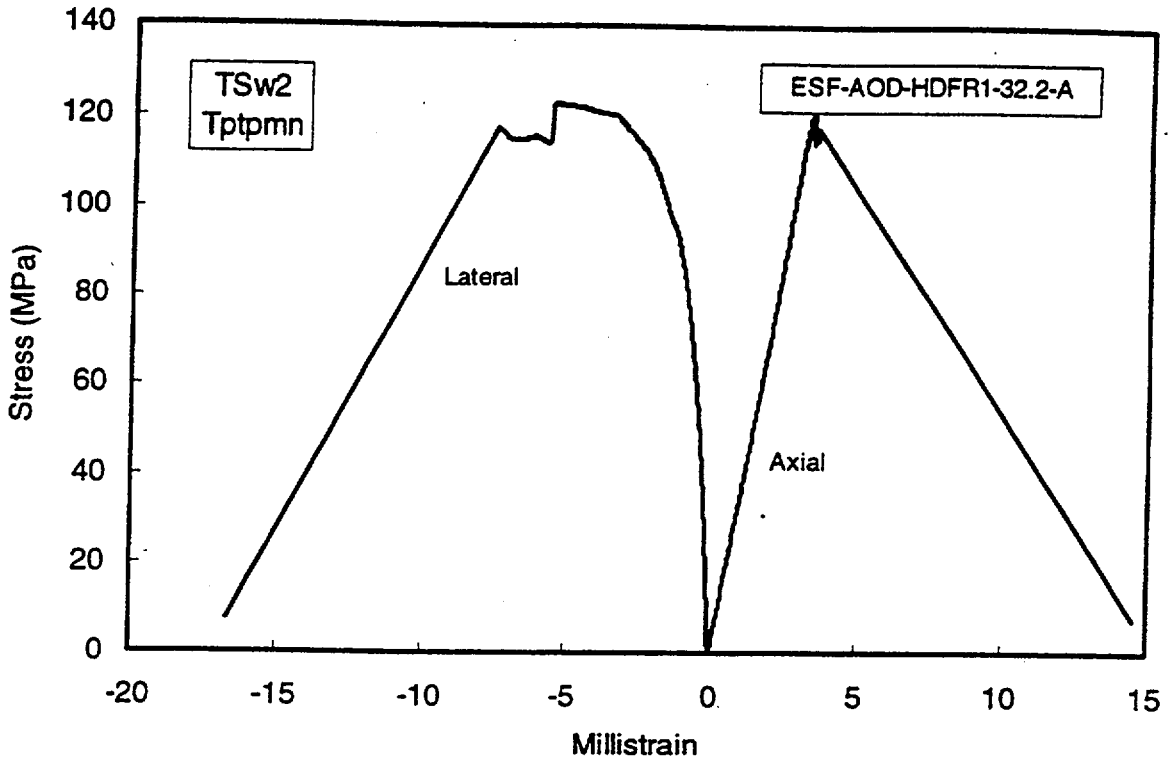

NOTE: Specimen is from TSw2 thermal/mechanical unit and Tptpmn lithostratigraphic unit.

Figure C-11. Stress-Strain Curves for Test UCDST011 on Specimen ESF-AOD-HDFR1-32.2-A

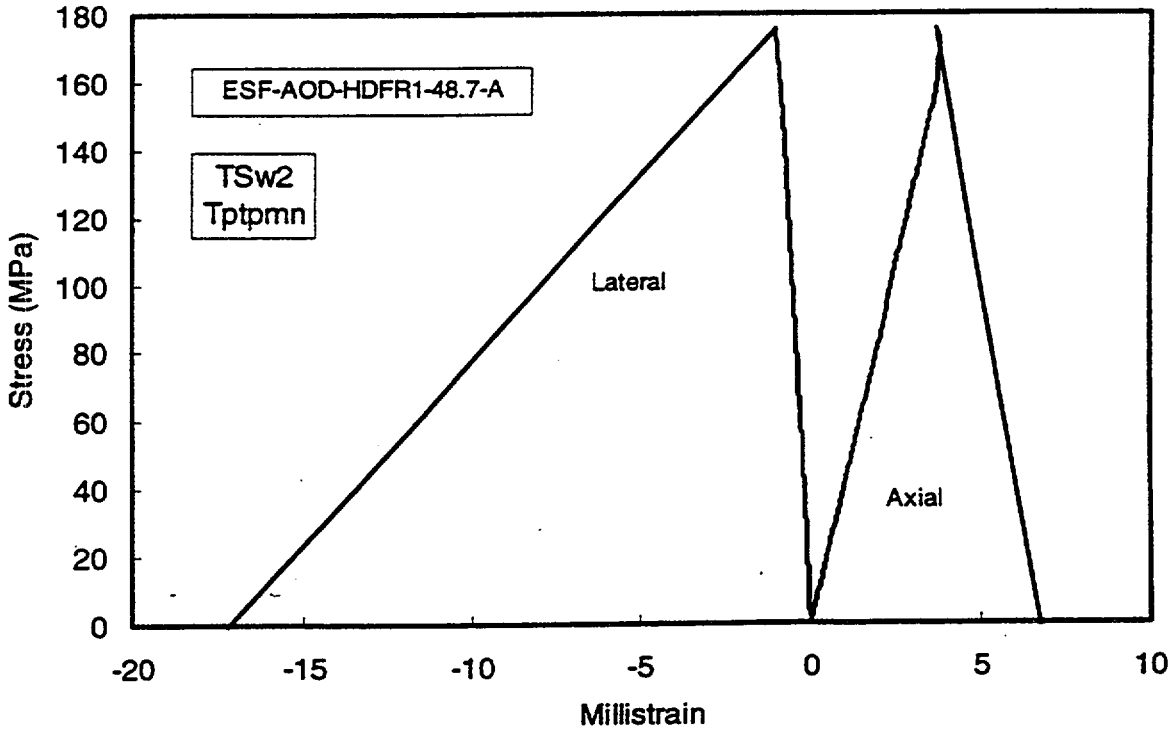

NOTE: Specimen is from TSw2 thermal/mechanical unit and Tptpmn lithostratigraphic unit.

Figure C-12. Stress-Strain Curves for Test UCDST012 on Specimen ESF-AOD-HDFR1-48.7-A

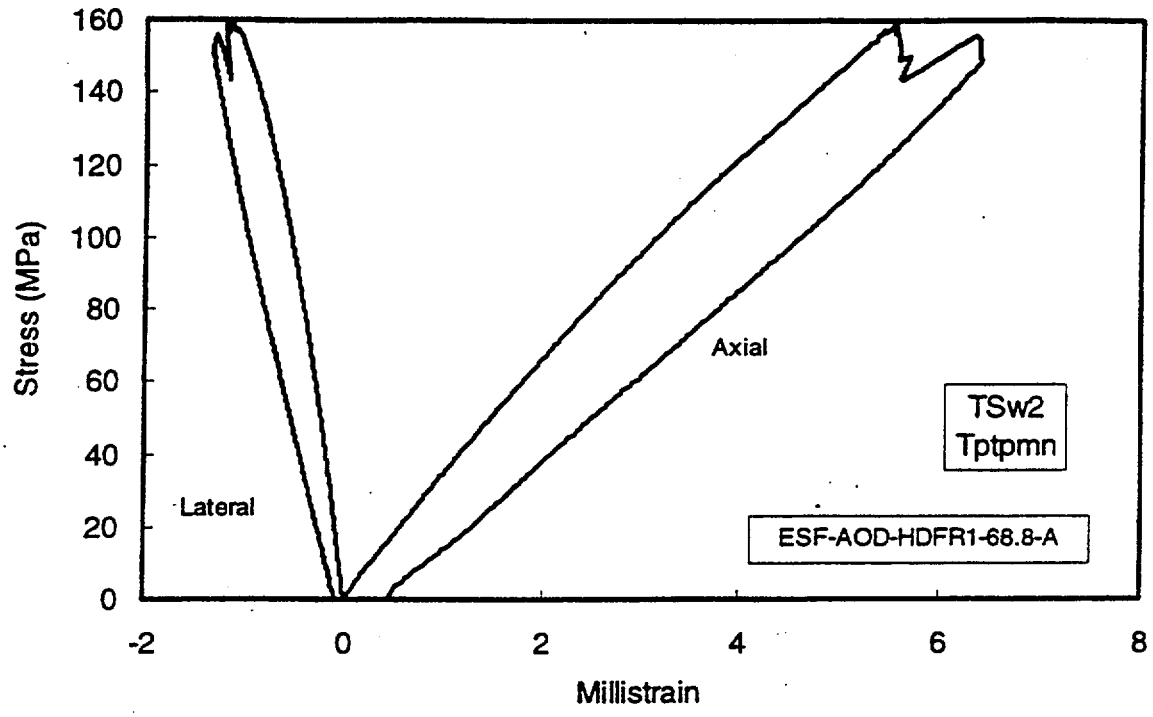

NOTE: Specimen is from TSw2 thermal/mechanical unit and Tptpmn lithostratigraphic unit.

Figure C-13. Stress-Strain Curves for Test UCDST013 on Specimen ESF-AOD-HDFR1-68.8-A

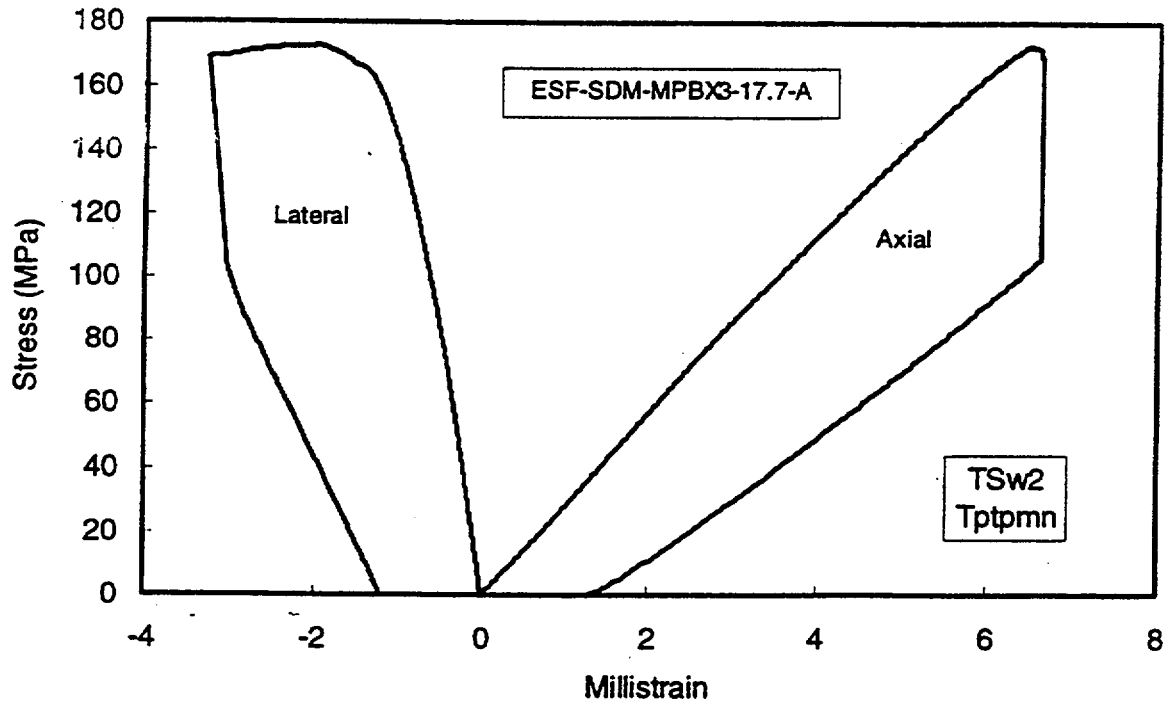

NOTE: Specimen is from TSw2 thermal/mechanical unit and Tptpmn lithostratigraphic unit.

Figure C-14. Stress-Strain Curves for Test UCDST014 on Specimen ESF-SDM-MPBX3-17.7-A

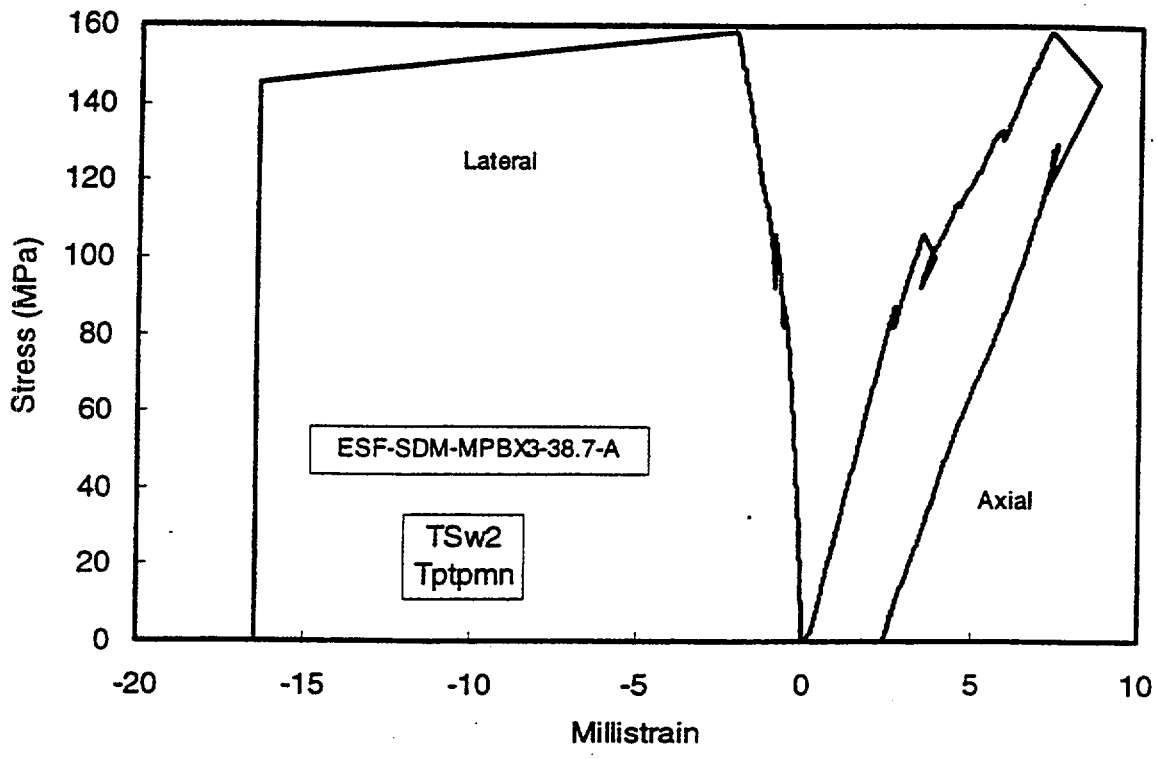

NOTE: Specimen is from TSw2 thermal/mechanical unit and Tptpmn lithostratigraphic unit.

Figure C-15. Stress-Strain Curves for Test UCDST015 on Specimen ESF-SDM-MPBX3-38.7-A

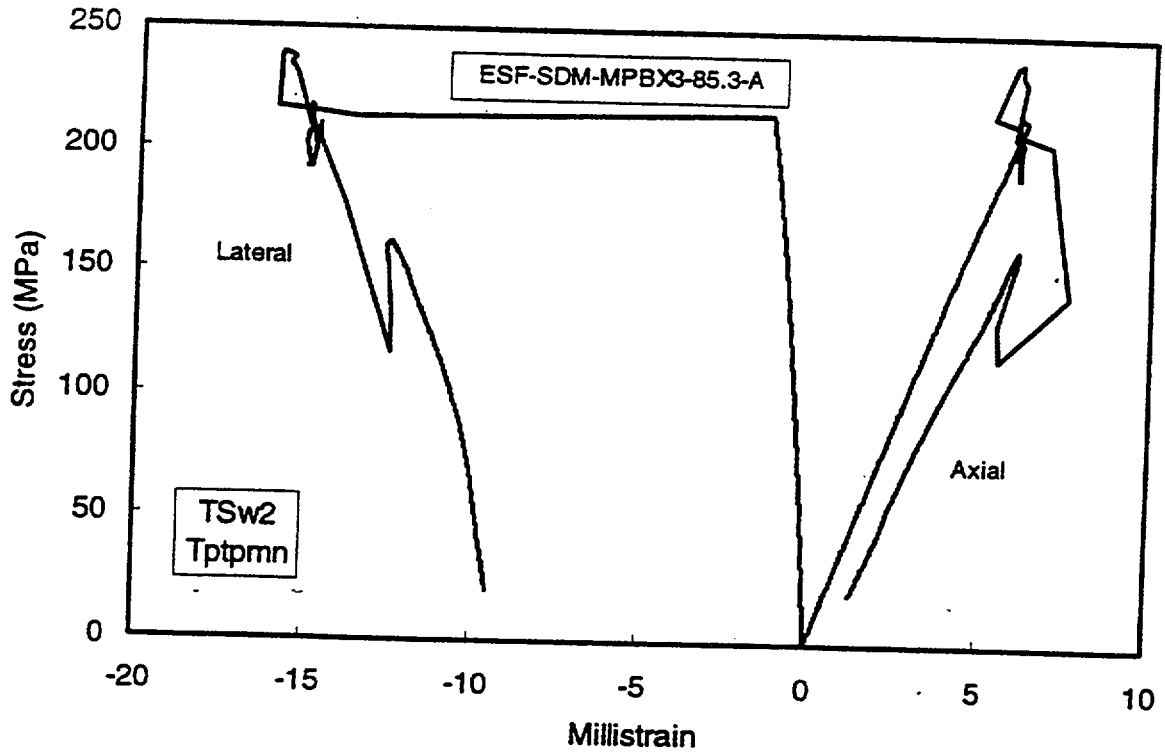

NOTE: Specimen is from TSw2 thermal/mechanical unit and Tptpmn lithostratigraphic unit.

Figure C-16. Stress-Strain Curves for Test UCDST016 on Specimen ESF-SDM-MPBX3-85.3-A

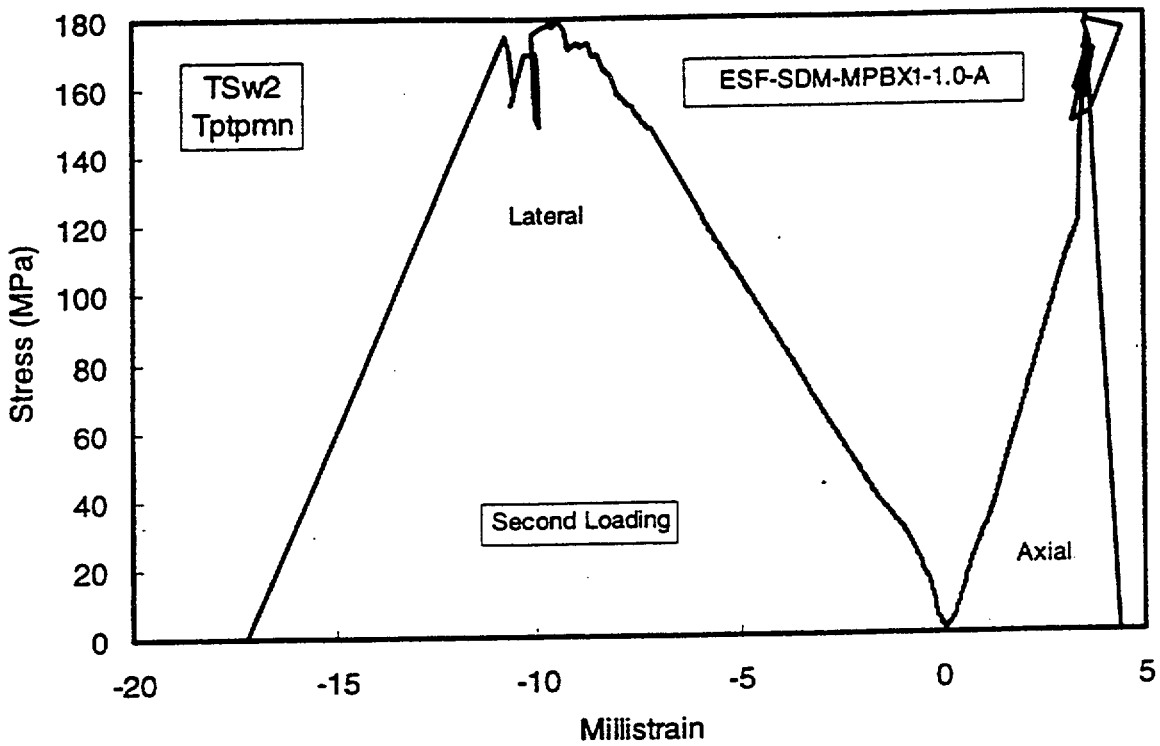

NOTE: Specimen is from TSw2 thermal/mechanical unit and Tptpmn lithostratigraphic unit.

Figure C-17. Stress-Strain Curves for Test UCDST017 on Specimen ESF-SDM-MPBX1-1.0-A

INTENTIONALLY LEFT BLANK

APPENDIX D

HYDROLOGICAL PROPERTIES DATA: GRAPHICAL PRESENTATION

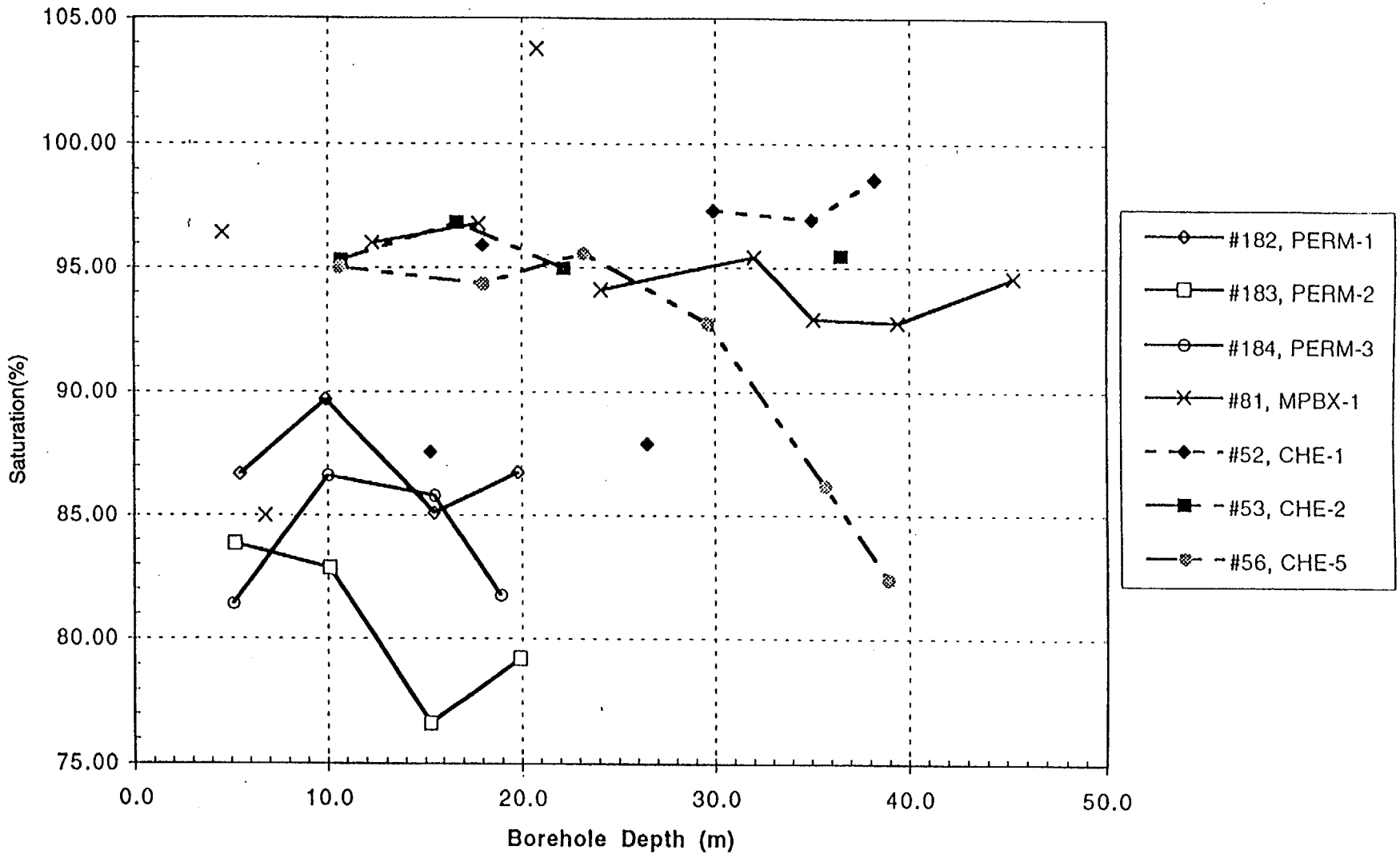

Figure D-1. DST Saturation: DST Dry and Wet Drilled Core Measurement

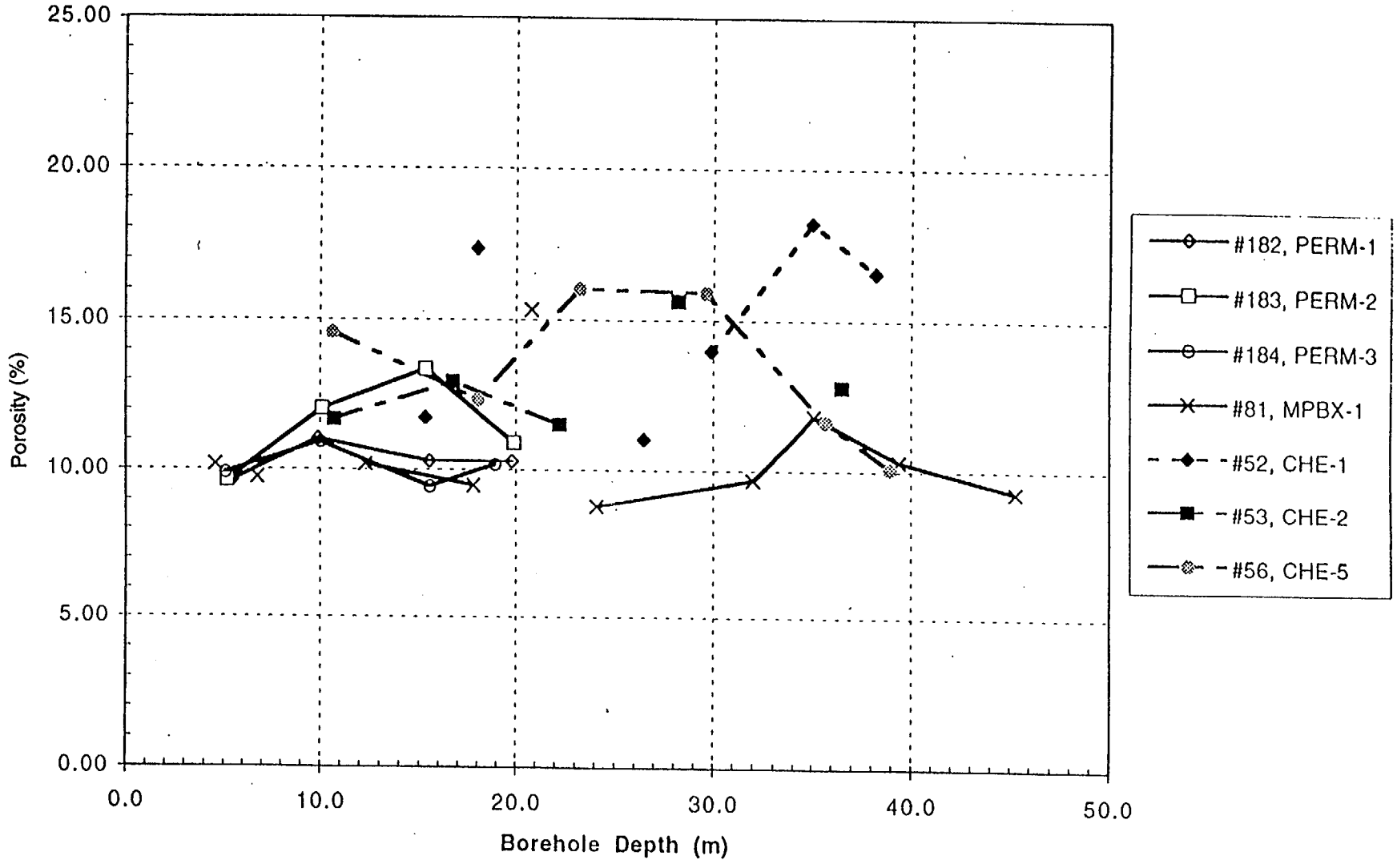

Figure D-2. DST Porosity: DST Dry and Wet Drilled Core Measurement

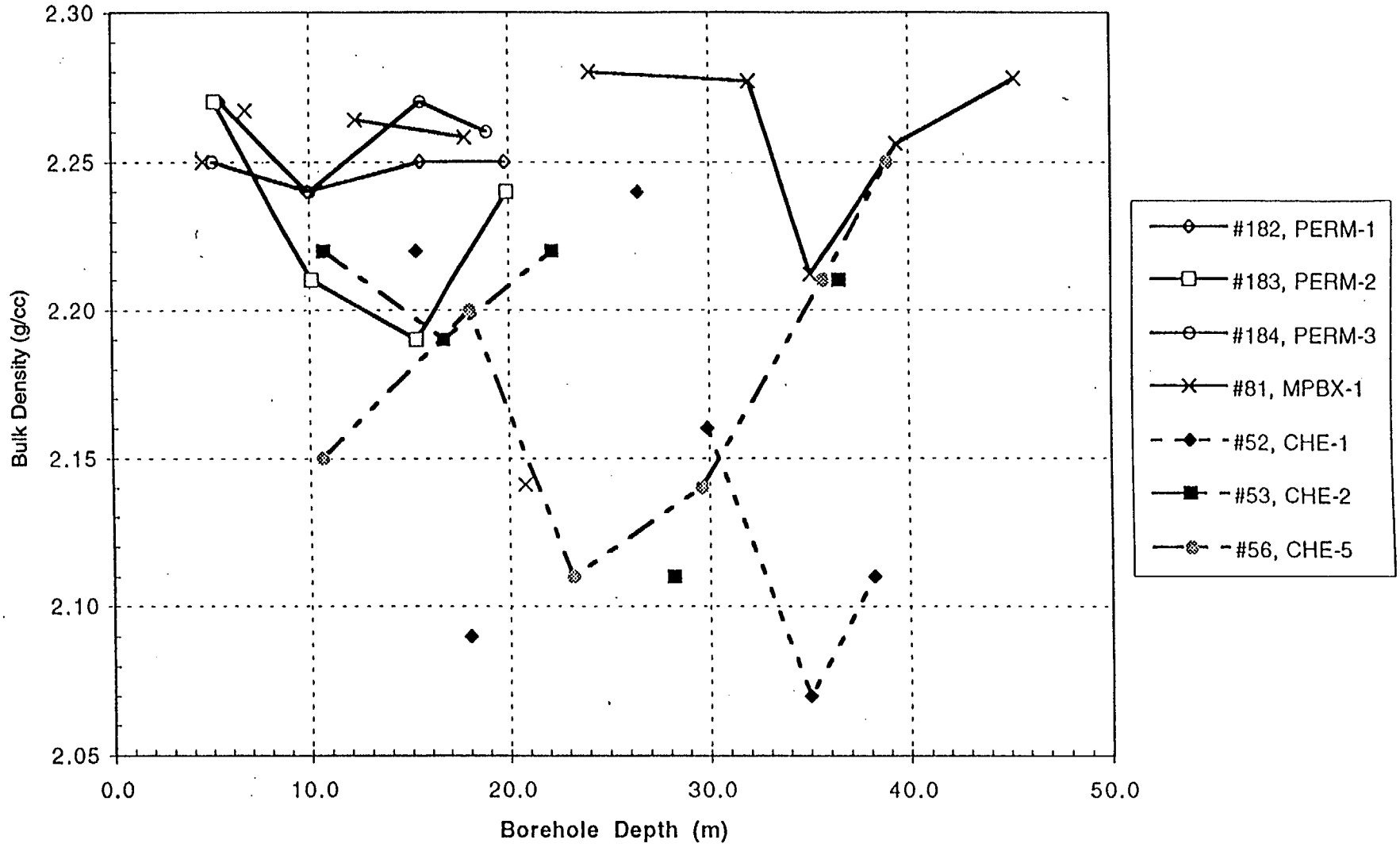

Figure D-3. DST Bulk Density: DST Dry and Wet Drilled Core Measurement

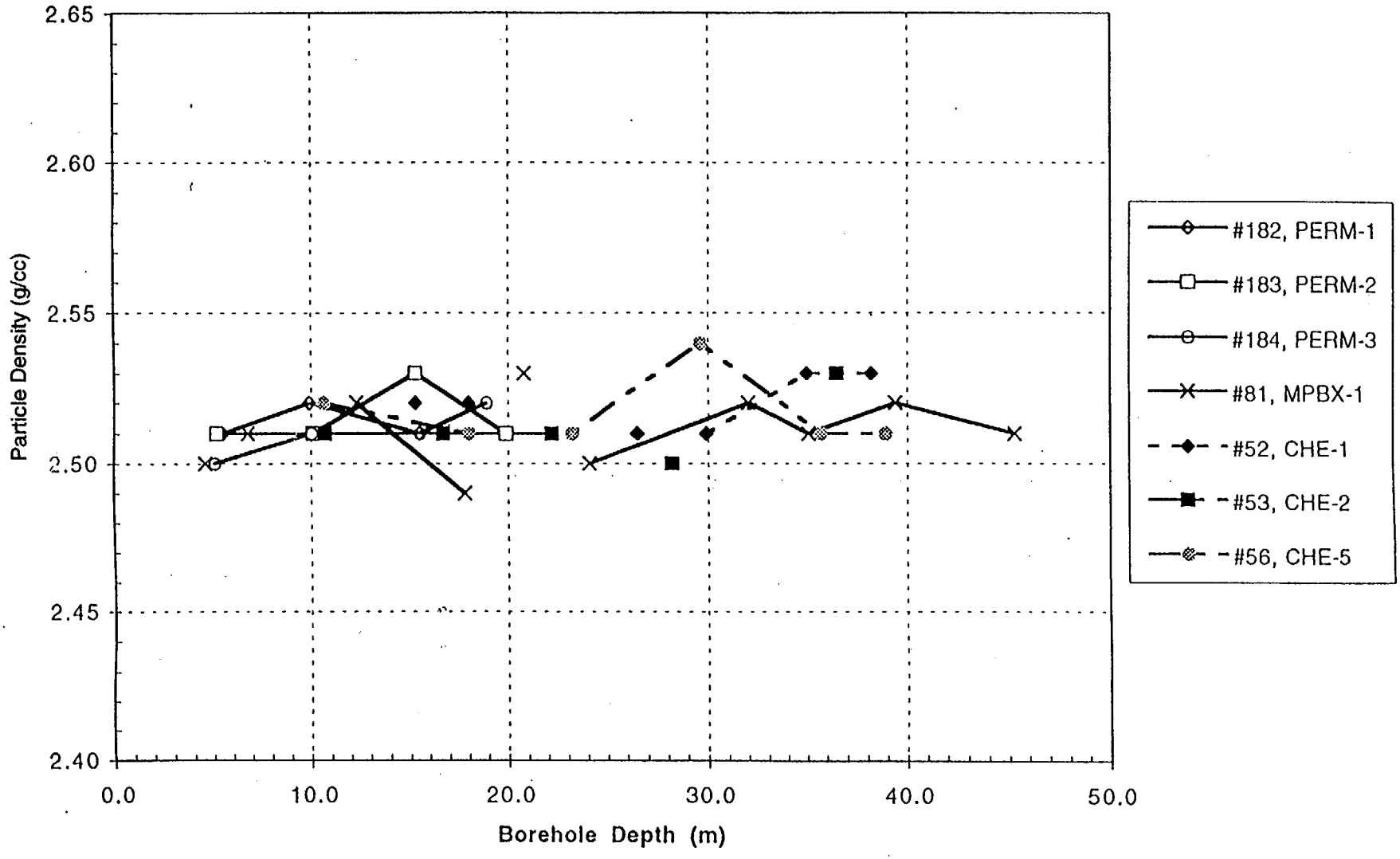

Figure D-4. DST Particle Density: DST Dry and Wet Drilled Core Measurement

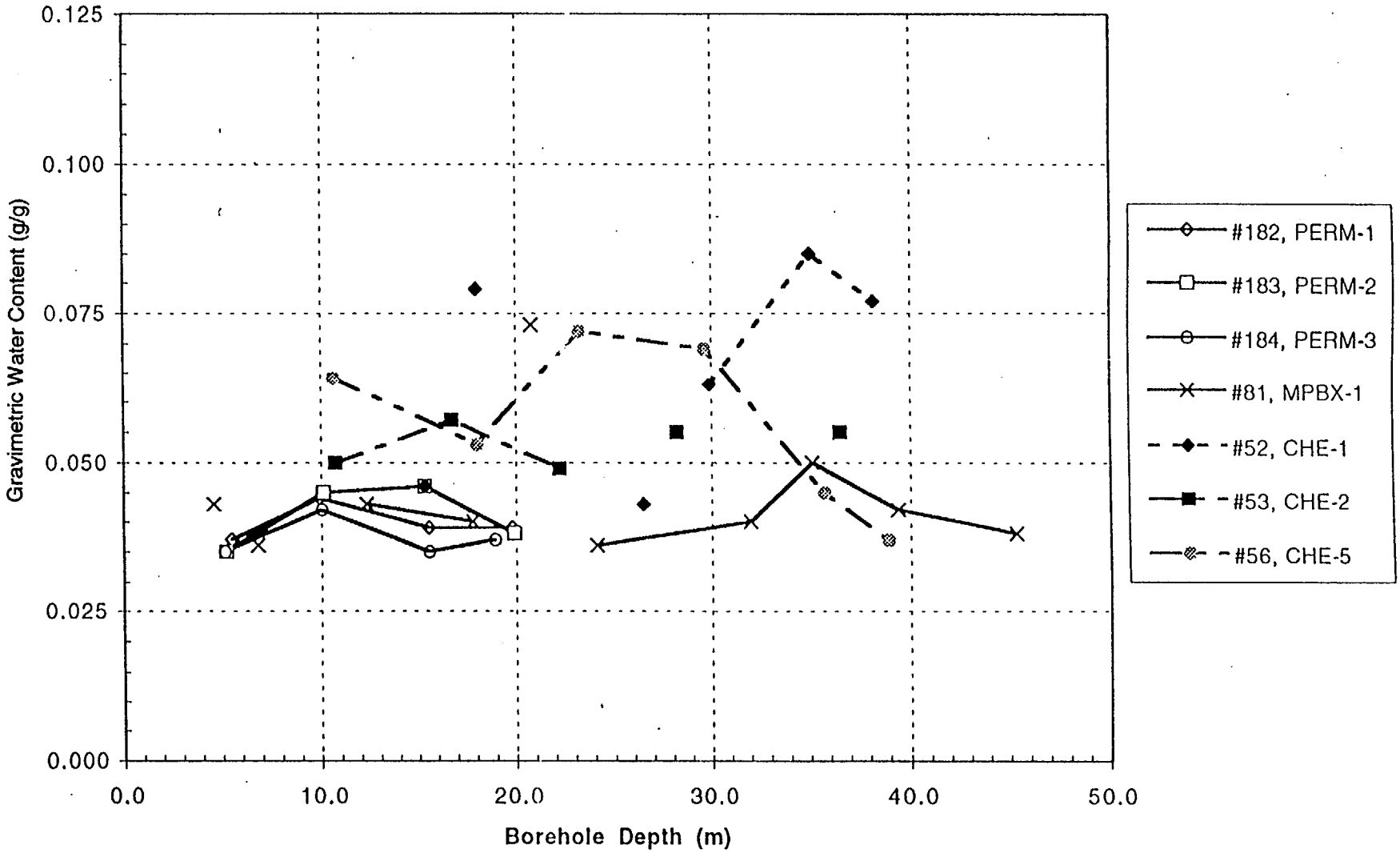

Figure D-5. SHT Gravimetric Water Content: DST Dry and Wet Drilled Core Measurement

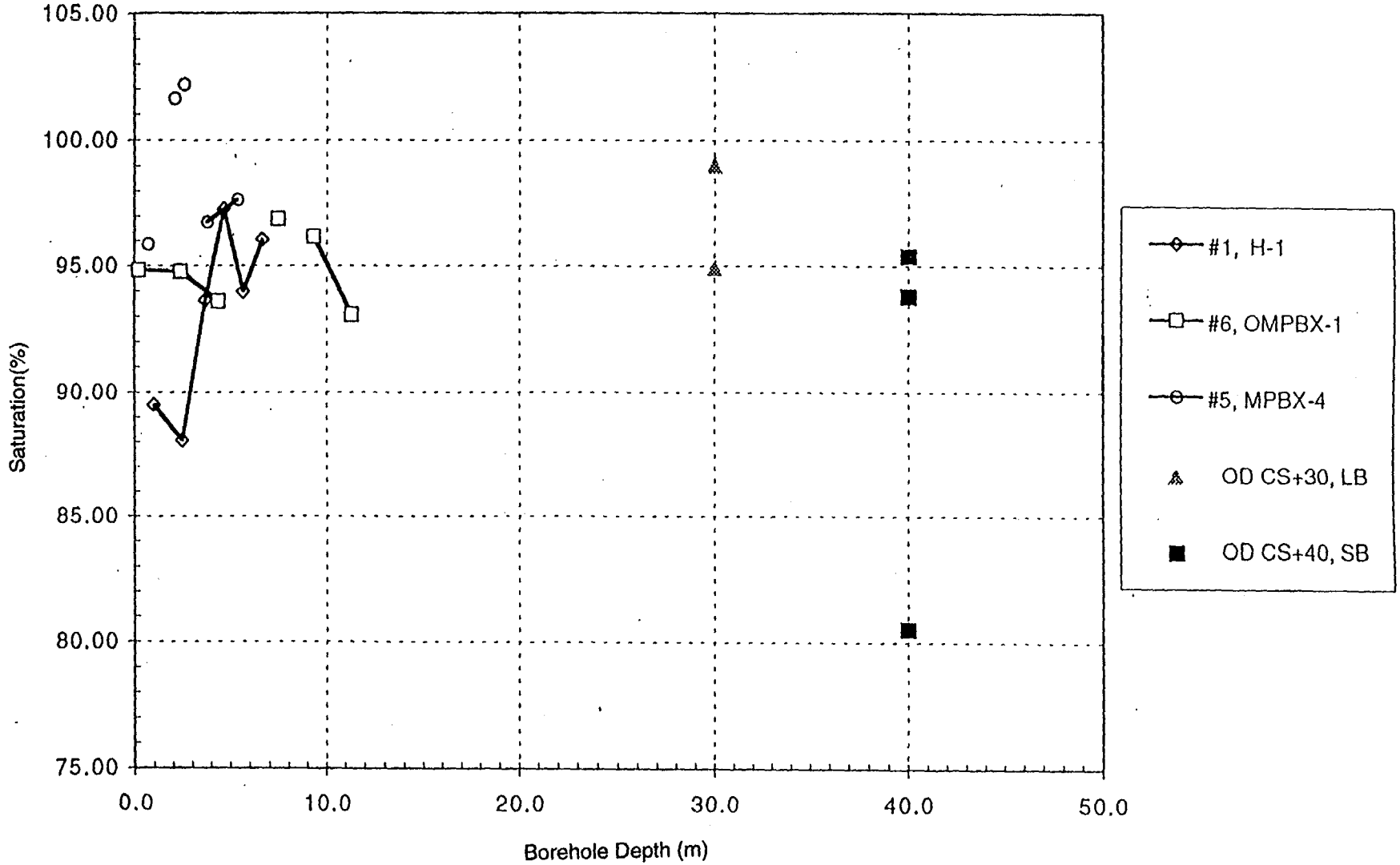

Figure D-6. SHT Saturation: SHT Wet Drilled Core & Grab Sample Measurement

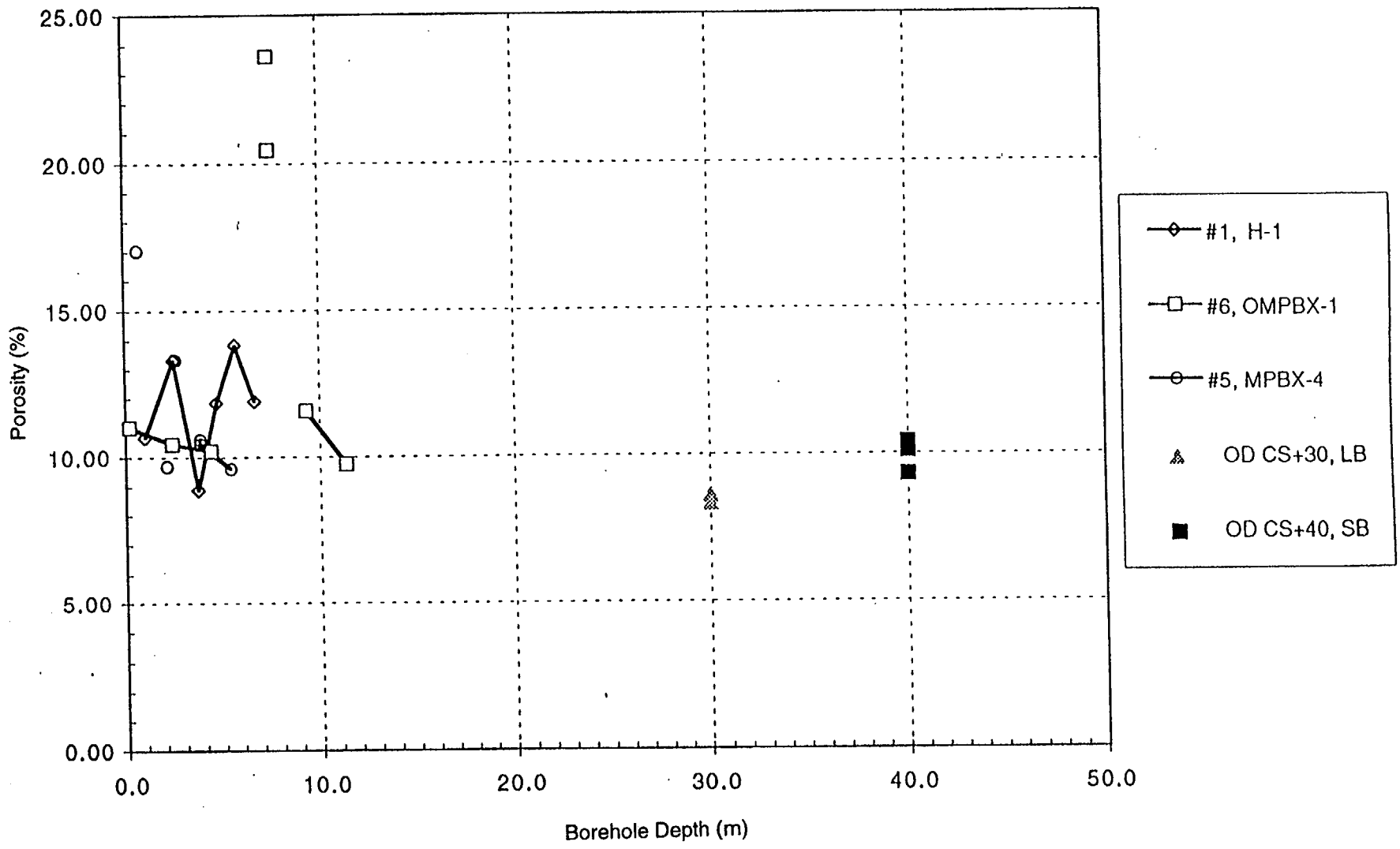

Figure D-7. SHT Porosity: SHT Wet Drilled Core & Grab Sample Measurement

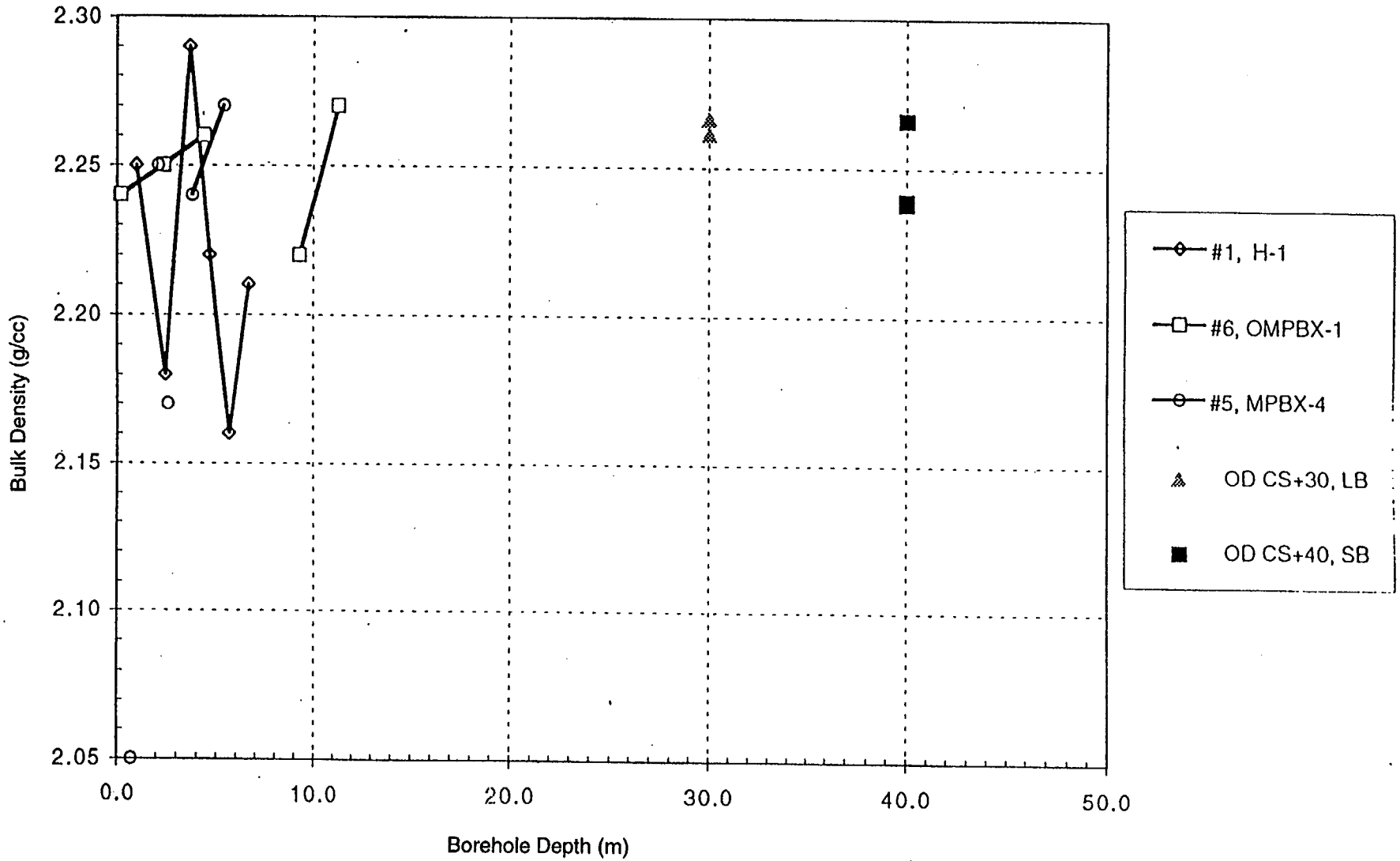

Figure D-8. SHT Bulk Density: SHT Wet Drilled Core & Grab Sample Measurement

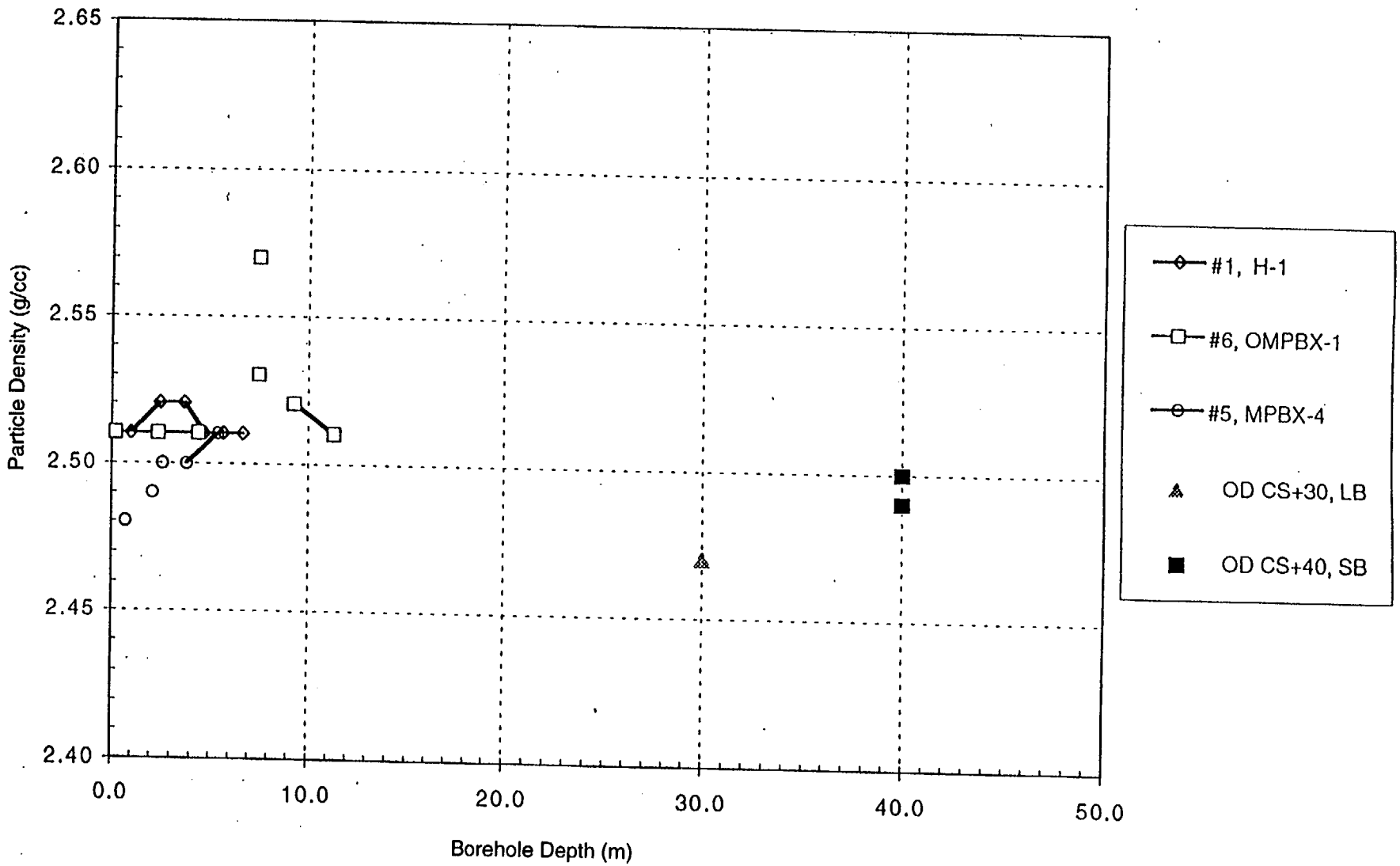

Figure D-9. SHT Particle Density: SHT Wet Drilled Core & Grab Sample Measurement

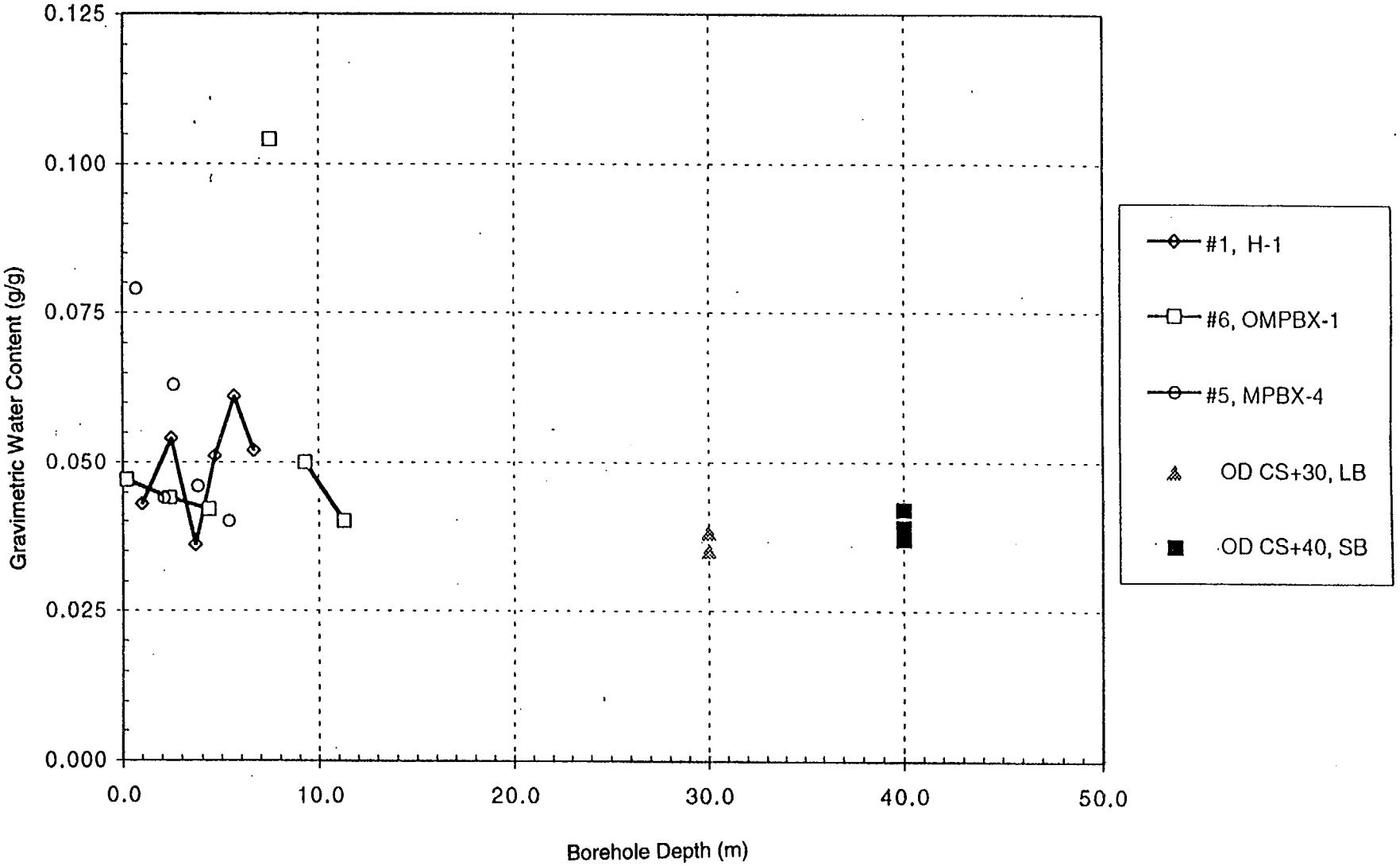

Figure D-10. SHT Gravimetric Water Content: SHT Wet Drilled Core & Grab Sample Measurement